UNIVERSITY OF Southampton

Faculty of Engineering and Physical Sciences

Bioengineering Unit

Elucidating Nanoclay-Stem Cell Interactions for Enhancing Bone Regeneration

by

Mohamed Mousa

Thesis for the degree of Doctor of Philosophy

September 2020

ABSTRACT

Bone fractures and degenerative diseases are a major socioeconomic problem that is on the rise with an aging population. Therefore, there is a pressing, yet unmet, clinical need for treatment approaches to repair damaged/degenerated bone tissues. A promising approach to address this problem is to develop new bioactive materials that can direct and enhance the osteogenic differentiation of human bone marrow stromal cells (hBMSCs). Recently, clay nanoparticles (herein Laponite) have received growing interest in this context due to their exciting potential to enhance cellular functions including adhesion, proliferation and differentiation, most notably for osteogenesis. However, the mechanism(s) of interaction between nanoclay and hBMSCs, which is the key for the successful harnessing of nanoclay for bone regeneration, remain poorly understood. In this thesis the ability of clay nanoparticles to promote hBMSCs osteogenesis (differentiation into the osteogenic lineage) was investigated followed by an investigation of various modes through which nanoclay may influence hBMSCs osteogenic function, in particular, the of Laponite endocytosis and subsequent release of Laponite degradation products ($Si(OH)_4$, Mg^{2+} and Li^+).

The osteogenic effects of clay nanoparticles on hBMSCs were determined at varying doses and culture time by determination of alkaline phosphatase (ALP) activity, calcium phosphate mineralization and osteogenic gene expression. The role of nanoclay endocytosis and subsequent release of degradation products, in particular lithium, was tested through the use of the endocytosis inhibitor chlorpromazine hydrochloride (CPZ) and the use of lithium modified Laponite formulations developed with BYK-ALTANA (Widnes, Cheshire, UK). Finally, the cellular uptake kinetics, intracellular transport pathway(s), and fate of internalized clay nanoparticles were tracked using inductively coupled plasma mass spectrometry (ICPMS), confocal and electron microscopy.

Clay nanoparticles were biocompatible up to a concentration of 100 μg/mL and promoted osteogenic differentiation of hBMSCs in a dose- and time-dependent manner. Inhibition of nanoclay endocytosis significantly attenuated (reduced) the ability of nanoclay to enhance ALP activity of hBMSCs, while nanoclay degradation products, applied at concentrations equivalent to that present in Laponite, failed to induce any significant increase in ALP activity. Furthermore, no significant differences were observed in ALP activity and calcium deposition between standard Laponite and lithium modified Laponite structures and both null and high lithium nanoclays showed similar effects on osteogenic gene expression of hBMSCs indicating that nanoclay osteogenic bioactivity is not principally an effect of nanoclay degradation products.

Clay nanoparticles strongly interacted with hBMSCs distributing intracellularly, extracellularly and on the cell membrane as clusters/aggregates. Clay nanoparticles were readily internalized by hBMSCs through clathrin-mediated endocytosis and their uptake kinetics followed a linear increase with incubation time. Following endocytosis, clay nanoparticles were observed entrapped within endosomal and lysosomal compartments, but clay nanoparticles were not free in other cell organelles. Internalized nanoclay underwent degradation with endosomal-lysosomal maturation and exocytosis. Nanoclay uptake influenced cell physiological functions as demonstrated by nanoclay-induced hBMSCs autophagy which stands as potential mechanism for Laponite osteogenic bioactivity.

This thesis provides a clear understanding of how nanoclay interact with hBMSCs for enhanced osteogenic differentiation and sets a basis for the successful control and manipulation of nanoclay for biomaterial design and regenerative medicine.

Contents

List of tables

List of figures

Declaration of Authorship

I, Mohamed Mousa, declare that this thesis and the work presented in it are my own and have been generated by me as the result of my own original research.

Elucidating Nanoclay-Stem Cell Interactions for Enhancing Bone Regeneration

I confirm that:

1. This work was done wholly or mainly while in candidature for a research degree at this University.
2. Where any part of this thesis has previously been submitted for a degree or any other qualification at this University or any other institution, this has been clearly stated.
3. Where I have consulted the published work of others, this is always clearly attributed.
4. Where I have quoted from the work of others, the source is always given. With the exception of such quotations, this thesis is entirely my own work.
5. I have acknowledged all main sources of help.
6. Where the thesis is based on work done by myself jointly with others, I have made clear exactly what was done by others and what I have contributed myself.

Signed:

Date:

Abstracts and Publications

Parts of this work has been published as:

Review paper

M. Mousa, N. D. Evans, R. O. C. Oreffo, and J. I. Dawson, "**Clay nanoparticles for regenerative medicine and biomaterial design: A review of clay bioactivity**," Biomaterials, vol. 159. pp. 204–214, 2018.

Original research articles

M. Mousa, O. Kelly, J. Doyle, N. D. Evans, R. O. C. Oreffo, and J. I. Dawson, "**The role of lithium in the osteogenic bioactivity of clay nanoparticles**," Biomaterials Science, Submitted.

P. Shi, Y. H. Kim, M. Mousa, R. R. Sanchez, R. O. C. Oreffo, and J. I. Dawson, "**Self-Assembling Nanoclay Diffusion Gels for Bioactive Osteogenic Microenvironments**," Adv. Healthc. Mater., vol. 7, no. 15, 2018.

Abstracts

"**Lithium modified clay nanoparticles for injectable osteogenic stem cell microenvironment**"; Poster presentation at: Conference of the Tissue and Cell Engineering Society (TCES), 2017 July 5-7, Manchester, UK.

"**Towards understanding why nanoclays are osteogenic**"; Oral presentation at: Conference of the Tissue Engineering and Regenerative Medicine International Society (TERMIS), 2019 May 27-31, Rhodes, GR.

Contributors

All experiments and data analysis were performed by the author in the Bone and Joint Research Group laboratory, Academic Unit of Human Development and Health, Faculty of Medicine, Southampton University Hospital, University of Southampton, with the following exceptions:

Section 5.3.2

Synthesis of lithium modified Laponite clay nanoparticles, in terms of structural lithium, was performed by BYK-ALTANA but modification of exchanged lithium in/on Laponite was performed by the author under the supervision of Dr Oscar Kelly in the Research & Development department, BYK-ALTANA. Characterization of lithium modified Laponite clay minerals was performed under the supervision of Dr Oscar Kelly in the Research & Development Laboratories, BYK-ALTANA.

Section 6.3.1

Sample preparation for confocal microscopy was conducted by the author in the Bone & Joint Group Laboratory but confocal imaging was performed under the supervision of Dr David Johnston in the Biomedical Imaging Unit, Faculty of Medicine, University of Southampton.

Section 6.3.2

Sample preparation for ICP-MS analysis was performed by the author in the Bone & Joint Group Laboratory and the National Oceanography Centre, the School of Ocean and Earth Science, University of Southampton under supervision of Ms Agnes Michalik. ICPMS instrumental analysis of prepared samples was performed under the supervision of Professor J. Andy Milton, National Oceanography Centre, the School of Ocean and Earth Science, University of Southampton.

Section 6.3.3

Sample preparation for TEM-EDX imaging and analysis was conducted by the author the Bone & Joint Group Laboratory and TEM imaging was performed under the supervision of Dr Patricia Goggin in the Biomedical Imaging Unit, Faculty of Medicine, University of Southampton.

Acknowledgements

First and above all, I wholeheartedly thank my mighty God Allah for giving me the vision, power and spirit to complete this interesting research work. O Allah, without your guidance and help I would have been lost and would not have been able to reach this level. Second, I'm deeply thankful to my love and excellent exemplar my prophet Mohamed, peace and blessings be upon him. All success I achieved in my life because I followed your path.

I express my deepest gratitude and appreciation to my whole family who has been an important and indispensable source of spiritual spirit and more specifically my true mentors: my mother, Mme. Nadya SAYED and my father, Mr. Abdelsattar MOHAMED who have been always giving me the strength to carry on and reach my goal.

I would like to thank my supervisors Dr Jon Dawson, Dr Nick Evans and Prof. Richard Oreffo for their continuous help and support in all the time of research and writing of this thesis. I'm very grateful indeed to Dr Jon Dawson, who was an excellent supervisor, for encouraging me to express and develop my research ideas and providing me with his excellent feedback and comments. Dr Dawson's supervision hugely helped me develop as an independent researcher during the course of my PhD.

My thanks goes to members of the Bone and Joint Research Group for having such great and friendly research environment. Special thanks goes to Ms Julia Wells and Dr María Carmen De Andrés for training me in tissue culture and molecular biology techniques. I'm also grateful to Dr David Johnston, Dr Patricia Goggin and Prof. Andy Milton for their excellent help with the confocal microscopy, TEM-EDX and ICPMS analysis.

Abbreviations

3-MA	3-methyladenine
3T3	embryonic fibroblast cell line
AAS	atomic absorption spectroscopy
AL	Autolysosome
ALP	alkaline phosphatase
ALPL	Alkaline Phosphatase, Liver/Bone/Kidney
ALT	alanine aminotransferase
AP	Autophagosome
APC	adenomatous polyposis coli
ARS	alizarin red stain
AST	aspartate aminotransferase
ATF4	activating transcription factor 4
ATR	attenuated total reflectance
BGLAP	bone gamma-carboxyglutamate protein (gene coding for osteocalcin)
BIU	biomedical imaging unit
BMD	bone mineral density
BMP	bone morphogenetic protein
BMP2	bone morphogenetic protein 2
BMPR	Bone morphogenetic protein receptor
BSP	bone sialoprotein
CaP	calcium phosphate
Cbfa1	core-binding factor alpha 1
C_{clay}	Concertation of clay
CCM	cell culture media
CD	cluster of differentiation
cDNA	complementary DNA
CEC	cation exchange capacity
CFU-F	colony-forming unit-fibroblast
CHO	Chinese hamster ovary cells
CLSM	Confocal Laser Scanning Microscopy
COL1	collagen type 1
COL1A1	collagen type 1, alpha chain 1
CPZ	chlorpromazine hydrochloride
CQ	chloroquine
DAPI	4′,6-diamidino-2-phenylindole
dH_2O	distilled water
DI	deionised (water)
DLX5	distal-less homeobox 5
DMEM	Dulbecco’s modified Eagle medium
DMSO	dimethyl sulphoxide
DNA	deoxyribonucleic acid
DNase	Deoxyribonuclease
dNTP	deoxynucleoside triphosphates
DOX	Doxorubicin

DPBS	Dulbecco's phosphate-buffered saline
dsDNA	double stranded DNA
Dvl	Dishevelled protein
ECM	extracellular matrix
EDTA	Ethylenediaminetetraacetic acid
EDX	energy dispersive X-ray
EGF	Epidermal growth factor
EGFR	Epidermal growth factor receptor
ER	endoplasmic reticulum
ERK	extracellular signal-regulated kinase
FA	folic acid
FACS	fluorescence-activated cell sorting
FAK	focal adhesion kinase
FBS	fetal bovine serum
FGF	fibroblast growth factor
FGFR	fibroblast growth factor receptor
FITC	Fluorescein isothiocyanate
FTIR	Fourier transform infrared spectroscopy
Fz8/Fc	Frizzled-8/Fc chimeric protein
Fzd	frizzled
GA	Golgi apparatus
GAPDH	Glyceraldehyde 3-phosphate dehydrogenase
GelMA	gelatin methacrylate
GLI	glioma-Associated Oncogene Homolog
GPA	glycophorin A
GSK3β	glycogen synthase kinase 3
HA	Hydroxyapatite
hASCs	human adipose-derived stem cells
Hb	hemoglobin
hBMSCs	human bone marrow stromal cells
HEPES	4-(2-hydroxyethyl)-1-piperazineethanesulfonic acid
HIF-1α	hypoxia-inducible factor 1α
HL	high lithium (Laponite)
HNT	halloysite nanotube
hSSCs	human skeletal stem cells
HUVECs	Human umbilical vein endothelial cells
Ibsp	Integrin Binding Sialoprotein
IC50	half maximal inhibitory concentration
ICPMS	inductively coupled plasma mass spectrometry
ICP-OES	inductively coupled plasma atomic emission spectroscopy
IGF	insulin-like growth factor
IHh	Indian hedgehog signaling molecule
LAP	Laponite
LC3	microtubule-associated protein light chain 3
LD50	median lethal dose
LDH	lactate dehydrogenase
LDH	layered double hydroxide (anionic clay)
LRP5/6	low density lipoprotein receptor-related protein 5/6

MAPK	mitogen-activated protein kinase
MCF-7	michigan cancer foundation-7 (breast cancer cell line)
MEK	MAPK/ERK kinase
MEM	membrane desalting buffer
M^{II}	divalent metal cation
M^{III}	trivalent metal cation
MMT	Montmorillonite
mRNA	messenger RNA
MSCs	mesenchymal stem cells
MSX2	msh homeobox 2
MT	Microtubule
NHDF	Normal Human Dermal Fibroblasts
NL	null lithium (Laponite)
NP	Nanoparticle
OCN	Osteocalcin
OI	osteogenesis imperfects
OPN	Osteopontin
OSE2	osteoblast-specific cis-acting element
OSX	Osterix
P0	primary passage culture
PCL	Polycaprolactone
PCN	polymer-clay nanocomposite
PDGF	platelet-derived growth factor
PEG/PEO	Polyethylene glycol
PFA	paraformaldehyde
PGC-1α	peroxisome proliferator-activated receptor gamma coactivator 1α
PGS	poly(glycerol sebacate)
Pi	inorganic phosphate
PIPES	piperazine-N,N′-bis(2-ethanesulfonic acid)
PKC	protein kinase C
PLCγ	phospholipase Cγ
PLGA	poly(lactic-co-glycolic acid)
PLT	platelet
PM	plasma membrane
PNIPA	poly-N-isopropylacrylamide
pNP	p-nitrophenol
pNPP	p-nitrophenyl phosphate
PPi	Pyrophosphate
PTCH	patched receptor
PU	Polyurethane
PXRD	powder X-ray diffraction
RBITC	Rhodamine B isothiocyanate
RCF	relative centrifugal force
RGD	Arginine-Glycine-Aspartic Acid
RNA	ribonucleic acid
RNase	ribonuclease
RNS	reactive nitrogen species
ROS	reactive oxygen species

ROS	reactive oxygen species
rpm	revolutions per minute
RT	reverse transcription
RT-qPCR	real-time quantitative polymerase chain reaction
RUNX2	runt-related transcription factor 2
SBF	simulated body fluid
SD	standard deviation
SEM	scanning electron microscopy
Sfrp1	Secreted Frizzled Related Protein 1
SHh	Sonic Hedgehog Signaling Molecule
SL	standard lithium (Laponite)
SL^{ex}	standard lithium Laponite with exchanged lithium
SMO	smoothened receptor
SP7	gene coding for osterix
SPARC	secreted protein acidic and rich in cysteine (gene coding for osteonectin)
SPP1	secreted phosphoprotein 1 (gene coding for osteopontin)
SSA	specific surface area
SSCs	skeletal stem cells
SSEA-4	stage-specific embryonic antigen 4
STRO-1	cell surface trypsin-resistant antigen expressed by CFU-F
T/E	trypsin/EDTA
TCF/LEF	T-cell factor/lymphoid enhancer-binding factor (transcription factors)
TCP	tissue culture plastic
TE	Tris/EDTA
TEM	transmission electron microscopy
TGFβ	transforming growth factor beta
T-O	tetrahedral-octahedral clay layer
T-O-T	tetrahedral-octahedral-tetrahedral clay layer
Tris	tris(hydroxymethyl)aminomethane
UV	Ultraviolet
WBC	white blood cells
Wnt	Wingless-related integration site
XRF	X-ray fluorescence
ZPC	zero point of charge
αMEM	minimum essential medium alpha

Chapter 1: Introduction

Overview

The demand for bone regenerative therapies is an increasing yet unmet clinical need. In particular, large bone defects due to severe disease, injury or trauma are beyond the intrinsic capacity of bone tissue for self-healing and repair and necessitates the intervention of surgical treatments (bone grafts) which are associated with high cost and severe side effects. The field of biomaterials and regenerative medicine offers a new safer alternative approach for bone tissue repair. Clay nanoparticles are emerging as a new class of biomaterials with exciting potential for bone regenerative therapies due to their capacity to enhance stem cell functions including adhesion, proliferation and osteogenic differentiation. This has encouraged a growing number of studies seeking to harness the potential of clay nanoparticles, applied either alone or in polymer clay nanocomposites, to direct and control function and fate of seeded stem cells for enhanced bone formation. However, there remains paucity of information of how clay nanoparticles modulate stem cell function which is the key to successfully harnessing these materials for biomaterial design, regenerative medicine and ultimately patient benefit. The main aims of this thesis are to investigate the osteogenic potential of clay nanoparticles on human bone marrow stromal cells and understand the interaction mechanisms between nanoclay and hBMSCs.

Before turning to explore these aims, this chapter will introduce the core concepts underlying this investigation. After introducing fundamental aspects of bone biology, structure and function including the definition and role of skeletal stem cells and their osteogenic differentiation, the following will review the need for biomaterials and regenerative medicine as a new alternative approach for bone fracture repair. It is in this context that I highlight the promise of clay nanoparticles. In particular, I will introduce clay composition and structure and explore its relevance for bone tissue engineering in relation to polymers for scaffold design, to proteins for controlled drug delivery and to with cells for direct stimulation of osteogenesis. At the end of this chapter, we discuss the various hypothesized mechanisms through which nanoclay can modulate osteogenic cell function.

1.1 Bone structure and function

Bone is a complex, living, constantly remodelling connective tissue, which has mechanical, metabolic and haematopoietic function[1,2]. It provides supportive and protective environment for organs inside the body against injury or trauma and enables body movement and locomotion by acting as levers communicating with muscles, tendons, ligaments and joints. Regarding its metabolic functions, bone acts as a major reservoir for inorganic minerals such as calcium and phosphorus and play a vital role in calcium homeostasis and energy metabolism in the body. The production of blood cells (haematopoiesis) is governed by red bone marrow which resides within bone cavities and contains hematopoietic stem cells[3].

Bone, in common, is composed of two main components: mineralized extracellular matrix (ECM) and bone cells with ratios of 90% and 10%, respectively[4]. ECM is composed of an organic matrix reinforced by an inorganic phase, although water also is a major constituent - in adult human cortical bone, ECM is a composite of mineral/organic matrix/water in approximately 60%/20%/20%, a ratio which is crucial for balance between bone stiffness and flexibility[5]. The inorganic phase of ECM is calcium hydroxyapatite HA (Ca_{10} (PO_4)$_6$ (OH)$_2$), a calcium phosphate mineral with Ca/P ratio of <1.67[4]. It provides compressive strength for bone. On the other hand, the organic matrix is predominantly composed of type I collagen COL1 (90%), while the remaining 10% is represented by non-collagenous proteins such as osteocalcin (OCN), osteopontin (OPN), osteonectin (ONC) and bone sialoprotein (BSP) in addition to proteoglycans, growth factors and cytokines[6,7]. In addition to providing structural integrity for bone, extracellular matrix proteins play a key role in regulating bone cell functions such as adhesion, migration, proliferation and differentiation as well as in matrix mineralisation[8,9]. A list of extracellular matrix components with their corresponding functions are included in **table 1.1**.

There are four types of cells which constitute bone tissue: osteoblasts, osteocytes, bone-lining cells and osteoclasts[10]. While the former three originate from local osteoprogenitors, which arise from differentiated mesenchymal stem cells (MSCs), osteoclasts are formed from fusion of mononuclear precursor cells originating from hematopoietic stem cell origin[1]. Osteoblasts are cuboidal mononuclear cells located along the bone surface and considered as bone-building cells as they synthesize and secrete organic bone matrix and control bone mineralisation[11–13]. Subsequently,

osteoblasts can undergo apoptosis, become bone lining cells covering the surface of newly formed bone or become entrapped in the newly-formed extracellular matrix and mature into osteocytes[14]. Osteocytes are former mature osteoblasts located within lacunae, surrounded by mineralised bone matrix, and account for 90-95% of bone cells in adult bone[15]. Osteocytes are characterised by their long cytoplasmic processes which cross canaliculi to communicate with neighbouring osteocytes via gap junctions and with cytoplasmic processes of osteoblasts and bone lining cells on bone surface, to facilitate transport of small molecules between bone cells thus maintaining cell-cell communication and bone homeostasis[16]. In contrast, osteoclasts are large multinucleated cells formed from fusion of mononuclear precursor cells of the monocyte-macrophage lineage[17]. Osteoclasts are responsible for bone resorption through a coordinating action with other bone cells including osteoblasts, osteocytes and bone lining cells[18,19].

Histologically, there are two types of bone, which differ mainly according to ECM pattern and organisation: primary (woven) bone and secondary (lamellar) bone[20]. The first is formed by osteoblasts and subsequently replaced by the second. While woven bone is characterised by a random pattern of collagen fibrils and mineralisation, which makes it relatively weak, lamellar bone constitute collagen fibrils with a high degree of parallel alignment resulting in higher mechanical strength[21].

Lamellar bone is formed of periosteum, cortical (compact) bone and cancellous (spongy) bone, moving from outside to inside of the bone tissue[7] (**Figure 1.1**). The periosteum is formed of an outer fibrous layer containing mainly fibroblasts and an inner cambium layer containing progenitor cells which develop into osteoblasts. It provides a good blood supply to the bone tissue and it is the point of attachment with muscles. The cortical bone is denser and stiffer than the cancellous bone and surrounds both the cancellous bone and medullary cavity, which contains the red bone marrow. The basic building block of cortical bone is the osteon, which consists of layers of compact bone, called lamellae, concentrically organised around the Haversian canal which contains blood vessels and nerves. Osteocytes are embedded in between lamellae forming a complex network with the bone matrix[7,20].

In contrast, trabecular bone is composed of an irregular, interconnected porous network of osteons. However, unlike the case in cortical bone, trabecular osteons lack

Haversian canal and exhibit irregular structure. While cortical bone provides mechanical and protective environment, trabecular bone is characterised by its metabolic functions and it responds more rapidly to stimuli than the cortical bone[20].

Component	Function
Collagenous proteins	
Type 1 collagen (COL1A1)	- Maintain mechanical support; scaffold of bone cells[22]. - Promote osteoblast differentiation through interaction with integrins[23,24] & control hydroxyapatite nucleation and deposition[25].
Non-collagenous proteins	
Bone sialoprotein (BSP)	- Necessary for initiation of mineralisation; act as a hydroxyapatite crystal nucleator[26]. - Promote osteoblast differentiation through its RGD integrin binding sequence[27].
Osteopontin (SPP1)	-Necessary for initiation of mineralisation; act as mineralisation inhibitor[28]; Ensure right crystal (HA) is formed[26]. -Inhibit osteoblast differentiation through inhibition of BMP2 responsiveness[29]; negative feedback regulator of osteogenesis and mineralisation.
Osteocalcin (BGLAP)	-Regulate growth/maturation rate and size of hydroxyapatite crystals[30]. -Promote osteoblast differentiation[31].
Osteonectin (SPARC)	-Binds selectively to both collagen and hydroxyapatite to regulate hydroxyapatite crystal growth[32]. -Promote osteoblast differentiation through the p38 MAPK pathway[33].
Inorganic ECM	
Hydroxyapatite crystals	- Provide compressive strength for bone[4] -Storage of calcium, phosphate and other minerals (calcium homeostasis)[34]. .

Table 1. 1 Components of the extracellular matrix in bone tissue with their corresponding functions.
Based on Lin et al., 2020[22].

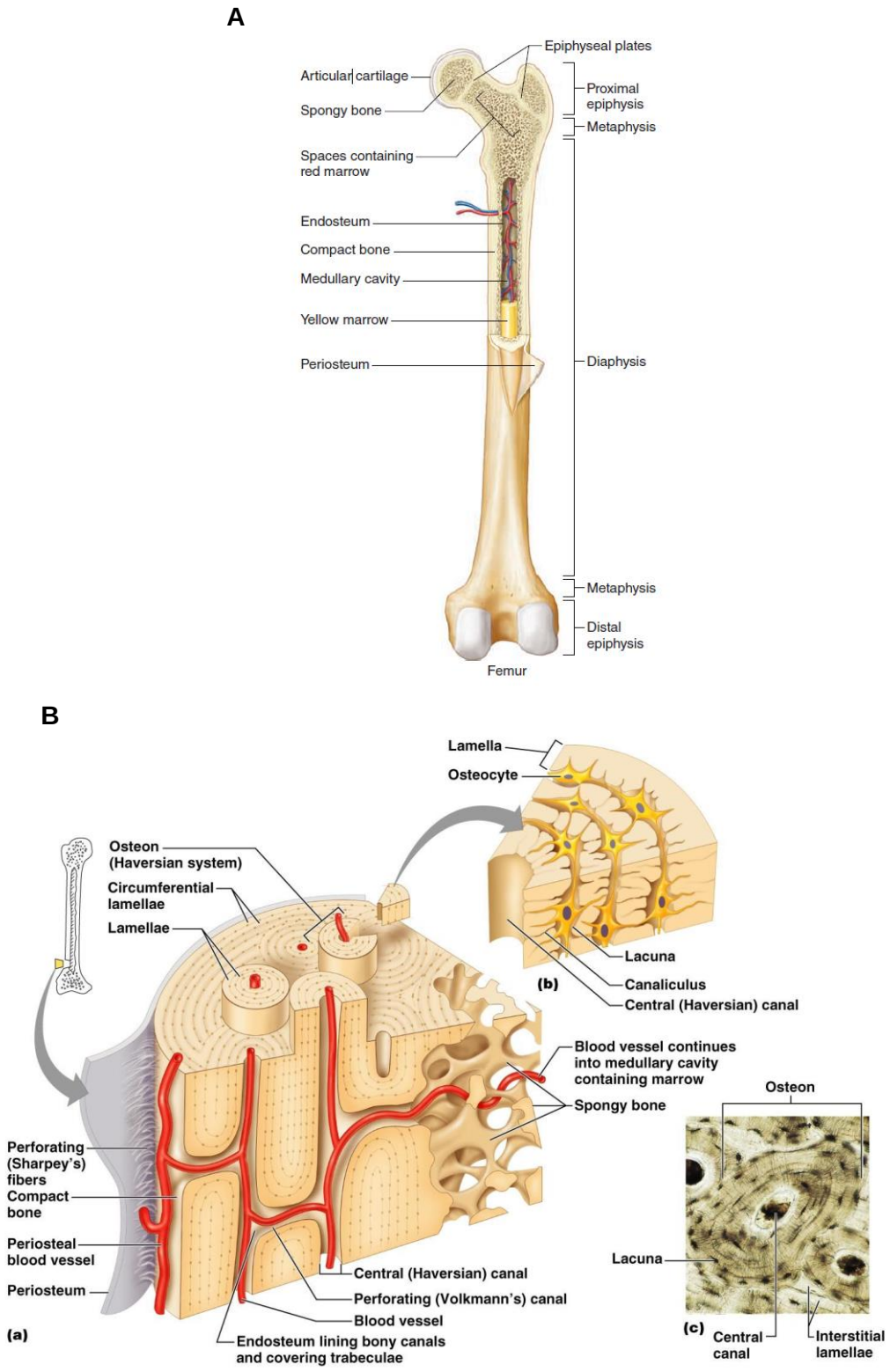

Figure 1. 1 Bone structure
Structure and anatomy of human long bone[34] (A) and cross section of cortical (compact) bone[35] (B).

1.2 Skeletal stem cells and osteoblast differentiation

Human skeletal stem cells (hSSCs) are present within the bone marrow stroma at the outer surface of sinusoids and are a part of a three-dimensional perivascular stromal compartment called the "bone marrow niche"[36]. hSSCs play a central role in bone development and homeostasis and have shown great promise for bone tissue repair and regeneration both *in vitro* and *in vivo*[37,38]. Therefore, they represent an attractive target for clinical bone regenerative therapies.

Human skeletal stem cells are characterized by their plastic adherence, clonal expansion, self-renewal capacity and multilineage differentiation potential into osteogenic, chondrogenic and adipogenic lineages *in vitro*[36,39–41]. However, the defining feature of hSSCs is their ability to generate heterotopic ossicles upon *in vivo* transplantation[36]. These are miniature bone organs containing multiple differentiated cell types of the donor (osteoblasts, adipocytes and fibroblasts) and hematopoietic cells of the host[36,39]. In addition to their multipotential differentiation capacity, hSSCs play critical roles in regulating the hematopoietic stem cell niche within the bone marrow [42–45].

The term human skeletal stem cells (hSSCs) is often used interchangeably in literature with human bone marrow stromal cells (hBMSCs) and human mesenchymal stem cells (hMSCs). However, hSSCs are a subset of hBMSCs, which are heterogeneous cell population that may contain hSSCs and are not stem cells themselves[46,47]. Moreover, the improper use of the term "mesenchymal stem cells" for "skeletal stem cells" should be abandoned because: i) it refers to stem/progenitor cells with differentiation potential into all cells derived from the mesenchyme - not only adipocyte, chondrocyte and osteoblasts lineages but also tenocytes, cardiac and smooth muscle myocyte; and 2) it assumes that these stem/progenitor cells are present not only in the bone marrow but also a number of other tissues (e.g. muscle and adipose tissue) and virtually all postnatal organs. Neither of these points have been proven *in vivo*. In particular, "MSCs" in extra-skeletal tissues and organs do not display skeletogenic properties assayable *in vivo* and are not generated by skeletal progenitors found in the bone marrow[36,37,39].

Human skeletal stem cells can be isolated from bone marrow through two different approaches: conventional and prospective[36,37,48]. While the former is based on plastic

adherence of clonal cultures but not the haematopoietic cell fraction, the latter is based on surface phenotype markers, which enrich for the skeletal stem cell population. Briefly, the conventional procedure involves plating the bone marrow cell suspension at low/clonal density (0.14–14.0 x10^3 nucleated cells/cm^2) which result in multiple colonies where each colony is the clonal progeny of a single stromal progenitor or stem cell (colony forming units-fibroblast CFU-F). It should be noted however that when the bone marrow cell suspension is plated as a bulk, the resultant cell population is a monolayer of both stromal stem/progenitors and other types of cells present among the adherent fraction of bone marrow aspirates (osteoblasts, endothelial cells, stromal fibroblasts etc.). While these populations are often described in the literature as MSCs it is more accurate to use the source related term: bone marrow stromal cells. Regarding the prospective method, several studies have used fluorescence-activated cell sorting (FACS) to enrich for hSSCs based on the expression of one or a group of specific surface markers such as STRO-1[49–51], CD146[52], CD271[53] and SSEA-4[54]. However, the presence of a reliable cell surface marker which can enrich for a homogenous skeletal stem cell population remains elusive[55]. For example, SRO-1, which represents antibody with the highest affinity and efficiency for isolating clonogenic SSCs, is expressed by heterogenous cell populations including glycophorin A+ (GPA+) erythroid progenitors and a subset of stromal cells[49]. In this thesis, hSSCs were isolated based on clonal cultures of human bone marrow stromal cell suspension at low density which has the benefit of enriching for cells capable of density independent growth at an early stage of culture – but which nevertheless still represent a heterogeneous bone marrow stromal population[48] . Therefore, the term "human bone marrow stromal cells" will be used for the cell fractions isolated and cultured in the studies presented throughout this thesis.

Differentiation of skeletal stem into osteoblasts is pivotal for bone development, growth, homeostasis and fracture healing/repair[56,57]. The primary commitment and subsequent differentiation of skeletal stem cells into specific lineage (i.e. osteoblastic, chondrogenic or adipogenic) is governed by activity of the so-called "master switch/transcription factors"[58]. Runt-related transcription factor 2 (RUNX2/Cbfa1) is known as the master switch for osteogenic differentiation – it directs multipotent skeletal stem cells to the osteoblast lineage and inhibit their differentiation to the

chondrogenic and adipogenic phenotypes[59]. The essential role of RUNX2 in osteogenesis is demonstrated by complete lack of both intramembranous and endochondral ossification in RUNX2-deficient (RUNX2 $^{-/-}$) mice due to arrest of osteoblasts differentiation and maturation[60,61]. RUNX2 directly regulate the expression of osteoblast-specific genes such as osteocalcin (BGLAP), osteopontin (SPP1), collagen type 1 (COL1A1) and bone sialoprotein (BSP) through binding to the osteoblast-specific cis-acting element (OSE2) found in the promoter region of these genes[62]. Another transcription factor which proved essential for osteoblast differentiation and bone formation is the zinc finger-containing transcription factor Osterix (SP7)[63,64]. In OSX-null mice, expression of almost all osteoblast marker genes is absent despite normal expression levels of RUNX2 compared to those found in wild-type osteoblasts/embryos, and OSX expression is absent in RUNX2-null mice. This indicate that OSX function downstream of RUNX2 and both transcription factors collaborate and play essential role in regulating osteoblast differentiation[63]. In particular, RUNX2 direct multipotential skeletal stem cells to immature preosteoblasts which then differentiate into mature osteoblasts, through the action of OSX, to express high levels of osteoblast marker genes[63].

Once RUNX2 is activated, skeletal stem cells become committed to osteoprogenitors which undergo 3 main successive developmental stages of osteogenic differentiation with each stage characterized by expression of certain molecular markers[58,65,66]. In stage 1, termed as proliferation stage, osteoprogenitors rapidly proliferate and express COL1A1 which is the most abundant protein in bone matrix. In stage 2, or so-called matrix maturation stage and cells termed as preosteoblasts, cells exit the cell cycle and start differentiation while synthesizing and secreting alkaline phosphatase ALP, COL1A1 and bone sialoprotein BSP. In addition, the extracellular matrix undergoes a series of modifications in composition and organization rendering it competent for the subsequent mineralization stage. In stage 3 (matrix mineralization) mature osteoblasts deposit osteopontin, osteonectin and osteocalcin and ECM undergo calcium phosphate mineralisation (**Figure 1.2**). Therefore, alkaline phosphatase, collagen type 1 and bone sialoprotein represent early markers of osteogenic differentiation, while osteopontin, osteonectin, osteocalcin and ECM mineralisation are typically viewed as late markers[65,67].

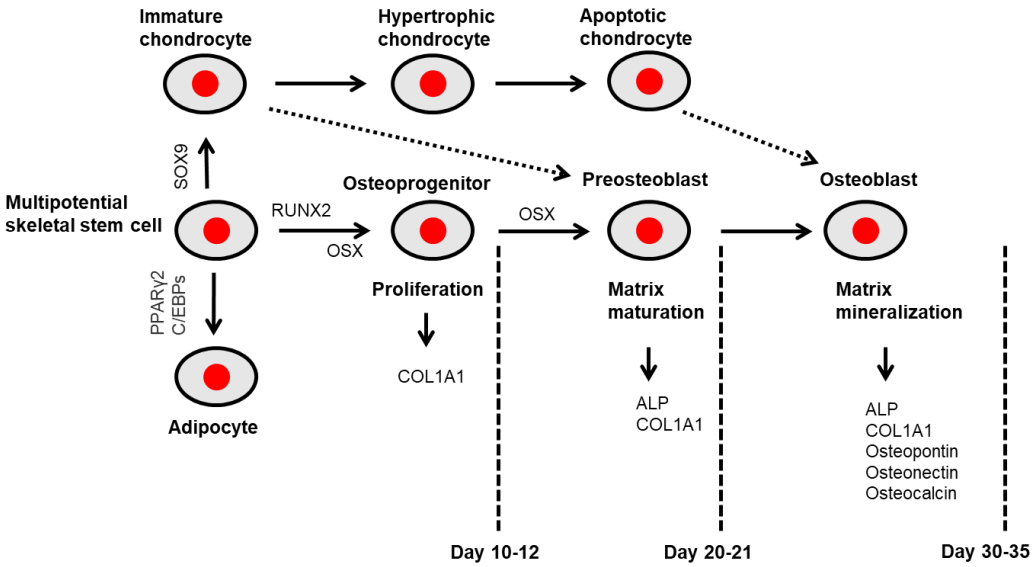

Figure 1. 2 Suggested developmental stages of skeletal stem cell differentiation into osteoblasts.
During intramembranous ossification, induction of RUNX2 expression, for example using an external osteogenic stimulus, drives SSCs towards commitment into osteoprogenitors which undergo extensive proliferation then differentiate into preosteoblasts under action of OSX which function downstream of RUNX2. During endochondral ossification, chondrocytes formed from SSCs under the activation of SOX9 enter the osteoblast lineage for terminal bone formation. Preosteoblasts express and secrete ALP and COL1A1 for matrix development and maturation. Then, preosteoblasts continue differentiating to mature osteoblasts which express and deposit extracellular non-collagenous matrix proteins osteopontin, osteonectin and osteocalcin for ultimate mineralization of the extracellular matrix with the help of ALP and COL1A1. The time scale for SSCs osteogenic differentiation is explained showing proliferation stage until day 10-12, matrix maturation stage until day 21 and mineralization stage until day 30-35 of cell culture/induction. Based on Aubin et al., 2002[58], Karperien et al., 2015[65], Aghajanian et al., 2018[68] and R.T. Franceschi, 1999[67].

Different signaling pathways have been reported to regulate, either alone or in concert, osteoblast commitment and differentiation including transforming growth factor-beta/bone morphogenic protein (TGFβ/BMP), Wnt/β-catenin, mitogen-activated protein kinase (MAPK), fibroblast growth factor (FGF) and Hedgehog signaling pathways [69].These osteogenic pathways respond to, and can be modulated by, various biochemical (e.g. growth factors and cytokines) and biophysical (e.g. mechanical stress and topographical features) cues, therefore they represent an attractive target for directing stem cell fate and ultimately successful bone regenerative therapies[70,71].

1.2.1 Wnt/β-catenin signaling pathway

The Wnt/β-catenin signaling pathway, or so-called the canonical Wnt cascade, is involved in embryonic skeletal development as well as fracture healing and repair in

adulthood[72,73]. The importance of Wnt signaling in bone was discovered when mutations of the low-density lipoprotein receptor-related protein 5 (LRP5) gene, a co-receptor for Wnt, were found to be responsible for osteoporosis-pseudoglioma syndrome, a disease characterized by low bone mass[74]. On the other hand, transgenic expressing *Wnt10b*, Wnt agonist, and mice lacking the Wnt antagonist secreted frizzled-related protein 1 (*Sfrp1*) exhibit a postnatal increase in bone mass[75]. Since then, the canonical Wnt signaling pathway has received a great attention and various drugs have been developed to target this pathway for treating osteogenic disorders[76]. Regarding skeletal stem cells, it was found that the canonical Wnt signaling plays a vital role in regulating cell growth, proliferation, motility and cell-fate determination[77]. However, the role of Wnt signaling in osteogenesis is complex between stimulating and inhibiting[78,79,80]. For example, Wnt signaling activation by exogenous Wnt3a or LiCl suppress dexamethasone-induced osteogenic differentiation of hMSCs as shown by Wnt-induced inhibition of ALP activity, ECM mineralization and osteogenic gene and protein expression[80,81]. Moreover, this inhibitory effect of Wnt on osteogenesis was attenuated with the addition of Wnt inhibitor Frizzled-8/Fc chimeric protein (Fz8/Fc)[81]. On the other hand, opposite effects of Wnt signaling have been observed demonstrated upregulated RUNX2 and osteocalcin expression[82]. These conflicting data regarding the role of Wnt signaling on skeletal stem cell osteogenesis are mainly attributed to various experimental factors which include Wnt concentration, cell type, stage of osteoblasts differentiation[77].

In the absence of Wnt ligands/modulators cytoplasmic β-catenin, which is the central player of this pathway, is constitutively phosphorylated and subsequently undergo proteasomal degradation by a protein destruction complex composed of glycogen synthase kinase 3β (GSK3β), Axin and adenomatous polyposis coli (APC)[73,83] (**Figure 1.3**). However, the canonical Wnt signaling is active when a Wnt ligand, such as Wnt3a, binds to frizzled (Fzd) receptor and its co-receptor low-density lipoprotein receptor-related protein (LRP)-5/6, causing phosphorylation of the intracellular protein disheveled (Dvl). Phosphorylated Dvl inhibits glycogen synthase kinase 3 (GSK3β) from phosphorylating β-catenin. As a result, β-catenin accumulates in the cytoplasm and translocate into the nucleus to bind with and activate transcriptional factor complex consisting of T-cell factor (Tcf)/lymphoid enhancer-binding factor

(Lef-1). RUNX2 expression and promoter activity is enhanced and thereby expression of osteogenic target genes is upregulated[82].

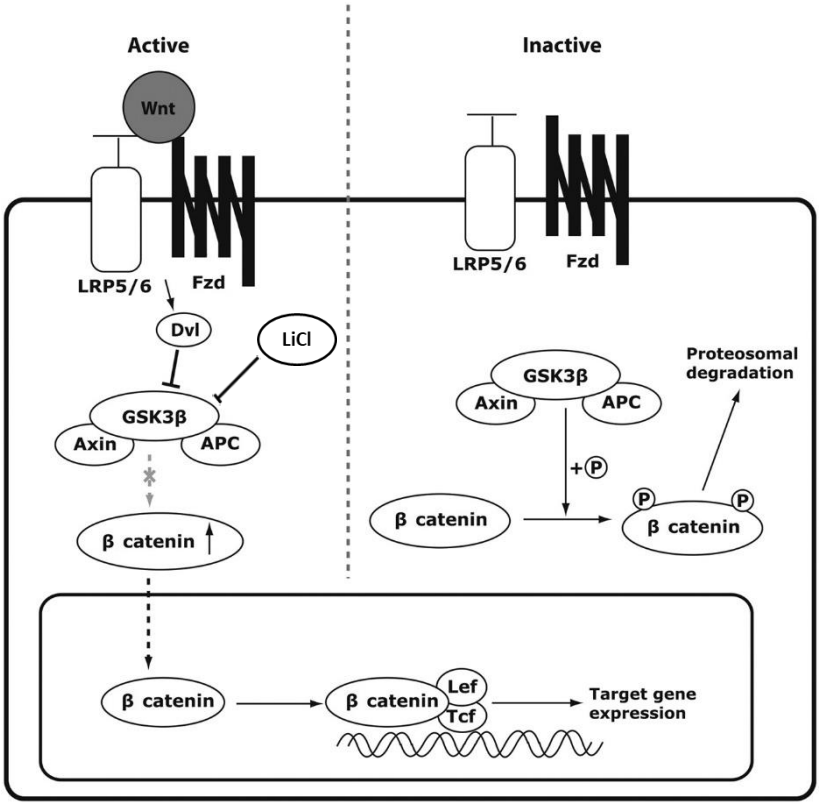

Figure 1. 3 Representation of the Wnt/β-catenin signaling pathway.
In the absence of Wnt ligands, β-catenin levels in the cytoplasm and nucleus are low because of the continuous phosphorylation by the destruction complex GSK3β/Axin/APC. Upon Wnt signaling activation by Wnt agonist binding to Fzd/LRP receptors, Dvl inhibits the destruction complex from phosphorylating and degrading β-catenin which translocate to the nucleus to activate Wnt-responsive gene expression. LiCl acts intracellularly by inhibiting GSK3 β. Adapted from Kim et al., 2013[73].

1.2.2 TGFβ/BMP pathway

The critical role of TGFβ/BMP signaling pathway in the commitment of multipotent skeletal stem cells to the osteogenic lineage has been convincingly demonstrated[84,85]. BMPs, which are members of the TGFβ superfamily, are the main inducers of osteogenic differentiation[86]. BMP-2, BMP-6, BMP-7 and BMP-9 are the main inducers of osteogenesis both *in vitro* and *in vivo* of this group. BMP signaling pathway is activated when one of the BMP proteins bind to heterodimer receptor complex (BMPR1/2). This leads to phosphorylation of Smad 1/5/8 proteins (also called R-Smads) which subsequently forms a heteromeric complexes with Co-Smad (Smad4) and translocate to the nucleus to induce the expression of key osteogenic genes[87,88,89] (**Figure 1.4**).

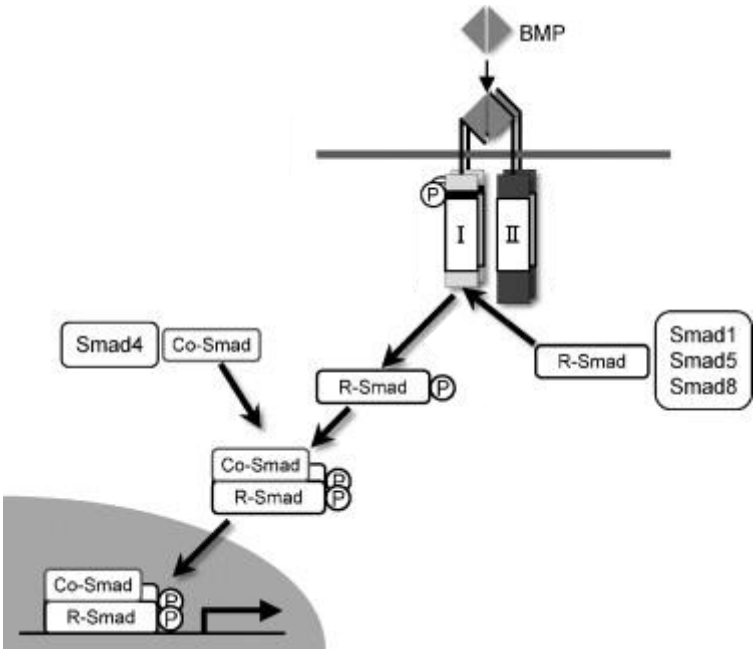

Figure 1. 4 BMP signaling pathway.
BMP protein binding activates BMPRs which phosphorylate R-Smad. Smad 4 forms a complex with activated R-Smad then translocate to the nucleus to activate target bone-related genes. Adapted from Jimi et al., 2010[89].

1.2.3 MAPK pathway

The MAPK-extracellular signal regulated kinase (ERK) pathway represents an important link between the extracellular matrix, cell membrane and nucleus to control cell functions including proliferation and differentiation[90]. Its responds to a variety of signals including hormone/growth factor stimulation[91], ECM-integrin binding[92,93] and mechanical loading[94]. It plays an essential role in osteoblast differentiation and skeletal development both *in vitro* and *in vivo*[90,95]. For example, mice lacking MEK1/2, upstream of ERK, suffers from severe osteopenia and Cleidocranial Dysplasia which is accompanied with decreased activation of the master transcription factor *RUNX2*.[95]. When MAPK pathway is activated, for example through binding of epidermal growth factor **(**EGF) to epidermal growth factor receptor **(**EGFR) or binding of ECM proteins to integrins on cell surface, receptor undergo dimerization and autophosphorylation and focal adhesion kinase **(**FAK) is activated. As a result, FAK activates Ras (a small GTPase) which directly interacts with and activates Raf. Raf phosphorylates and activates MEK, which in turn phosphorylates and activates ERKs. ERK1/2 translocate to the nucleus to activate target transcription factors such as RUNX2[96] (**Figure 1.5**).

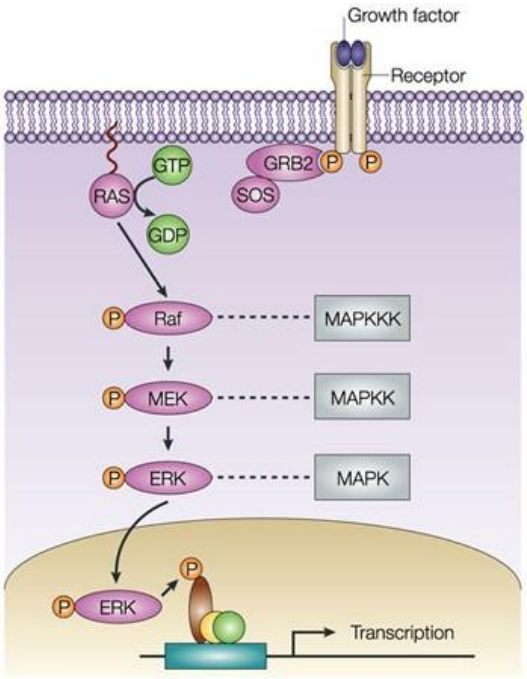

Figure 1. 5 Schematic representation of the ERK-MAPK signaling pathway[97].

1.2.4 Hedgehog signaling pathway

Activation of the Hedgehog (Hh) signaling pathway has been reported to promote the osteogenic differentiation of SSCs, both *in vitro* and *in vivo*[98,99]. The Hedgehog signaling is active when one of the three different Hedgehog ligands Sonic Hh (SHh), Indian Hh (IHh) or Desert Hh binds to a cell surface complex composed of two proteins, patched (PTCH) and smoothened (SMO). This leads to conformational changes of the receptor complex and subsequent activation of transcription factor glioma-associated oncogene homologs (GLI) 1, 2 or 3 which then translocate to the nucleus to activate the expression of target genes[72].

1.2.5 FGF signaling pathway

FGFs play critical function in regulating intramembranous and endochondral signaling in osteoprogenitors[100]. Mutations in the FGF pathway lead to craniofacial and long bone abnormalities[101]. When FGFs bind their fibroblast growth factor receptors (FGFRs), a family of tyrosine kinase receptors, it induces intrinsic tyrosine phosphorylation and activation of signal transduction pathways such as Raf, mitogen-activated protein (MAP) kinases, extracellular signal-regulated kinases (Erks), src and p38 MAP kinases, phospholipase Cγ (PLCγ), and protein kinase C (PKC). This leads to activation of genes involved in cell proliferation, migration, survival and differentiation[102] (**Figure 1.6**).

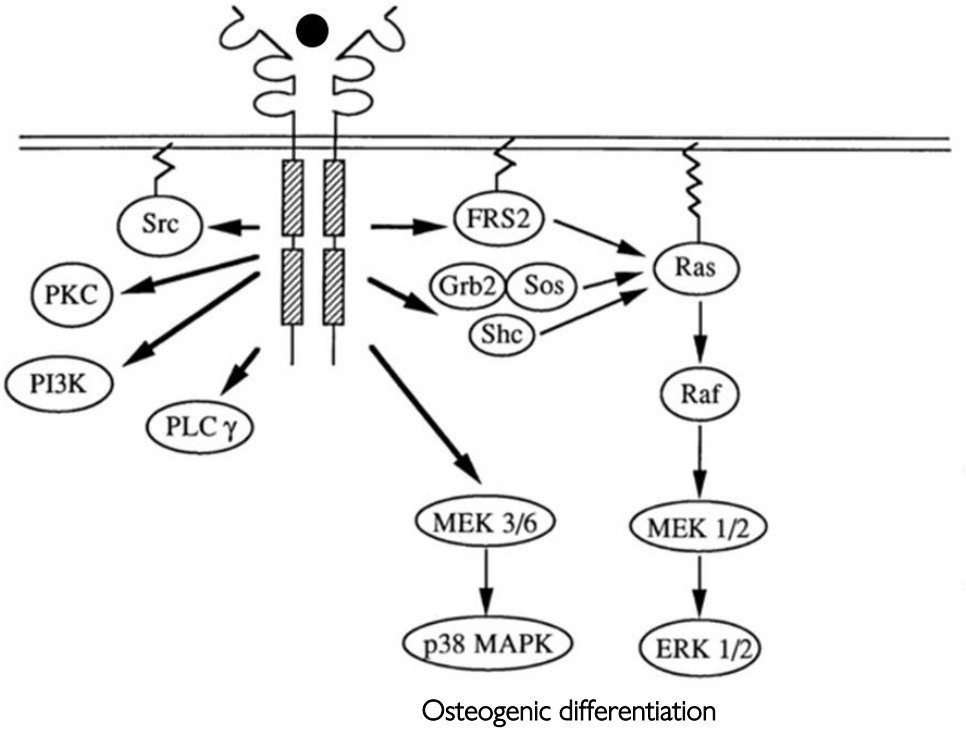

Figure 1. 6 Representation of FGF signaling pathway[103].

A schematic representation of the different signaling pathways which govern and regulate osteogenic differentiation of skeletal stem cells as well as their orchestrated interaction is presented in **Figure 1.7**.

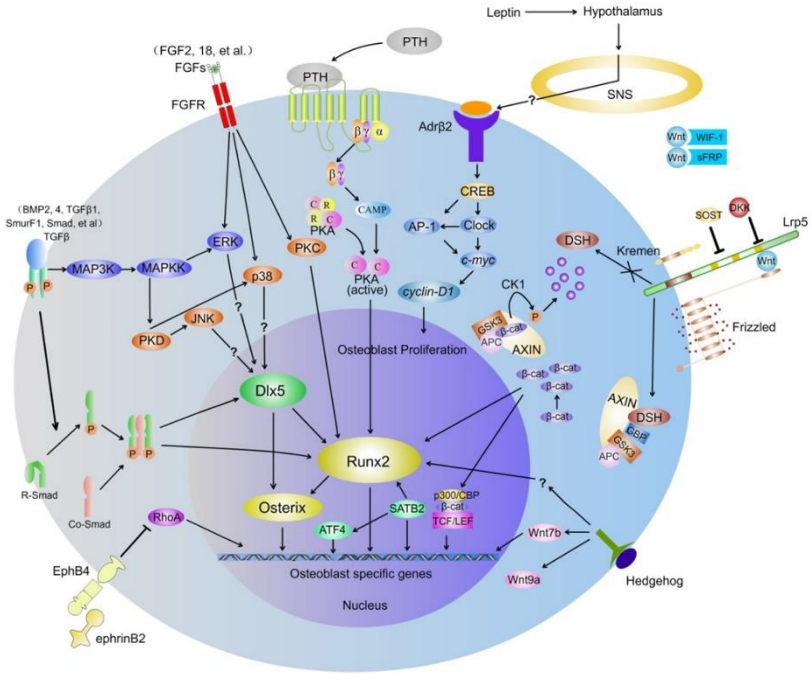

Figure 1. 7 Signaling pathways that control osteoblast commitment and differentiation and their orchestrated interactions[104].

1.3 Bone fractures and treatments

Despite its capacity for regeneration and self-repair, some bone defects caused by severe trauma, disease or high-energy injury fail to heal properly leading to delayed or non-union even under the best surgical treatments[105]. In the UK alone, over 2 million people suffer from bone fracture every year[106] and around 10% of bone fractures worldwide lead to nonunion[107]. The National Health Service (NHS) cost for treating non-unions range between £7,000 and £79,000 per person[108].

The most common treatment method for bone defects, delayed unions and non-unions is bone grafts which include autografts and allografts[109,110].

1.3.1 Autografts

Autografts refer to transplanting bony tissue from one site to another in the same patient[111]. Autograft is still considered the 'gold standard' in bone repair, among all clinically available bone grafts and substitutes[112]. This is because autograft possesses all properties essential for bone formation, namely osteoconductivity, osteogenicity and osteoinductivity. Autograft contains osteogenic cells, growth factors and bone structural proteins with no associated immune or infective-related risks and it can integrate into the host bone more rapidly and completely[109,111]. In autogenous bone grafting, bone can be harvested from non-essential bones, such as the iliac crest or the fibula. However, there are major side effects associated with this approach – autograft transplantation is expensive, painful and constrained by severe volume limitations and donor site morbidity due to infection and hematoma[113–116].

1.3.2 Allografts

Allograft refers to transplanting bony tissue from one individual (donor) to another (patient). Based on the limitations of autografts, allografts represent a suitable alternative for autografts[117]. Allografts may be harvested from living donors (e.g. the femur head of patients undergoing total hip replacement surgeries) or non-living donors. Allograft must be processed within a bone tissue bank and it is available in a variety of forms including cortical, cancellous and highly processed bone derivatives (i.e., demineralized bone matrix)[111]. Despite being osteoconductive, allograft is weakly osteoinductive (the ability of a material to stimulate stem cell differentiation towards osteoblasts and induce new bone formation when implanted *in vivo*). For example, allografts require sterilisation (e.g. via gamma irradiation) which show detrimental

effects on mechanical properties of bone, and deactivation of structural proteins. Moreover, the immune response and inflammatory cells produced due to the introduction of allografts, as they are immunogenic, cause necrosis of osteoprogenitor cells[109]. Despite that allograft circumvent some of the drawbacks of autograft by eliminating donor site morbidity and issues of volume limitations, its clinical application is also limited by various factors such as costs, laborious procedures required for tissue harvesting and processing, limited osteoinduction, and risks of tissue rejection by the patient's immune system and the possibility of introducing infection or disease from the donor to the patient[113,118].

1.4 Biomaterials and regenerative medicine as an alternative approach for bone repair

The field of tissue engineering and regenerative medicine aims to regenerate damaged tissues, instead of replacing them, by developing biological substitutes that restore, maintain, or improve tissue function[119,113]. Bone tissue engineering has the potential to overcome limitations of currently available treatments[120]. Biomaterial scaffolds, stem cells and growth factors are the vital components for bone tissue engineering[121]. Biomaterials scaffolds play a crucial role in bone tissue regeneration by acting as a carrier for cells and signals and a template for tissue formation – they provide the suitable biophysical and biochemical environment for the cells to grow, proliferate and differentiate leading to extracellular matrix synthesis and new tissue formation while the scaffold material itself undergoes slow degradation[113,122].

According to the European Society for Biomaterials, biomaterials are defined as "'a material used in a medical device, intended to interact with biological systems"[113]. For a biomaterial to satisfy the requirements for an ideal scaffold, it must be biocompatible, biodegradable into nontoxic products, with adequate porosity and mechanical properties, support cell adhesion and proliferation and induce/promote osteoblast differentiation[71]. Several classes of biomaterials have been reported for bone tissue engineering including ceramics (such as hydroxyapatite, β-tricalcium phosphate and bioactive glass), natural polymers (such as collagen, gelatin, silk fibroin and chitosan), synthetic polymers (such as poly(lactic acid), poly(lactic-co-glycolic acid) and polycaprolactone) and metals[71,122]. However, difficulties persist with many of these materials such as lack of osteoinductivity, insufficient degradation, low mechanical strength and/or shortage for cell adhesion[123].

Recently, nanoparticles have emerged as an interesting class of materials able to enhance the potential of biomaterial scaffolds for bone regeneration by improving biomaterial's mechanical properties, allowing control over key stem cell functions including adhesion, proliferation, migration and differentiation and providing controlled and sustained delivery of growth factors for guiding stem cell fate[124,125]. Moreover, incorporation of nanoparticles in the scaffold better recapitulate the nanoscale nature of bone[126]. One such recently emerging new class of nanoparticles which showed exciting potential for bone regenerative medicine are clay nanoparticles.

1.5 Clay nanoparticles for biomaterial design and regenerative medicine

Recent studies have shed new light on the potential of clay nanoparticles and composites for biomaterial design and regenerative medicine[127–129]. Clay nanoparticles are biocompatible at doses significantly higher than most other nanomaterials [130,131] and their degradation products are non-toxic, absorbable and of relevance to osteogenic cell function[132,133,134]. Furthermore, several studies have convincingly demonstrated direct, beneficial, concentration-dependent effects of clay nanoparticles on cellular adhesion, proliferation and differentiation [130–132,135–138]. These new observations combined with the well-established utility of clay nanoparticles to impart attractive mechanical or rheological properties to polymeric hydrogels and scaffolds [135–138,139, 140], and the opportunities afforded by their classic use as drug delivery modifiers[141,142], suggest the striking potential of clays for the creation and development of new bioactive scaffolds.

1.5.1 An overview of clay chemistry

Broadly, clay minerals are structured of two principal units: tetrahedral (T) and octahedral (O) sheets[143,144]. Each tetrahedron consists of a central cation (mostly Si^{4+}) coordinated to four O^{2-} anions and linked to adjacent tetrahedra through three shared oxygens on the corners (basal oxygens O_b) which allow basal oxygens to reach stability according to the bond valence model and result in infinite 2D hexagonal mesh (**Figure 1.8**). The fourth O^{2-} (apical oxygen O_a) remains unshared lying perpendicular to the tetrahedral sheet and is the main site of interaction with the octahedral sheet. Each octahedron consists of a metal cation (M^{n+}) coordinated to six O^{2-} and/or OH^- anions. Adjacent octahedra are linked to each other by sharing edges (two O^{2-} or OH^-), forming an octahedral sheet. If M^{n+} is divalent (e.g. Mg^{2+}), a

trioctahedral or *brucite-like* sheet is produced, if it is trivalent (e.g. Al^{3+}), then 2 out of every 3 octahedral sites are occupied leaving a vacant site and the generation of a *dioctahedral* or *gibbsite-like* sheet.

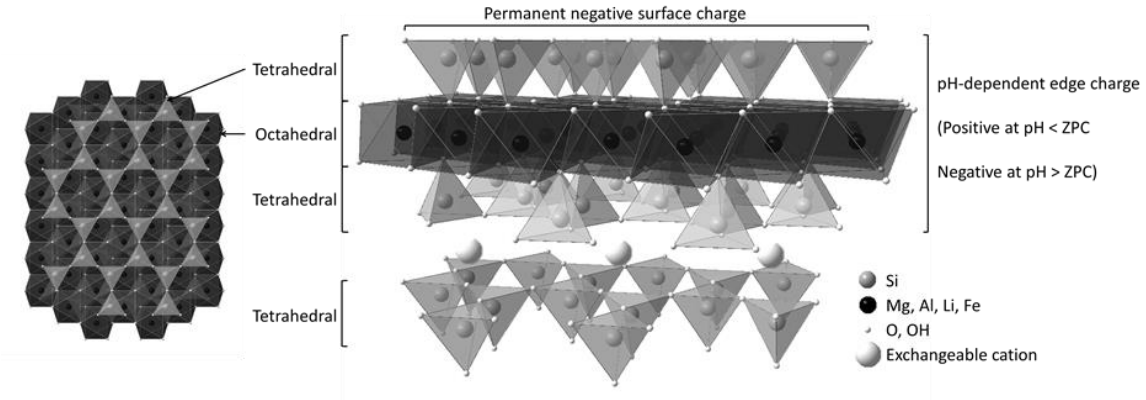

Figure 1. 8 The structure of smectites
Clays are formed of layered tetrahedral (T) and octahedral (O) sheets. In the case of smectites an octahedral sheet of metal oxides (usually Mg^{2+} or Al^{3+}) is sandwiched between two tetrahedral silica sheets. Two types of charges originate on smectite clay particle: i) permanent negative charges on the surface due to isomorphous cation substitution in the tetrahedral and/or octahedral sheets (e.g. Li^{+} for Mg^{2+} in Laponite) balanced by exchangeable cations such as Na^{+} or Ca^{2+} in the interlayer gallery. ii) Positive (amphoteric) charges on the edges due to broken Si-O, Al-OH and Mg-OH groups. At pH < Zero Point of Charge (ZPC), these edge charges become positive with anion exchange capacity while at pH > ZPC they become negative with a cation exchange capacity. Adapted from Dawson et al., 2013[127].

Clays can be classified into 1:1 and 2:1 types according to the layering of tetrahedral and octahedral sheets. 1:1 (or T-O) clay minerals consist of a single tetrahedral sheet linked to a single octahedral sheet, and 2:1 (or T-O-T) clay minerals consist of a single octahedral sheet sandwiched between two tetrahedral sheets (**Figure 1.9**).

In the case of 1:1 clay minerals, each particle consists of 1:1 layers stacked one above the other, with the half unit formula $M_xSi_2O_5(OH)_4$. For *dioctahedral* species, M_x = Al_2 (e.g. kaolinite and halloysite) while in case of *trioctahedral* species $M_x = Mg_3$ (e.g. serpentine). The 1:1 layers are electrically neutral and weak hydrogen bonding and van de Waals forces hold the adjacent layers. Given no isomorphous substitution takes place in the 1:1 layer, these clay minerals carry no structural (permanent) charges and the total layer charge is only accounted for by edge pH-dependent charges. Consequently, their cation exchange capacity (CEC) is typically low (<10 meq/100 g) and these clay minerals do not undergo interlayer swelling in water

making them of less interest for biomedical application than the 2:1 class. One exception in this regard is halloysite, whose hydrated 1-1 sheets roll up into nanotubes/nanocylinders giving rise to a higher specific surface area (SSA) and total pore volume[145] that confers several interesting possibilities, particularly for intracellular drug delivery[146].

For 2:1 clay minerals each particle consists of 2:1 layers stacked one above the other, with the half unit formula $M_xSi_4O_{10}(OH)_2$. In the case of *dioctahedral* species, M_x = Al_2 (pyrophyllite) while in the case of *trioctahedral* species M_x = Mg_3 (talc). Pyrophyllite and talc are of low reactivity (SSA ≈ 20 m^2/g) and their layered structure is electrically neutral. In contrast, smectites, mica and vermiculite groups are characterized by isomorphous cation substitutions in the tetrahedral and/or octahedral sheets producing clay particles with a wide range of net surface charges, ion exchange capacities, surface reactivity, swelling and gelation properties.

The smectite group is represented by two key clay minerals: dioctahedral montmorillonite (MMT) $Na_m(Al_{2-m}Mg_m)Si_4O_{10}(OH)_2.nH_2O$ and trioctahedral Laponite (LAP) $Na_h(Mg_{3-h}Li_h)Si_4O_{10}(OH)_2.nH_2O$, a synthetic Hectorite manufactured by BYK-ALTANA, which are the most investigated among all phyllosilicates in regenerative medicine. Their relatively low net charge (0.2–0.6/structural formula unit) allows smectite platelets to undergo complete dissociation by osmotic swelling enabling a rich surface chemistry[147]. Laponite in particular is notable for: i) its small particle size of 25-30 nm diameter and 1 nm thickness[148] yielding a high specific surface area (800 m^2/g) and cation exchange capacity (80-150 meq/100 g)[149,150] and, ii) its charge anisotropy and heterogeneity in the form of a permanent negative charge on the surface and positive amphoteric charges on the edges [151]. These features result in a rich array of possible interactions with biomolecules or polymers, and yield unique rheological properties following dispersal in water, including the generation of arrested gel or glassy states[152].

In contrast to the smectites, vermiculites display a higher layer charge (0.6–0.9/unit structure) which restricts water accessibility in the interlayer region. As a result vermiculites undergo crystalline, rather than osmotic, swelling and do not undergo delamination[149]. Nevertheless, vermiculites possess a high SSA (750 m^2/g) and high CEC (120–200 meq/100 g). Similarly, illites possess a still higher net charge (0.8–

1.0/unit formula) which further reduces swelling and thus yields a low SSA (30 m^2/g) and low CEC (10-40 m^2/g) [149,150].

Finally sepiolite and palygorskite are distinct from other clay minerals due to their inverted 2:1 ribbons which feature rectangular channels running parallel to the opposing ribbons, thus giving these clay minerals a fibrous morphology with high SSA (≈900 m^2/g) and high surface reactivity[153,154]. The rheology of sepiolite and palygorskite depends on physical entanglement and so, in contrast to other clays, is relatively stable at different ionic strengths and pH[153,154].

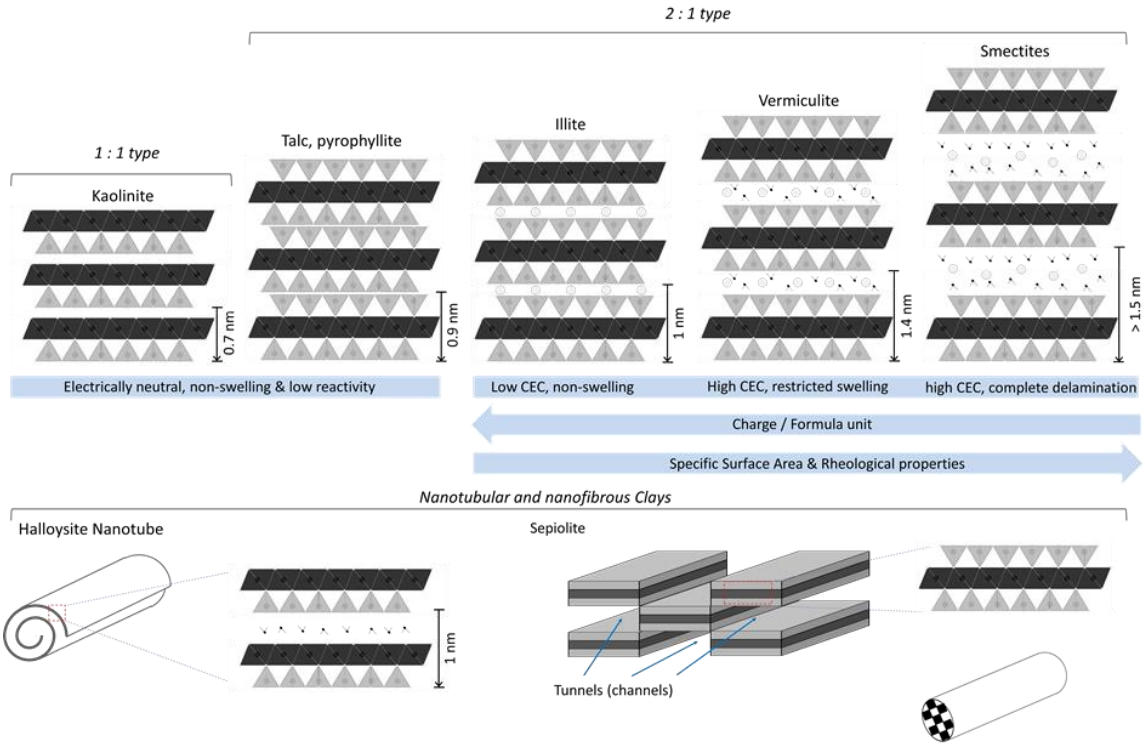

Figure 1. 9 Clay structure and reactivity.
The reactivity of clays is largely a function of their swelling capacity. Kaolinite (of the 1:1 clay family) and talc and pyrophyllite (of the 2:1 clay family) possess no structural charges and consequently are non-swelling and of low adsorption capacity. The high layer charge on vermiculite and illite restrict their swelling and gelling tendency although their surface area and CEC are relatively high. Smectites are characterized by their relatively low layer charge which allow their particles to undergo complete dissociation in water and give them interesting rheological/gel forming properties and surface reactivity. Halloysite is formed of hydrated 1:1 layers which role up into nanotubes (alumina sheet on the inside and silica sheet on the outside surface) and sepiolites (and palygorskite) are characterized by their inverted 2:1 ribbon structures. Such arrangements confer large SSA, porosity and sorptive capacity. Adapted from Dawson et al., 2013[127].

1.5.2 Clays in biomaterial design

The surface reactivity of clays, in particular the high adsorption and exchange capacity, specific surface area and charge heterogeneity described above, allow for a range of possible interactions of relevance for biomaterial design. This includes interactions with synthetic scaffold materials, organic and inorganic components of the extracellular matrix and soluble factors as well as direct interactions with cell surfaces and intracellular signalling pathways. Before exploring cell-clay interactions we briefly survey the relevance of clay interactions with polymers, and proteins for biomaterial design.

1.5.2.1 Clay-polymer interactions for scaffold design

The potential of polymer-clay nanocomposites to achieve materials with greatly improved mechanical properties is evidenced by the significant volume of literature and their use across almost the full scope of modern material applications [155]. In the context of biomedical applications, inorganic clay mineral (along with silicon and calcium phosphate) nano-phases are increasingly being incorporated into polymers with established biocompatibility to enhance the mechanical and degradation properties of the polymeric base. For example, clay nanoparticles can act as physical cross-linkers in hydrogels that combine the dynamic properties of physical gels, such as self-healing for minimally-invasive delivery, with significantly improved mechanical strength and toughness [132,137,156,157,158]. For example, the incorporation of Laponite in poly(N-isopropylacrylamide) hydrogel (PNIPA) led to a nanocomposite with increased mechanical toughness and flexibility compared to clay-free PNIPA control as shown by the ability of PNIPA/Laponite nanocomposite to withstand high levels of deformation such as elongation, bending and compression[159] (**Figure 1.10**). Clay nanoparticles can also significantly improve the mechanical strength, toughness and degradation properties of hard scaffolds, allowing the generation of porous matrices with mechanical properties that approximate that of bone matrix[136,159,160,161].

The ability of clay minerals to interact with polymeric matrices has been reported for both uncharged as well as positively and negatively charged polymers through various mechanisms[162,163 ,164]. The negative silanol groups on the external surface of clay minerals are the main sites of electrostatic interaction with cationic groups on positively charged polymers, which are able undergo intercalation/exfoliation between clay layers. In contrast, negatively charged polymers tend to be adsorbed via

electrostatic interactions on the positive rims of clay minerals and/or through cation bridging on the negative clay surfaces, although ligand exchange and van der Waals interactions also may play a role.

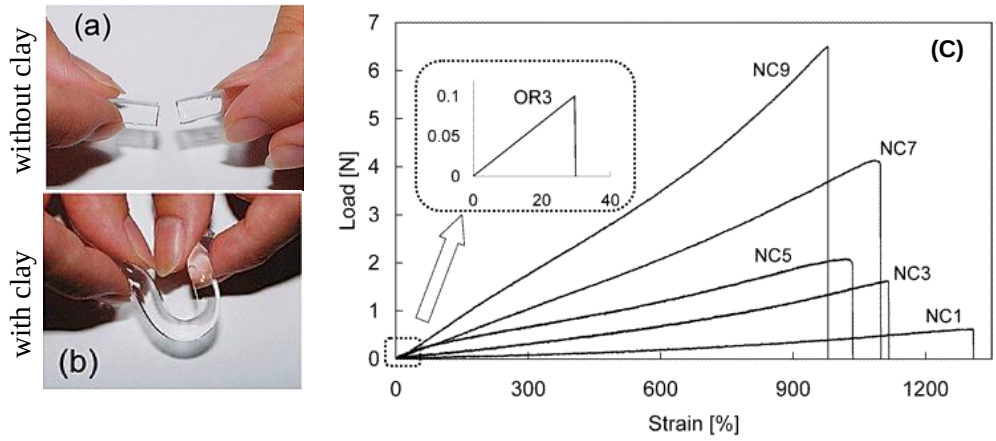

Figure 1. 10 Clay as multi-functional cross linkers for enhanced mechanical/rheological properties of polymeric matrices.
(a-b) In contrast to conventional chemically cross-linked poly(N-isopropylacrylamide) hydrogels (OR gels) which are weak and exhibited brittle fraction, clay-containing poly(N-isopropylacrylamide) hydrogels (NC gels) showed interesting mechanical properties withstanding high levels of deformation. (c) load-strain curves of NC gels as a function of clay content. NC1-NC9 refer to nanocomposite with increasing clay content. From Haraguchi et al., 2002[159].

Recent approaches have employed the dynamic mechanical properties conferred by clay nanoparticles in the optimization of 3D printing inks to allow the formation of tough hydrogels in various complex structures by controlling the pre-gel solution's viscosity and shear thinning properties as a function of clay loading. For example, recent studies have shown that methylcellulose-alginate-nanoclay hydrogels could be 3D printed into various biocompatible constructs of clinically-relevant, preserved shapes[165]. Indeed, the thixotropic and yield stress properties of the higher concentration (>5 weight percent) colloidal Laponite gels alone were themselves found to allow the printing of self-supporting structures in air without the need for a crosslinking water bath[166].

1.5.2.2 Clay-biomolecule interactions for delivery of soluble factors

The capacity of clay particles to bind biological molecules has been known by scientists for over fifty years. Clinicians observed that the presence of certain drugs in the blood stream was severely reduced when patients simultaneously received clay-based anti-diarrheal treatments[167]. This was found to result as a consequence of

binding of drugs by the clay particles. This property is now utilised in the design of tablets to carefully control the release and action of a range of drugs.

Various mechanisms underlie clay associations with biomolecules. These can include intercalation within the interlayer gallery through cation exchange reactions, adsorption via electrostatic interactions on their positive and/or negative surfaces, binding of polar biomolecules at hydrophilic (octahedral) and hydrophobic (tetrahedral) sites, as well as ligand exchange, cation/water bridging, hydrogen bonding and van der Waals interactions. [127,168] Such utility has been extensively explored in the development of drug delivery systems as for example in the use of smectites for controlled release of ibuprofen[169], Donepezil[170], nicotine[171], timolol[172] and many others[127,173,174]. From a regenerative medicine perspective, our group have shown the potential for clay nanoparticles to self-organise, via electrostatic interactions, into gels under physiological conditions. These clay hydrogels display the ability to take-up and bind bioactive molecules to direct the differentiation of endogenous cell behaviour or cell populations encapsulated within the gel **(Figure 1.11**). This approach has been applied to initiate the formation of new blood-vessels at an injury site through localisation of vascular endothelial growth factor[141] and to induce bone at significantly reduced doses of an osteoinductive (bone morphogenetic protein) growth factor[142].

The data for the use of pure Laponite gels as growth factor delivery vehicles suggest rather minimal release of clay bound molecules making their bioactivity dependent on the invasion of responsive cell populations into the gel itself. While this ability to sustain a localized regenerative microenvironment may have advantages in certain contexts, other clinical scenarios require sustained release of a molecule to the surrounding tissue. Such an effect can be achieved by combining clays with polymers to form a nanocomposite for the purpose of modified drug delivery[174,175,176]. For example, a recent study observed negligible release of fibroblast growth factor-2 (FGF2) from pure Laponite gels but achieved a tuneable release profile with varying concentrations of the glycosaminoglycan heparin which associated with Laponite to form a shear-thinning (and thus injectable) hydrogel. Heparin itself has a physiological role in binding biological molecules which resulted in a bi-modal effect of heparin concentration on FGF2 release implying competitive binding between the clay, the polymer and the growth factor [177]. As well as smectites, halloysite nanotubes

(HNTs) have also been used for modified drug release, for example to achieve sustained release of dexamethasone[178]. Such studies underline the potential of clay-based strategies for modifying the release of bioactive agents to initiate and sustain regenerative responses at sites of injury or disease.

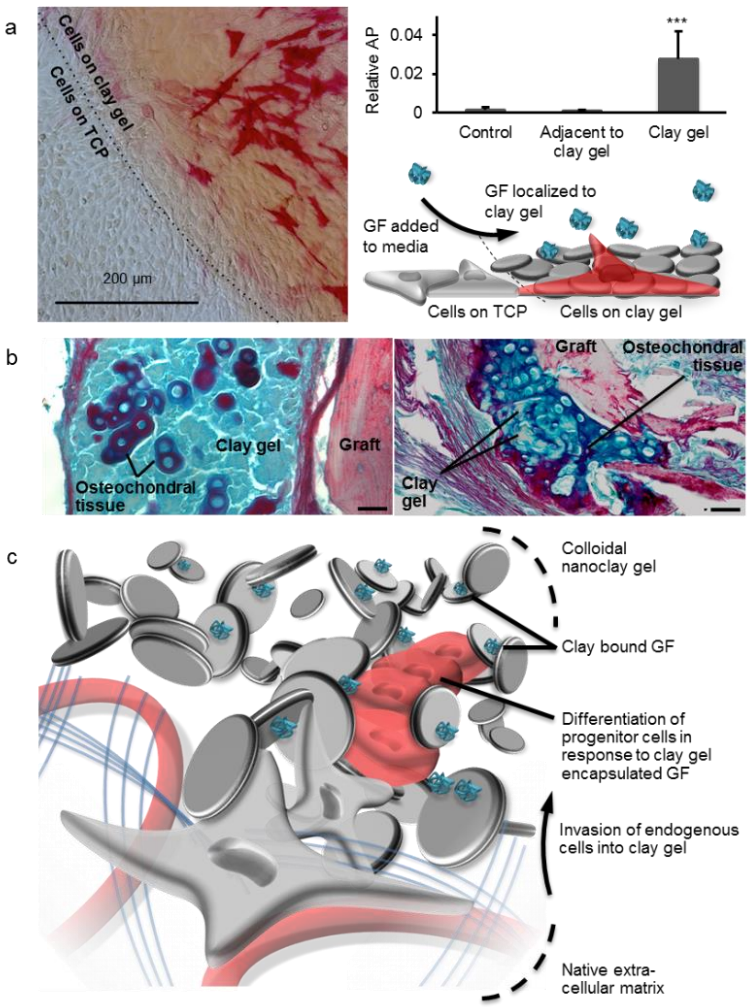

Figure 1. 11 Clay gels for growth factor localisation.
Laponite gels display the ability to take-up and bind bioactive molecules to direct the differentiation of endogenous cell behaviour. Clay gel films localize otherwise sub-efficacious doses of BMP2 to induce a) osteogenic differentiation of C2C12 myoblasts *in vitro* and b) clay-gel localised endochondral ossification *in vivo*. b) blue stain refers to endochondral ossification (proliferating and hypertrophic chondrocytes) localised within clay gel in response to encapsulated/localised BMP2 while red stain refers to non-viable human trabecular bone graft scaffold perfused with clay gel. Scale bar = 50 µm. c) Schematic representation of proposed mechanism for endogenous stem/progenitor cell differentiation in response to clay-mediated growth factor delivery and localization . In contrast to conventional drug release strategies, the growth factor remains localised within the clay gel requiring invasion of endogenous cells from native tissue. This allows a highly localised response to the growth factor and for templating by the clay gel of new tissue formation. TCP = tissue culture plastic control. Adapted from Gibbs et al., 2016[142].

1.5.3 Clay-cell interactions for osteogenesis

A growing number of studies have investigated the biocompatibility of clays and their direct interactions with cells and tissues (**Table 1.2**). These studies have yielded unanticipated observations of clay dependent enhancements to cellular responses such as cell adhesion and differentiation. Before turning to examine the evidence for such enhancements it is important to review the evidence for the biocompatibility of clay nanomaterials and their uptake by cells.

1.5.3.1 Cellular uptake of clay

Following release from a degrading polymer matrix or via addition as a dispersion to cell culture media, cells are likely to encounter clays as free-floating particles or aggregates. Clay particles are characterized by their nanoscale size and anisotropic charge distribution and thus consideration of cellular-nanoparticle responses are relevant. Since cellular physiological responses are directly and strongly affected by their uptake of nanoparticles[179,180], understanding the extent and mechanism by which clay nanoparticles enter cells is of importance to understanding their bioactivity and may present further opportunities for tissue regeneration applications.

Species	Mode of presentation	Studies demonstrating cellular interactions / effects			
		Cyto-compatibility	Cellular uptake	Enhanced adhesion & proliferation	Enhanced differentiation
Halloysite	Dispersed particles, PCNs	181,182,183,184,185	181	186,187,188	189,190,191
MMT	Dispersed particles, PCNs	192,193,194,195,196,197,198,199,200,201	193	202,203,204,205,186,206,207	138,192,208,209,210
Laponite	Dispersed particles, colloidal gels, PCNs	130,131,132,133,135,136,211,212,213,201	130,131	131,211,213,214,215,216,217,218,219,220,221	130,131,132,135,136,137,141,142,211,222,223,216,224,225,226
Sepiolite	Dispersed particles	227	227		

Table 1. 2 Key clay mineral species used for tissue engineering and regenerative medicine applications with their mode of presentations, and cellular interactions / effects. PCNs = Polymer-clay nanocomposites. MMT = Montmorillonite.

Nanoparticle-cell interactions are highly dependent on particle size, shape and charge[228]. The optimal particle size for cellular endocytosis is in the order of 25–30 nm[229] which suggests Laponite particles in particular (25–30 nm diameter sheets) are likely to be endocytosed, and several lines of evidence support this. Confocal analysis following addition of dispersed Laponite to adipose derived stromal cells indicated internalisation and cytoplasmic distribution of clay particle/aggregates but with some accumulation on cell membranes[131]. The addition of colchicine (to impede clathrin-mediated endocytosis) resulted in a reduction of the number of cells associated with rhodamine-labelled Laponite as measured by flow cytometry. From this reduction of Laponite associated cells, the authors inferred an internalisation efficiency of at least 40% (depending on Laponite concentration) and confirmation of a role for clathrin-mediated endocytosis in cellular uptake[131] (**Figure 1.12**).

Larger sized MMT particles (100s nm diameter) were shown to interact with cell membranes of Chinese Hamster Ovary cells at a concentration similar to that reported for Laponite (100 μg/mL) but with no clear evidence of cellular uptake [193]. Halloysite nanotubes, on the other hand, vary in length between 1-15 microns but, presumably due to their high aspect ratio were efficiently internalised into the cytoplasm of both MCF-7 and HeLa cell lines without modulation of cell phenotype or preventing cell proliferation up to a concentration of 75 μg/mL [181].

As well as particle size and shape, direct interaction of the cationic edge charges of the clay nanoplatelet with the anionic glycoproteins and phospholipids of the cell membrane may also facilitate cellular transport and uptake,[131,179,230,231]. Layered double hydroxides are characterised by the general formula $[M^{II}_{1-x}M^{III}_{x}(OH)_2]^{x+}[A^{m-}_{x/m}.nH_2O]^{x-}$, in which the isomorphous substitution of divalent metal cation (M^{II}) by trivalent metal cation (M^{III}) gives the brucite-like layers positive charges rather than a negative surface charge as in the case of cationic clays[232]. These positively charged particles were found to form electrostatic interactions with anionic cell surfaces to facilitate receptor-mediated endocytosis[233,234].

Other studies have shown that internalization of clays is not restricted to receptor mediated endocytosis. Smirnov et al found that the addition of chloroquine (an endocytosis inhibitor) resulted in a 20% reduction of sepiolite internalization efficiency by mammalian cells and amiloride (a macropinocytosis inhibitor) reduced

the sepiolite internalization efficiency by 50% suggesting macropinocytosis to represent the main cellular uptake pathway of sepiolite nanofibers[227]. Time-lapse video microscopy showed spontaneous internalization/exclusion of sepiolite by the cells and, interestingly, its transmission between neighbouring cells[227].

Understanding the fate of clay nanoparticles following cellular uptake including their degradation profiles and the extent of endosomal release into the cytoplasm will be important for elucidating mechanisms behind clay bioactivity and resolving ongoing questions regarding cytocompatibility.

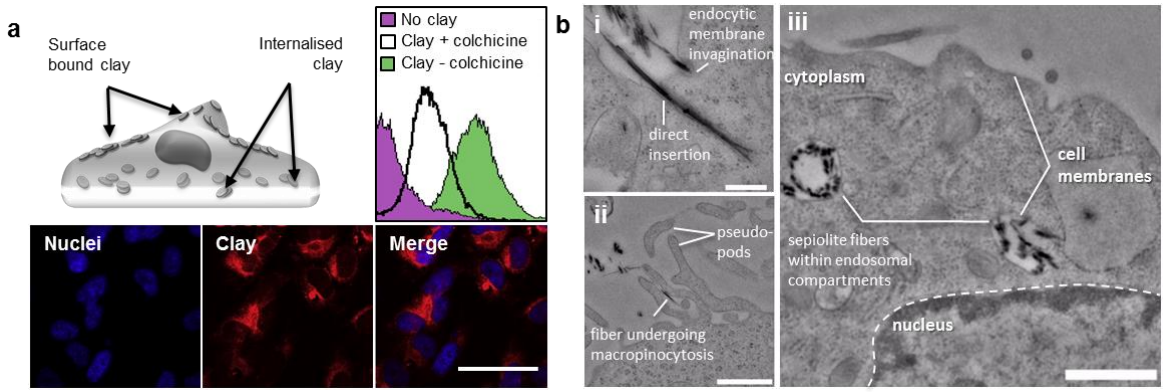

Figure 1. 12 Cellular uptake of clay.
a) Laponite directly interacts with stem cells through both attachment to the cell surface and wide distribution in the cell cytoplasm. Rhodamine-labelled Laponite nanoparticles (10 µg/ml) locate around the nucleus of human adipose-derived stem cells (hASCs) following 24 culture. Scale 50 µm. A significant reduction in clay cellular uptake is observed as a result of an endosomal inhibitor. b) transmission electron microscopy (TEM) of sepiolite uptake shows endocytic and direct routes of uptake (i) as well as evidence of macropinocytosis via psuedopod formation (ii). Cytoplasmic regions clearly show sepiolite fibers within endosomal compartments (iii). (a) Adapted from Mihaila et al., 2014[131]. (b) Adapted from Castro-Smirnov et al., 2017[227].

1.5.3.2 Toxicology of clay

Most toxicology studies to date have demonstrated negligible effects of clay nanoparticles on human or animal cells at relevant physiological concentrations. Oral ingestion of MMT did not affect the mortality of exposed Sprague-Dawley rats up to a dose level of 5700 mg/kg body weight – median lethal dose (LD50) >5700 mg/kg[193]. In another study, MMT orally administered at doses up to the highest level tested (1000 mg/kg) indicated rapid clearance within 2 h and no clay accumulation observed in the long term in any specific organ[194]. An increasing number of studies reporting

implantation of smectite based biomaterials have yet to note any indication of toxicity or persistent inflammation[133,135,136,182,212] . For example, unlike carbon nanotube based composites MMT-based composites did not increase local vascularization and pro inflammatory markers against controls following subcutaneous implantation[195].

When applied directly to cells *in vitro*, Laponite nanoparticles dispersed in cell culture media showed no significant effect on cell morphology, viability or proliferation of human bone marrow and adipose derived stromal cells up to a concentration of 100 μg/mL over 7 days [130,131]. At higher clay doses, a decrease in metabolic activity was observed. Interestingly, it is notable that the half maximal inhibitory concentrations (IC50s) determined (4 mg/mL and 1 mg/mL for bone marrow and adipose derived cells, respectively) remained around ten-fold higher in comparison with other commonly investigated nanoparticles such as hydroxyapatite (IC50 = 250 μg/mL) and silica (IC50 = 400 – 500 μg/mL) [130,131,235–237].

Likewise, *in vitro* cytotoxicity of MMT on Hamster Ovary cells (CHO) was only evident at >1 mg/mL[193]. Examination of cell viability and proliferation profiles of human dermal fibroblasts (NHDF) remained close to 100% for all MMT concentration tested (5-300 μg/mL)[196]. Furthermore, no or negligible genotoxic effects of exfoliated MMT were observed up to a concentration of 1mg/mL across three separate assays: i) the Comet assay (DNA damage evaluation) on CHO cells *in vitro*, ii) the micronucleus assay (chromosomal damage evaluation) on Peripheral-blood cells *in vivo*, and, iii) the *Salmonella* gene mutation assay[193].

Some studies have however observed a more acute response following the addition of clay. A study of proliferation and colony formation of human normal intestinal cells revealed inhibition even at low concentrations of MMT (5 μg/mL) within 24 h[194]. Another study observed a significant loss of viability in the human hepatic cell line HepG2 in response to low concentrations of both unmodified and organically modified MMT nanoclays[197]. An important factor in both these studies is the well characterised flocculation behaviour of clay colloids at increasing concentrations and in the high salt concentrations of cell culture media. In such conditions clay particles will typically aggregate into micro-sized clusters/agglomerates with a tendency to accumulate around cells. Such an accumulation can block membrane channels and impair cellular metabolism and cytoskeleton organization[130,131,198,199]. Thus, MMT

was found to inhibit cell proliferation and colony formation independently of any direct effect on cell viability in the short term. This was evidenced by lactate dehydrogenase (LDH) based assessments of membrane integrity which was compromised at very high concentrations (1 mg/mL) and reactive oxygen species (ROS) generation which was observed only after 48 h despite clear inhibition of proliferation within 24 h[194]. The authors inferred an indirect effect of clay aggregation and accumulation on cell proliferation rather than a direct cytotoxic effect. Consistent with this conclusion is the observation that clay nanoparticle incorporation as a dispersed phase within a polymeric network allows considerably higher dispersion stability [173,162] and typically preserves good cytocompatibility at considerably higher concentrations of nanoclay [132,135,211,192 ,213, 200].

As well as dispersion stability, particle shape and size are of importance to cytocompatibility. For example, a study observing slightly lower cytotoxicity for MMT compared with Laponite suggested the lower aspect ratio of MMT (300:1 vs 25:1) to be an important factor [201]. More pronounced is the pro-inflammatory response and lower threshold cytotoxic concentration observed for the 1:1 tubular clay mineral, halloysite. Both human epithelial adenocarcinoma (HeLa) and human breast cancer (MCF-7) cell lines maintained their viability at >70% when incubated in HNTs-containing media, at concentrations up to 75 μg/mL above which pronounced cytotoxicity was observed[181]. Another study observed good viability and membrane integrity up to halloysite concentrations of 100 μg/mL[183,184] , but detected significant pro-inflammatory effects at HNTs concentrations as low as 1 μg/mL and significant changes in protein expression at high halloysite content (100 μg/mL) [183]. Interestingly, surface coating of halloysite by PEG polymer significantly improved halloysite cytocompatibility even at much higher doses (<500 μg/mL)[185].

While the current available *in vitro* and *in vivo* studies indicate a good toleration of clay nanoparticles, even at relatively high doses if dispersion stability is maintained, long-term implantation and bio-distribution studies are warranted and remain to be undertaken. To date, there remains a paucity of information detailing the biodegradation and clearance profiles of clay nanoparticles and nanocomposites surgically implanted or parenterally delivered or indeed, their modulation of acute and chronic inflammatory events. In addition, exposition of the mechanisms behind the cytotoxic effects observed *in vitro* and the relative importance of dispersion stability,

surface charge, ion exchange capacity and particle size and morphology on such dose-dependent effects remains to be demonstrated.

Despite some ambiguity regarding the cytotoxic assessment of clay nanoparticles, a growing number of studies exploring the biocompatibility of various polymer-clay nanocomposites have observed, not only minimal cytotoxicity but direct clay-dependent enhancements to cell functions such as cell adhesion, proliferation and differentiation offering new potential biomedical applications.

1.5.3.3 Cell adhesion and proliferation

Poly-ethylene glycol (PEG/PEO), like most polymeric hydrogels, is hydrophilic, non-fouling and does not support protein and cell adhesion[238,239]. Laponite incorporation in PEG hydrogels at 40-70% (wt.%) was shown to enhance cell adhesion, spreading and proliferation of NIH 3T3 mouse fibroblasts[213,214], MC3T3-E1 mouse preosteoblasts[211,215] , and human bone marrow stromal cells (hBMSCs) [216] in a clay dose-dependent manner. Cells cultured on PEG/Laponite films with <40% clay showed poor cell adhesion and growth and exhibited non-adherent spherical morphology with disrupted and disorganised F-actin fibres. Following an increase in the clay fraction, however, (40%-70%), hBMSCs were observed to readily grow and proliferate, displaying a flat morphology and resulting in a confluent monolayer after 14 days' culture [211,213,214,216] (**Figure 1.13**). 3D encapsulation of mouse embryonic fibroblasts led to vinculin expression in the PEG clay nanocomposite hydrogel but not its clay-free counterpart, indicating the formation of focal adhesions[215]. Similarly, only Laponite-containing poly-*N*-isopropylacrylamide (PNIPA) hydrogels were able to support adhesion, spreading and proliferation of HepG2 human hepatoma, human dermal fibroblasts, and human umbilical vein endothelial cells (HUVECs). In this case the effect was dose dependent up to a maximum concentration (C_{clay} of 6×10^{-2} molar) above which cell adhesion was impeded[217].

Similar clay-dependent effects on cell spreading and proliferation have been observed following the addition of montmorillonite to gelatin-cellulose [202], polyurethane (PU)[203], and chitosan-based[204] scaffolds. In the case of chitosan, a direct comparison between an MMT based composite and a hydroxyapatite based composite revealed increased cell spreading and proliferation on the clay-based nanocomposite[205]. Halloysite nanotubes have also been employed for enhanced cell attachment in

nanocomposites to similar effect. Enhanced cell spreading was observed after surface treatment of a polyelectrolyte film with halloysite compared with MMT. Interestingly, with both treatments improved adhesion and proliferation was observed against untreated controls[186]. Dose-dependent positive effects on adhesion and proliferation were also observed upon addition of halloysite to poly(vinyl alcohol)[187] and alginate[188] based nanocomposites.

Various factors have been suggested as possible mechanisms behind clay-enhanced cell adhesion and spreading. Indirect enhancement of cell adhesion via the adsorption of cell adhesive proteins such as fibronectin or vitronectin from serum supplemented media is frequently cited and likely to play a role [216–219]. Interestingly though, even in serum-free media, fibroblast attachment and spreading was observed on PEO/clay surfaces following a clay concentration dependent trend. This contrasts with PEO alone or, indeed, standard tissue culture plastic, which typically does not support cell attachment or spreading in the absence of serum [213] suggesting that direct clay-cell interactions facilitate cell adhesion. Clay nanoparticles may therefore act directly as focal adhesion sites through the provision of reactive functional groups (e.g. >Si-OH_2^+) for cell attachment [216, 217, 219]. Alternatively, in some cases, the particular hydrophobicity/hydrophilicity balance between hydrophobic polymer chains and the hydrophilic clay dispersion could directly mediate cell adhesion as well as promote protein adsorption[217, 240,241]. Another possible mechanism could be increased local concentrations of divalent cations such as Ca^{2+} or Mg^{2+} which exchange on clay surfaces preferentially over monovalent ions given their increased charge density. Such divalent ions are essential for the function of integrins, the transmembrane receptors that mediate cell interactions with ECM[242]. It has also been suggested that Mg^{2+} ions arising from the dissolution of Laponite could promote cell adhesion [218,220], however, the concentration of clay dissolution expected in physiological buffers is disputed[243] and the concentration of divalent ions in cell culture media is also unlikely to be limiting.

Finally, modification of clays with exchangeable organic compounds, an approach widely used to improve the intercalation of non-polar polymers for nanocomposites, has also been explored as a means to biochemically functionalise clays to modulate adhesion and other cell functions. Bongartz and Barlas et al., reported an approach to control the capacity and selectivity of Cloisite for cell adhesion and proliferation via

folic acid (FA) modification[206,207]. In contrast to A549 cells (FA receptor-negative), the adhesion and proliferation behaviour of HeLa cell line (FA receptor-positive) showed a FA-dependent enhancement compared to the unmodified Cloisite[206]. Similarly, intercalating polydopamine into clay nanosheets significantly improved the cell affinity of clay-polyacrylamide hydrogels compared to polydopamine unmodified controls[221]. Such approaches suggest new avenues for modulating clay based nanocomposites to achieve specific cell responses[221].

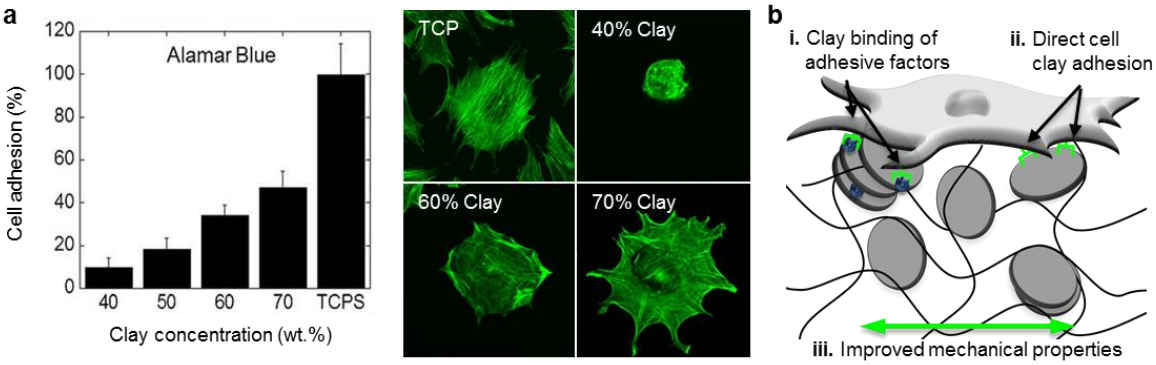

Figure 1. 13 Clay mediated improvements to cell adhesion and spreading.
a) The incorporation of clay nanoparticles in PEG polymeric hydrogel, which alone is non-cell-adhesive, significantly improves hBMSCs adhesion and spreading in a dose-dependent manner. b) Schematic showing possible mechanisms of clay-enhanced cell adhesion and spreading: i) clay nanoparticles adsorb cell adhesive proteins from serum (indirect effect), ii) clay nanoparticles themselves act as focal adhesion sites thus facilitating cell attachment and spreading through a direct clay-cell interaction, iii) clay nanoparticles confer improved stiffness or other physical properties that promote cell spreading. Adapted from Gaharwar et al., 2011[211] and Gaharwar et al., 2012[216].

1.5.3.4 Clay and osteogenesis

In addition to the utility of clays for drug and growth factor delivery, various studies have highlighted a direct bioactive effect of clays on the osteogenic differentiation of skeletal populations. Gaharwar and colleagues reported an improved osteogenic response of preosteoblast cell line MC3T3[132,136,211,224,225] and bone marrow stromal cells[135,216,222] as a direct function of modulating Laponite content in PEO[211,216], poly(glycerol Sebacate) PGS[136,224] , PEG[225], polycaprolactone (PCL)[222] and gelatin methacrylate (GelMA)[132,135] polymer nanocomposites. The authors found increasing Laponite concentrations from 40% to 70% in PEO led to a 10-fold increase in alkaline phosphatase (ALP) activity and calcium phosphate (CaP) mineralisation by day 28[211]. Likewise, GelMA-clay nanocomposite hydrogels were able to support osteogenic

differentiation of both surface seeded[132] and encapsulated[135] skeletal populations. Su et al observed enhanced ALP activity and bone-related gene expression in silk fibroin hydrogels with addition of Laponite[137]. The bioactivity of clay in its dispersed form has also been convincingly demonstrated. Dispersion of Laponite in cell culture media up to a concentration of 100 μg/mL resulted in a dose-dependent and stage specific upregulation of osteogenic gene expression (RUNX2, BGLAP and SPARC), increased ALP activity, type I collagen synthesis and CaP deposition in hMSCs and hASCs cultures[130,131] (**Figure 1.14**). Interestingly, the osteogenic effects were apparent even in the absence of the standard osteogenic differentiation media supplements dexamethasone, ascorbate-2-phosphate and beta-glycerophosphate suggesting the possibility of direct interaction with select osteogenic pathways.

Several groups have also demonstrated a similar osteogenic effect for other clay mineral types in nanocomposite biomaterials. For instance hBMSCs cultured on silk/MMT surfaces showed an up-regulation in osteogenic gene expression in a clay dose-dependent manner[192]. Ishikawa and colleagues found imogolite ($Al_2SiO_3(OH)_4$) addition resulted in increased ALP activity and mineralization by MC3T3s [244], compared to carbon nanotubes which did not affect differentiation over tissue culture plastic (TCP) controls. The incorporation of HNTs within PCL scaffolds resulted in a doubling of hBMSC ALP activity[189] and 1% HNTs increased hBMSC osteogenic gene expression over pure PCL control, equivalent to that seen with the addition of 5% nano-hydroxyapatite [190].

Furthermore, a common feature of enhanced osteogenesis in association with clays is a strong and early enhancement in calcium phosphate mineralisation suggesting that clays may have a direct effect on CaP nucleation, growth and/or deposition (**Figure 1.14**)[130,131,132,135,138,192,211]. For example, the culture of skeletal populations on Laponite-containing nanocomposites yielded almost double the mineralised matrix in comparison to controls[130,211,245]. Few studies have also provided evidence for the intrinsic 'bioactivity' of certain clays, understood in this context as the specific ability to initiate biomineralisation in simulated body fluid (SBF). Laponite addition to polycaprolactone electrospun fibres increased calcium phosphate deposition in 10x SBF[222] and a sintered Laponite bioceramic induced hydroxyapatite formation and deposition on its surface after 7 days in 1.5x SBF[223]. Interestingly, incorporation of Laponite nanorods in poly(butylene succinate) scaffold led to a strong apatite

mineralization in 1x SBF solution as demonstrated by SEM-EDX analysis showing Ca/P ratio of 1.65 which is close to natural apatite mineral[246]. The mechanism for clay mediated biomineralisation remains poorly understood. The anisotropic and heterogeneous charge structures of clay particles and their aggregates, as well as the affinity of silica for calcium ions[247,248] may provide favourable nucleation sites facilitating adsorption of Ca^{2+} and HPO_4^{2-} to reduce the energy barrier for calcium phosphate deposition [249].

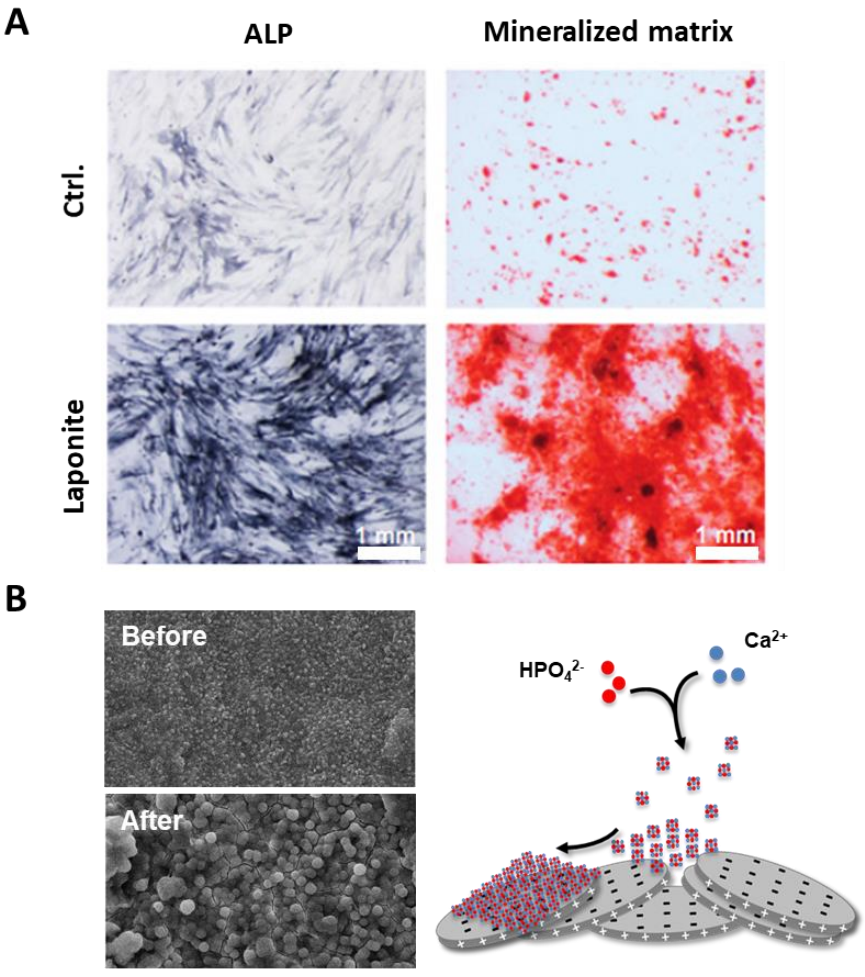

Figure 1. 14 Clay promotes osteogenic differentiation of human skeletal stem cells. (A) Laponite addition, as culture media supplements, to skeletal stem cells results in a significant enhancement of early (ALP) and late (matrix mineralisation) osteogenic markers[250]. (B) SEM images of Laponite bioceramic surface before and after soaking in 1.5x simulated body fluid for 7 days[223]. Laponite surface/SBF interaction resulted in the deposition of hydroxyapatite layer which plays an essential role for the growth and integration of biomaterial/tissue interface.

The mechanism(s) behind clay promotion of osteogenic differentiation remain poorly understood. As far as we know, the only study available in literature exploring the mechanisms of Laponite osteogenic bioactivity is the one reported by Carrow et al in which they reported Laponite promotion of osteogenic differentiation through the MAPK signalling pathway[250]. However, this study was based on utilising high-throughput sequencing technology at the whole transcriptome level to identify the osteogenic signalling pathways involved in nanoclay osteogenic bioactivity without paying much attention to how nanoclay exert their osteogenic character for example through biochemical vs biophysical models or intracellular vs extracellular roles. Herein, biochemical models refer to osteogenic character exerted by Laponite degradation and subsequent release of osteogenic degradation products, while biophysical model rerefer to the osteogenic influence of intact Laponite particles though interaction with cell organelles.

Based on the above-mentioned discussion of clay regenerative medicine, we hypothesize various routes through which Laponite promote osteogenic differentiation (**Figure 1.15**). The known osteogenic effects of clay degradation products are frequently cited [130–132,140]. In the case of Laponite, $Si(OH)_4$, Mg^{2+} and Li^+ have each been associated with enhanced osteogenic cell function. For example, magnesium ions are involved in activating osteogenesis-regulating pathways ((HIF-1α and PGC-1α)[251,252] and are essential for integrin adhesion to biomaterial surfaces [253], orthosilicic acid ($Si(OH)_4$) promotes collagen type 1 synthesis and osteoblast differentiation[254] and lithium is known to activate canonical Wnt-responsive osteogenic genes through the inhibition of GSK3β[255,73]. However, the rate and extent of clay dissolution within endosomal (or lysosomal) intracellular compartments or in cell culture solutions remains to be confirmed. In addition osteogenic effects have been seen using clays such as MMT[138,192], halloysite[189,191] and attapulgite[256] each with different dissolution products. Wang et al. observed similar osteogenic effects with addition to electrospun poly(lactic-co-glycolic acid) PLGA nanofibers of both Laponite[226] and the aluminium phyllosilicate, attapulgite[256] also in the absence of additional osteogenic culture additives. In both these studies, clay addition resulted in improved surface hydrophilicity and mechanical properties of the PLGA nanofibers which had a clear effect on cell adhesion and proliferation compared to pure PLGA – factors that are also likely to contribute to a stronger osteogenic response.

According to Thompson et al.[134], Laponite degradation takes place according to equation 1 which is a direct function of solution pH (< 9) and Laponite concentration (< 2 mg/mL). It was reported that Laponite degradation starts by the attack of H^+ on Laponite surface and/or edges, possibly through cation exchange with compensating ions adsorbed in/on Laponite such as Na^+, leading to the formation of protonated complexes on Laponite surfaces and/or edges (M-OH^{2+}) causing polarization and loosening of metal bonds with other atoms in the crystal lattice, in presence of water[257,258].

$$Na_{0.7}Si_8Mg_{5.5}Li_{0.3}O_{20}(OH)_4 + 12H^+ + 8H_2O \longrightarrow 0.7Na^+ + 8\,Si(OH)_4 + 5.3Mg^{2+} + 0.4Li^+ \quad (Eq1)$$

Various other models for how clays may influence differentiation pathways independent of clay dissolution could be proposed. Modulation of local calcium phosphate dissolution/formation dynamics is known to play an important role in the osteogenic activity of mineralised or mineralising biomaterials such as ceramics and bioactive glasses suggesting one potential mode of osteogenic action for bioactive clays[259]. Furthermore, intracellular accumulation of calcium phosphates is known to play a role in both mineral deposition[260] and osteogenic differentiation[259], and thus intracellular delivery of calcium phosphate nanoparticles was able to promote osteogenic commitment in skeletal populations[261]. It is therefore possible that cellular uptake of clays may aid the transport of calcium phosphate minerals and/or their ions to promote these pathways. Similarly, clay-protein interactions, in addition to their ability to stabilize extracellular growth factor concentrations[141,142] may also enhance osteogenesis by aiding the cellular uptake of bioactive molecules[262]. Such utility has been applied directly through the use of clays as nanocarriers for drugs and plasmids[173,263]. Intracellular clay-protein interactions may also directly influence intracellular signalling events following clay uptake for example through catalysis via co-localisation of an enzyme and its substrate. To provide one rather striking example, a study seeking to mimic pre-cellular biochemical processes during early-life evolution found that Laponite clay gels were able to consistently enhance the transcription and translation of nucleic acids (a process involving more than 30 enzymatic reactions) in a cell lysate solution compared to clay free controls[264].

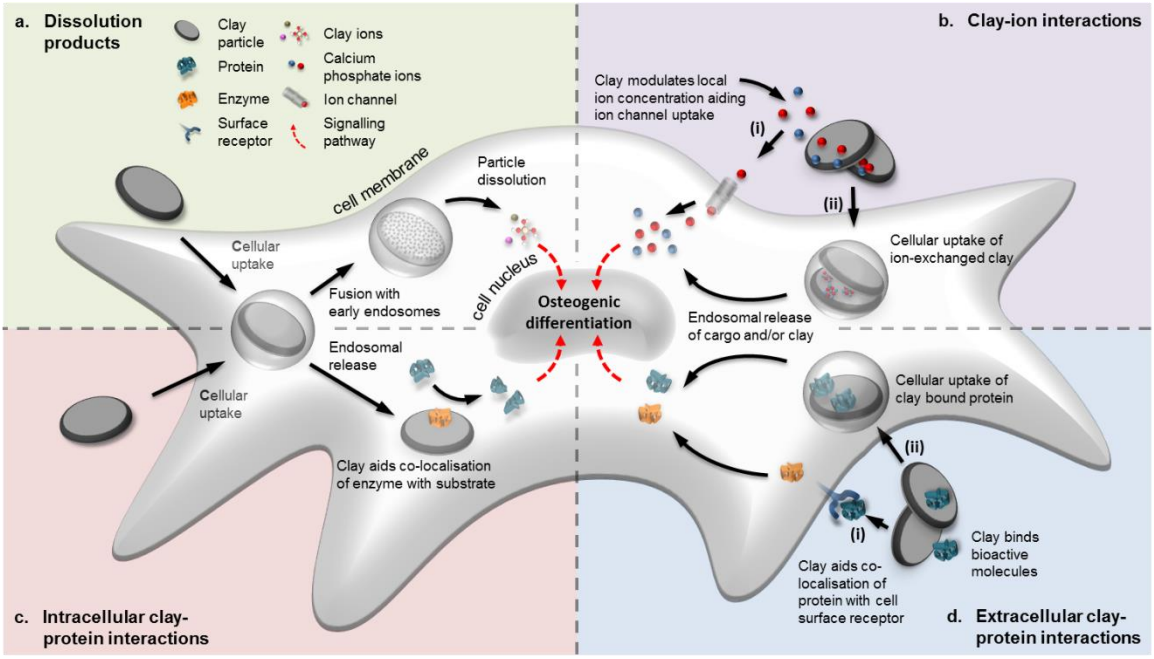

Figure 1. 15 Possible modes of action for clay osteogenic bioactivity.
Clay enhancement of osteogenic differentiation of responsive populations could be mediated via various possible routes. **a.** Following cellular uptake clay nanoparticles may undergo degradation within the low pH endosomal or lysosomal intracellular compartments to release dissolution products ($Si(OH)_4$, Mg^{2+} and Li^{+}) known to influence osteogenic cell function; **b.** Clay nanoparticles may facilitate the transport of extracellular Ca^{2+} and PO_4^{3-} ions across the cell membrane by modulating extracellular ion concentrations (i) or via uptake of ion-exchanged particles (ii) to promote mineralisation. **c.** Internalised clay nanoparticles may modulate intracellular signalling pathways through clay-protein interaction, as for example through alteration of enzyme activity as a result of adsorption/immobilization on clay surfaces. **d.** Clay nanoparticles may aid receptor interaction (i) or uptake (ii) of bioactive molecules.

Hypothesis and aims

The overall hypothesis of this thesis is that Laponite clay nanoparticles induce osteogenic differentiation of human bone marrow stromal cells and that Laponite osteogenic bioactivity is mediated by a range of interactions the most prominent of which is Laponite endocytosis and subsequent release of osteogenic degradation products.

The project tested four different hypotheses through specific aims as follows:

Hypothesis 1

Laponite clay nanoparticles are cytocompatible and induce osteogenic differentiation of hBMSCs and that Laponite osteogenic bioactivity directly depend on Laponite dose and exposure time.

Aims

1. Test the effect of Laponite clay nanoparticles on hBMSCs viability and morphology.
2. Test the osteogenic differentiation potential of hBMSCs in response to Laponite addition.
3. Treat hBMSCs with varying Laponite doses and exposure time to determine the optimal Laponite osteogenic culture conditions.

Hypothesis 2

Laponite enhance ALP activity in hBMSCs cultures through direct interaction with ALP enzyme and through Laponite endocytosis and subsequent release of osteogenic degradation products ($Si(OH)_4$, Mg^{2+} and Li^{+}).

Aims

1. Measure the capacity of Laponite for ALP adsorption and subsequent influence on ALP activity.
2. Determine the effect of Laponite endocytosis inhibition on ALP activity of hBMSCs.
3. Test the effect of $Si(OH)_4$, Mg^{2+} and Li^{+} ions, applied as salt solutions, vs. intact Laponite particles on hBMSCs ALP activity.

Hypothesis 3

Lithium is involved in imparting the osteogenic bioactivity of Laponite through activating the canonical Wnt signaling pathway and that modulation of Laponite lithium will modify Laponite osteogenic bioactivity accordingly.

Aims

1. Explore the effect lithium content of Laponite on Wnt signalling activation.
2. Generate a family of lithium modified Laponite clay minerals in terms of both structural and adsorbed lithium.
3. Explore the effect of lithium modified Laponite formulations on hBMSCs osteogenic differentiation.

Hypothesis 4

Laponite nanoparticles are endocytosed by hBMSCs for intracellular trafficking through the lysosomal degradative pathway leading to intracellular Laponite degradation.

Aims

1. Track Laponite uptake kinetics and *in vitro* distribution in hBMSCs culture.
2. Track Laponite colocalisation with intracellular organelles and determining which intracellular trafficking pathway(s) Laponite pursue.
3. Track the fate of internalised Laponite nanoparticles.
4. Track the effect internalised Laponite influence on cell physiological functions.

Chapter 2: General methods

2.1 Isolation of human bone marrow stromal cells

The vast majority of cell studies in this thesis were performed using human bone marrow stromal cells (hBMSCs). hBMSCs were isolated from femoral bone marrow samples obtained from haematologically normal osteoporotic or osteoarthritic patients undergoing hip replacement surgery, following full informed patient consent, at Southampton General Hospital or Spire Hospital Southampton and with the approval of the appropriate Local Research Ethics Committee (LREC 194/99/1).

hBMSCs were isolated from bone marrow aspirates from patients' femurs. The donated samples typically included small fragments of trabecular bone and traces of fat. To flush out the soft marrow tissue, around 10 ml plain α-MEM (Lonza) was added into the obtained sample, shaken vigorously and the liquid transferred to a new 50 mL Falcon tube. The last step repeated until the sample appeared pale pink to white - the stage at which most cells were isolated, then the hard-trabecular bone tissue discarded into Virkon. Next, the as-obtained cell suspension was centrifuged at 1100 rpm for 5 min, the supernatant was discarded into Virkon and the cell pellet was re-suspended in 20 mL plain α-MEM. The last obtained cell suspension was passed through a 70 μm cell strainer on top of a new 50 mL Falcon tube to isolate the cell population from the residual bone chips and remaining unwanted tissues. Cell number was counted in the filtered cell suspension (total volume = 20 mL) using the haemocytometer method. Ideally, 50 μL of cell suspension was mixed with 50μL of 0.1% acetic acid, to lyse red blood cells, and 100 μL trypan blue dye, to differentiate between live and dead cells, in Eppendorf tube. 25 μL of this 200 μL pipette was added into haemocytometer for counting. The formula used for calculating cell number is:

Cell number = (mean no. of counted cells in 16x16 small squares) x 10^4 x 4(dilution factor) x total volume of cell suspension (e.g. 20 mL)

Cells, the whole nucleated fraction, were seeded at a density of 5 x 10^3 cells/cm^2 in T175 tissue culture flasks containing 20 mL basal medium to set up clonal cultures of the obtained hBMSCs population. After 3 h incubation at 37 °C and 5% CO_2, existing media discarded and the cells were washed twice with DPBS (Lonza) to remove the non-adherent cell fraction (red blood cells) while the adherent hBMSCs were grown out in basal media (~ 20 mL/T175 flask) at 37 °C and 5% CO_2 for 12-14 days, before

being passaged for culture expansion. The discrete distribution of colonies was confirmed at day 7. Cells at this stage are at passage P0.

When reached 70-80% confluence per colony, which usually occurs at day 11-12 post-cell isolation, hBMSCs were passaged in order to a) redistribute cells and prevent regions of very high density occurring and b) allow for enough cell yield for subsequent experiments. For subculture, cells were detached with the use of collagenase IV (1 mg/mL) and 0.5 mg/mL trypsin for 30 and 5 min, respectively, at 37 °C and 5% CO_2. The ratio for passaging was 1:1 to redistribute cells from high colony-confluence to throughout the tissue culture flask. Cells incubated in basal medium at 37 °C and 5% CO_2 until reaching 70-80% confluence/flask which usually takes 6-7 days. Culture media was replenished every 3-4 days. At 70-80% confluence/flask, cells were frozen-down and banked at liquid nitrogen for later Laponite-hBMSCs experiments. Cells at this stage are at passage 1 (P1).

Basal culture medium composed of α-MEM (Lonza) containing 10% FBS (Gibco) and 100 μg/mL penicillin/streptomycin (Sigma).

2.2 Culture of human bone marrow stromal cells

For all stages before cell seeding for Laponite interaction, cells were grown in basal medium at 37 °C in humidified CO_2 atmosphere until reaching 70-80% confluence/flask. Culture medium was changed every 3-4 days. At this confluence, cells were either passaged in a ratio 1:2 or seeded at the required density in well culture plates for subsequent interaction with Laponite nanoparticles. For all experiments, the obtained hBMSCs were used before passage 4.

2.3 Preparation of Laponite dispersion in cell culture medium

Freshly prepared Laponite dispersions were used for all experiments. First, 0.5% (w/v) Laponite dispersion in dH_2O was prepared as a stock for subsequent preparation of Laponite-containing cell culture media. Briefly, 0.25 g Laponite powder (particle size = 25-30 nm) was sterilized using Blak-Ray B-100AP High intensity UV Lamp (UVP, Upland, CA, USA) for 15 min then added in a very slow manner to sterile-filtered dH_2O (18.2 MΩ) while under rapid agitation/stirring sufficient to produce a vortex (at 700 rpm stirring speed) and left to stir for ~2 h until a clear dispersion is formed.

Dilutions of the as-prepared 0.5% stock solution were performed using basal or osteogenic cell culture medium according to experimental conditions. 49 mL culture medium were allowed to stir at 700 rpm forming a vortex, then 1 mL of Laponite /H_2O stock was added in the middle of this vortex through 5 consecutive times (200 µL/time with 1 min time interval) to avoid Laponite particle aggregation in cell culture media which is a spontaneous character of Laponite. The resultant media dispersion has a net Laponite concentration of 100 µg/mL and was used as a stock for the subsequent preparation of lower Laponite concentrations (e.g. 1/10 and 1/4 dilutions for 10 and 25 µg/mL, respectively). For Laponite-free media (negative control), 1 mL dH_2O was added to 49 mL culture medium under the same conditions for consistency.

It is worth noting that all the materials and equipment used were pre-sterilized via autoclaving and all stages of preparation were performed under the fume hood to ensure complete sterilization of the as-obtained Laponite dispersions.

Osteogenic culture media composed of basal medium supplemented with 100 µM ascorbate-2-phosphate and 10 mM β-Glycerophosphate and 10 nM dexamethasone (Sigma).

2.4 Osteogenic differentiation assays and markers

2.4.1 Alkaline phosphatase activity – staining

ALP staining was performed using naphthol AS-MX phosphate alkaline solution (Sigma 85-5) as substrate and fast violet salt (Sigma F1631) as diazonium salt. Naphthol AS-MX is liberated, due to of activity of ALP, and coupled with the diazonium salt producing an insoluble visible pigment. At each selected time point, existing media discarded into Virkon, cells washed twice with DPBS then fixed with 95% ethanol at 4 °C for around 10 min. Next, ethanol was removed, and the fixed cells were further washed with DPBS and left to dry for 20 min at room temperature. In the meanwhile, ALP reaction solution was prepared by combining naphthol AS-MX phosphate (1/25 dilution in dH_2O) and fast violet salt (final concentration 0.24 mg/mL). Fixed cells were incubated with the as-prepared ALP reaction solution for 10-60 min in the dark depending on ALP conc. and activity of the obtained sample. When color changed from yellow to red, which is due to the activity of ALP, liquid was discarded and cells rinsed with dH_2O to stop the reaction. Next, cells were

imaged using: 1) Carl Zeiss Axiovert 200 microscope with AxioVision imaging software (Zeiss) and 2) Zeiss Stemi 2000 microscope with Canon Power Shot G10 digital camera.

2.4.2 Alkaline phosphatase activity – quantification assay

ALP activity was quantified using an an end-point colorimetric assay based on the conversion of p-nitrophenol phosphate (pNPP) to yellow p-nitrophenol (pNP) by ALP enzyme. First, cell lysates were collected for ALP activity and DNA quantification as following: at each selected time point culture media discarded and cells washed twice with DPBS then incubated with CelLytic M (Sigma C2978) for 15 min on an orbital shaker at room temperature. Cell lysates were collected by continuous scrapping and pipetting and transferred to sterilized collection tubes then centrifuged at 12000 *xg* for 15 min at 4 °C to separate unwanted cell debris from the protein-containing supernatant which was transferred to chilled tubes for ALP and DNA quantification.

Standards (0-200 nmol/mL) were prepared using 4-nitrophenol (Sigma N7660-100ML), which is end product of ALP enzymatic reaction. ALP activity of tested samples was read-off from the standard curve. The substrate solution was prepared by dissolving 40 mg phosphatase substrate (Sigma P47441G) in 10 mL of 1.5 M alkaline buffer solution (Sigma A9226-100ML) and 20 ml dH_2O. Along with the samples and standards, sample background controls were used to extract any interference caused by coloured samples in the absorbance readings.

Standards (100 µL/well), samples (20 µL/well) and background controls (20 µL/well) were added in triplicates in clear, flat-bottom, 96-well plate. 80 µL/well of the previously prepared substrate solution was added to both samples and backgrounds, then immediately 1M NaOH (100 µL/well) was used to stop the reaction only in the background controls. The plates were incubated in the dark at 37 °C and 5% CO_2 for 10-60 min until samples changed color to yellow (product) but not as intense as the 200 nmol/mL standard. Exactly at the time of color change, plates taken out of the incubator and the reaction stopped by adding 1M NaOH (100 µL/well) to both samples and standards but not the background controls. Finally, the the colour intensity/absorbance was measured using ELx800 microplate reader (BioTek, Winooski, USA) at 415 nm. The ALP activity was calculated as conc. of product/hour

based on the obtained absorbance, standard curve and incubation time then normalized to the corresponding DNA content assayed as below.

2.4.3 dsDNA quantification – cell number & proliferation

Double-stranded DNA (dsDNA) quantification was performed on the same cell lysate samples used for ALP quantification above to control for cell number. Quant-it™ PicoGreen® dsDNA Assay Reagent (Invitrogen LifeTech) was used according to the manufacturer protocol. Standard curve was established using standards at 0-1000 ng/mL prepared from 2 μg/mL stock DNA solution. Standards (100 μL/well), and samples (20 μL/well) were pipetted in triplicates in black, 96-well plate then diluted with 80 μL/well 1x TE buffer (Tris/EDTA, Sigma). Next, 100 μL/well of 0.5% PicoGreen in 1x TE buffer was added to both samples and standards, followed by incubation for 5 min at room temperature in the dark. Fluorescence was measured using FLx800 fluorescence microplate reader (BioTek) at an excitation/emission of 480/520 nm. The standard curve was used for the conversion of the detected absorbance to concertation as described above with the case of ALP quantification.

2.4.4 Calcium mineralization – alizarin red staining

Calcium deposition/mineralisation in extracellular matrix was determined using alizarin red dye (ARS) which binds selectively to calcium slats and is widely used for calcium histochemistry. Calcium forms an Alizarin Red S-calcium complex in a chelation process and the end product is a bright red stain. Alizarin red stain working solution was prepared fresh at 2% (w/v) in dH_2O while under rapid agitation/stirring and left for stirring for 3 h in the dark. pH of the resulting ARS solution was adjusted to 4.1–4.3 using 10% NH_4OH and 10% HCl, then filtered and used for staining calcium deposits in cell culture.

At each selected time point, existing culture media discarded, cells washed twice with DPBS (without Ca^{2+} or Mg^{2+}) then fixed in 4% paraformaldehyde (PFA) for 15 min at room temp. Next, the PFA fixative was aspirated off and cells washed twice with DPBS. The as-prepared ARS (pH = 4.1–4.3) was added to the fixed cells at a volume that covers the entire surface of the well then incubated at room temperature in the dark on an orbital shaker for 20 min. Finally, ARS discarded and cells washed several times with dH_2O to remove excess un-bound dye. The stained cell monolayer was visualised by 1) Carl Zeiss Axiovert 200 microscope with AxioVision imaging

software (Zeiss) and 2) Zeiss Stemi 2000 microscope with Canon Power Shot G10 digital camera. Image quantification was performed using Cell Profiler software (Broad Institute Inc.).

2.4.5 Osteogenic gene expression – RT-qPCR

2.4.5.1 RNA extraction

Total RNA extraction was performed using ISOLATE II RNA Mini Kit (Bioline, BOI-52073) according to manufacturer protocol. At each selected time point, culture media discarded, cells washed twice with DPBS and lysed in 350 µL RLY lysis buffer. Cell lysis was collected in new DNase/RNase free sterile collection tubes, vortexed vigorously and immediately processed for RNA extraction or snap-frozen for later processing.

First, cell lysate was filtered through loading onto ISOLATE II Filter (**violet**) in a 2 mL collection tube and centrifuged at 11000 *xg* for 1 min. The **violet** column discarded and the flow-though was mixed very well with an equivalent volume of 70% ethanol, then transferred onto ISOLATE II RNA Mini Column (**blue**) in a new 2 mL collection tube to bind RNA and centrifuged at 11000 *xg* for 30 s. The flow-through discarded while the **blue** column was transferred to a new 2 mL collection tube. 350 µL of Membrane Desalting Buffer (MEM) was added onto the **blue** column and centrifuged for 1 min at 11000 xg to dry membrane and eliminate salts which reduce DNase activity in the next steps. Flow-through was discarded and the blue column was put again on the same 2 mL collection tube. To digest DNA, 95 µL DNase I reaction mixture (10 µL reconstituted DNase **I** to 90 µL Reaction Buffer for DNase I) was applied directly onto the centre of the silica membrane and incubated at room temperature for 15 min. Then, the silica membrane undergone 3 cycles of wash using RW buffers as following: 1) in the 1st. wash, 200 µL Wash Buffer RW1 was added onto the column and centrifuged for 30 s at 11000 *xg*. Flow-through discarded and the column was placed into a new 2 mL collection tube. 2) the 2nd wash was the same as the first one but using 600 µL Wash Buffer RW2. iii) in the 3rd wash, 50 µL Wash Buffer RW2 was added onto the column and centrifuged for 2 min at 11000 *xg* to dry membrane completely. Flow-through discarded and the column was transferred to in new nuclease-free 1.5 mL collection tube. Total RNA was eluted by applying 60 µL RNase-free water directly onto centre of the column and centrifugation at 11000

xg for 1 min. The column was discarded and the flow-through (eluted RNA) was directly kept on ice post-centrifugation to keep RNA intact from degradation.

Concentration and quality of eluted RNA was determined using NanoDrop ND-1000 spectrophotometer (Thermo Fisher). Samples were either stored at -80 °C or proceeded for cDNA synthesis. Samples with a 260/280 absorbance ratio of ~2 were considered as pure RNA.

2.4.5.2 Reverse transcription – cDNA synthesis

RNA samples reverse transcribed using TaqMan Reverse Transcription kit (Applied Biosystems, N8080234) for complementary DNA (cDNA) synthesis according to manufacturer protocol. Briefly, 7.7 µL of each sample, containing 250 ng RNA, was mixed very well with 12.3 µL Reverse Transcription reaction mix in 200 µL-micro reaction tubes and placed in Mastercycler Gradient (Eppendorf) with the following reaction settings: 10 min at 25 °C for primer incubation, 30 min at 48 °C for reverse transcription, 5 min at 95 °C for reverse transcriptase inactivation, hold at 4 °C – reaction volume of 20 µL. Samples were either proceeded for gene expression analysis or stored at -20 °C. Reverse transcription reaction mix composed of: 10x TaqMan RT Buffer (PCR Buffer II), 25 mM Magnesium chloride, DeoxyNTPs mixture (2.5 mM each dNTP), Random Hexamer (50 µM), RNase Inhibitor (20 U/µL) and MultiScribe Reverse Transcriptase (50 U/µL), with the following ratios: 2, 4.4, 4, 1, 0.4 and 0.5 µL/sample, respectively.

2.4.5.3 RT-qPCR

Expression of genes of interest was quantified by RT-qPCR using Applied Biosystems reagents and AB7500 cycler, according to manufacturer protocol. The genes analysed include: β-Actin and GAPDH as house-keeping genes, bone-related genes (ALP, RUNX2, osteocalcin, collagen 1, osteopontin and osteonectin) and non-template control (primer mix without cDNA). For each gene expression, 1 µL of each cDNA sample was mixed with 19 µL primer mix (10 µL GoTaq + 4 µL F+R primers (5µM) + µL nuclease-free H_2O) for a total reaction volume of 20 µL/sample. Reactions were performed in the AB7500 Applied Biosystems cycler (Foster, USA) with the following settings: 50 °C for 2 min, 95 °C for 10 min, followed by 40 cycles of 95 °C for 15 s and 60 °C for 60 s. Each sample was run in triplicates and relative expression of target genes was calculated using the $2^{-\Delta\Delta Ct}$ method by normalising first

against reference gene β-Actin or GAPDH then against corresponding negative control (e.g. Laponite-free samples). All primers used in this project were designed and validated by Bone & Joint research group at the University of Southampton. Details of primers sequences are included in **table 2.1**.

Primer name	Forward primer sequence(5′-3′)	Reverse primer sequence(5′-3′)	Product length
β-actin	GGCATCCTCACCCTGAAGTA	AGGTGTGGTGCCAGATTTTC	82pb
GAPDH	GACAGTCAGCCGCATCTTCTT	TCCGTTGACTCCGACCTTCA	86pb
RUNX2	GTAGATGGACCTCGGGAACC	GAGGCGGTCAGAGAACAAAC	78pb
Osterix (SP7)	ATGGGCTCCTTTCACCTG	GGGAAAAGGGAGGGTAATC	75pb
ALP	GGAACTCCTGACCCTTGACC	TCCTGTTCAGCTCGTACTGC	86pb
Collagen type 1 (COL1A1)	GAGTGCTGTCCCGTCTGC	TTTCTTGGTCGGTGGGTG	52pb
Osteocalcin (BGLAP)	GGCAGCGAGGTAGTGAAGAG	CTCACACACCTCCCTCCT	102pb
Osteopontin (SPP1)	GTTTGCGAGACCTGACATCC	CATTCAACTCCTCGCTTTCC	80pb
Osteonectin (SPARC)	GAGGAAACCGAAGAGGAGG	GGGGTGTTGTTCTCATCCAG	95pb

Table 2. 1 List of primers used in the RT-qPCR analysis.

2.5 Statistical analysis:

Statistical analysis was performed using GraphPad Prism 8 software (GraphPad, USA). Quantitative results are presented as mean ± standard deviation (SD). The N number in the figure legend represent the number of experimental replicates in each experiment. One-way ANOVA was used for comparison of means of 3 or more groups in response to one independent variable, whereas for comparing means of 3 or more groups in response to two independence variables, two-way ANOVA analysis was performed. This was followed by Tukey's multiple comparisons test. The difference between groups was considered statistically significant at $P < 0.05$. Details on the presentation and statistical tests used are detailed in the figure legends.

Chapter 3: Exploring the osteogenic bioactivity of Laponite

3.1 Introduction

As discussed in chapter 1, a growing number of studies have convincingly demonstrated biocompatibility and intrinsic osteogenic bioactivity of Laponite clay nanoparticles applied either alone or in combination with polymeric matrices[265,130,137]. However, these studies lack a clear explanation of I) the method followed to prepare Laponite dispersion in cell culture media and II) the influence of Laponite-cell culture conditions, for example Laponite dose and exposure time, on Laponite promotion of osteogenic differentiation. Understanding these points is the basis for the ultimate aim of this thesis – exploring the mechanism(s) underlying Laponite osteogenic bioactivity.

The method of nanoparticle preparation in cell culture media (CCM) plays a key role in determining nanoparticle influences on cell functions such as uptake, viability and differentiation[266]. Laponite is characterized by its rich surface chemistry, heterogenous charge distribution and therefore spontaneous flocculation in cell culture media[134,267]. Therefore, direct dispersion of Laponite in CCM, as vaguely explained in previous studies[268], suffers from the background of strong Laponite aggregation/flocculation which makes Laponite biocompatibility and osteogenic bioactivity results difficult to interpret. Moreover, nanoparticle influence on bone marrow stromal cell function and fate is also affected by other factors such as extraction and isolation techniques as well as number and osteogenic potential/stage of osteoblast progenitors[269,270] which might differ from the above-mentioned studies and necessitates the need for validating the biocompatibility and osteogenic bioactivity of Laponite in our cell culture model (clonal cultures of hBMSCs).

Another limitation of the above-mentioned Laponite-investigating studies is that they did not pay attention to the role of the fundamental culture conditions in terms of clay dose and incubation time which achieve the optimal Laponite osteogenic effect. It is believed that Laponite exert its osteogenic characters through both intracellular and extracellular processes as for example though providing osteogenic chemical cues intracellularly and acting as a growth nuclei for matrix and/or mineral maturation extracellularly[265,130]. This strongly depends on both the amount and availability of clay nanoparticles in the intra- and extracellular vicinity and thus clay dose and exposure time. Moreover, this represents an important approach for optimising and

selecting the right culture conditions to track Laponite/hBMSCs mechanistic interactions in subsequent chapters.

3.2 Hypothesis and aims

Experiments in this chapter were performed to test the hypothesis that Laponite clay nanoparticles are cytocompatible and induce osteogenic differentiation of hBMSCs and that Laponite osteogenic bioactivity directly depend on Laponite dose and exposure time.

In summary, the aim of the work in this chapter is to

1. Test the effect of Laponite clay nanoparticles on hBMSCs viability and morphology.
2. Test the osteogenic differentiation potential of hBMSCs in response to Laponite addition.
3. Treat hBMSCs with varying Laponite doses and exposure time to determine the optimal Laponite osteogenic culture conditions.

3.3 Methods

3.3.1 Physicochemical characterization of Laponite

Most of this thesis was mainly based on using standard Laponite XLG (batch number SR4871), herein used interchangeably as Laponite SL, which was kindly gifted from BYK-ALTANA. According to the manufacturer, this clay mineral is characterised by the molecular formula $Na^{+0.7}[(Si_8Mg_{5.5}Li_{0.3})O_{20}(OH)_4]^{-0.7}$ with particle diameter of 25-30 nm and thickness of 1 nm. We were not directly involved in synthesis of standard Laponite XLG for BYK patent reasons.

To investigate Laponite crystal structure and whether there is phase transformation or crystal defects, samples undergone powder X-ray diffraction (PXRD) analysis. PXRD experiments were carried out with Bruker D2 Phaser diffractometer using CuKα radiation (λ = 1.5415 Å). The XRD patterns were recorded over the 5°-70° 2θ range using a step of 0.02° and a counting time of 0.3 s per step.

Attenuated total reflectance Fourier transform infrared spectra (ATR-FTIR) were measured using Nicolet iS5 FTIR spectrometer equipped with iD7 ATR accessory. The FTIR spectra were collected after 32 scans within 400–4000 cm^{-1} wavenumber and at a resolution of 8 cm^{-1}.

Energy dispersive X-ray (EDX) analysis was recorded using Carl Zeiss Leo 1450VP scanning electron microscope (SEM) equipped with Oxford Instruments X-Act 10 mm^2 area silicon drift detector for elemental quantification by EDX. Briefly, samples were prepared by dispersing dry powder in ethanol on holder with double-sided conductive adhesive tape and carbon coated for EDX analysis.

For measuring lithium content of Laponite by atomic absorption spectroscopy (AAS), Laponite powder was dispersed in deionised H_2O at 2 mg/mL and digested with of 68% nitric acid before dilution with deionised H_2O (dilution factor = 10). Samples and standards were measured, in terms of lithium ion, using the M Series ‘SolAAr’ AA Spectrometer.

3.3.2 Effect of Laponite on cell viability and morphology

hBMSCs viability was determined using WST-1 colorimetric assay (Roche, Germany). The technique is based on the cleavage of tetrazolium salts to formazan dye by mitochondrial dehydrogenases produced by viable cells. Cells were seeded in clear flat-bottom 96-well plates at varying densities of 1.5 x 10^3 – 12 x10^3 cells/cm^2 in

basal medium and allowed to adhere for 24 h at 37 °C and 5% CO_2. Background controls contained basal medium without cells. After the 24 h incubation, existing media discarded and replaced with fresh basal media containing standard Laponite at concentrations 10-1000 μg/mL. Fresh Laponite-free basal media was added for backgrounds and negative control. Then the cells were incubated for another 24 h at 37 °C and 5% CO_2. The next day, existing media was discarded and replaced with fresh basal media supplemented with WST-1 (1:10 dilution) for the Laponite-treated samples, negative control and background. Then plates were put on an orbital shaker for one min to ensure homogenous distribution of color, followed by 1 h incubation at 37 °C, 5% CO_2. Finally, the absorbance of the samples was measured using EL-800 Universal Microplate Reader (BioTek Instruments Inc., Winooski, USA) at 450 nm. The absorbance/color intensity produced by formazan product correlates with the number of viable cells in the samples. Cell viability was expressed as a percentage relative to the control groups after subtraction of the background absorbance.

For assessing the effect of Laponite internalisation on hBMSCs adhesion and morphology, cells were treated with Rhodamine B-labelled standard Laponite nanoparticles and imaged using confocal microscopy. First, Laponite powder was fluorescently labelled with Rhodamine B isothiocyanate RBITC dye (20653, Cayman Chemicals, USA). Briefly, 0.5 g Laponite powder was dispersed in 25 mL of 1 mg/mL RBITC solution, prepared in anhydrous DMSO (ThermoFisher). The mixture was kept under continuous stirring overnight in dark conditions at 300 rpm at 4 °C. Repeated washing-centrifugation steps, at 3000 rpm and 21 °C for 15 min per step, with absolute ethanol were performed until supernatant appeared colourless indicating complete removal of excess dye. The resulting Laponite-RBITC powder was separated via filtration using Buckner funnel, air dried at room temperature and stored, protected from light, until further use.

At 70-80% confluence, hBMSCs (P2) were detached from culture flasks and seeded at density 10^4 cells/cm^2 in a 24-well plate on # 1.5 sterilised glass coverslips. Cells allowed to adhere in basal medium for 24 h. RBITC-labelled Laponite powder was dispersed in basal culture medium at 100 μg/mL as reported in **section 2.3**. Cell culture media aspirated, cells washed twice with DPBS and replaced with Laponite - containing vs Laponite-free basal media for clay-treated vs negative control groups,

respectively. Cells allowed to interact with RBITC-labelled Laponite for 24 h at 37 °C and 5% CO_2. Next, cells washed gently twice with pre-warmed DPBS (0.5 mL/well) and fixed with 4% PFA (0.5 mL/well) for 15 min at room temperature. Fixative removed, cells washed twice with PBS and permeabilised in 0.1% Triton™ X-100 in PBS (0.5 mL/well) for 15 min at room temperature. Triton removed, cells washed twice with DPBS and actin filaments were stained with 0.5 mL/well FITC-phalloidin (F432, Invitrogen), at 1/1000 dilution in PBS of 165 µM stock prepared in anhydrous dimethyl sulfoxide (DMSO), for 30 minutes at room temperature. Phalloidin aspirated, cells washed three times with DPBS, then incubated with 0.5 mL/well nuclear stain DAPI (D1306, Invitrogen), at 1/2500 dilution in PBS of 5 mg/mL stock prepared in dH_2O, for 15 min at room temperature. Finally, DAPI solution removed, cells washed three times with DPBS, mounted and stored in the dark at 4 °C for next day imaging using Leica TCS-SP8 Confocal Microscope equipped with Leica LAS-X software.

3.3.3 Effect of Laponite on hBMSCs osteogenic differentiation – concentration examination

When reaching 70-80% confluence, hBMSCs were detached from culture flasks using trypsin/EDTA 1x, seeded at density of 10^4 cells/cm^2 in basal medium and allowed to adhere under 37 °C and 5% CO_2 conditions for 24 h. Next day, existing media discarded, cells washed twice with pre-warmed DPBS and cultured with osteogenic culture medium containing 0, 1, 10 and 100 µg/mL standard Laponite nanoparticles and incubated (with Laponite) under 37 °C and 5% CO_2 conditions for 3 days. For negative control Laponite-free medium was used. At day 3, culture media was replaced with freshly prepared Laponite-free osteogenic media and cells incubated under the same culture conditions (37 °C and 5% CO_2) for 14 days. Media change was performed every 3-4 days with Laponite-free osteogenic culture media. On day 3 post-Laponite addition, ALP staining and activity assay as well as osteogenic gene expression of hBMSCs were performed as described in **sections 2.4.1, 2.4.2** and **2.4.5** respectively, while calcium phosphate mineral deposition at day 7 and 14 was assayed using alizarin red staining as reported in **section 2.4.4**.

3.3.4 Effect of Laponite on hBMSCs osteogenic differentiation – Laponite exposure time examination

For monitoring the effect of Laponite-hBMSCs contact time on Laponite osteogenic properties, hBMSCs were treated with standard Laponite XLG for 3 and 7 days followed by assessing osteogenic markers ALP and extracellular matrix mineralisation. Briefly, hBMSCs at 70-80% confluence and passage 2 were detached from culture flasks using trypsin/EDTA 1x, seeded at 10^4 cells/cm^2 in basal medium in 24-well plates and allowed to adhere for 24 h at 37 °C and 5% CO_2. Next day, existing media discarded, cells washed twice with DPBS and Laponite-containing osteogenic culture media was added at final Laponite concentration of 100 µg/mL. hBMSCs were incubated with Laponite nanoparticles for 3 vs 7 days, denoted "d-3" and "d-7", respectively. In the d-3 condition, cells were in contact with Laponite nanoparticles in osteogenic media for only 3 days, without media change, after which media change was performed with fresh clay-free osteogenic media, every 3-4 days, for a total incubation time of 14 days. On the other hand, in the case of d-7 cells incubated with Laponite nanoparticles in osteogenic media for complete 7 days, without media change, followed by changing media with clay-free osteogenic media every 3-4 days until day 14. Therefore, d14-3 for example refers to assay performed on day 14 on cells incubated with clay for only 3 days, while d14-7 indicates the assay performed on day 14 but on cells incubated with nanoclay for 7 days (**Figure 3.1**). At day 1, 3, 7 and 14 post-Laponite addition ALP staining, activity assay and dsDNA quantification were assayed as reported in **sections 2.4.1, 2.4.2 and 2.4.3** respectively. On day 14, extracellular matrix mineralisation was monitored using ARS as described in **section 2.4.4**.

For evaluating the reproducibility of Laponite-induction of calcified nodule formation across various patients, hBMSCs were cultured with dispersed Laponite nanoparticles in osteogenic culture medium for complete 7 days as described above for the "d-7" group. On day 3, ALP activity was assayed as in **section 2.4.1**, while ARS staining was investigated as in **section 2.4.4.**

Finally, the influence of Laponite on temporal bone-related gene expression of hBMSCs during the first week of clay induction was analyzed by RT-qPCR (**section 2.4.5**) on hBMSCs cultured with Laponite for 7 days as in the group "d-7" at day 7 post-Laponite addition.

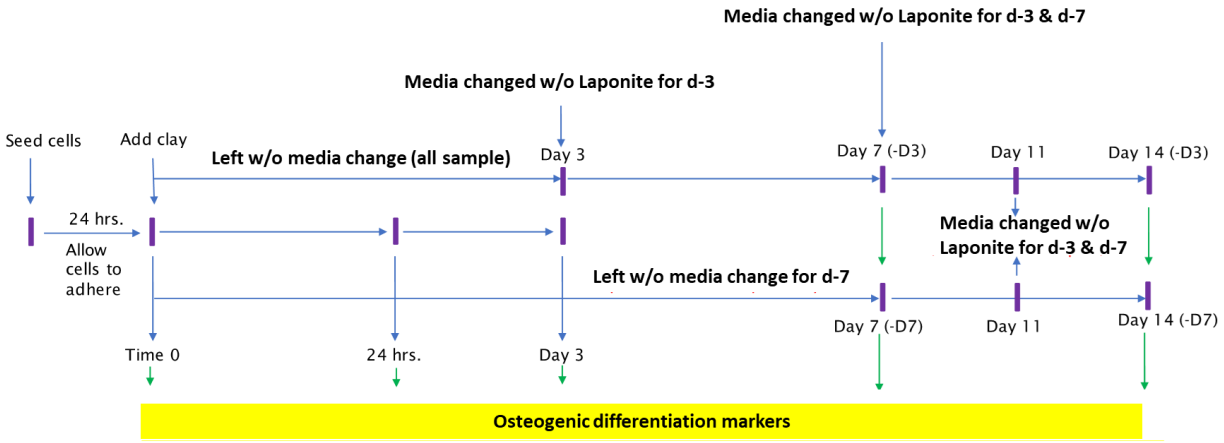

Figure 3. 1 Schematic representation of methodologies used to evaluate the effect of Laponite exposure time on hBMSCs osteogenic differentiation.

3.4 Results

3.4.1 Physicochemical characterisation of Laponite

Structure and composition of nanoparticles play a direct role on stem cell responses such as cellular uptake, toxicity, proliferation and differentiation[265]. Therefore, characterisation/authentication of Laponite clay nanoparticles, obtained from BYK-ALTANA, was performed using a range of materials characterisation techniques.

Crystal structure was investigated by powder X-ray diffraction (PXRD and Fourier transform infrared spectroscopy (FTIR) while chemical composition of the obtained nanoclay was analysed using energy dispersive X-ray (EDX) and atomic absorption spectroscopy (AAS). As expected, X-ray diffractogram (**Figure 3.2A**) shows peaks ascribed to a typical Na-synthetic Hectorite, according to Brindley & Brown[144], without phase transformation or precipitate impurities and with the following characteristic reflections:

1. Basal *00l* reflection of the 001 plane, with d_{001} = 13 Å in the low angle region (2θ = 6.8°). Shifts in the 001 peak position indicate either an increase, hence greater separation of the clay layers, or decrease in the d-spacing – i.e. interlayer region thickness.

2. Broad *hk0*, *0k0*, *00l* and *h00* reflections in the middle angle region (2θ = 20-40°), with $d_{110,\ 020}$ = 4.5 Å at 2θ ~ 20°, d_{004} = 3.18 Å at 2θ ~ 28°, and $d_{130,\ 200}$ = 2.56 Å at 2θ ~ 35°.

3) Broad *hk0* and *0k0* reflections in the high angle region (2θ = 50-61°, with $d_{150,\ 240}$ = 1.72 Å at 2θ ~ 53° and $d_{060,\ 330}$ = 1.52 Å at 2θ ~ 61°.

On the other hand, in agreement with the XRD diffractogram, the FTIR results (**Figure 3.2B**) show stretching and bending vibrations of the functional groups characteristic of magnesium silicate clay mineral, including[271]: i) Si-O stretching and Si-O-Si bending of the tetrahedral sheet, at 980 cm^{-1} and 427 cm^{-1}, respectively, ii) Mg-OH bending of the octahedral sheet at 650 cm^{-1} and iii) H-O-H bending of adsorbed and interlayer water at 4304 cm^{-1} and 3630 cm^{-1}.

Energy dispersive X-ray analysis (**Figure 3.2C**) revealed the presence of oxygen (48.5%), silicon (31.45%), magnesium (18.23%), sodium (1.7%) and calcium (trace), with stoichiometry similar to standard Laponite XLG reported in literature. Lithium

content was measured by AAS (3.11 g/kg), as EDX is less useful for determination of elements with Z<11. The half unit formula of nanoclay under analysis was calculated according to V. Olphan[147] (**Figure 3.2D**) based on elemental composition determined by EDX and AAS, which was similar to reported Laponite XLG but with higher sodium content and trace adsorbed Ca ions ($Si_{4.06}$ Mg $_{2.72}$ $Li_{0.15}$) $Na_{0.27}$ $Ca_{0.01}$.

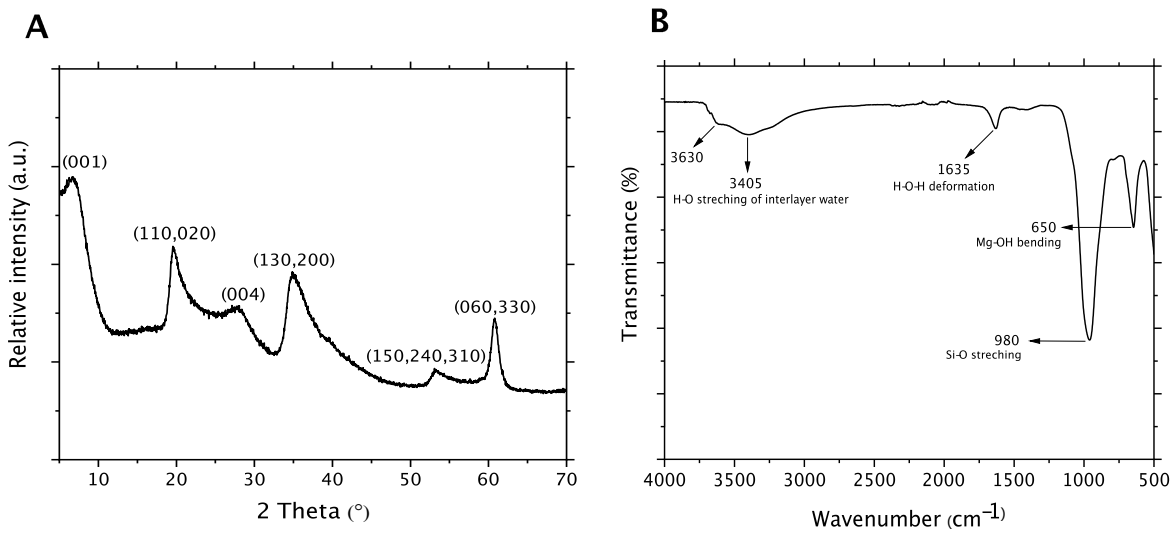

C

Element	Wt.%	Atomic %	Oxide	Oxide %	Number of cations
O	48.50	60.88			11
Na	1.70	1.49	Na_2O	2.049	0.27
Mg	18.23	15.07	MgO	29.97	2.72
Si	31.45	22.49	SiO_2	67.80	4.062
Ca	0.147	0.073	CaO	0.20	0.01
Total	100	100		100	7.06

D

Half Unit Formula
($Si_{4.06}$ Mg $_{2.72}$ $Li_{0.15}$) $Na_{0.27}$ $Ca_{0.01}$

Figure 3. 2 Nanoclay physicochemical characterisation.
(A) XRD diffractogram and (B) FTIR spectrum showing peaks and vibrational bands representative of synthetic Na-hectorite. (C) Elemental analysis of studied Laponite clay mineral as determined by EDX confirming and (D) its calculated half unit formula.

3.4.2 Effect of Laponite on cell viability and morphology

Prior to examining the potential osteogenic role of Laponite on hBMSCs, Laponite cytotoxicity was investigated. WST-1 assay was performed to assess the metabolic activity of hBMSCs cultured at varying cell seeding densities (1.5×10^3 – 12×10^3 cells/cm^2) and Laponite doses (0–1000 µg/mL) for 24 h. For all cell densities tested Laponite clay nanoparticles exhibited good cytocompatibility up to a concentration of 100 µg/mL (**Figure 3.3A**). However, at higher clay doses and particularly at the

highest cell density used (12 x10^3 cells/cm^2) the cellular metabolic activity decreased significantly (P = 0.0046). Therefore, Laponite concentrations of ≤ 100 µg/mL were selected for subsequent experiments. F-actin staining (FITC-phalloidin) confirmed normal cell spreading and morphology in the presence of 100 µg/mL Rhodamine B-labelled Laponite nanoparticles which appeared associated with the cells in monolayer cultures (**Figure 3.3B).**

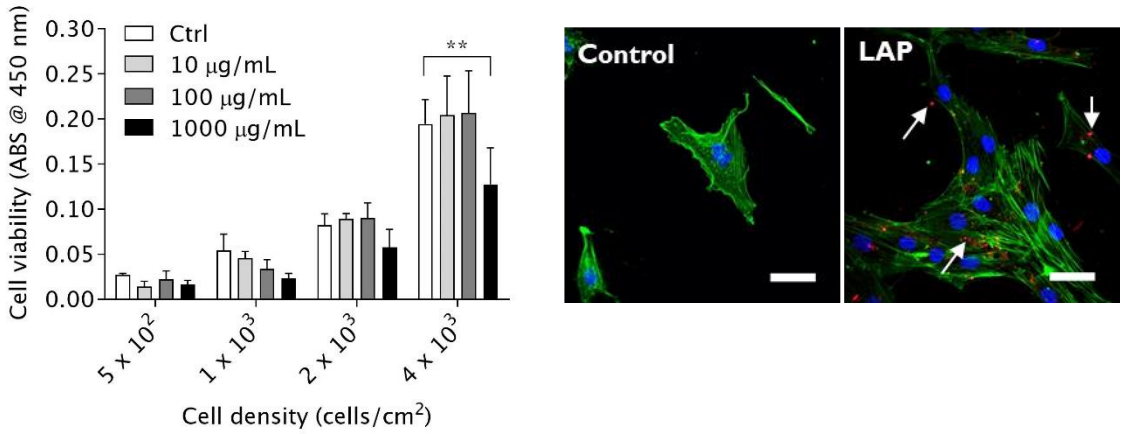

Figure 3. 3 Cytocompatibility of Laponite clay nanoparticles.
(A) Laponite clay nanoparticles, dispersed in cell culture media, are biocompatible up to a concentration of 100 µg/mL as measured by WST1 assay. (B) Laponite NPs (100 µg/mL) associate with cells in monolayer culture, but do not interfere with cell adhesion and spreading as seen by staining of F-actin filaments. Scale bar = 20 µm. Laponite labelled with RBITC (red) while cell cytoskeleton and nucleus were stained with FITC-phalloidin (green) and DAPI (blue), respectively. Statistical analysis was performed using two-way ANOVA followed by Tukey's multiple comparisons test. Data represent mean ± SD, N = 3. **P < 0.01.

3.4.3 Effect of Laponite on hBMSCs osteogenic differentiation – concentration examination

Based on the cell viability results, the osteogenic bioactivity of Laponite nanoparticles on hBMSCs was investigated at concentration of 1-100 µg/mL. While 1 and 10 µg/mL Laponite concentrations did not significantly affect ALP activity, an early marker of osteoblast differentiation, addition of 100 µg/mL Laponite led to significant enhancement of hBMSCs ALP activity compared to clay-free control (P < 0.0001) as demonstrated by both ALP assay and staining (**Figure 3.4).**

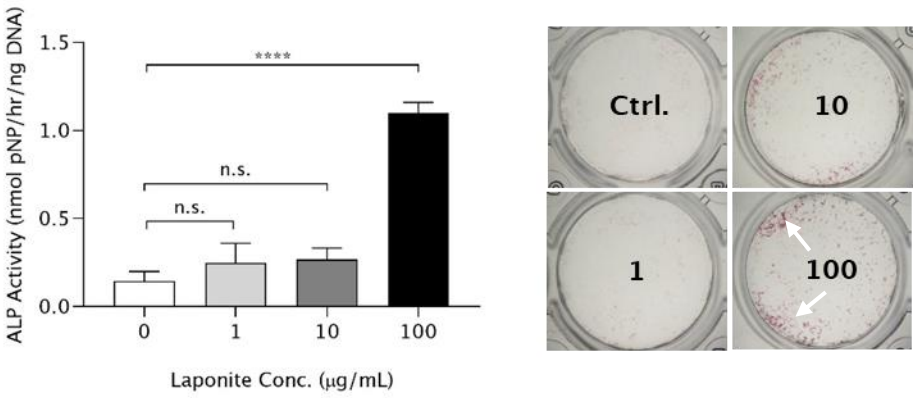

Figure 3. 4 Role of nanoparticle dose in Laponite osteogenic bioactivity assayed by ALP staining and activity quantification on day 3.
The addition of Laponite nanoparticles, up to a conc. of 100 μg/mL, promoted an early increase of hBMSCs ALP activity (A) and staining intensity (B) in a dose dependent manner, reaching statistically significant levels at 100 μg/mL. Statistical analysis was performed using one-way ANOVA followed by Tukey's multiple comparisons test. Data represent mean ± SD, N = 3. ****P < 0.0001; n.s. = not statistically significant.

Such clay-enhanced ALP activity was in agreement with a significant up-regulation of osteogenic genes expression with the addition of clay nanoparticles in cell culture media (**Figure 3.5**). At day 3, the presence of Laponite at 1-10 μg/mL did not result in any statistically significant influence on the mRNA expression levels of both early (RUNX2, ALP & COL 1) or late (OPN & OCN) genes tested. When Laponite concentrations was increased to 100 μg/mL, the expression of both ALP and Collagen type 1 was significantly upregulated reaching around 5- (P = 0.007) and 7-fold (P = 0.0053) increase, respectively, when compared to their respective negative controls. However, this clay-induced upregulation of hBMSCs ALP and COL1 expression was not accompanied by an effect on RUNX2. As expected at this early time point, even at the highest Laponite dose tested, there was no significant influence of Laponite on the expression profile of late osteogenic marker genes OPN and OCN.

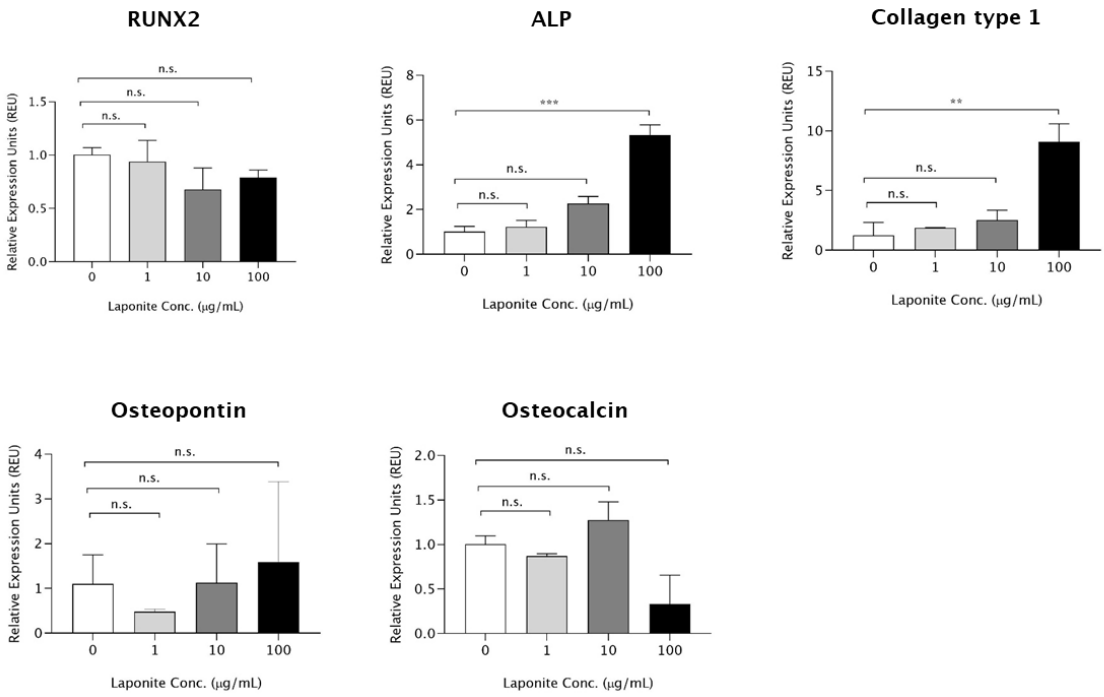

Figure 3. 5 Role of nanoparticle dose in Laponite osteogenic bioactivity assayed by RT-qPCR on day 3.
The cells exhibited a clay-mediated upregulation of early osteogenic gene expression (ALP & COL1) at Laponite concentration of 100 µg/mL. Laponite treatment, however, did not change the mRNA expression level of RUNX2, OPN and OCN. Statistical analysis was performed using one-way ANOVA followed by Tukey's multiple comparisons test. Data represent mean ± SD, N = 3. **P < 0.01; ***P < 0.001; n.s. = not statistically significant.

Next, the effect of Laponite concentration on extracellular calcium mineralisation was assessed at later time points (day 7 & 14), by alizarin red staining. In agreement with the ALP and gene expression data, Laponite concentrations below 100 µg/mL did not trigger significant hBMSCs mineralization at either day 7 or 14. However, hBMSCs treated with 100 µg/mL Laponite showed enhanced mineralization levels with a more intense overall staining and higher number of mineralized regions compared to hBMSCs cultures without Laponite at day 14 (**Figure 3.6**). This was confirmed with staining quantification which showed the highest Laponite dose tested with around 20-fold higher mineralization levels ($P < 0.0001$) compared to the negative control. Moreover, the ARS quantification levels at 1-10 µg/mL Laponite were not statistically different from the negative control at both day 7 and 14, a trend similar to 100 µg/mL Laponite at day 7.

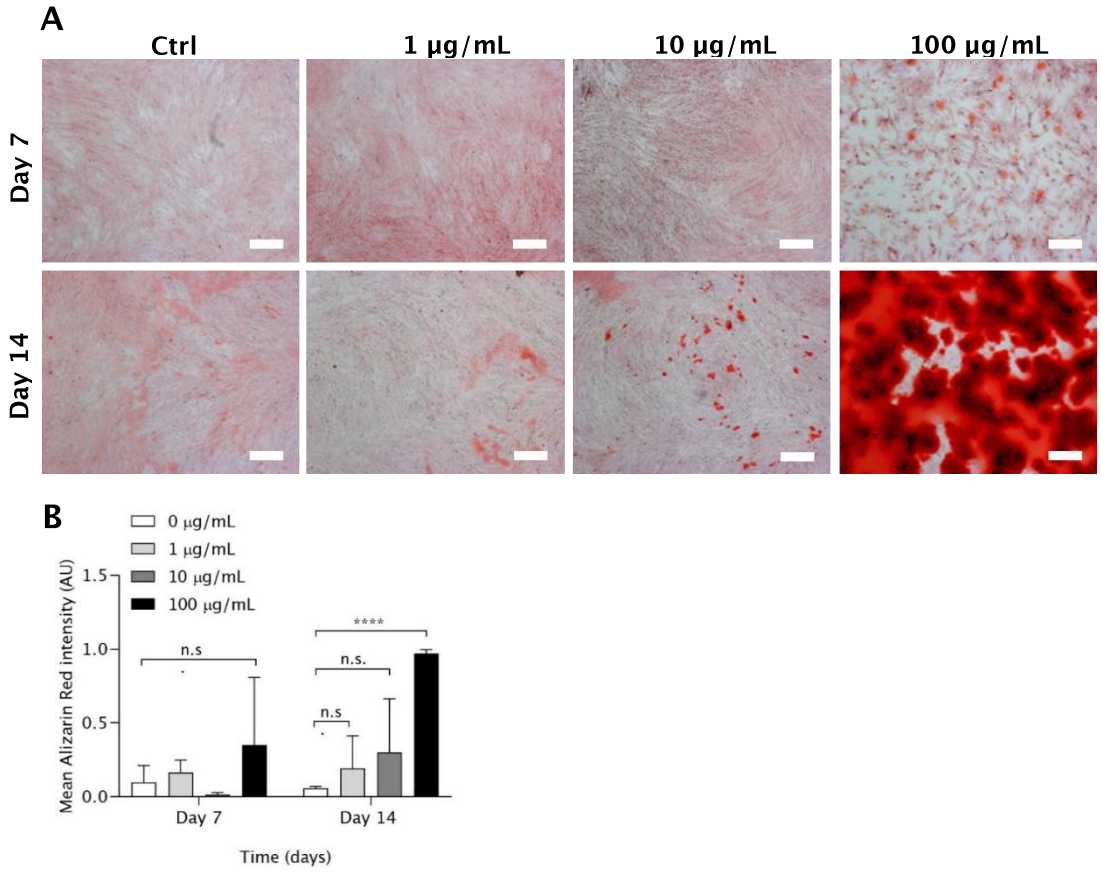

Figure 3. 6 Role of nanoparticle dose in Laponite osteogenic bioactivity as assayed by CaP mineralisation.
(A) Images were taken with Carl Zeiss Axiovert 200 microscope at 2.5x magnification on day 7 and 14 post-exposure to Laponite nanoparticle dispersions. Scale bar = 400 µm. White arrows refer to small mineralised nodules. (B) Quantification of ARS showed clay-mediated enhancement in hBMSCs mineralised nodule formation at 100 µg/mL Laponite on day 14. Cells were treated with Laponite for 3 days followed by media change without Laponite. Statistical analysis was performed using two-way ANOVA followed by Tukey's multiple comparisons test. Data represent mean ± SD, N = 3. ****P < 0.0001; n.s. = not statistically significant.

3.4.4 Effect of Laponite on hBMSCs osteogenic differentiation – role of Laponite exposure time on hBMSCs activity

In order to test the role of Laponite/cell contact time on Laponite osteogenic bioactivity, hBMSCs were incubated with Laponite dispersions for either complete 3 or 7 days denoted d-3 and d-7, respectively, followed by media change without Laponite every 3-4 days. ALP activity, bone-related gene expression and calcium phosphate mineral deposition was assessed at days 1-14 post-Laponite addition. As expected, Laponite significantly increased ALP activity of hBMSCs at both the intracellular (**Figure 3.7A**) and extracellular (**Figures 3.7B**) levels, reaching more than 6-fold increase (****$P < 0.0001$) compared to clay-free negative control. This

clay-enhanced ALP activity trend was sustained until day 14 for both treatment groups. Interestingly, ALP activity of the d7-7 group was significantly higher than that of d7-3 (P= 0.0414). When comparing d14-3 vs d14-7 the ALP staining distribution was different. The d14-3 group showed a more homogenous distribution of ALP stain while the d14-7 group exhibited areas of very high cell density, expressing ALP forming interconnected bridges between aggregated cell structures. Small nodules exhibiting higher ALP staining intensity could be observed at high magnification.

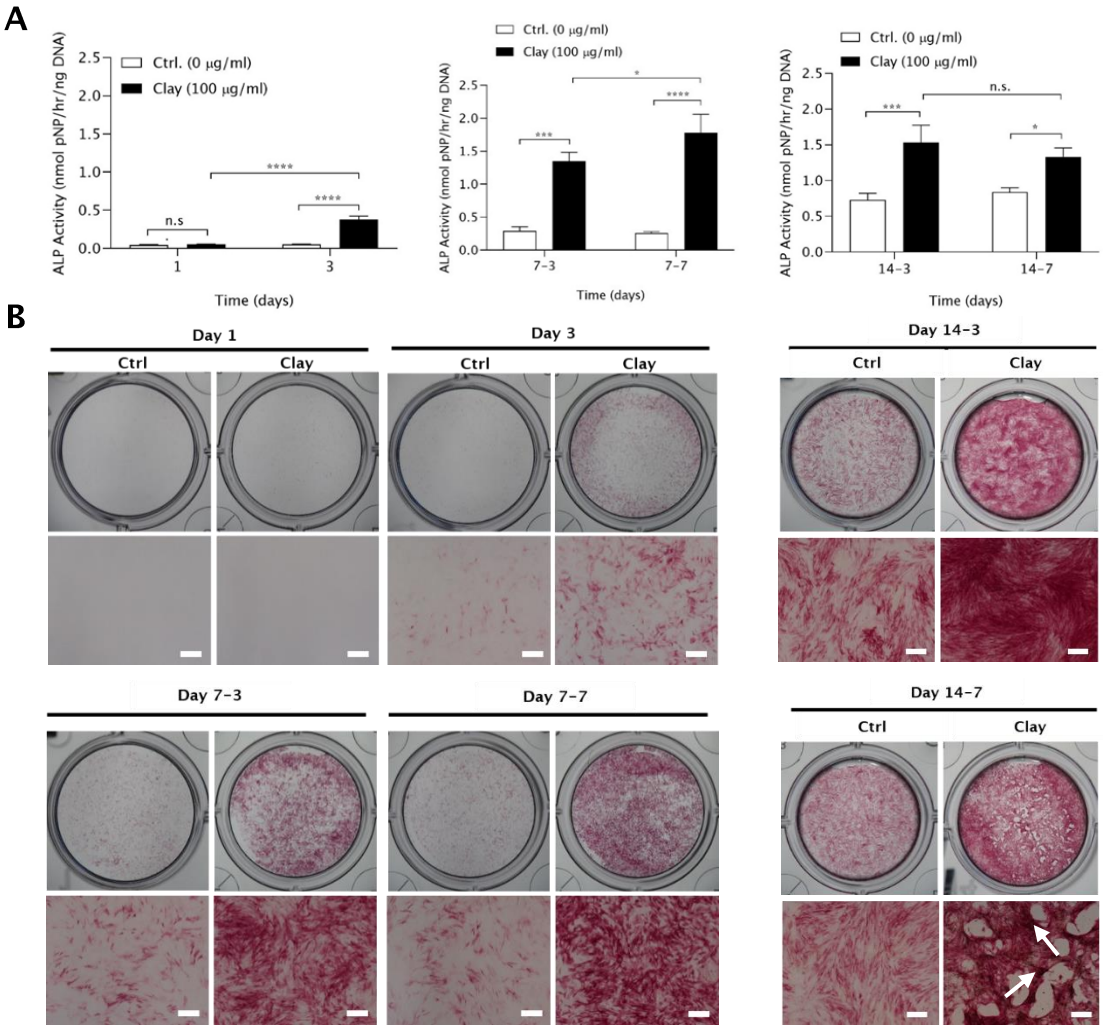

Figure 3. 7 Effect of clay exposure time on intracellular ALP activity (A) and extracellular ALP staining (B) at day 1-14 post-Laponite addition.
High magnification images were taken with Carl Zeiss Axiovert 200 microscope at 2.5x magnification, while whole well images were recorded with Zeiss Stemi 2000 microscope. Scale bar = 400 µm. White arrows refer to areas of intense ALP staining regions which localise with mineralised nodule formation. Cells were treated with Laponite for 3 (d-3) or 7 (d-7) days followed by media change without Laponite. Statistical analysis was performed using two-way ANOVA followed by Tukey's multiple comparisons test. Data represent mean ± SD, N = 3. *P < 0.05; ***P < 0.001; ****P < 0.0001; n.s. = not significant. Day -3 and -7 refer to cells incubated with LAP for 3 and 7 days, respectively.

In order to explore the effects clay nanoparticles exert on osteoblast proliferation/differentiation interrelationship, we investigated the cell proliferation profile of hBMSCs in response to clay exposure time, as previously described for ALP activity experimental design, using PicoGreen dsDNA quantification assay. The addition of Laponite nanoparticles had no or negligible effects on hBMSCs proliferation profile until day 7 for all clay dose conditions tested (d-3 & d-7), except a small decrease in the case of d7-7 clay-treated group although was not statistically significant (**Figure 3.8**). On day 14, although there was no significant effect of both the d14-3 and d14-7 clay-treated groups on cell proliferation when compared to their corresponding negative controls, the d14-7 clay-exposed cells exhibited significantly lower cell number (****$P < 0.0001$) compared to the d14-3 clay-treated ones. This might be attributed to the media change conditions in the d-3 vs d-7 groups rather than a clay exposure time-dependent effect, but when comparing the d14-3 and d14-7 negative controls only (*P <0.05), the statistical difference was not as significant as when adding clay to the system. These data together indicate the effect of clay dose/exposure on hBMSCs proliferation which play an important interrelationship with its osteogenic potential.

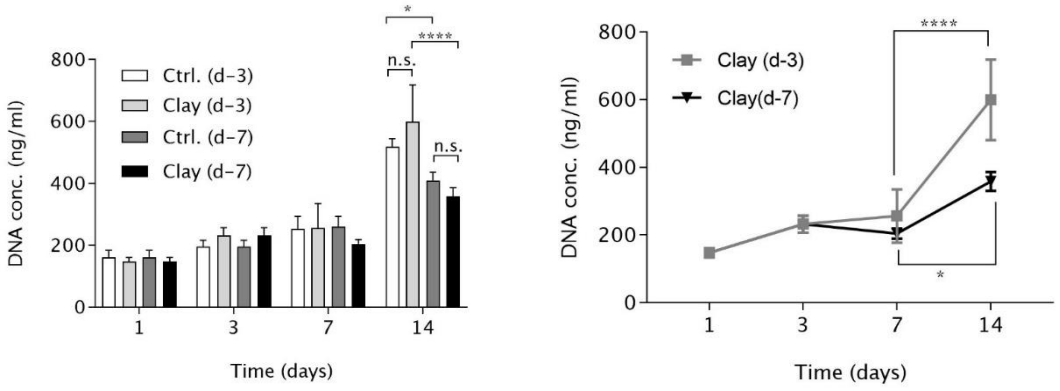

Figure 3. 8 Effect of clay exposure time on hBMSCs proliferation.
Statistical analysis was performed using two-way ANOVA followed by Tukey's multiple comparisons test. Data represent mean ± SD, N = 3. *P < 0.05; ****P < 0.0001; n.s. = not significant.

The effect of clay exposure time on calcium phosphate mineralisation was assessed using alizarin red staining on day 14. As shown in **figure 3.9**, in the absence of Laponite clay nanoparticles, there was not any detectable calcium phosphate minerals in both culture conditions (d-3 & d-7). Likewise, treating hBMSCs with Laponite nanoparticles for only 3 days did not have any significant impact on their mineralisation potential as in the case of negative controls. Interestingly, however, incubating hBMSCs with Laponite nanoparticles for a full period of 7 days, strongly enhanced calcium phosphate mineral growth and deposition and resulted in calcified nodule formation. Furthermore, phase contrast images for the fixed cells in the case of d14-7 clay-treated group showed the formation of dark osteoblast/ECM 3D nodule-like structures.

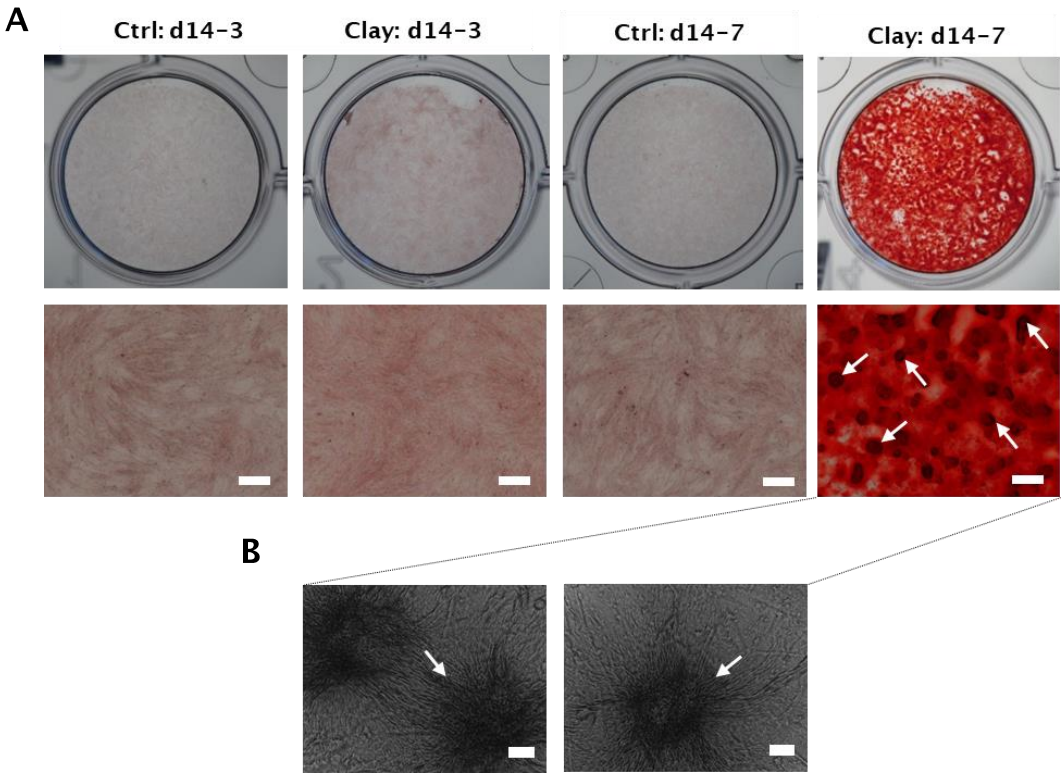

Figure 3. 9 Effect of clay exposure time on hBMSCs-mediated CaP mineralisation. While d14-3 treatments did not have an effect on hBMSCs mineralisation potential, Laponite treatment for 7 days resulted in the formation of bone-like nodules at day 14. High magnification images were taken with Carl Zeiss Axiovert 200 microscope at 2.5x magnification, while whole well images were recorded with Zeiss Stemi 2000 microscope. Scale bar = 400 μm for **A** & 20 μm for **B**. White arrows refer to small mineralised nodules.

These data confirm the strong potential of clay nanoparticles to induce and support terminal *in vitro* osteogenic differentiation of hBMSCs which strongly depends on clay dose and culture time.

The formation of mineralised bone-like nodules starting from human primary stromal cells is challenging with scarcely available data in literature. We decided to the test the reproducibility of Laponite-induced bone nodule formation potential of hBMSCs across different patients. Briefly, ALP activity at day 3 and mineralised nodule formation at day 14 were investigated among the tested patients. As shown in **figure 3.10**, the as-observed clay-enhanced ALP activity of hBMSCs was reproducible among all tested patients, showing more intense staining compared to the negative control in the case of patients 3 and 4 vs. patients 1 and 2.

Interestingly, cells incubated with Laponite in both patients 1 and 2 were able to deposit calcium phosphate crystals in the form of mineralised bone-like nodules with specific mineralisation at the mineralised nodule regions (white arrows). On the other hand, patients 3 and 4 exhibited widespread nonspecific mineralisation across the whole culture which might indicate clay-mediated dystrophic calcification. Moreover, data suggest a positive correlation between the effect of clay particles on early ALP activity and its effect on mineralisation, indicating that there is a level of clay-enhanced early ALP activity above which it leads to non-specific/dystrophic calcification. In agreement, phase contrast high magnification imaging at day 7 showed difference in cell behaviour between both patient groups. For example, in patient 2, cells formed dense clusters with selective mineralisation while in the case of patient 3 the cell monolayer started to be covered with non-specific calcium minerals. These data indicate the complexity in reproducing the as-observed Laponite-induced bone nodule formation of hBMSCs, which might be attributed to the complex patient variation factors such as age, sex, nutrition and medication status which is beyond the time and scope of this thesis.

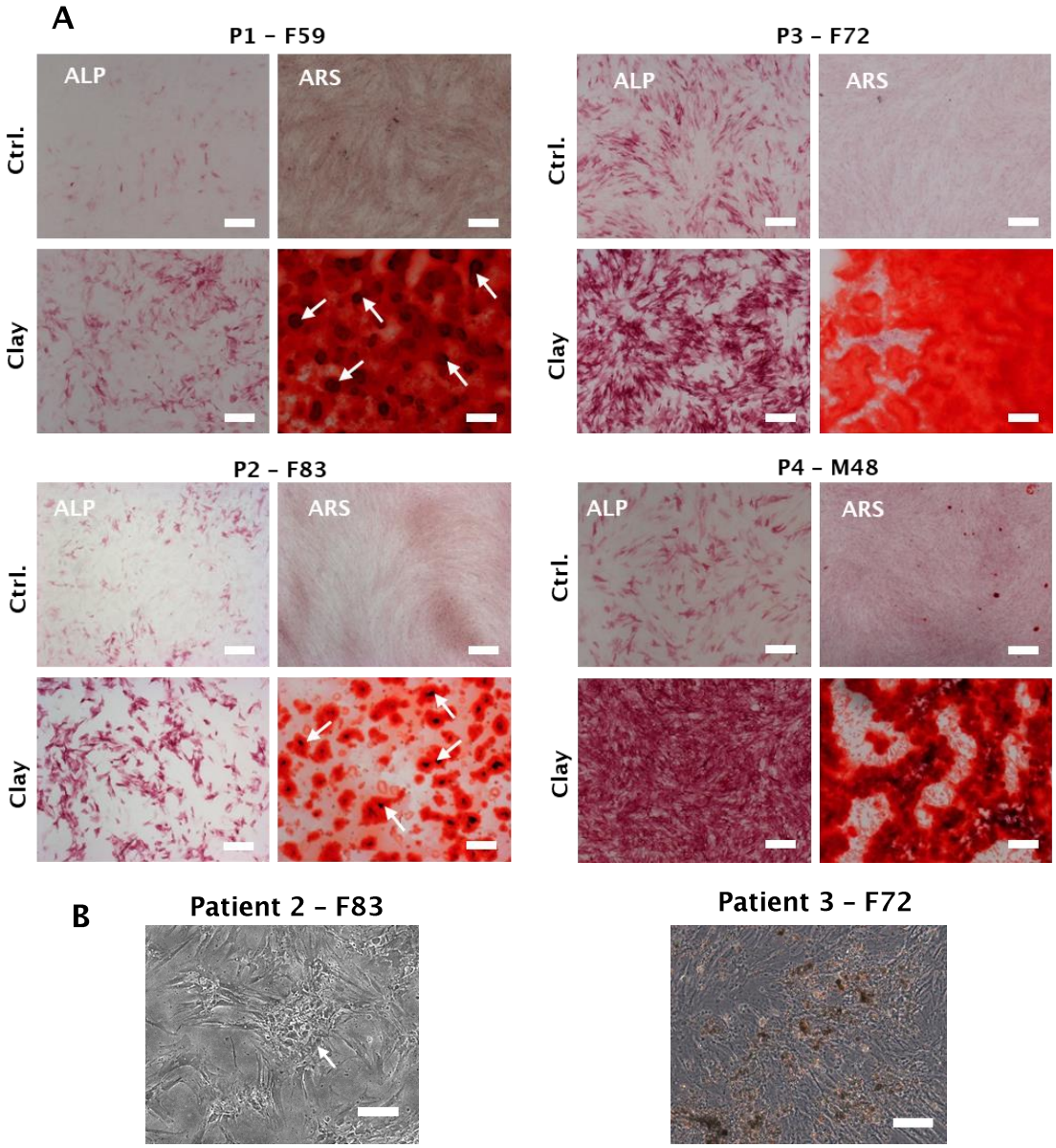

Figure 3. 10 Effect of Laponite clay addition on hBMSCs- mediated mineralised nodule formation across patients.
(A) Patients 1 and 2 showed specific mineralisation in nodular regions, but patients 3 and 4 indicated nonspecific mineralisation across the whole culture. This was found to be correlated with the effect of Laponite on early ALP activity of hBMSCs. (B) Phase contrast imaging at day 7 showing cell clusters formed with patient 2 while wide distribution of nonspecific mineralisation with patient 3. High magnification images were taken with Carl Zeiss Axiovert 200 microscope at 2.5x magnification; Scale bar = 400 μm (A) and 10x magnification; scale bar = 100 μm (B).

Following validating Laponite osteogenic bioactivity on hBMSCs and optimising Laponite/hBMSCs culture conditions in terms of Laponite dose and incubation time we tracked Laponite/hBMSCs interactions at the molecular level during the first week of clay induction (**Figure 3.11**) – a selected time window for subsequently understanding the mechanisms underlying the as observed early Laponite promotion of osteogenesis. The addition of Laponite did not have any significant effect on the gene expression level of both RUNX2 and Osterix transcription factors, except a significant clay-induced decline in Osterix expression at day 7 compared to the negative control ($P < 0.0001$). The effect of Laponite on the early osteogenic markers ALP and COL 1 was strong and sustained. Laponite strongly increased the mRNA expression level of ALP reaching around 15 and 5-fold increase compared to the negative control on day 3 and 7, respectively ($P < 0.0001$). Such clay-induced upregulation of gene expression was also evidenced with COL1 which exhibited around 100% increase in response to clay exposure ($P < 0.0001$ for both day 1 & 7). As expected, the late osteogenic markers OPN and OCN did not exhibit any significant response to Laponite addition in terms of gene expression profile.

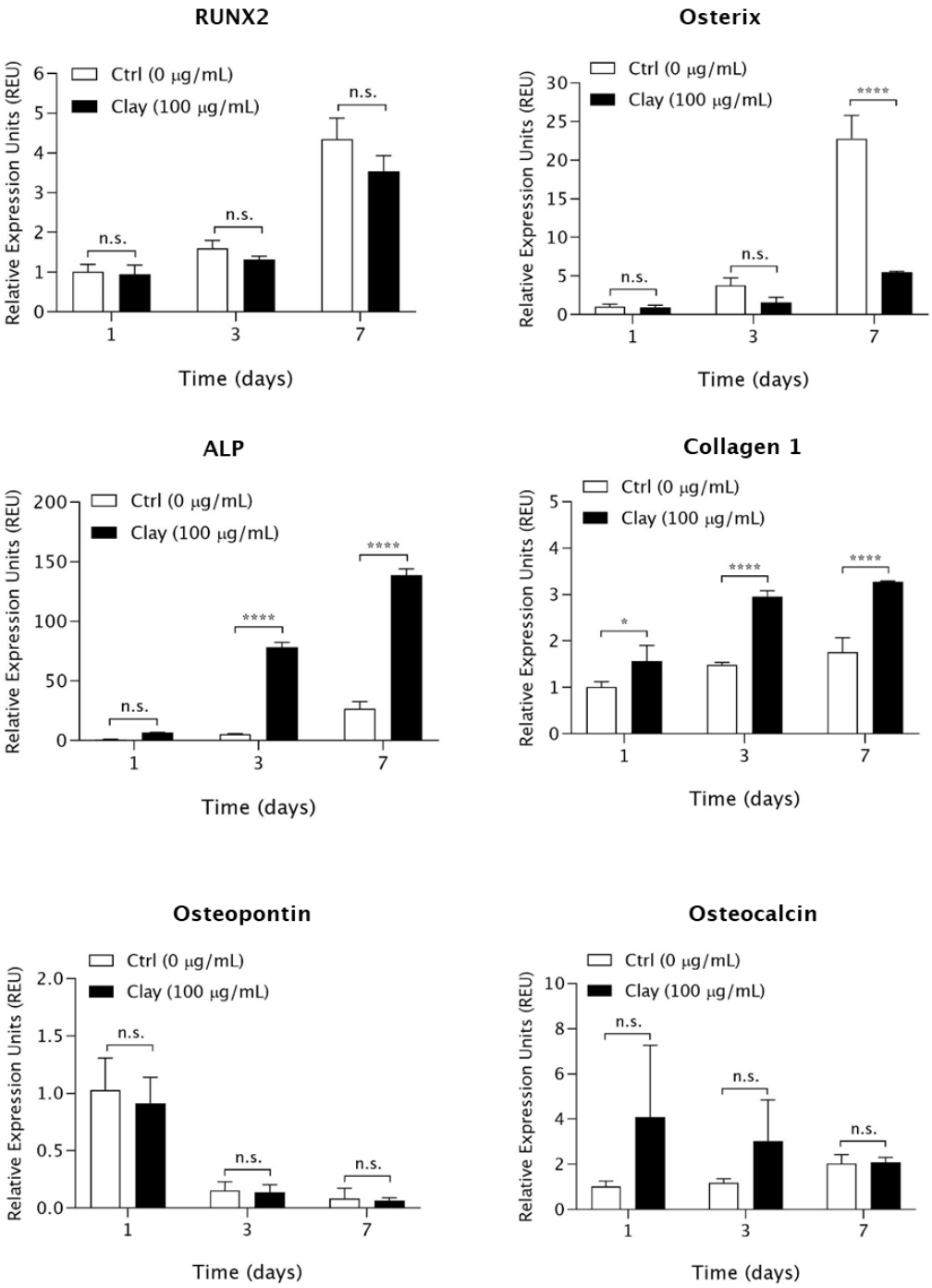

Figure 3. 11 Effect of Laponite on hBMSCs osteogenic gene expression assayed by RT-qPCR during first week of clay induction.
While there was no significant clay influence on gene expression of RUNX2, there was a significant clay-mediated decrease in OSX expression at day 7. Laponite strongly upregulated both ALP and COL1 expression during the tested time-points. However, the late osteogenesis markers OPN and OCN were not affected. Statistical analysis was performed using two-way ANOVA followed by Tukey's multiple comparisons test. Data represent mean ± SD, N = 3. *P < 0.05; ****P < 0.0001; n.s. = not significant.

Discussion and analysis

In this chapter, the cytocompatibility and osteogenic potential of Laponite clay nanoparticles was investigated using human bone marrow stromal cells. An optimisation of Laponite dose and exposure time was performed for reaching the optimal culture conditions to be used for exploring the mechanisms underlying Laponite osteogenic bioactivity in subsequent chapters. Results showed that Laponite nanoparticles are cytocompatible and support cell adhesion and proliferation up to a concentration of 100 µg/mL above which Laponite start to cause cytotoxicity. Laponite was able to induce osteogenic differentiation of hBMSCs in a dose- and time-dependent manner. A clay concentration of 100 µg/mL was an optimal bioactive concentration and a clay exposure duration of 7 days showed enhanced clay osteogenic bioactivity compared to 3 days exposure. This was confirmed by a strong Laponite-enhanced ALP activity, calcified nodule formation and upregulated osteogenic gene expression.

Biocompatibility is a critical prerequisite for the successful application of nanoparticles, in general, for the biomedical field. Results of this study showed that dispersed Laponite nanoparticles are cytocompatible up to 0.1 mg/mL without interfering in cell adhesion, morphology or proliferation profile. This is in agreement with recent studies which confirmed *in vitro* biocompatibility of Laponite at similar concentration range as demonstrated by unaffected cell metabolic activity, plasma membrane integrity as well as reactive oxygen species (ROS) and reactive nitrogen species (RNS) production[130,131,250,268]. Furthermore, Laponite degrade into nontoxic absorbable products ($Si(OH)_4$, Mg^{2+}, Li^+ & Na^+) which makes Laponite an attractive new nano-/biomaterial[134,243,272]. The biocompatibility of Laponite have been convincingly demonstrated *in vivo* as well[273]. Mice injected with Laponite stayed quite healthy exhibiting nearly complete clearance of Laponite at 45 days post-treatment, normal levels of blood routine parameters (Hb, WBC & PLT) and serum biochemistry parameters (AST, ALT, total Bilirubin, Creatinine & Carbamide) and no noticeable organ damage/abnormality[273].

An interesting observation of this study is that above the previously mentioned biocompatible Laponite dose (>0.1 mg/mL) Laponite led to a significant reduction in cell metabolic activity. This is in agreement with various studies which reported a conc. threshold for Laponite above which Laponite start to be cytotoxic[130,131,250,268].

One possible explanation is that at such high clay concentration Laponite particles start to aggregate into small clusters which cover the cell surface, physically block most of the membrane channels and consequently impair cellular metabolism and cytoskeleton organisation[147,130,131, 267]. Alternatively, these Laponite aggregates might accumulate inside the cell to interact with subcellular compartments such as mitochondria and endoplasmic reticulum and restrict cellular functionality as for example inducing cell oxidative stress[274]. Therefore, a Laponite dose of 1-100 μg/mL was selected for subsequent experiments investigating the osteogenic bioactivity of Laponite.

After confirming biocompatibility of Laponite nanoparticles, Laponite osteogenic bioactivity was investigated. Laponite was able to stimulate early osteogenic differentiation of hBMSCs. This is evidenced by Laponite-mediated enhancement of osteogenic markers including ALP activity, bone-related gene expression and calcium phosphate mineral deposition. The osteogenic differentiation of hBMSCs follows a temporal pattern of sequential stages characterised by expression and synthesis of certain molecular markers namely proliferation, ECM development and maturation and ECM mineralisation stages[58]. Briefly, upon osteogenic induction, bone-related transcription factors such as RUNX2 and OSX become activated and the cells committed to osteoprogenitors which enter the proliferation stage and express collagen type I and fibronectin. In stage 2, the cells exit the cell cycle and start differentiation while synthesizing and secreting alkaline phosphatase and collagen type I for the extracellular matrix maturation. In stage 3, the ECM becomes enriched with osteocalcin and osteopontin and calcium phosphate mineral deposition takes place. Therefore, ALP and COLI represent early markers of hBMSCs osteogenic differentiation while OPN, OCN and calcium deposition represent late osteogenic markers[11]. Therefore, we observed a significant and sustained increase in ALP activity during the first two weeks of clay induction starting from day 3. ALP is a key phenotypic marker of osteogenic differentiation and plays a critical role in ECM mineralisation by releasing inorganic phosphate (Pi) from pyrophosphate (PPi) [275,276].Another early osteogenic marker that was significantly activated upon clay addition even at very early stage (day 3) is collagen type 1, which is the most abundant extracellular protein in bone, gives bone its tensile strength and play essential role in bone formation and mineralisation[2,25]. Interestingly, however, such

observed clay promotion of osteogenesis was independent of RUNX2 activation and accompanied by a strong suppression of Osterix gene expression. RUNX2 and Osterix are well-known as the master transcription factors which regulate osteoprogenitor commitment and differentiation either independently or in an orchestrated manner[60,61,63,64,277]. During normal osteogenesis, RUNX2 and Osterix induce MSCs commitment to immature osteoblasts whereas RUNX2/Osterix has to be downregulated for differentiation into mature osteoblasts[278]. Moreover, other transcription factors have been reported to control osteoblast differentiation even in a RUNX2-independent pathway such as Msh homeobox 2 (MSX2), distal-less homeobox 5 (DLX5) and activating transcription factor 4 (ATF4)[277 279]. Therefore, it is possible that Laponite may induce hBMSCs commitment to the osteogenic lineage through one of these transcription factors independent of RUNX2 to downregulate OSX expression at later stage of osteoblast maturation or that the main role of Laponite might be promoting osteogenic development of immature osteoblasts already committed though other pathways not involving Laponite – for example the effect of osteogenic supplements and growth factors present in culture media. Further experiments are warranted to test this interpretation.

Regarding late osteogenic markers. Laponite addition led to formation of calcified bone-like nodules at an early stage (day 14) as observed by specific 3D cellular aggregates rich in calcium phosphate minerals. The formation of bone-like nodules represents a late stage of osteoblast differentiation and data available in literature showing terminal *in vitro* osteogenic differentiation starting from human (primary) bone marrow stromal cells, especially at day 14, are lacking[270]. However, a limitation of this study is that we relied on ARS staining and microscopy morphological examination which does not confirm the phase/nature of calcium minerals deposited for example whether it is nonspecific dystrophic calcification of amorphous calcium phosphate or ECM-mediated mature hydroxyapatite crystals. This must be evidenced by more advanced chemical techniques for example using SEM-EDX[280,281,] for determination of 3D nodule structure and elemental ratios of calcium, phosphorus, and carbon combined with Raman spectroscopy to detect functional groups for cells, ECM and tissues[280,282] with native bone as positive control[280]. These are important future experiments that need further exploration to correctly confirm and harness the ability of Laponite for bone tissue regeneration. Another limitation here is that the

gene expression data were only at the first week of clay induction which is not enough time window to highlight the role of late osteogenic markers OCN and OPN which are activated during the late stage of mineralisation. Therefore, we did not observe any significant influence of Laponite on OCN or OPN until day 7 which makes interpreting the observed clay-mediated nodule formation at day 14 difficult to interpret. Several studies suggest the role of OCN in regulating bone mineral maturation and turnover[283,284]. OPN plays an important role in bone remodeliing[284,285]. The expression of these late marker genes OPN and OCN is a good indicator of upcoming formation of mineralised bone-like nodules which can further develop into 3D mineralised structures. Future experiments are warranted to extend examining the influence of Laponite on temporal molecular profile of hBMSCs to longer time points (at least until day 14). We focused on the first week of clay induction as the early observed clay promotion of ALP activity is intriguing, reproducible and represent an attractive model for screening the various complex pathways of Laponite bioactivity.

After validating the biocompatibility and osteogenic bioactivity of Laponite, the role of Laponite culture conditions, including clay dose and incubation time on Laponite osteogenic bioactivity, was investigated. The results show that Laponite exerts its osteogenic character in a dose- and time-dependent manner. The highest Laponite dose (0.1 mg/mL) and exposure time (7 days) achieved the strongest osteogenic effect. This dose- and time-dependent osteogenic effect of Laponite can be interpreted from different angles including: 1) Extracellular model: the effect of clay nanoparticles on hBMSCs osteogenesis might be not restricted to intracellular effects but extracellular role as well and using low Laponite dose or washing Laponite off on day 3 make this extracellular clay-mediated effect on the cell insufficiently induced or interrupted, respectively. Examples of the extracellular osteogenic role of Laponite include Laponite-cell membrane, Laponite-extracellular protein and Laponite-culture media interactions[265,130,131,250,265]. 2) Intracellular role: It could be that Laponite exert its osteogenic action mainly through intracellular modes by interacting with specific intracellular osteogenic signalling pathway. Therefore, it is possible that low Laponite dose (<0.1 mg/mL) or 3 days culture period was not enough to trigger these intracellular pathways. This necessitates the need for ICP-MS and TEM uptake study which until now not explored[265,130,131,250,265]. Gaharwar and colleagues reported a similar dose-dependent osteogenic effect of Laponite on mesenchymal stem cells but

with no attention to the role of exposure time[130,131,268]. Most previous work on nanoparticles rely on using relatively low dosage at short period of time which does not mimic the real exposure environment of implanted material *in vivo*[286]. Results of this study show a persistent/sustained osteogenic properties of Laponite with increasing incubation time and before Laponite clearance which better mimic *in vivo* target for bone regeneration.

3.6. Conclusion

The main objective of this study was to investigate the biocompatibility and osteogenic bioactivity of Laponite clay nanoparticles and optimize Laponite culture conditions with hBMSCs for subsequent understanding of the mechanisms underlying Laponite bioactivity – the central aim of this thesis. Laponite proved biocompatible at doses lower than 0.1 mg/mL, supported cell adhesion and promoted osteoblast differentiation in a dose- and time-dependent manner. A clay concentration of 0.1 mg/mL and 7 days exposure time showed an optimal Laponite osteogenic effect therefore these conditions were selected for next chapters to track Laponite-hBMSCs interaction mechanisms. This chapter validate the exciting potential of Laponite as a new bioactive additive and/or scaffold for bone formation and sets the basis for elucidating the right mechanism(s) behind Laponite bioactivity which is the focus of the subsequent chapters of this thesis.

Chapter 4: Exploring Laponite effects on alkaline phosphatase activity

4.1 Introduction

The previous chapter demonstrated the consistent ability of Laponite clay nanoparticles to enhance alkaline phosphatase gene expression and enzyme activity even at a very early stage of hBMSCs culture. Alkaline phosphatase is an accepted phenotypic marker for osteoblast differentiation and necessary for postnatal bone formation[287]. Loss-of-function mutation in *ALPL* gene is associated with a severe skeletal disease, hypophosphatasia, which is characterized by bone mass loss and, consequently, pathological fractures[288]. Moreover, ALP upregulation *in vitro,* in response to external osteogenic stimuli, showed interesting correlation with the capacity of BMSCs to form bone *in vivo* [289,290]. Therefore, we were particularly interested in understanding how Laponite nanoparticles drive such strong enhancement of hBMSCs ALP activity. Answering this question may provide important insights into the mechanism(s) behind Laponite osteogenic bioactivity.

Based on the hypothesis drawn in the introduction chapter this chapter will explore three potential pathways by which Laponite may exert its osteogenic effects on hBMSCs – focusing particularly on induction of alkaline phosphatase activity. Given the strong affinity of clays for protein, as well as their well-known applications in catalysis it is important to consider the possibility of a direct effect of Laponite on the alkaline phosphatase enzyme itself. To provide one rather striking example, a study conducted by Yang et al. seeking to mimic precellular biochemical processes during early-life evolution found that Laponite clay gels were able to consistently enhance the transcription and translation of nucleic acids (a process involving more than 30 enzymatic reactions) in a cell lysate solution compared to clay free-controls[264]. Although various studies have explored this pathway on different clay minerals such as kaolinite, montmorillonite, and illite[291–293], data regarding the influence of Laponite on ALP activity are lacking.

Regarding Laponite-cell interaction, Laponite nanoparticles might affect cell osteogenic function intracellularly, extracellularly or through direct interaction with the cell membrane[265]. Endocytosis is frequently suggested as playing a key role in the cellular response to Laponite. In particular, endocytosed Laponite particles might release osteogenic cues such as silicon[130–132,140], interact with proteins involved in osteogenic signals or enhance transport of bioactive molecules/ions [259, 260]. However, the role of extracellular Laponite can't be neglected as its rich surface chemistry

combined with its heterogenous charge distribution allow for a wide range of interactions not only with the cells but also with extracellular components. For example, compared to dispersed Laponite nanoparticles applied as culture media additives, similar osteogenic properties of clay were also clearly observed when incorporated in polymeric matrices as 2D or 3D scaffolds or applied as clay gel[245] which limit/slow nanoparticle uptake indicating a possible extracellular role of clay[245,132]. Therefore, the first question we decided to explore is which of these main pathways (intracellular vs extracellular) is responsible for the osteogenic effect of Laponite. An intracellular effect is likely to be mediated by endocytosis and while endocytosis of clay has been confirmed in other studies[250], its requirement for Laponite promotion of hBMSCs osteogenic differentiation demonstrated in ALP activity has not been explored. Answering this question will allow us to narrow the focus of subsequent investigations.

Following Laponite endocytosis and fusion with lysosomal bodies, as reported by previous studies[250], Laponite is expected to undergo dissolution into nontoxic ionic products (Na^+, Li^+, Mg^{2+} & $Si(OH)_4$) due to the action of lysosomal digestive environment mediated by low pH (~4.5) and hydrolytic enzymes[265,294]. In addition, Laponite degradation seems possible for extracellular particles in cell culture media. It was found that at clay concentration below 2 mg/mL and at medium pH < 9, Laponite particles are vulnerable for chemical degradation with decreasing pH value according to the following equation[134,243,258].

$$Na_{0.7}Si_8Mg_{5.5}Li_{0.3}O_{20}(OH)_4 + 12H^+ + 8H_2O \longrightarrow 0.7Na^+ + 8\,Si(OH)_4 + 5.3Mg^{2+} + 0.4Li^+ \quad (Eq1)$$

These Laponite degradation products $Si(OH)_4$, Mg^{2+}, and Li^+ have been frequently hypothesised as the main mode of action for nanoclay bioactivity due to their inherent osteogenic properties reported in literature. Orthosilicic acid promote collagen type 1 synthesis and osteoblast differentiation[254], silicon play an important role in bone calcification[295] and silicate ions (SiO_3^{2-}) significantly enhanced bone-related expression and mineralised nodule formation[296]. Magnesium ions are involved in activating osteogenesis-regulating pathways ((HIF-1α and PGC-1α)[251,252] and are essential for integrin adhesion to biomaterial surfaces[253]. Lithium is known to activate canonical Wnt-responsive osteogenic genes through the inhibition of GSK3β and in

turn stimulate stem cell osteogenic differentiation[255,73]. Despite their intriguing osteogenic properties, almost no data are available in literature exploring their role in nanoclay osteogenic character demonstrated in ALP activity.

In this study the role of Laponite-ALP interaction vs Laponite-cell interaction was explored as possible mechanisms behind Laponite-promotion of ALP activity. The former started with exploring the adoption capacity and isotherm of ALP by Laponite and the subsequent Laponite-mediated change in catalytic activity of immobilized ALP. The role of Laponite endocytosis was investigated by blocking/inhibiting Laponite cellular uptake using an endocytosis inhibitor and subsequently assessing ALP activity at day 3. Finally, the role of Laponite degradation products in Laponite-enhanced ALP activity was investigated by incubating hBMSCs with salt solutions at concentrations that provide lithium, magnesium and silicate ions at exactly the same concentration to be released from Laponite assuming complete particle degradation at clay dose 0-100 µg/mL.

4.2 Hypothesis and aims

This study was performed to test the hypothesis that Laponite enhance ALP activity in hBMSCs cultures through direct interaction with ALP enzyme and through Laponite endocytosis and subsequent release of osteogenic degradation products ($Si(OH)_4$, Mg^{2+} & Li^{+}).

In summary, the aim of the work in this chapter is to:

1. Measure the capacity of Laponite for ALP adsorption and subsequent influence on ALP activity.
2. Determine the effect of Laponite endocytosis inhibition on ALP activity of hBMSCs.
3. Test the effect of Si, Mg and Li ions, applied as salt solutions, vs. intact Laponite particles on hBMSCs ALP activity.

4.3 Methods

4.3.1 Role of Laponite-ALP enzyme interaction

The effect of Laponite on ALP enzymatic activity was monitored using lyophilized ALP from bovine intestinal mucosa (P7640, Sigma Aldrich) in a cell-free system. First, the adsorption kinetics of ALP on/in Laponite was investigated to determine the optimal ALP/Laponite incubation time for subsequent experiments. Two separate solutions were prepared including 10 mg/mL Laponite and 1 mg/mL ALP in Tris-buffered saline (25 mM Tris, 150 mM NaCl and pH 7.6). 0.5 mL of the Laponite dispersion was mixed with an equivalent volume of ALP solution for a final Laponite and ALP concentrations of 5 mg/mL and 0.5 mg/mL respectively. Then, the mixture was gently shaken in the dark at 37 °C and 5% CO_2 for 0, 10, 30, 60, 120 and 240 min. These conditions both represent cell-mimicking physiological conditions and are optimal for ALP activity according to manufacturer protocol. Samples were run in triplicates. At each selected time point, the ALP/Laponite mixture was centrifuged at 12,000 *xg* for 15 min at 4 °C to separate clay-adsorbed ALP from the free unbound enzyme in supernatant. Next, the supernatant was transferred to chilled Eppendorf tubes for protein (ALP) quantification using Pierce™ Coomassie (Bradford) Protein Assay Kit (23200, ThermoFisher Scientific). The amount of enzyme adsorbed was calculated from the difference between the amount of enzyme added and that remaining in the supernatant according to the following formula: $Q_e = \frac{(C_0 - C_e)V}{w}$; where Q_e is the amount of adsorbed ALP in µg/mg Laponite, C_0 is the initial concentration of ALP (before adsorption) in µg/mL, C_e is the concentration of ALP at equilibrium (after absorption; in supernatant) in µg/mL, V is the volume of reaction/adsorption solution (1 mL) and W is the weight of adsorbent/Laponite (5 mg).

For protein quantification of supernatant ALP sample, ALP standards at conc. 0–2 mg/mL were prepared in Tris-buffered saline (TBS). 30 µL of unknown sample or standard was pipetted into 2 mL test tube, mixed well with 1 mL Coomassie reagent and incubated in the dark for 10 min at room temperature. Absorbance was measured at 595 nm using standard spectrophotometer. Coomassie dye changes its absorption maximum from 465 nm to 595 nm when binds a protein. The average 595 nm measurement for the Blank replicates was subtracted from the 595 nm measurements of all other individual standard and unknown sample replicates. Then, ALP conc. of each unknown sample was determined from the plotted standard curve.

Based on adsorption equilibrium time which was found 120 min, adsorption isotherm of ALP on/in Laponite was explored at fixed 5 mg/mL Laponite vs. a series of ALP concentrations 0, 0.1, 0.25, 0.5, 1, 1.5 & 2 mg/mL in Tris-buffered saline (pH = 7.6). Mixtures were gently shaken in the dark at 37 °C for 2 h. Mixtures were centrifuged, and supernatant collected for protein quantification as described above. The adsorption isotherm was obtained by plotting the series of equilibrium ALP conc. (C_e) vs the corresponding amounts of adsorbed ALP (Q_e).

Based on results from the adsorption experiments, the effect of Laponite on ALP activity was investigated by comparing the activity free unbound enzyme vs it's immobilised from. In summary, Laponite/enzyme complex was prepared by mixing Laponite and ALP solutions at final concentration of 5 mg/mL and 0.25 mg/mL, respectively, in Tris-buffered saline. On the other hand, ALP enzyme alone in Tris-buffered saline at 0.25 mg/mL was used as positive control (free enzyme). Samples were run in triplicates and shaken gently for 2 h at 37 °C, 5% CO_2 in the dark. Next, both clay/enzyme complex and free enzyme samples were moved for assessing ALP activity. No centrifugation/separation was performed here as under these conditions (0.25 mL ALP & 2 h incubation) 100% of the enzyme was adsorbed by Laponite. 20 µL of each unknown sample was pipetted into transparent flat bottom 96-well plate to which added 80 µL/well increasing phosphatase substrate concentrations (0-1000 µM) in 1.5 M Alkaline buffer (Sigma A9226). Plates were incubated in dark at 37 °C, 5% CO_2 for 10 min and the reaction stopped by adding 100 µL/well 1 M NaOH. Finally, colour absorbance was measured using ELx800 microplate reader (BioTek, Winooski, USA) at 415 nm. ALP activity of free and bound enzyme was calculated as conc. of product/hour based on the obtained absorbance, ALP product standard curve and incubation time.

4.3.2 Role of Laponite endocytosis

4.3.2.1 Cytocompatibility of endocytosis inhibitor

We first started with screening for the cytocompatibile dose of endocytosis inhibitor, here chlorpromazine hydrochloride (CPZ), to be used for subsequently assessing the effect of Laponite endocytosis blocking on Laponite promotion of ALP activity. hBMSCs at 70-80% confluence (P2) were seeded at 96-well plates at density of 10^4 cells/cm^2 in basal media and allowed to adhere overnight at 37 °C, 5% CO_2. Then,

CPZ was prepared in dH_2O, filter-sterilised then diluted in basal culture medium at final concentration range 0-10 µg/mL. dH_2O was used as vehicle control in basal medium (negative control). Culture media was replaced with CPZ-containing vs. CPZ-free media and incubated for 6, 12 and 24 h. At each selected time point, cell variability using the WST-1 assay as described above. Briefly, culture media discarded, cells washed twice with DPBS and added fresh basal media supplemented with WST-1 (1:10 dilution). Then plates were put on an orbital shaker for one minute to ensure homogenous distribution of color, followed by 1 h incubation at 37 °C, 5% CO_2. Finally, the absorbance of the samples was measured using EL-800 Universal Microplate Reader (BioTek Instruments Inc., Winooski, USA) at 450 nm. Cell viability was expressed as a percentage relative to the control groups (without CPZ) after subtraction of the background absorbance.

4.3.2.2 Validation of endocytosis inhibitor efficacy

For assessing the inhibition efficacy of chlorpromazine hydrochloride on Laponite uptake, cells were seeded at density of 10^4 cells/cm^2 in a 24-well plate on # 1.5 sterilised glass coverslips in basal medium and left to adhere for 24 h. Next, culture media was discarded, cells washed twice with DPBS and were pre-treated with basal media with or without CPZ at 5 µg/mL for 2 h then replaced by either plain basal media for negative control or basal media containing RB-Laponite in presence or absence of 5 µg/mL CPZ for clay-treated groups. Cells incubated for 24 h at 37 °C, 5% CO_2. Next, samples were prepared for confocal imaging as following: culture media discarded, then cells washed with DBPS, and incubated with DAPI staining (D1306, Invitrogen), (1/2500 dilution of the 5 mg/mL stock), at room temperature for 15 min. Then, DAPI solution was removed and cells washed with DBPS and incubated with CellMask™ Deep Red plasma membrane stain (C10046, Invitrogen) at 5 conc. of µg/mL in DPBS for 10 min at 37 °C. Cell mask stain removed, cells washed twice with DPBS and detached through incubation with 0.2 mL/well trypsin/EDTA 1x for 5 min at 37 °C, 5% CO_2. Tapped gently to detach the cells and added 0.8 mL basal media/well to deactivate trypsin/EDTA action then put in 1.5 Eppendorf for centrifugation at 400 RCF for 5 min at 21 °C. Supernatant discarded, and cell pellet resuspended and fixed in 0.2 mL 4% PFA and for 10 min at room temperature. Fixed cell suspension was transferred into µ-Slide 8 Well Glass Bottom chamber (80827, Ibidi) freshly coated with 1% Alcian Blue in H_2O. Cells were

imaged immediately by Leica TCS-SP8 Confocal Microscope equipped with Leica LAS-X software.

4.3.2.3 Effect of endocytosis inhibition on Laponite induction of ALP

hBMSCs at 70-80% confluence and passage P2 were detached from culture flasks and seeded at 10^4 cells/cm^2 in 24-well plate in basal medium and allowed to adhere overnight. Next day, basal culture media with and without CPZ were prepared by first dissolving CPZ in dH_2O at a conc. of 1 mg/mL, filter-sterilized and diluted in basal culture media for a final conc. of 5 µg/mL. CPZ-free dH_2O was used for negative control (cells without CPZ). Culture media was discarded, cells washed twice with DPBS then incubated with or without CPZ in basal media for 2 h. Then, Laponite nanoparticles were dispersed in basal and osteogenic culture media at final conc. of 100 µg/mL which then supplemented with either CPZ (final conc. is 5 µg/mL) or dH_2O for CPZ-treated and CPZ-free sample groups respectively. Therefore, 4 sample groups were generated including cells alone (without Laponite & without CPZ), cells + CPZ (without Laponite), cells + Laponite (without CPZ) and cells + Laponite + CPZ. Then, the as-prepared basal and osteogenic culture media with or without Laponite/CPZ were added to the corresponding cell wells and incubated at 37 °C, 5% CO_2 for three days (**Figure 4.1**). At day 3, ALP activity was assayed as described in **section 2.4.2.**

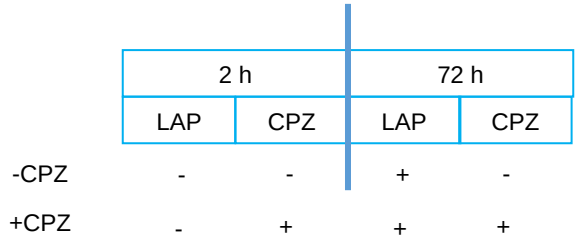

Figure 4. 1 Representation of procedures followed for assessing the role of particle endocytosis on Laponite osteogenic bioactivity.

4.3.3 Role of Laponite degradation products

For clarifying the role of Laponite degradation products in Laponite osteogenic bioactivity, hBMSCs were incubated with osteogenic culture media supplemented with LiCl, $MgSO_4$ and Na_2SiO_3 salt solutions at concentrations that provide Li, Mg and Si ions at exactly the same concentration present in Laponite at nanoclay dose 0-100 µg/mL (**Table 4.1**). Salt in group A and Group B were called providing and excluding salts, which provide the ion of interest and exclude the role of counter ion,

respectively. Standard Laponite powder was used at the same nanoclay conc. (0, 25, 50 & 100 µg/mL) as a positive control.

Briefly, hBMSCs were seeded at 10^4 cells/cm^2 in 24-well plates and allowed to adhere overnight in basal culture media. Next day, intact Laponite particles in osteogenic media were prepared at conc. of 0, 25, 50 and 100 µg/mL as described previously in **section 2.3.** Providing and excluding salts for Li, Mg and Si ions in osteogenic culture media were prepared as following: Salt powder was dissolved in plain alpha MEM, filter-sterilized then diluted to the required final ion conc. reported in **table 4.1** using osteogenic culture media. Then, existing culture media was replaced with osteogenic media containing Laponite, Li, Mg and Si salts and incubated for 3 days. At day 3, ALP activity was assayed as in **section 2.4.2.**

Laponite Conc. (µg/mL)	Salt & corresponding ion conc. (µg/mL)					
	Group A (Na_2SiO_3) – to provide Si^{4+}			Group B (NaCl) – to exclude Na^+		
	Salt	Si	Na	Salt	Si	Na
0	0	0	0	0	0	0
25	31.835	7.325	10.3	26.15	0	10.3
50	63.67	14.65	20.6	52.3	0	20.6
100	127.34	29.3	41.2	104.6	0	41.2

Laponite Conc. (µg/mL)	Salt & corresponding ion conc. (µg/mL)					
	Group A ($MgSO_4$) – to provide Mg^{2+}			Group B (Na_2SO_4) – to exclude SO_4^{2-}		
	Salt	Mg	SO_4	Salt	Mg	SO_4
0	0	0	0	0	0	0
25	21.675	4.375	17.25	25.5	0	17.25
50	43.35	8.75	34.5	51	0	34.5
100	86.7	17.5	69	102	0	69

Laponite Conc. (µg/mL)	Salt & corresponding ion conc. (µg/mL)					
	Group A (LiCl) – to provide Li^+			Group B (NaCl) – to exclude Cl^-		
	Salt	Li	Cl	Salt	Li	Cl
0	0	0	0	0	0	0
25	0.4125	0.0675	0.345	0.56875	0	0.345
50	0.825	0.135	0.69	1.1375	0	0.69
100	1.65	0.27	1.38	2.275	0	1.38

Table 4. 1 Concentration of providing and excluding salts and the corresponding ionic concentrations used to test the effect of clay degradation products on Laponite bioactivity. Highlighted cells refer to Si, Mg, and Li ion concentrations obtained assuming complete clay particle degradation at clay corresponding clay doses of 0, 25, 50 & 100 µg/mL.

4.4 Results

4.4.1 Role of Laponite-ALP interaction

4.4.1.1 Adsorption kinetics of ALP on Laponite

Clay minerals have shown strong affinity for enzyme adsorption/immobilization and subsequent enzyme activity alteration[291,292,293] – a likely scenario through which Laponite might enhance ALP activity in hBMSCs cultures. To test this hypothesis, we first explored whether Laponite adsorbs ALP and the associated adsorption kinetics. At only 10 min of enzyme-clay interaction time, around 50% of initial ALP was rapidly adsorbed indicating strong affinity of Laponite for ALP immobilisation (**Figure 4.2**). Next, longer stirring times exhibited a slower rate of enzyme adsorption with 90% of total ALP adsorbed at 120 min and saturation level achieved at 240 min. 2 h was selected as an optimal stirring time for subsequent experiments.

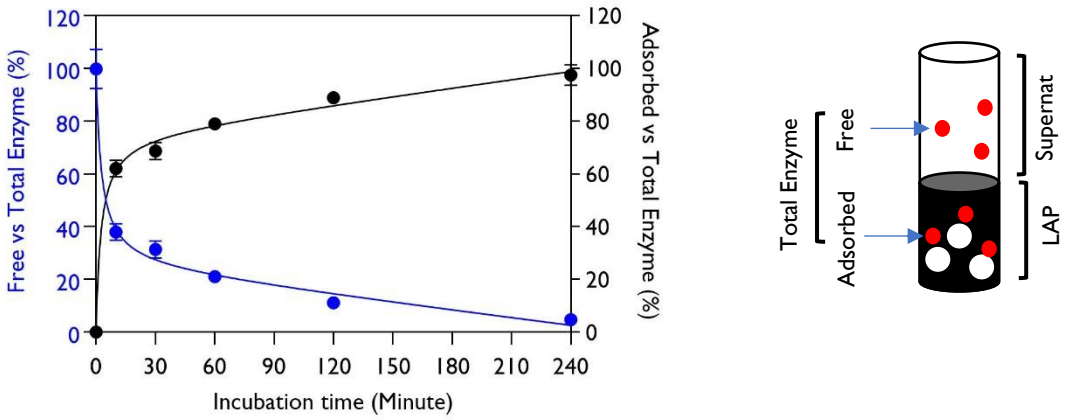

Figure 4. 2 Amount of ALP enzyme adsorbed on/in Laponite (black line) and free in the supernatant (blue line) as a function of duration of incubation.
Error bars represent ± SD, N=3.

4.4.1.2 Adsorption isotherm of ALP on Laponite

Next, we moved to explore which isotherm model best fit/describe ALP adsorption on Laponite. As shown in **Figure 4.3A**, the adsorption curve belonged to the L-type with strong adsorption capacity of Laponite at low doses of ALP (0-250 µg/mL) then followed a lower increase behaviour of adsorbed ALP amount until 500 µg/mL adsorbate. The adsorption saturation level was reached at ALP conc. ≥ 500 µg/mL. This indicates that ALP adsorption capacity of Laponite is not a simple linear increase with increasing initial ALP concentration but reaches a limit at specific ALP/Laponite ratio (here is ~1:10 wt./wt.).

Two main adsorption isotherm models of clay minerals have been used to describe the experimental results of ALP adsorption on clay minerals - Langmuir & Freundlich. The linear form of Langmuir isotherm is expressed by the following equation $Q_e^{-1} = Q_{max}^{-1} + (K_L^{-1}*Q_{max}^{-1}*C_e^{-1})$; where Q_e is the amount of adsorbed ALP (µg ALP/mg Laponite), Q_{max} is the maximum adsorption capacity (µg ALP/mg Laponite), K_L is Langmuir constant and related to the free energy of adsorption (L/mg clay) and C_e is the conc. of free enzyme in liquid phase at equilibrium (µg/mL). Freundlich model is expressed by the equation $\text{Log } Q_e = 1/n*\text{Log } C_e + \text{Log } K_F$; where where K_F (mg/g) $(mg/L)^{1/n}$ and n are Freundlich adsorption constants related to the adsorption capacity and intensity of the adsorbents, respectively. The linear plots of Langmuir and Freundlich isotherms are presented in **Figure 4.3B**. The Langmuir model has a better fit with higher degree of correlation (R^2=0.9951) than Freundlich model (R^2=0.8534).

The values of Q_{max} and K_L for Langmuir as well as K_F and n for Freundlich were calculated from the intercept and slope of the previous equations and presented in **Figure 4.3C**. The highest adsorption monolayer capacity of Laponite for ALP (Q_{max}) was 107.53 µg/mg clay. K_L is a measure of the affinity of adsorbate (ALP) to adsorption sites. Specifically, the dimensionless separation factor (R_L) which is a function of K_L and initial ALP conc. C_0 ($R_L=1/(1+K_L*C_0)$ is indicates either the adsorption isotherm to be unfavorable (RL > 1), favorable (0 < RL > 1), linear (RL = 1), or irreversible (RL = 0)[297].The R_L values for the tested C_0 conc. (100-2000 µg/mL) were in the range of 0.014-0.25 indicating the favourable adsorption of ALP on/in Laponite. For Freundlich model, K_F is an indicator of adsorption capacity and has a value of 13.2404 L/mg. 1/n Values specify whether adsorption is irreversible (1/n = 0), favorable (0 < 1/n < 1) or unfavorable (1/n > 1). 1/n value was 0.3223 confirming, with the K_L values, favorable adsorption of ALP on Laponite.

A

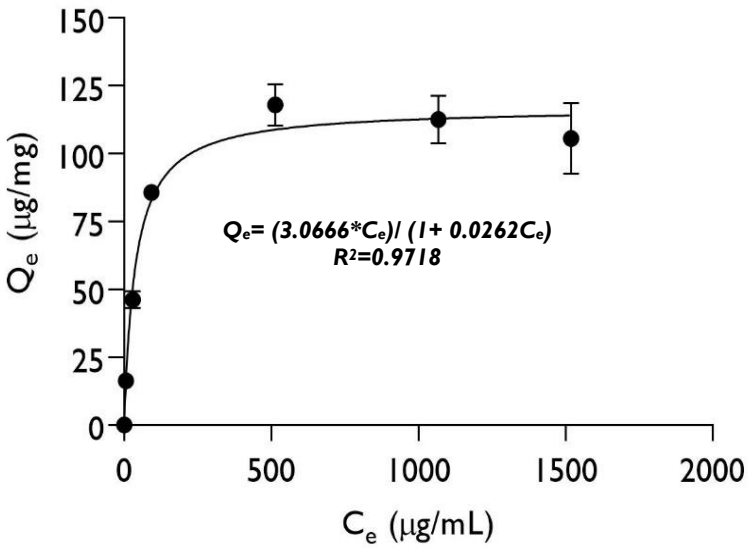

B

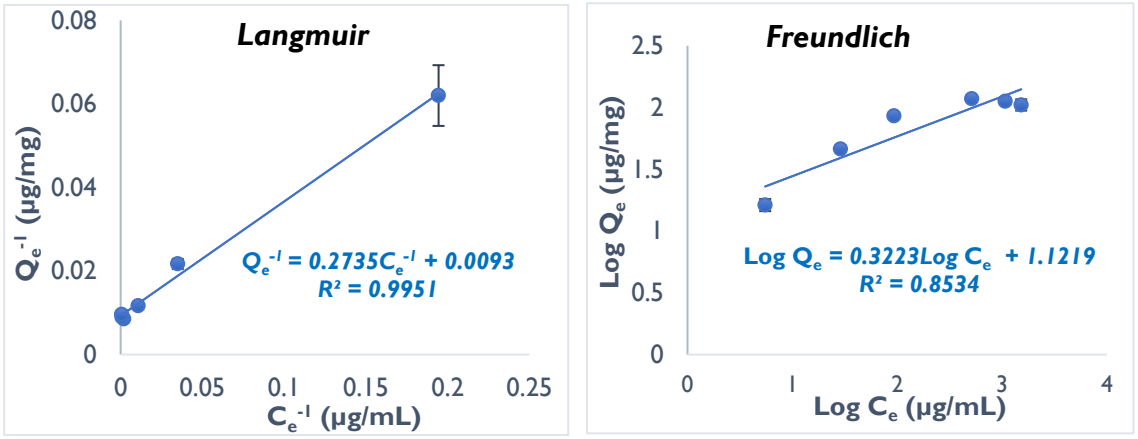

C

MODEL	LANGMUIR			FREUNDLICH		
EQUATION	$Q_e^{-1} = Q_{max}^{-1} + K_L^{-1}*Q_{max}^{-1}*C_e^{-1}$			Log Q_e = 1/n*Log C_e + Log K_F		
PARAMETERS	Q_{max} (µg/mg)	K_L	R^2	n	K_F	R^2
VALUES	107.53	0.034	0.9951	3.1027	13.2404	0.8534

Figure 4. 3 Adsorption isotherm of ALP on Laponite.
(A) The experimental isotherm of ALP adsorption on/in Laponite showing relationship between liquid enzyme conc. at equilibrium (C_e) vs amount of adsorbed ALP (Q_e). (B) Linearized plots of Langmuir and Freundlich models confirming Langmuir isotherm fitting to the experimental obtained data of ALP adsorption by Laponite. (C) Adsorption isotherm parameters and constants for the immobilization of ALP by Laponite based on the linear plots of both Langmuir and Freundlich models. Error bars represent ± SD, N=3.

4.4.1.3 Activity of adsorbed ALP

Activity kinetics of free vs adsorbed ALP was fitted with the Michaelis–Menten model (R^2 = 0.9970 & 0.9706, respectively), which is based on the equation $V=(V_{max}*[S])/(K_m+[S])$. V refers to enzyme velocity (µmol pNP/h), [S] is the substrate conc. (µM), V_{max} is the maximum reaction velocity (µmol pNP/h) and K_m is the Michaelis–Menten constant (µM) which is a measure of the of the affinity of an enzyme for its substrate – the higher K_m, the lower its affinity for substrate and vice versa[298]. As shown in **Figure 4.4**, plotting V vs [S] showed a hyperbolic curve for both free and immobilized ALP in which V is directly proportional to [S] at low [S], but the velocity tends towards a maximum at high [S]. Interestingly, adsorption of ALP on/in Laponite led to a significant (~10-20-fold) decrease of the enzyme activity/velocity at all substrate concentrations ($P<0.0001$), indicating strong inhibitory role of Laponite on ALP enzymatic activity.

Although the adsorption process preserved the Michaelis behavior of the enzyme (R^2=0.9706), the enzyme kinetics parameters (V_{max} & K_m) were severely affected. Specifically, K_m of the adsorbed enzyme was almost double that of its free form (6127 and 3478 µM, respectively). This indicate that the affinity of ALP for its substrate was significantly reduced when adsorbed on/in Laponite. V_{max} value of the enzyme-clay complex was only 13% of V_{max} calculated for free ALP enzyme, confirming strong reduction in activity of adsorbed ALP. In agreement, V_{max}/K_m ratio, which is an indicator of the catalytic efficiency of an enzyme[292,293], was strongly decreased in presence of Laponite (from 3.9×10^{-3} to 2.9×10^{-4}). Moreover, the decreased V_{max} and increased K_m of ALP with the addition of Laponite, indicate that Laponite acts as a mixed inhibitor which binds to the enzyme alone in absence of substrate as a competitive inhibitor, but can bind to either the enzyme alone or the enzyme-substrate complex as uncompetitive inhibitor in presence of both the enzyme and substrate. V_{max} is decreased in both cases, but K_m is increased only when the inhibitor favors binding to the free enzyme which was seen in our system. This suggests that Laponite more closely mimics competitive inhibitor action on ALP.

A

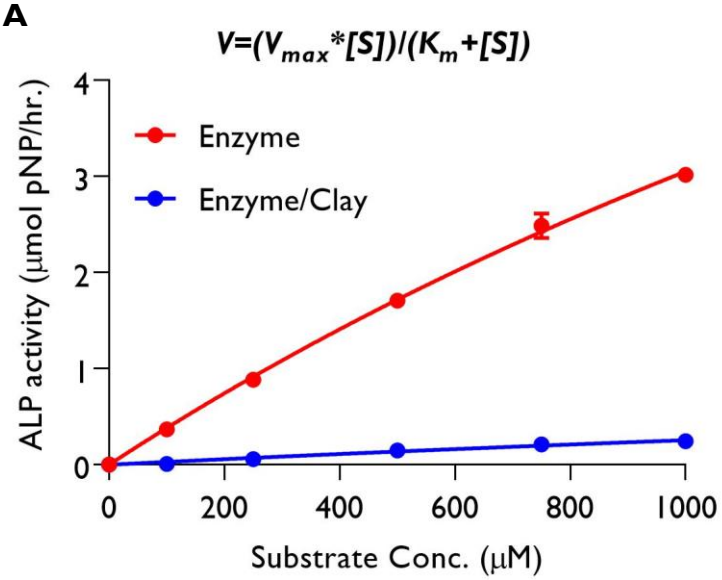

B

Enzyme				***Enzyme/Clay***			
V_{max} (µmol pNP/hr.)	K_m (µM)	V_{max}/K_m	R^2	V_{max} (µmol pNP/hr.)	K_m (µM)	V_{max}/K_m	R^2
13.67	3478	$3.9*10^{-3}$	0.9970	1.822	6127	$3*10^{-4}$	0.9706

Figure 4. 4 Activity of free ALP enzyme in solution (Red curve) vs. enzyme adsorbed on Laponite (Blue curve) as a function of ALP substrate (pNPP).
(**A**) Bothe curves were fitted with the Michaelis–Menten equation with high degree of correlation (R^2). (**B**) Kinetics parameters (V_{max} & K_m) of free vs immobilized ALP enzyme calculated using the Michaelis–Menten equation. Error bars represent ± SD, N=3.

4.4.2 Role of Laponite endocytosis

The other route through which Laponite might enhance ALP activity in hBMSCs culture is Laponite endocytosis - direct interaction with the cell - which is subdivided into four main pathways discussed in chapter 1. Herein, we tracked whether blocking Laponite endocytosis would reduce or inhibit Laponite induction of ALP.

4.4.2.1 Cytocompatibility of endocytosis inhibitor

Chlorpromazine hydrochloride (CPZ) was selected as specific inhibitor of clathrin-mediated endocytosis which has been recently cited as the main cellular uptake pathway of Laponite nanoparticles[131,250]. The effect of CPZ on cell viability was tested to select the optimal concentration which is both cytocompatible and able to block Laponite uptake for subsequent experiments. As shown in **Figure 4.5** cells stayed metabolically active to concentration of 5 µg/mL, however, 10 µg/mL resulted in a significant decrease of cell viability reaching around 50% decrease after 24 h compared to the negative control. Therefore, 5 µg/mL CPZ represents the upper concentration limit for the inhibitor cytocompatibility. In addition, ~5-10 µg/mL CPZ

was used an effective optimized dose for inhibiting cellular uptake of nanoparticles, such as silica, silver and clay, by human mesenchymal stem cells[250,299,300]. Therefore, 5 µg/mL CPZ was selected for subsequent experiments for validating the efficacy of CPZ to reduce/inhibit Laponite endocytosis.

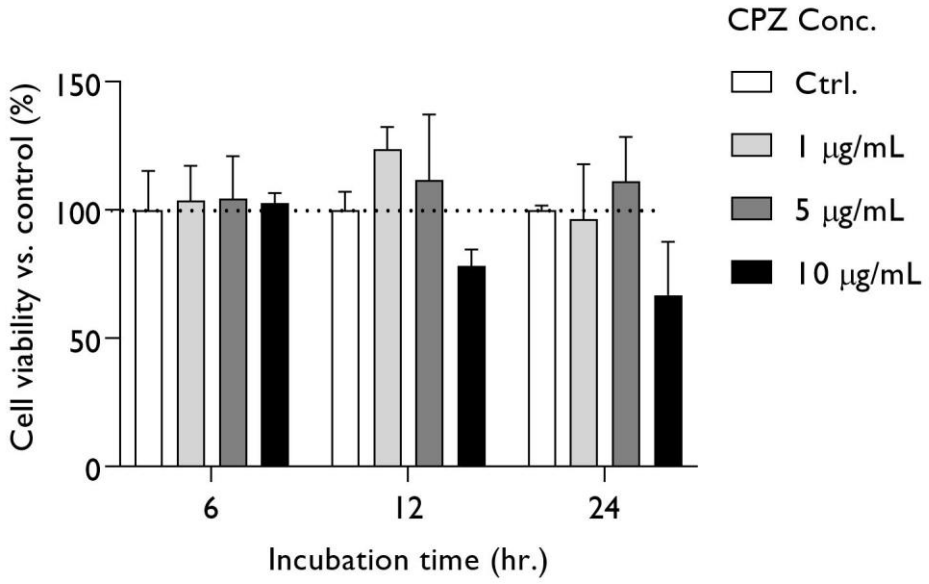

Figure 4. 5 Cytocompatibility of chlorpromazine hydrochloride on hBMSCs.
CPZ was cytocompatible up to a dose of 5 µg/mL. Statistical analysis was performed using two-way ANOVA followed by Tukey's multiple comparisons test. Data represent mean ± SD, N = 3.

4.4.2.2 Validation of endocytosis inhibitor efficacy

Next, the efficacy of the selected dose of CPZ on Laponite cellular uptake was validated using confocal microscopy. Uptake of Laponite nanoparticles by hBMSCs was clearly inhibited following treatment with CPZ compared to clay-exposed cells in absence of CPZ as shown by confocal microscopy (**Figure 4.6**). Image quantification showed that the addition of CPZ resulted in ~90% reduction in the amount of internalized Laponite particles by hBMSCs. This confirmed selection of 5 µg/mL CPZ as an effective dose for subsequently assessing the role of particle endocytosis on Laponite bioactivity.

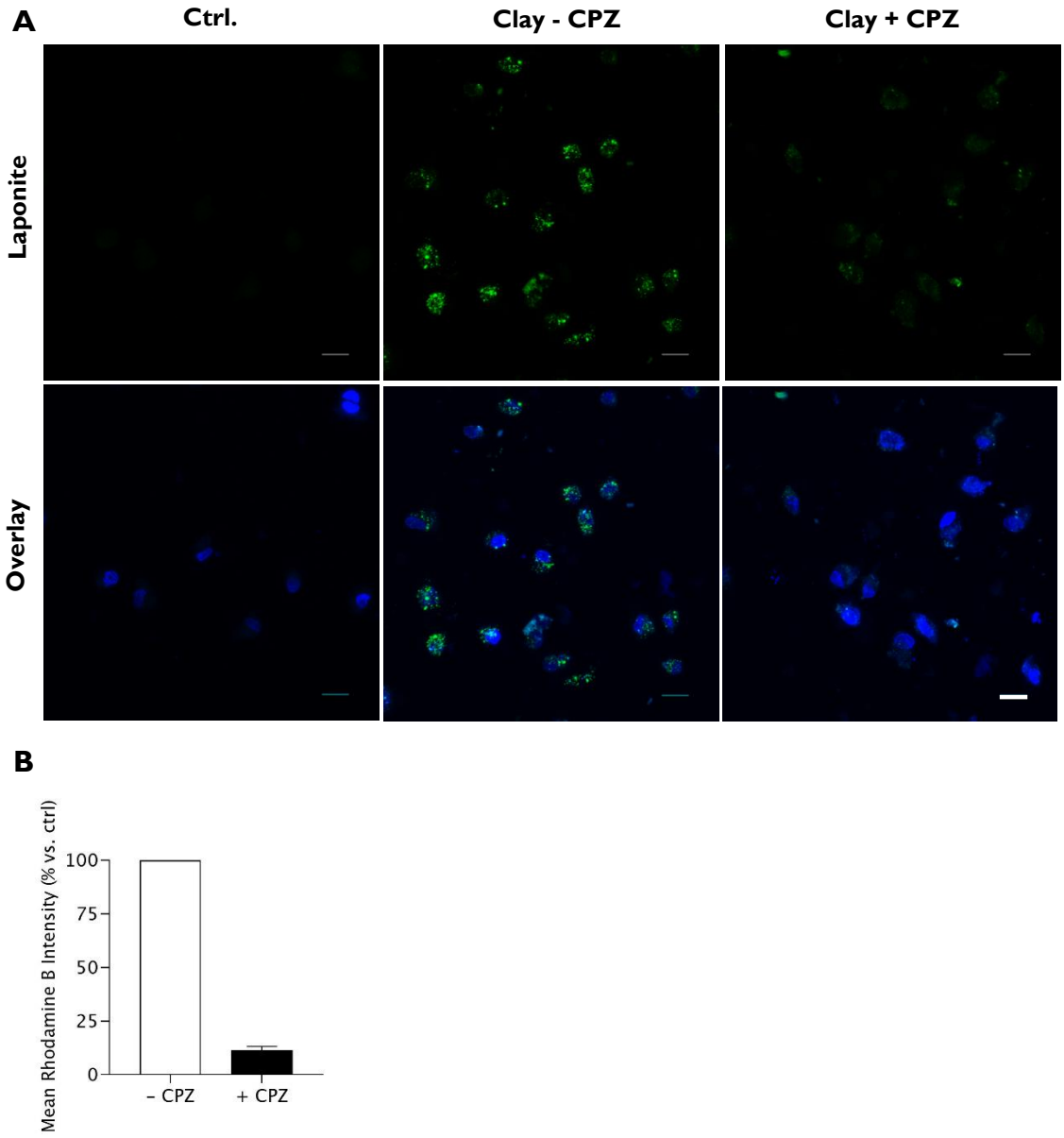

Figure 4. 6 Effect of chlorpromazine hydrochloride on Laponite uptake by hBMSCs. (A) Cells were incubated with RBITC-labeled Laponite dispersions in presence or absence of 5 µg/mL CPZ for 24 h and particle internalization was visualized by confocal microscopy through z-stacking of detached cell suspension. Scale bar = 20 µm. (B) Staining quantification of Laponite uptake in presence and absence of CPZ. Uptake intensity was normalized to Ctrl (cells with Laponite but without CPZ). CPZ = chlorpromazine hydrochloride inhibitor.

4.4.2.3 Effect of endocytosis inhibition on Laponite induction of ALP

Having confirmed an effective and cytocompatible dose of CPZ able to inhibit Laponite cellular uptake, the effect of clay endocytosis inhibition on Laponite-induction of ALP activity was investigated. Cells were treated with CPZ for 2 h prior to Laponite addition (0-100 µg/mL) in presence or absence of CPZ for 72 h. We did

not wash out CPZ as this might reverse its inhibitory action[301]. As shown in **Figure 4.7**, co-administration of an inhibitor of endocytosis with Laponite significantly attenuated ALP activity enhancement induced by Laponite alone across the Laponite concertation range tested in both basal and osteogenic cultures and (P<0.0001). However, compared to the negative control the addition of Laponite was still able to enhance ALP activity of hBMSCs at 100 µg/mL which might be attributed to residual clay particles that have been internalized (10% of initially applied clay). Overall, data suggest that endocytosis of Laponite nanoparticles play a key role in their ability to trigger ALP induction in hBMSCs culture and necessitates the need for further exploring this pathway for Laponite osteogenic bioactivity.

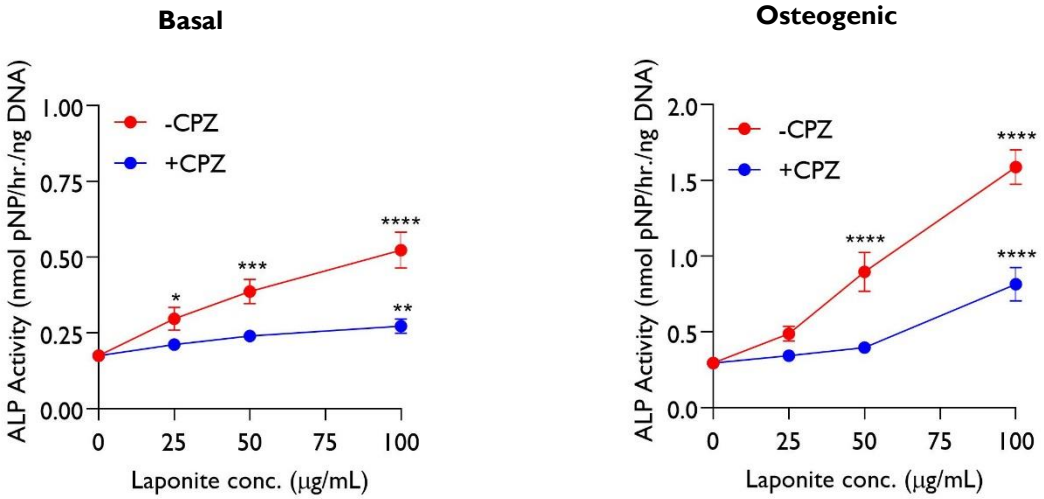

Figure 4. 7 Effect of Laponite endocytosis inhibition on ALP activity of hBMSCs. Blocking Laponite endocytosis resulted in significant attenuation of Laponite-induction of ALP activity at day 3 across the Laponite dose range tested, implying that Laponite endocytosis is crucial for its osteogenic character reflected in ALP activity. Statistical analysis was performed using two-way ANOVA followed by Tukey's multiple comparisons test. Data represent mean ± SD, N = 3. *P < 0.05; ****P<0.0001.

4.4.3 Role of Laponite degradation products

As expected, the addition of dispersed Laponite nanoparticles, in their intact/undegraded form, resulted in a significant dose-dependent increase in ALP activity at conc. 0-100 µg/mL. Neither Mg^{2+} nor Li^{+} ions were able to trigger any statistically significant effect on hBMSCs ALP activity at the whole tested concentration rage (**Figure 4.8**). There was no significant difference for both providing ($MgSO_4$ & LiCl) and excluding (Na_2SO_4 & NaCl) salts when compared to negative control, indicating that Mg^{2+} and Li^{+} are not involved in Laponite osteogenic

bioactivity. The addition of sodium silicate Na_2SiO_3 led to a dose-dependent increase in ALP activity although only statistically significant at the high dose 127.2 µg/mL ($P<0.05$). However, when normalized to the role played by counter ion (Na^+), assayed using NaCl, the effect of silicon ion on ALP activity was negligible as in the case of Mg and Li ions.

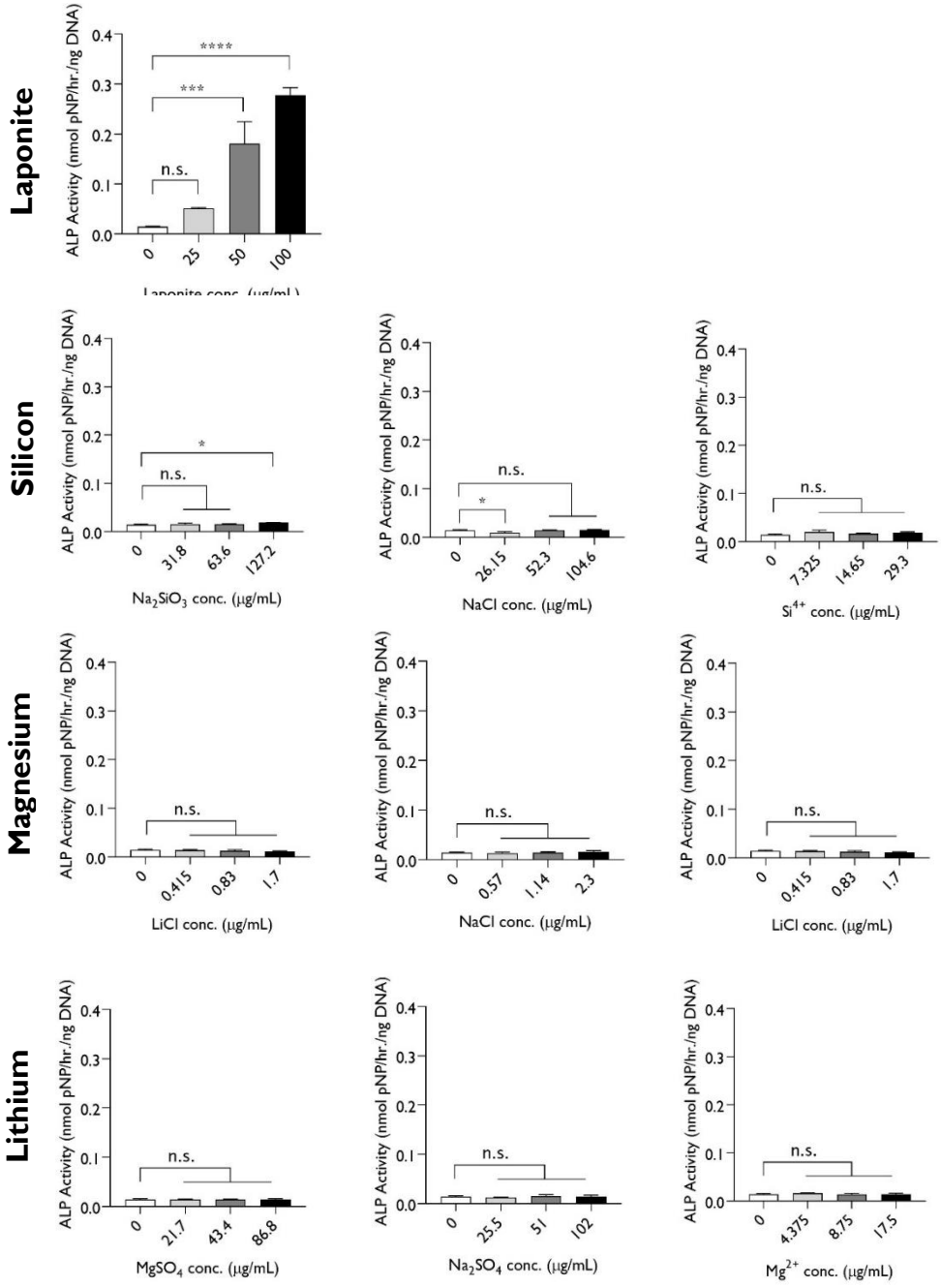

Figure 4. 8 Role of clay degradation products Si, Mg and Li in Laponite osteogenic bioactivity.

None of the tested dissolution products were able to significantly participate in Laponite bioactivity. Statistical analysis was performed using one-way ANOVA followed by Tukey's multiple comparisons test. Data represent mean ± SD, N = 3. ***P < 0.001; ****P < 0.0001; n.s. = not significant.

4.5 Discussion and analysis

The goal of this study was to explore possible mechanisms which may drive Laponite early induction of hBMSCs ALP activity. Two main routes have been examined: i) cell-independent– through interaction of Laponite with ALP enzyme; and ii) cell-dependent – through Laponite endocytosis by hBMSCs. Results showed that ALP adsorption by Laponite is a favorable and rapid process which best fit the Langmuir adsorption isotherm ($Q_e^{-1} = Q_{max}^{-1} + (K_L^{-1} * Q_{max}^{-1} * C_e^{-1})$). ALP enzyme activity was strongly reduced (~10-20 fold) as a result of its adsorption/immobilisation on Laponite, as confirmed by Laponite-mediated significant changes in Michaelis–Menten parameters K_m and V_{max}. This necessitated the need for further exploring role of direct Laponite-cell interaction through endocytosis and subsequent release of degradation products. The addition of a clathrin mediated endocytosis inhibitor chlorpromazine hydrochloride strongly blocked cellular uptake of Laponite nanoparticles by hBMSCs. Inhibition of Laponite endocytosis strongly attenuated the dose-dependent Laponite induction of ALP activity indicating that Laponite endocytosis is crucial for exerting its osteogenic character. However, the addition of silicon, magnesium and lithium at concentrations corresponding to that present in Laponite failed to induce any significant change in ALP activity of hBMSCs indicating that Laponite induction of ALP is almost independent of its degradation products.

The initial question was whether Laponite is able to enhance the catalytic activity of ALP secreted by the cell. We first tracked ALP enzyme adsorption kinetics on Laponite to determine the optimal contact time to select for subsequent experiments. ALP adsorption kinetics followed an L-type curve with rapid adsorption at the first 30 min then reaching near-saturation at 2 h. This in agreement with Yu[168] and Ghiaci[302] et al, studies which found 2 h as sufficient contact time to attain ALP adsorption equilibrium by smectites and preserve enzyme activity which was reduced by longer stirring times (> 2 h)[302,303]. Therefore, 2 h was select as an optimal incubation time.

Adsorption isotherm provides useful understanding of sorption mechanism and surface properties affinity of Laponite for ALP. It expresses the amount of adsorbate (e.g. ALP) removed from solution by unit mass of adsorbent (Laponite) at constant temperature. In agreement with various studies[293,292], our results best fit the Langmuir adsorption isotherm with high degree of correlation. Langmuir model is based on the

assumptions that adsorption is a monolayer process on homogenous surface and reaches a saturation level at specific ligand (ALP) concentration[293]. Moreover, the calculated Langmuir and Freundlich constants K_L and K_F confirmed that ALP adsorption by Laponite is a favourable process. As previously discussed, nanoclay are characterised by their rich heterogeneous surface chemistry which allow for different modes of interaction with proteins for example though electrostatic interaction, hydrophobic interaction and hydrogen bonding on different surfaces such as negative silica surface, interlayer gallery and particle edges[265,168]. According to manufacturer protocol, the isoelectric point of ALP in this investigation is 4.4-5.8. Therefore, ALP would have a net negative charge under Tris-HCl buffer used in this study (pH=7.6). Under these physiological pH conditions, which is < zero point of charge for Laponite, Laponite particles carry permanent negative charge on the surface and positive charge on the edges[258]. In accordance with other studies, this suggests that electrostatic interaction play an important role in ALP-Laponite interaction and explains Laponite strong affinity for ALP adsorption[293,292].

ALP absorption on/in Laponite particles strongly reduced enzyme activity and affinity for substrate suggesting that Laponite works as an enzyme inhibitor. This is clear from the calculated Michaelis–Menten parameters maximum reaction velocity V_{max} and enzyme affinity for substrate K_m – K_m was almost doubled, and V_{max} was reduced by ~90% as a result of enzyme adsorption on Laponite. Other clay minerals such as montmorillonite have shown similar influence on ALP enzyme activity and affinity for the substrate[293,292]. For example, Zhu et al. reported decrease in V_{max} from 3.7 to 0.8 µmol pNP/h and K_m increase from 0.9 to 1.4 mM as a result of ALP adsorption by montmorillonite[293] and Shindo et al. showed that K_m and V_{max} of ALP-montmorillonite enzyme complex were, respectively, double and 20% that of free enzyme[292]. Such reduction in ALP activity by clay minerals might be attributed to changes induced in the active conformation of the enzyme or by blocking of active centers[304,305]. In fact, protein conformational change (e.g. denaturation, unfolding, change in orientation and aggregation) is a common consequence of protein adsorption on clay minerals as observed with culture media model proteins such as bovine serum albumin[306,307].

Overall, these data indicate that Laponite exerts its effects on the cell phenotype/physiology, rather than directly enhancing the activity of the enzyme itself.

Inhibition of ALP activity can lead to accumulation of ALP substrate (pyrophosphate PPi and β-Glycerophosphate) and shortage of ALP product (inorganic phosphate Pi) which acts as a negative feedback loop stimulus to inhibit enzyme activity[298]. It is at least possible therefore that the strong negative influence of Laponite on the enzyme itself could influence this regulatory pathway by establishing a positive feedback loop causing the cell to produce more enzyme – though we are not aware of this effect on the pathway being reported in the literature. More likely, given the rapid and strong clay-mediated upregulation of ALP gene expression (a 100-fold increase compared to negative control) is a direct nanoclay-stem cell interaction Overall therefore, these results indicate that a direct interaction between Laponite and secreted ALP is not the main pathway through which Laponite promotes ALP production and activity.

Regarding Laponite-cell interaction, we first tracked whether the dominant/primary route through which Laponite promote ALP production/activity is through intracellular or extracellular processes by testing the dependency of ALP activity on endocytosis. Blocking Laponite endocytosis strongly attenuated Laponite-induction of ALP activity implying that Laponite endocytosis is essential, and represents the main pathway, for Laponite osteogenic effects. This agrees with the vast number of publications which report that nanoparticle modulation of hMSCs osteogenic differentiation require nanoparticle uptake. For example, gold nanoparticles promote osteogenic differentiation of hMSCs by acting as an intracellular mechanical stimulus[59] and the osteogenic potential of silica nanoparticles require particle cellular uptake to release the osteogenic element silicon[308] and induce autophagy through direct binding with LC3 and p62 (two key proteins involved in autophagosome formation)[309].

Another important conclusion from this study is that Laponite degradation products, upon which most recent papers have relied as main mode of action for nanoclay osteogenic bioactivity, doesn't seem to play a significant role in Laponite osteogenic character. It should be noted that the rate and extent of clay dissolution within endosomal (or lysosomal) intracellular compartments, or in cell culture solutions, remains to be confirmed[265]. Therefore, we assumed complete degradation of clay particles and used the corresponding ionic concentrations of Si, Mg and Li. This results is expected given that fact that the concentration of Si, Mg and Li ions released from Laponite dispersions at conc. up to 100 µg/mL is not sufficient to trigger

significant osteogenic influence. In this study, the concentration of Mg was 0-17.5 µg/mL (0-0.7 mM), which is lower than that previously reported to enhance osteogenic differentiation in literature[251,310–312] Zhang et al., reported that while Mg^{2+} conc. ≥ 1.3 mM significantly inhibited ECM mineralization of hBMSCs in a dose-dependent manner, there was no significant effect of Mg^{2+} at conc. ≤ 1.05 mM compared to control[310]. Moreover, other studies found Mg^{2+} dose of 5-20 mM as an optimal osteogenic dose which significantly enhanced ALP activity, ECM mineralization and bone-related protein synthesis of hBMSCs[251] and osteoblasts[311,312]. However, at doses above 20 mM, Mg^{2+} inhibited cell osteogenesis and showed no significant influence at concentration ≤ 2 mM[311]. Concentration of Li used in this study is 0-0.27 (0-0.04 mM) which is far below that reported to have a significant effect on SSCs osteogenic differentiation (20-40 mM), although complex between stimulating and inhibitjng[313,314]. In addition, while some studies showed an effect at Li conc. of 5 mM[315], others reported that lithium at < 5 mM did not significantly influence SSCs osteogenic function[313,314]. On the other hand, studies exploring the effect of silicon on cell osteogenic differentiation[296,316] showed an osteogenic effect of Si at concentrations similar to the range used in our study (0-1.04 mM). Si concentrations at 0.625, 1.25 and 5 mM significantly enhanced osteogenic gene expression and mineralized nodule formation of bone marrow stromal cells[296]. In agreement, Xing et al., reported that Si at concentration range 7.96–31.84 µg /mL significantly enhanced ALP activity, ECM mineralization and bone-related gene expression of hBMSCs compared to negative control[316]. The discrepancy between these studies and results in this chapter might be attributed to experimental factors such as cell type, seeding density and/or timing of ALP activity measurement. For example, Valerio et al., showed that osteoblasts cultured with silicon, released from bioactive glass, at 40 µg/mL exhibited similar ALP activity levels at day 3 compared to TCP control[317]. It should be noted that the used concentrations of Mg, Li and Si ions in this study are based on assuming complete Laponite particle degradation, however, the percentage of particle endocytosed by hBMSCs and whether they completely degrade inside the cell still remain unknown. This can be answered through the use of ICPMS analysis.

Despite that we excluded the possible osteogenic role of Laponite degradation products individually, combinations of these ions might play a role in Laponite

osteogenic bioactivity and warrants further investigations. For example, Tsigkou et al.[318] found that a combination of silicon and calcium promoted osteogenic differentiation of fetal osteoblasts and Naruphontjirakul et al.[319] found that strontium ions are needed in addition to silica and calcium, released from bioactive glass nanoparticles, to stimulate osteogenic differentiation of hMSCs. It should be noted however that Laponite is free from these ions such as calcium and strontium which showed, in literature, a synergistic osteogenic effect with silicon.

Conclusion

This is the first study to elucidate how nanoclay may influence osteogenic cell function, demonstrated by ALP activity, though screening two main pathways – cell-independent through Laponite-ALP interaction and cell-dependent through Laponite endocytosis and Laponite dissolution products (Si^{4+}, Mg^{2+} & $Li^{+)}$. Despite its strong affinity to adsorb ALP, Laponite strongly repressed ALP activity rather than enhanced it suggesting a direct nanoclay-cell interaction route. As a first step towards reaching the right cell-dependent mechanism, blocking Laponite endocytosis resulted in a strong attenuation of Laponite-induced ALP activity indicating the crucial role played by Laponite endocytosis which need further exploration. Interestingly, Laponite seem to exert its osteogenic character, as reflected by ALP activity, almost independent of its degradation products which necessitate the need for turning our attention to biophysical models such as nanoclay-cell membrane interaction, Laponite as a nanocarrier of bioactive molecules/ions and Laponite induction of cell stress (e.g. autophagy). However, before moving to explore these biophysical models, it's important to confirm excluding the role of Laponite degradation products through modulating the content of these elements in Laponite crystal which represent a more reliable approach and comes into discussion in next chapter.

Chapter 5: The role of lithium in the osteogenic bioactivity of Laponite clay nanoparticles

5.1 Introduction

Despite the interesting data of Si, Mg and Li ions salt solutions presented in chapter 4, using modified Laponite nanoparticles in terms of these elements represent a more reliable and consistent approach for testing the role Laponite degradation products. This is because; 1) The intra- and extra-cellular distribution profile of Laponite nanoparticles as well as the rate and extent of their degradation inside the cell or in cell culture media, to release degradation products, is not clear in the literature. Therefore, it is hard to calculate the exact/correct amount of Si, Mg or Li released from Laponite inside the cell to potentially have an action on osteogenesis. 2) cell interaction, for example cellular uptake pathways and kinetics[320], with inorganic ions is different from nanoparticles.

Among the degradation products reported herein, lithium has attracted considerable attention for bone regenerative therapies due to its well-documented role in prompting osteogenesis and bone formation[109,321]. For example, a study conducted by Zamani et al., reported that bone mineral density in several areas of 75 lithium-treated patients was significantly higher than that of normal participants[322] and current use of lithium (in contrast to past use) was associated with a decreased risk of fractures[323]. Recently, Jin et al., reported the ability of lithium to enhance implant osseointegration, implant fixation and bone formation in osteoporotic conditions[324] suggesting lithium as a promising therapeutic agent for bone formation and preventing implant failure. *In vitro*, various studies have reported the ability of lithium to promote proliferation and osteogenic differentiation of bone marrow-derived mesenchymal stem cells[314,315,325–327].

These interesting osteogenic properties of lithium are mainly attributed to its well-known pharmacological function as an agonist for the canonical Wnt signaling pathway[255] which plays a key role in modulating osteogenic gene expression. Lithium acts to inhibit glycogen synthase kinase 3 (GSK3β) from phosphorylating β-catenin, which subsequently escapes degradation and translocate to the nucleus to bind TCF/LEF transcription factor complex[73,255,315,325]. Aberrations or alterations in Wnt signaling pathway are known to lead to various osteogenic disorders in both animal and human models which reflects not only its crucial role in normal bone physiology but also its potential as an attractive therapeutic target for bone regeneration[73,328,329]. For example clinical trials using Wnt agonist drugs showed promising results

augmenting bone formation and increasing bone mineral density[73,328] and incorporation of lithium ions in bioactive ceramics[327] and mesoporous bioglass[315] significantly enhanced proliferation and osteogenic differentiation of bone marrow mesenchymal stem cells compared to lithium-free scaffolds. Despite these interesting properties of lithium and Wnt signaling in osteogenesis and the potential relevance to clay bioactivity, no data are currently available in literature to test the hypothesis that lithium release underlies the osteogenic effects of Laponite.

In this study, a family of lithium-modified Laponite clay formulations have been generated, in collaboration with BYK-ALTANA, and subsequently tested for their osteogenic potential on human bone marrow stromal stem cells. After testing the influence of Laponite on luciferase activity of a Wnt reporter cell line, the osteogenic response of hBMSCs to lithium modified Laponite analogues was explored by testing early and late markers of osteogenic differentiation. This investigation represents an opportunity not only to understand the role of lithium and Wnt signalling in Laponite bioactivity but may also lead to novel modified Laponite structures able to tune specific cell responses for regeneration.

5.2 Hypothesis and aims

This study was performed to test the hypothesis that lithium is involved in imparting the osteogenic bioactivity of Laponite through activating the canonical Wnt signaling pathway and that modulation of Laponite lithium content enhances Laponite osteogenic bioactivity.

Aims

1. Explore the effect of lithium content of Laponite on Wnt signalling activation.
2. Generate a family of lithium modified Laponite clay minerals in terms of both structural and adsorbed lithium.
3. Explore the effect of lithium modified Laponite formulations on hBMSCs osteogenic differentiation.

5.3 Methods

5.3.1 Luciferase activity

In order to investigate the role of Wnt signalling pathway in Laponite osteogenic bioactivity, luciferase assay was performed using of an engineered 3T3 mouse fibroblast cell line (ENZ-61001-0001, Enzo Life Sciences) which expresses the firefly luciferase reporter gene under the control of Wnt-responsive promoters (TCF/LEF). Luciferase activity from the reporter gene in this cell line can be up-regulated or down-regulated in response to the addition of Wnt agonists or antagonists, respectively, therefore, this technique can be used to screen the ability of small molecules and nanoparticles to modulate the canonical Wnt signaling pathway.

Cells were used at passage below 10 after defrosting as their Wnt responsiveness diminishes at higher passage numbers. Briefly, cells were seeded in white clear-bottom 96-well plates at density of 1.5 x 10^4 cells in 50 µL assay medium per well and incubated at 37 °C, 5% CO_2 for 24 h. Assay medium composed of DMEM, 25 mM HEPES (pH = 7.2–7.4), 5% FBS and 0.5% penicillin/streptomycin. Next day, Laponite and LiCl in DMEM were added to existing assay medium for total volume of 100 µL/well and final Laponite and LiCl concentration range of 0-100 µg/mL and 0–50 mM, respectively. 50 µL/well plain DMEM was added in the case of negative control - cells without Laponite or LiCl. Samples were run in triplicates and incubated at 37 °C and 5% CO_2 for 18 h. Next, added 100 µL/well luciferase substrate diluted in luciferase buffer (Steady-Glo, Promega, Madison, USA) and incubated at room temperature for 10 min in the dark. The chemiluminescence signal was immediately read (0.1 s/well) on a Varioscan Flash microplate reader (Thermo Scientific). To control for cell count, cell lysates were analysed for dsDNA content as described previously in **section 2.4.3.**

5.3.2 Preparation and physicochemical characterization of Lithium-modified Laponite nanoparticles

Two classes of Lithium-modified Laponite nanoparticles were generated in collaboration with BYK-ALTANA: structural- and exchanged-lithium clays. Briefly, structural lithium refers to lithium incorporated in the octahedral sheet of Laponite crystal while exchanged lithium is adsorbed in the interlayer space and/or on particle surface of Laponite.

Structural lithium was modified solely by BYK-ALTANA through tailoring the reactant molar ratios of SiO_4^{4-}: Mg^{2+}: Li^+: Na^+ salts during the initial stages of Laponite crystal synthesis. We did not include the methodology for this Laponite modification for BYK patent reasons and also because we were not directly involved in this synthesis. Standard, null and high structural-lithium Laponite formulations were successfully generated termed as Laponite SL, NL and HL, respectively (**Table 5.1**).

On the other hand, exchanged-lithium modification was conducted by our group and BYK through Na^+-Li^+ exchange reaction on the surface of standard Laponite SL. Briefly, 800 g of structural-lithium Laponite slurry (filter-cake) was reheated to 70 °C and filtered on a 24 cm Buchner filter funnel using a 541-filter paper then washed twice with 750 g deionised water/time at 70 °C. This was followed by 4 times washing of the filter-cake using 750 g of 15% Li_2SiO_4 solution/time at 70 °C. This allowed the Na^+-Li^+ cation exchange reaction to take place between Li^+ in the Li_2SO_4 solution and Na^+ in the interlayer space of Laponite particles. To remove excess cations from the reaction mixture, the filter-cake was washed several times with 750 g DI water at 70 °C/time until reaching the conductivity plateaux. pH and conductivity of filtrate at each washing step were measured and recorded to ensure reaching the conductivity plateaux. Next, the filter-cake was removed from the filter paper and dried on a glass dish in an oven at 110 °C overnight. Finally, the dried product was milled in a Janke and Kunkel A10 mill to a fine white powder.

Laponite Type	Lithium Location	Preparation Method	Laponite Symbol
Structural	In octahedral sheet	tailoring reactant molar ratios during Laponite crystal synthesis	Laponite SL (std.), HL (high) & NL (null)
Exchanged	In octahedral sheet , interlayer gallery & on negative surface	Laponite reaction with Li_2SO_4 to allow Na-Li exchange in/on clay crystal	Laponite SL^{ex}.

Table 5. 1 Classification and preparation method of obtained Lithium-modified Laponite nanoparticles.

Powder X-ray diffraction was carried out as described for standard Laponite in **section 3.3.1**. X-ray fluorescence spectroscopy (XRF) was used to measure elemental composition, in the form of oxides, of the as-prepared Laponite structures. However, XRF is less useful for measurement of elements with atomic number Z < 11, as in the case of lithium, due to weak fluorescence from these species. Therefore, Lithium content was analyzed by atomic absorption spectroscopy (AAS) as described in **section 3.3.1**.

5.3.3 Role of Laponite lithium content (structural & adsorbed) in Laponite osteogenic bioactivity

For evaluating whether lithium plays a significant role in the as-observed Laponite promotion of hBMSCs osteogenic differentiation, hBMSCs were cultured with lithium modified Laponite structures vs standard Laponite SL as a reference for 7 days. When reached 70-80% confluence, hBMSCs were seeded in 24 well plates in basal media and incubated at 37 °C and 5% CO_2 for 24 h to adhere. Next, existing media was replaced with both basal and osteogenic culture media supplemented with 100 μg/mL Laponite (standard or lithium modified) prepared as described in **section 2.3**. Cells were allowed to interact with both standard and lithium modified Laponite structures (Laponite NL vs SL vs HL & Laponite SL vs SL^{ex}) at 37 °C and 5% CO_2 for 7 days without media change to allow for sufficient time for Laponite particle degradation. On day 7, osteogenic markers were assessed including ALP staining and assay, alizarin red staining and bone-related gene expression as previously reported in chapter 2 (general methods).

5.4 Results

5.4.1 Role of lithium content of Laponite in Wnt signalling activation

The addition of Laponite to Wnt reporter fibroblast cell line at concentrations sufficient to enhance hBMSCs osteogenic differentiation (chapter 3) failed to induce any increase in luciferase Wnt reporter activity compared to the control indicating that the canonical Wnt signaling pathway does not play a significant role in Laponite bioactivity (**Figure 5.1A).** LiCl, here used as a positive control, caused a significant upregulation in TCF/LEF promoter activity in Wnt luciferase reporter cell line only at ≥ 25 mM which suggests lithium released from Laponite insufficient to activate the Wnt signaling pathway (**Figure 5.1B**). The addition of LiCl at concentrations which proved able to upregulate promoter activity in the reporter cell line led a significant dose-dependent down regulation, rather than enhancement, of hBMSCs ALP activity (**Figure 5.1C)**.

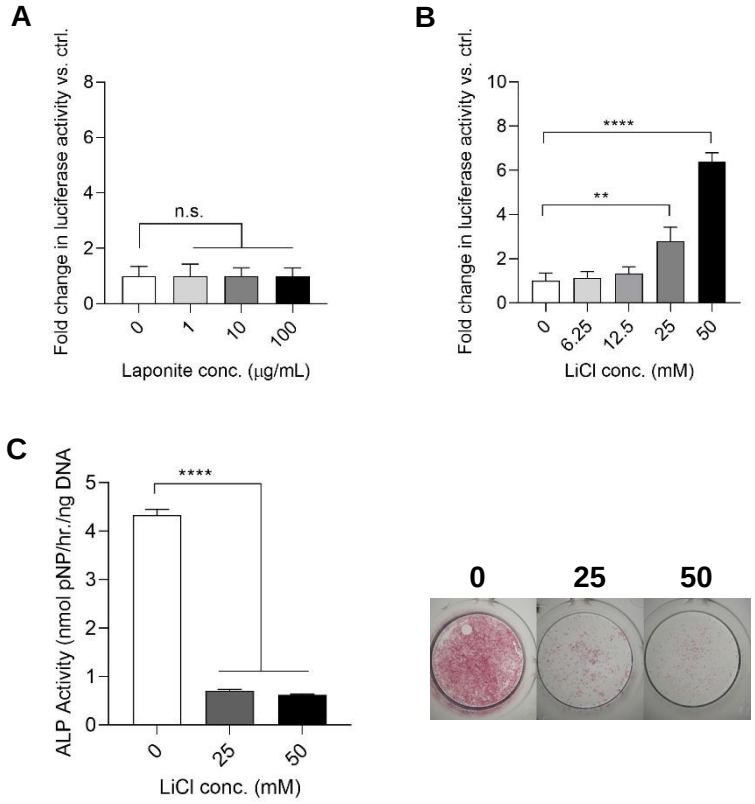

Figure 5. 1 Effect of lithium ions on osteogenic differentiation of hBMSCs though the canonical Wnt signaling pathway demonstrated in Wnt reporter fibroblasts.
While addition of Laponite did not have any significant effect on luciferase activity of Wnt reporter cell line (**A**), LiCl led to a significant dose-dependent increase in luciferase activity at ≥ 25 mM (**B**). LiCl addition to hBMSCs caused a dose-dependent decrease in ALP activity at conc. range which activated the Wnt signaling (**C**). Statistical analysis was performed using one-way ANOVA followed by Tukey's multiple comparisons test. Data represent mean ± SD. N = 3. **P<0.01; ****P < 0.0001; n.s. = non-significant.

5.4.2 Preparation and physicochemical characterization of Lithium-modified Laponite nanoparticles

Various lithium modified Laponite structures in terms of structural (NL vs SL vs HL) and adsorbed (SL vs SL^{ex}) lithium were generated to test their bioactivity on hBMSCs (**Figure 5.2A**). XRD diffractogram show that both standard and lithium modified Laponite clay minerals exhibit reflection peaks characteristic of pure Laponite crystal without phase transformation or impurities (**Figure 5.2B**).

X-ray fluorescence (XRF), and atomic absorption spectroscopy (AAS) analysis (**Figure 5.2C**) confirmed successful modification of lithium content in the octahedral sheets of HL and NL producing Laponite analogues with structural Lithium contents ranging from 0 to 5.5 mg/g in the order of HL > SL > NL. Efficient Na^{+}-Li^{+} exchange reactions for the generation of SL^{ex} grade Laponite were also confirmed by XRF and AAS which showed complete removal of Na_2O and a 2.6-fold increase in lithium concentration respective.

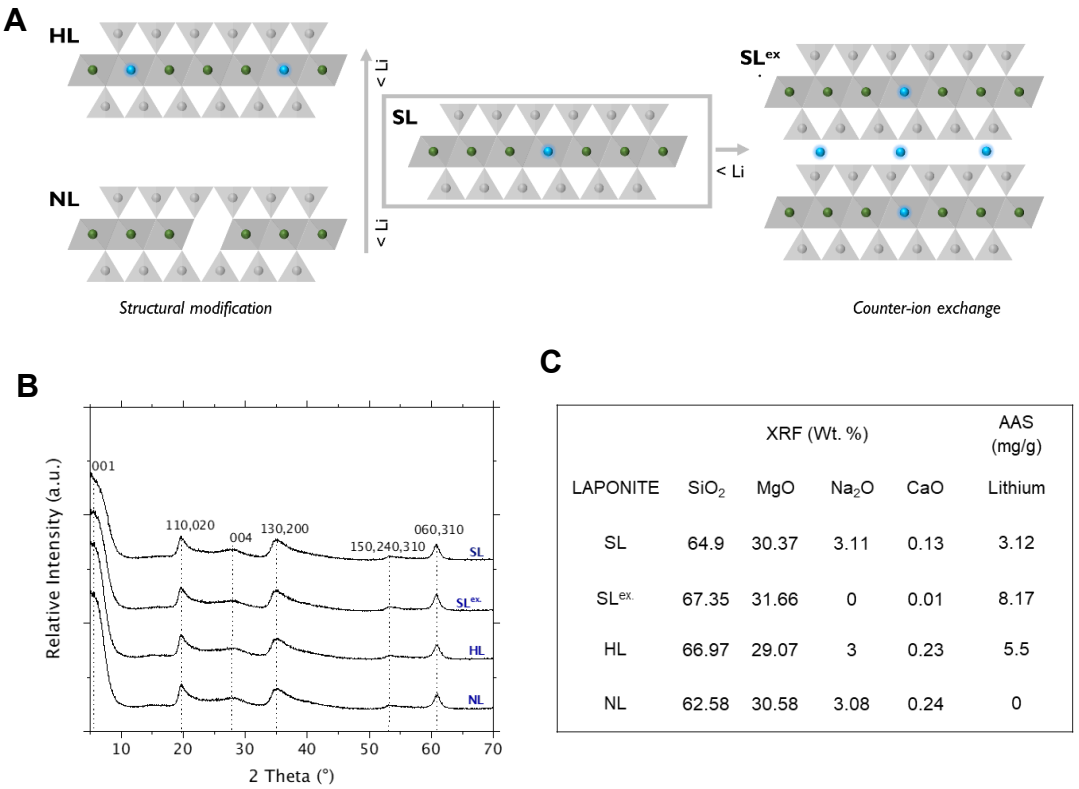

C

	XRF (Wt. %)				AAS (mg/g)
LAPONITE	SiO_2	MgO	Na_2O	CaO	Lithium
SL	64.9	30.37	3.11	0.13	3.12
$SL^{ex.}$	67.35	31.66	0	0.01	8.17
HL	66.97	29.07	3	0.23	5.5
NL	62.58	30.58	3.08	0.24	0

Figure 5. 2 Structural and compositional analysis of Lithium-modified Laponite clay nanoparticles.
(A) Schematic of Lithium modified Laponite analogues (lithium ions represented in blue). (B) XRD diffractogram showing reflection peaks characteristic of pure Na-hectorite clay mineral without impurities or phase transformation compared to standard Laponite. (C) Elemental analysis by XRF and AAS confirming successful modulation of Laponite lithium content.

5.4.3 Role of structural lithium in Laponite bioactivity

The role of structural Lithium in nanoclay bioactivity was investigated by incubating hBMSCs with Laponite NL and HL together with Laponite SL as a reference control for 7 days in both basal and osteogenic conditions. ALP activity was measured as an early osteogenic marker together with osteogenic gene expression. Compared to Laponite-free control, both standard and lithium-modified Laponite nanoparticles followed a similar pattern in enhancing ALP activity of hBMSCs ($P < 0.05$). However, it was hard to detect any significant difference between the clay formulations themselves in both culture media conditions as demonstrated by ALP assay and staining (**Figure 5.3**).

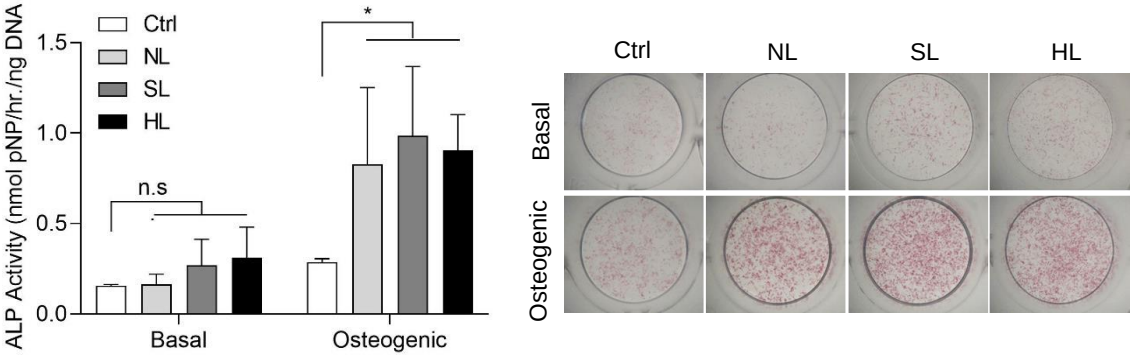

Figure 5. 3 Role of structural lithium in Laponite osteogenic bioactivity assayed by ALP activity of hBMSCs at day 7.
Both standard and modified structures showed clay-enhanced ALP activity compared to negative control but with no significant difference between the clay formulations. Statistical analysis was performed using two-way ANOVA followed by Tukey's multiple comparisons test. Data represent mean ± SD. N = 3. *P < 0.05; n.s. = non-significant

Interestingly however, both high lithium and null lithium Laponite effected a marked reduction in the expression of osteogenic genes (RUNX2, ALPL and COL1A1) compared to standard Laponite (**Figure 5.4).** This was particularly apparent under basal culture conditions where the strong upregulation of all three genes by standard Laponite was significantly attenuated in both Laponite analogues – neither of which effected a significant change relative to the Laponite-free control. With osteogenic supplements both null lithium and high lithium Laponite caused a significant upregulation of ALPL and COL1A1 gene expression relative to the Laponite-free control but again in both cases upregulation of ALPL and COL1A1 was significantly reduced compared to that observed for standard Laponite. No significant differences

were detected between standard and modified clays for SPP1 expression over the time frame tested.

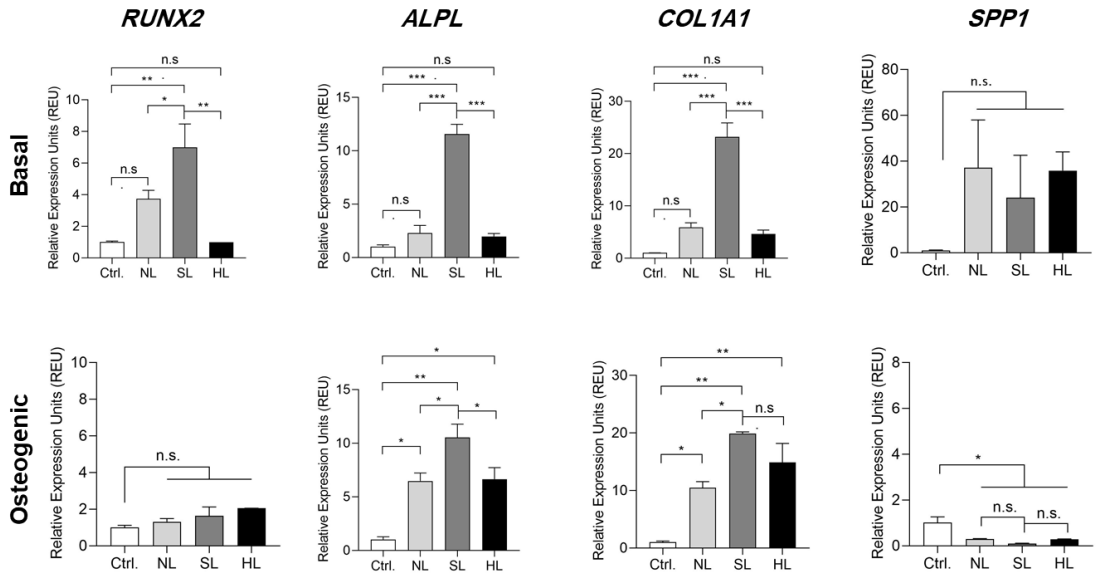

Figure 5. 4 Role of structural lithium in Laponite osteogenic bioactivity assayed by osteogenic gene expression of hBMSCs at day 7.
Both null- and high-lithium Laponite clays significantly attenuated the osteogenic effect of standard Laponite SL, however, no significant difference was observed between the former two in both culture conditions. The negative control in basal culture is basal media without Laponite while the negative control in osteogenic culture is composed of basal media with osteogenic supplements but without Laponite. Statistical analysis was performed using two-way ANOVA followed by Tukey's multiple comparisons test. Data represent mean ± SD. N = 3. *P < 0.05; **P < 0.01; ***P < 0.001; n.s. = non-significant

5.4.4 Role of exchanged lithium in Laponite bioactivity

Similar to the results for structurally modified Laponite, the exchange of the interlayer sodium for lithium did not appear to significantly affect the osteogenic character of standard Laponite on ALP activity or mineralisation. Both Laponite SL and SL^{ex} significantly reduced ALP activity of hBMSCs at day 7 (**Figure 5.5**) which was accompanied by a clay-enhanced calcium mineralisation (**Figure 5.6**) but with no significant difference between the two clays.

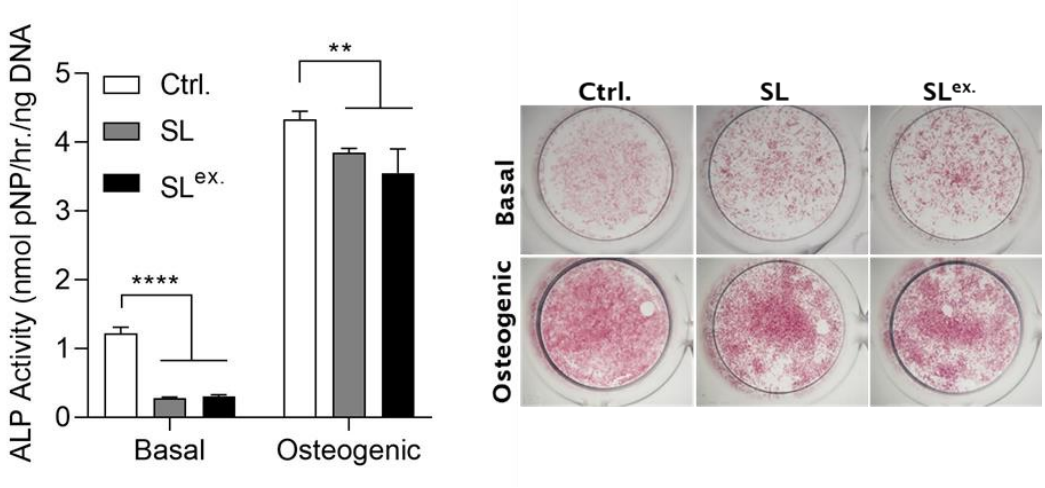

Figure 5. 5 Role of adsorbed lithium in Laponite osteogenic bioactivity assayed by ALP activity of hBMSCs at day 7.
Both Laponite SL ad SL^{ex} significantly attenuated ALP activity of hBMSCs but with no significant variation between the standard and modified clays. Statistical analysis was performed using one-way ANOVA followed by Tukey's multiple comparisons test. Data represent mean ± SD. N = 3. **P < 0.01; ****P < 0.0001.

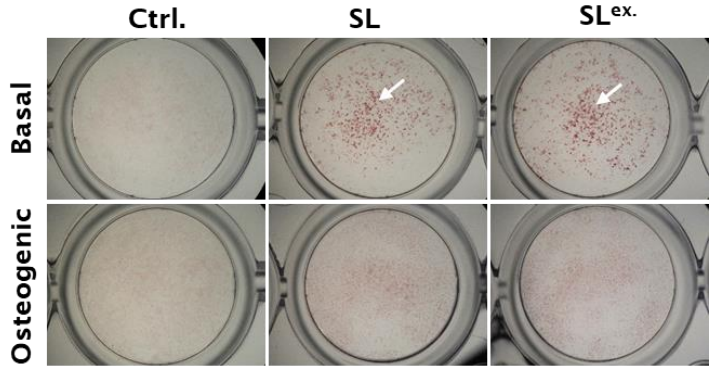

Figure 5. 6 Role of adsorbed lithium in Laponite osteogenic bioactivity assayed by CaP mineralization at day 7.
Exchanged lithium did not influence the osteogenic character of standard Laponite on mineralization.

In agreement with the role of structural lithium data discussed above, exchanged lithium tended to reduce the strength of the upregulatory effect of Laponite on osteogenic gene expression – an influence more evident in osteogenic media. Lithium exchange in/on Laponite reverted standard Laponite-induced upregulation of RUNX2 and ALPL gene expression back to control levels and attenuated the influence of standard Laponite on COL1A1 from 6-fold to 3-fold compared to control in osteogenic cultures. As expected, both Laponite SL and SL^{ex} failed to trigger any significant influence on late gene marker SPP1 regardless of culture media used (**Figure 5.7**).

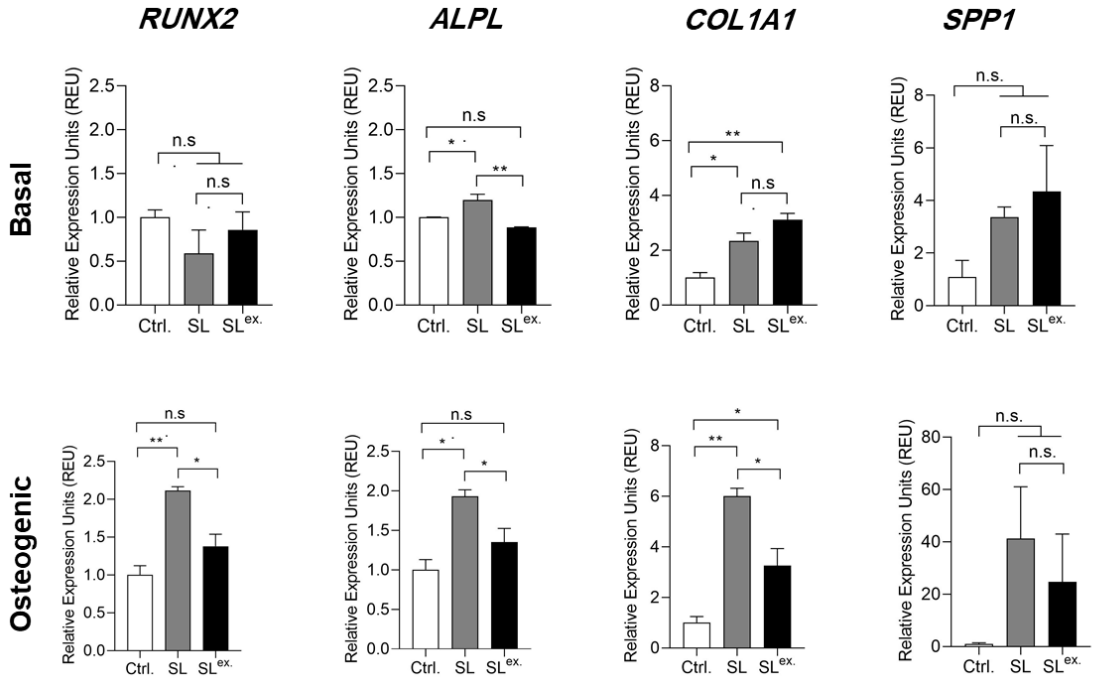

Figure 5. 7 Role of adsorbed lithium in Laponite osteogenic bioactivity assayed by osteogenic gene expression at day 7.
Adsorbed lithium significantly attenuated the enhancing effect of standard Laponite on RUNX2, ALPL & COL1A1. The negative control in basal culture is basal media without Laponite while the negative control in osteogenic culture is composed of basal media with osteogenic supplements but without Laponite. Statistical analysis was performed using one-way ANOVA followed by Tukey's multiple comparisons test. Data represent mean ± SD. N = 3. *P < 0.05; **P < 0.01; n.s. = non-significant.

Together these data suggest that Laponite osteogenic effects are not attributed to its lithium content, either structural or exchanged, and that standard Laponite achieved optimal osteogenic properties due to an uncontrolled variable associated with lithium modification.

5.5 Discussion and analysis

In this study, the role of lithium ion, as a Wnt signaling modulator, in Laponite osteogenic bioactivity was investigated using lithium modified Laponite clays. Results showed that Laponite clay nanoparticles exert their osteogenic character almost independent of its Lithium content, either structural or exchanged, and that the canonical/β-catenin Wnt signaling pathway does not play a key role in Laponite osteogenic bioactivity. These results exclude a frequently cited hypothesized mechanism for Laponite bioactivity upon which a large number of studies relied in their interpretation. In addition, they necessitate the need for turning attention to other mechanistic routes such as biophysical models of clay-cell membrane and clay-cell culture media interactions in order to elucidate the right mechanism for Laponite osteogenic bioactivity.

The first conclusion drawn from this study is that lithium released from Laponite is not sufficient to activate the Wnt signaling pathway. Assuming complete degradation of Laponite particles – an unlikely scenario - at the highest osteogenic conc. tested (100 µg/mL) the amount of released lithium is about 0.04 mM which is 50x lower than the reported inhibition constant K_i of 2 mM for GSK3β enzyme activity [330,331]. Moreover, this Laponite lithium content (0.04 mM) lies in the LiCl concentration range which proved unable to activate the Wnt signaling pathway reflected in luciferase Wnt reporter assay. In addition, even the lithium doses which proved sufficient for Wnt reporter activation (≥ 25 mM) led to a significant dose-dependent inhibition, rather than activation, of ALP activity in hBMSCs cultures in this study – a case opposite to that observed with Laponite. This is in agreement with studies carried out by Satija and colleagues which reported an inhibitory role of lithium on mesenchymal stem cell osteogenesis at similar concentration range[332,80]. For example, hMSCs at 20 mM LiCl exhibited significant inhibition in cell proliferation, colony formation and ALP activity which was accompanied by a LiCl-stimulated nuclear translocation of β-catenin[332]. These results stand against a role of lithium, as a Wnt signaling activator, in Laponite induction/promotion of osteogenesis in hBMSCs culture.

Having confirmed the inability of lithium in Laponite, at least at the osteogenic doses tested and reported in literatures, to activate the Wnt signalling pathway we asked whether lithium content of Laponite is still able to play a role in Laponite osteogenic

properties. To explore the relationship between osteogenesis and Laponite lithium therefore, Laponite analogues modified for lithium content were generated and their effect on hBMSCs osteogenic differentiation investigated. Overall, the results also support the conclusion above that Laponite osteogenic effects are not attributed to its lithium content. All Laponite analogues tested, including null-lithium Laponite, significantly enhanced ALP activity and osteogenic gene expression relative to the clay-free control. Furthermore, although removal of lithium somewhat attenuated the osteogenic effect of standard Laponite a very similar attenuation was also observed for high lithium analogues.

These findings are consistent with results presented in in chapter 4 which showed that the amount of lithium present in Laponite at the concentrations reported for its bioactivity (10-100 µg/mL) failed to trigger a response in ALP of hBMSCs when applied as lithium salt solutions. This is expected given the fact that concentration of lithium released from Laponite is also far below the limit to induce osteogenic action of stem cell populations – the above calculated 0.04 mM Li released from 100 µg/mL Laponite is more than 100-times lower than reported osteogenic dose of Lithium[315]. In agreement, a growing body of literature indicate such osteogenic effects *in vitro* to be a more generalised feature of clays – many of which do not contain lithium. For example, Kim et al. showed that dispersion of MMT ($Na_m(Al_{2m}Mg_m)Si_4O_{10}(OH)_2.nH_2O$) nanoparticles in cell culture media enhanced ALP activity, mineralization and expression of osteoblast differentiation markers (RUNX2, BMP2, COL1 & OCN) in an MG63 cell line[333] and Kang et al. reported similar osteogenic effects of anionic clays Mg_2Al-Cl and Zn_2Al-Cl on pre-osteoblasts[334]. Moreover, similar clay osteogenic effects were observed when comparing addition of Laponite[132] vs. halloysite[335] to gelatin methacrylate hydrogel and Laponite[226] vs. attapulgite[336] to electrospun PLGA nanofibers and Laponite[137] vs. MMT[192] to silk fibroin nanocomposites.

An interesting feature of the gene expression results was that all nanoclay modifications effected a slight but significant reduction in the osteogenic enhancement of Laponite. For example, at least 2-5-fold downregulation in mRNA expression levels of RUNX2, ALPL and COL1A1 was observed for both Laponite NL and HL in basal ($P < 0.001$) and osteogenic ($P < 0.05$) cultures compared to standard Laponite - though with no significant differences between the two. This is

notable as it suggests that relatively subtle changes in chemistry (subtle, certainly, compared to the differences between the various clays cited above) can in fact change the bioactivity of nanoclay. In this case, given that the effect does not correlate with lithium content, the change appears to be in an uncontrolled variable associated with lithium modification. For example, modification of structural lithium of Laponite will subsequently modify its cation exchange capacity[199,337] which, according to BYK-LTANA, has value of ~50 and ~75 meq/100g for Laponite SL and HL, respectively. Cation exchange capacity potentially influence amount and/or nature of proteins adsorbed on clay nanoparticle in cell culture media[265,168] leading to modified protein corona on clay surface[250]. This in turn lead to different particle internalization route and bioactivity potential[338]. Further experiments are warranted to confirm this interpretation regarding clay but they are beyond the objective of this study.

4.6. Conclusion

This study examined the role of lithium as a Wnt signaling activator in Laponite osteogenic bioactivity – a pathway which has been frequently cited behind Laponite promotion of osteogenesis. Results in this study convincingly demonstrated that the bioactivity of Laponite does not correlate with its lithium content, either incorporated in Laponite structure or adsorbed on Laponite surface and seems independent of the β-catenin Wnt signalling pathway. This suggests against the hypothesised role of lithium release in imparting Laponite bioactivity and that other physicochemical features of Laponite need to be explored to understand Laponite osteogenic effects. Moreover, these results convincingly suggest biophysical model(s) exerted by intact Laponite particles independent of Laponite degradation but before exploring such models it is essential to answer key questions regarding Laponite uptake, intracellular trafficking, fate and influence on physiological cell function which is discussed in next chapter.

Chapter 6: Tracking cellular uptake, intracellular trafficking and fate of Laponite nanoparticles in human bone marrow stromal cells

6.1 Introduction

Laponite nanoparticles have shown exciting potential for applications in the biomedical field including biomaterial design, regenerative medicine[127,265,294] and drug/gene delivery[273,174] due to their unique physicochemical properties including particle size and shape, specific surface area, density of charge and structural and exchanged cations. From a regenerative medicine perspective, we have confirmed in chapter 3 the intrinsic bioactivity of Laponite to induce osteogenic differentiation of hBMSCs. In chapters 4 and 5, we have excluded a fundamental frequently cited mode of action for Laponite-promotion of osteogenic differentiation – the role of degradation products. However, there remains essential questions that need to be resolved before moving to explore the exact biophysical mechanism behind Laponite bioactivity. In particular, what is the rate and kinetics of Laponite uptake by the cells? Where are they transported within the cell and with which intracellular organelles do they co-localize? How does their internalization affect cell function? And what about their intracellular fate, for example, are they degraded, released in the cytoplasm or exocytosed? The answers to these questions may shed light on the mechanism(s) behind Laponite bioactivity and inform future development of the exciting potential of these materials for various biomedical applications[339].

Since the ability of nanoparticles, in general, to alter cell osteogenic functions is strongly dependent on their cellular uptake[340,180,179] the first question we addressed is the extent and kinetics of Laponite uptake by hBMSCs. Recent studies have reported Laponite nanoparticles are readily internalised *in vitro* via clathrin-mediated endocytosis by different cell types[130,131,268,250]. However, the rate and kinetics of Laponite cellular uptake is not well characterized. This is critical to explain the observed enhanced Laponite osteogenic bioactivity with increasing Laponite-cell contact time in chapter 3. In summary, we observed a clay-stimulated formation of mineralized bone-like nodules when Laponite interacted with the cells for 7 days but not when exposed for only 3 days. This indicates that during the first week of clay addition Laponite nanoparticles increasingly accumulated inside the cell to trigger stronger osteogenic action.

When nanoparticles reach the cell membrane they enter the cell through different endocytosis mechanisms including phagocytosis, clathrin-mediated endocytosis, caveolin-mediated endocytosis, clathrin/caveolae-independent endocytosis and

macropinocytosis[339,341]. Following endocytosis nanoparticles are normally found in membrane-bound endosomal/lysosomal vesicles although bare/free nanoparticles in the cytoplasm or other cell organelles such as nucleus, mitochondria and endoplasmic reticulum are occasionally reported[341,342] .This normally leads to significant alteration of cell functions such as viability, proliferation and differentiation. For example, endocytosis of nanoparticles such as gold and silica increase osteoblast differentiation through induction/stimulation of autophagy and colocalization with autophagosomes[343,309]. In addition, other studies reported the ability of gold nanoparticles to colocalize with endoplasmic reticulum (ER) and promote MSCs osteogenic differentiation. This suggests a possible role for nanoparticle-induced ER stress in mediating nanoparticle osteogenic bioactivity[340]. In support of this hypothesis, various studies reported that moderate ER stress can accelerate bone formation both in *vitro* and *in vivo*[344,345,346]. Therefore, it is highly plausible that internalized clay nanoparticles or aggregates might co-localize and interfere with some of these cell organelles to shift cell fate to the osteogenic lineage. Such critical questions of how clay nanoparticles are distributed and evolve inside the cell and which cell organelles they interact with is seldom discussed. Moreover, while most recent studies rely on the role of clay degradation as a main mechanistic pathway for nanoclay bioactivity[294], they do not provide clear data explaining the intracellular fate of clay nanoparticles.

In this study Laponite cellular kinetics and *in vitro* distribution was investigated using confocal microscopy and ICPMS – a powerful sensitive tool for nanoparticle quantification. This was followed by tracking, using TEM-EDX, Laponite intracellular trafficking pathway, fate of internalised Laponite and ultimately the influence Laponite exert on cell physiological functions.

6.2 Hypothesis and aims

Experiments in this chapter were performed to test the hypothesis that Laponite nanoparticles are endocytosed by hBMSCs for intracellular trafficking through the lysosomal degradative pathway and ultimately Laponite degradation.

In summary, the aim of the work in this chapter is to:

1. Track Laponite uptake kinetics and *in vitro* distribution in hBMSCs culture.
2. Track Laponite colocalisation with intracellular organelles and determining which intracellular trafficking pathway(s) Laponite pursue.
3. Track the fate of internalised Laponite nanoparticles.
4. Track the effect internalised Laponite influence on cell physiological functions.

6.3 Methods

6.3.1 Tracking Laponite uptake kinetics using confocal microscopy

For tracking Laponite uptake kinetics by hBMSCs, cells were incubated with RB-labelled Laponite nanoparticles. Briefly, hBMSCs (70-80% confluence; P2) were detached from culture flasks and seeded at density 10^4 cells/cm^2 in a 24-well plate on # 1.5 sterilised glass coverslips. Cells allowed to adhere in basal medium for 24 h. RBITC-labelled Laponite dispersion in basal culture medium at 100 µg/mL was prepared. Cell culture media aspirated, cells washed twice with DPBS and replaced with Laponite-containing vs Laponite-free basal media for clay-treated vs negative control groups, respectively. Cells incubated with Laponite at 37 °C, 5% CO_2 for 1, 3 and 7 days without media change.

At each selected timepoint (day 1, 3 and 7), culture media discarded and cells washed twice with pre-warmed DPBS (0.5 mL/well). Then, cells were incubated with 0.5 mL/well CellMask™ Deep Red plasma membrane stain (C10046, Invitrogen), at 1/1000 dilution in DPBS of 5 mg/mL stock solution in DMSO, for 10 min at 37 °C. Cell mask stain removed, cells washed twice with DPBS and detached though incubation with 0.2 mL/well trypsin/EDTA 1x for 5 min at 37 °C, 5% CO_2. Tapped gently to detach the cells and added 0.8 mL basal media/well to deactivate T/E action then put in 1.5 Eppendorf for centrifugation at 400 RCF for 5 min at 21 °C. Supernatant discarded and cell pellet resuspended and fixed in 0.2 mL 4% PFA and for 10 min at room temperature. Fixed cell suspension was transferred into µ-Slide 8 Well Glass Bottom chamber (80827, Ibidi) freshly coated with 1% Alcian Blue in H_2O. Cells were imaged immediately by Leica TCS-SP8 Confocal Microscope equipped with Leica LAS-X software.

6.3.2 Tracking Laponite uptake and *in vitro* distribution by ICPMS

hBMSCs at 70-80% confluence and passage number P2 were detached from tissue culture flasks and seeded in 6-well plates at density of 10^4 cells/cm^2 in basal medium and left to adhere for 24 h. Then, culture media discarded, cells washed twice with DPBS (2 mL/well/time) and added fresh Laponite-free basal media for negative controls and media supplemented with Laponite nanoparticles at conc. of 100 µg/mL for clay-treated samples. Media volume of 5 mL/well was selected to be consistent in terms of Laponite/cell ratio which is 5 ng/cell across all Laponite -hBMSCs

interaction experiments of this thesis. Cells incubated with Laponite at 37 °C, 5% CO_2 for 7 days without media change. Selected time points are day 1, 3 and 7 and each sample was run in triplicates.

At each selected time point, cell culture media collected (≤ 5mL) in 15 mL Falcon tube – this is *supernatant 1* representing clay free in the system. Then, cells washed 3 times with DPBS (2 mL/well/time) to collect non-internalised particles adhered on cell membrane (total volume = 6 mL; in 15 mL Falcon tube). This is termed *supernatant 2*. Stored supernatants 1 & 2 at -20 °C for later analysis with ICPMS.

To collect internalized Laponite particles, cell monolayer was detached by incubation with 1 mL/well trypsin/EDTA 1x for 5 min at 37 °C, 5% CO_2 tapped gently to detach the cells, then add 1 mL basal medium to deactivate T/E action. Cell suspension transferred to 2 mL collection tubes, suspended very well and transfer 25 µL in the haemocytometer chamber for cell counting (duplicates/sample). Centrifugation was performed at 400 RCF for 5 min at 21 °C to separate the cells. Supernatant removed and cell pellet resuspended well in dH_2O at final volume of 1 mL/sample, and store at -20 °C for the ICP-MS analysis with supernatants 1 & 2. It's worth noting that all above-mentioned steps were formed in clean fume hood to avoid contamination by atmospheric particulates which might contain one or more the elements under investigation such as silicon. Also, avoided using tools/reagents which might contain Si, Mg or Li such as glass.

For sample digestion and analysis by ICPMS, each sample was homogenised very well by vortexing and repeated pipetting then representative 100 µL was added into digestion Teflon vessel. Pipettes were changed and cleaned with HCL then dH_2O between samples to prevent sample cross-contamination. Then, each sample was soaked in 1 mL conc. HNO_3 and 0.25 mL 30% H_2O_2 overnight and heated gradually to 130 °C until the solution was colourless and clear indicating complete sample digestion. Vessels containing HNO_3 and H_2O_2 and free from Laponite was used as blank controls. Samples cooled down and 0.2 mL was collected from each sample, after homogenisation through vortexing and repeated pipetting, and diluted up to 2 mL using 1.8 mL In/Re spiked 3% HNO_3 (dilution factor = 10). Finally, the Si and Li content were analysed using Thermo Scientific ELEMENT XR HR-ICPMS with indium as an internal standard. The concentration of elemental silicon and lithium in

solution was obtained, and the amount of Laponite internalized/cell, adhered on cell membrane, and remained free in extracellular space was calculated according to the following formula:

Conc. of Laponite (pg/cell) = measured conc. of Li (pg/cell)*(1/0.0027). Which is based on Laponite structural formula $\mathbf{Na^{+}_{0.7}[(Mg_{5.5}\ Li_{0.3})Si_8O_{20}(OH)_4]^{-0.7}}$ which show that each 1 pg Laponite contain 0.0027 pg Lithium.

To determine which element (Si vs. Li) best fit as a reliable marker for Laponite concertation measurement by ICPMS, a parallel study was performed. Laponite standards (0-100 µg/mL) were prepared in basal culture media as previously discussed in **section 2.2.4** and analysed by ICPMS as described above for collected supernatants 1 & 2 and cell pellets.

6.3.3 Tracking Laponite distribution, intracellular transport pathway and fate using TEM-EDX

Uptake mechanism, intracellular trafficking and fate of Laponite nanoparticles were investigated using using FEI Tecnai12 (ThermoFisher, Netherlands) coupled with energy dispersive X-ray unit based on protocol developed by the biomedical imaging unit, University of Southampton and modified from an earlier study[347]. hBMSCs at 70-80% confluence (P2) were detached from culture flasks using collagenase IV and trypsin/EDTA 1x as described above then seeded in 6-well plates at density of $0.5x10^6$ cells/well in basal media and incubated for 24 h. Next day, culture media removed and cells washed twice with DPBS and added Laponite-containing (100 µg/mL) and Laponite-free fresh basal media for the clay-treated and negative control samples, respectively. Cells were run in triplicate and incubated with Laponite at 37 °C and 5% CO_2 for 1, 3 and 7 days without media change. Samples were processed at day 1, 3 and 7 for TEM-EDX imaging and analysis as discussed below.

At each selected time point, cell culture media was discarded, cells washed with DPBS (2 mL/well/time) and trypsinized (1 mL/well T/E 1x) for 5 min at 37 °C, 5% CO_2 to detach cell monolayer tapped gently to detach the cells then added 1 mL basal media to deactivate trypsin action. Next, cell suspension was transferred to 2 mL collection tubes and centrifuged at 400 RCF for 5 min at 21 °C to collect cell pellet. Supernatant was discarded and cell pellet fixed in 1 mL fresh 37 °C pre-warmed 3% glutaraldehyde and 4% formaldehyde in 0.1 M PIPES buffer at pH 7.2 for 1 h at room

temperature then stored at 4 °C for later sample processing by the biomedical imaging unit, University of Southampton.

For sample processing/sectioning, cells were rinsed twice (10 min/time) in 0.1 M PIPES buffer at pH 7.2 followed by post-fixation in 1% osmium tetroxide in 0.1 M PIPES buffer at pH 7.2 for 1 h. Samples were rinsed twice again in 0.1 M PIPES buffer at pH 7.2 (10 min/time) followed by distilled water and 2% aqueous uranyl acetate for 30 s and 20 min, respectively. Next, the samples undergone dehydration in graded series of ethanol and eventually embedded in epoxy resin before being sectioned/cut into 90 nm sections using ultra-microtome. Ultrathin sections were examined using TEM-EDX at an accelerating voltage of 60 kV and magnifications 6-60000x.

6.4 Results

6.4.1 Tracking Laponite uptake kinetics using confocal microscopy

The first objective of this study was to track the extent and kinetics of clay nanoparticles cellular uptake. Confocal Laser Scanning Microscopy (CLSM) was applied to visualize cellular uptake of Rhodamine-labelled Laponite nanoparticles as defined by cell mask-stained cell membrane. As shown in **Figure 6.1**, Laponite particles were observed to strongly interact with hBMSCs and observed to be readily internalized in a time-dependent manner. At 24 h post-clay addition, almost all cells were noted to be positively stained for Laponite and the amount of Laponite internalized by the cells appears to increase with incubation time (day 1-7).

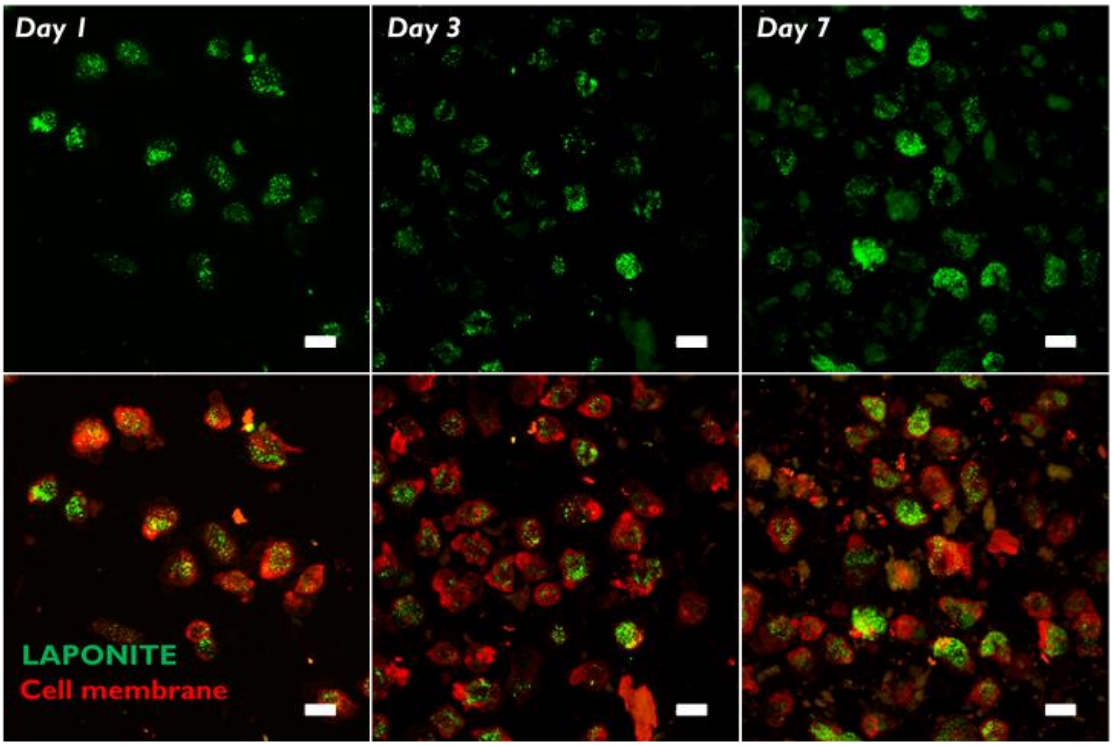

Figure 6. 1 Tracking cellular uptake of Laponite nanoparticles by confocal microscopy. Laponite exhibit strong affinity for internalization by hBMSCs, in a time-dependent manner. Scale bar = 20 µm. Top row images refers to Laponite particles labelled with rhodamine B (green) while bottom row refers plasma membrane stained with cell mask deep red (red).

Furthermore, as shown in **Figure 6.2**, Laponite was present inside the cell with perinuclear aggregates of various sizes distributed across the cell both near the plasma membrane and around the nucleus indicating strong interaction between the clay mineral and hBMSCs.

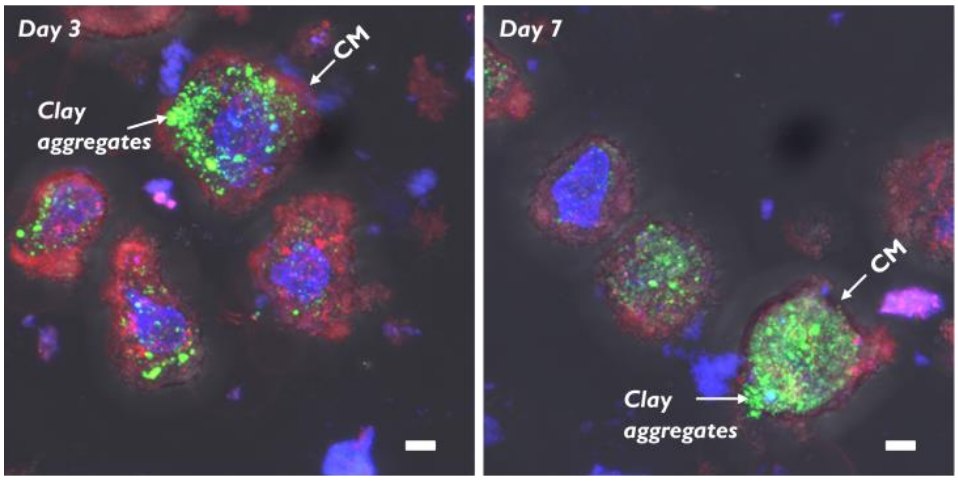

Figure 6. 2 High magnification confocal imaging demonstrating interaction of Laponite with hBMSCs as perinuclear aggregates of various sizes distributed across the cell. Green (RB-labelled Laponite particles); red (cell mask-stained plasma membrane); blue (DAPI-stained nucleus). Scale bar = 5 µm.

6.4.2 Quantifying intracellular vs extracellular Laponite using ICPMS

Despite these interesting results revealed by confocal microscopy, the levels of nanoclay particles internalized and nanoclay particles remaining free in the extracellular space are unclear using this methodology. Moreover, it is possible that clay particles adhered on the cell membrane were removed during the washing steps performed for confocal sample preparation. In addition, the observed clear clay aggregation in the system makes it difficult to quantify accurately the number of particles associated with the cell. Elucidating the correct percentages of Laponite present in, on and outside the cell is critical for understanding the mechanism(s) for Laponite bioactivity. This was analyzed with ICPMS which is a sensitive and powerful technique for analyzing the conc. of Laponite in the cell culture system based on elemental analysis of Si and Li.

First, we analyzed which element represented the best marker for quantifying Laponite concentration. Laponite doses 0-100 µg/mL were dispersed in cell culture media and the concentration of silicon and lithium analyzed by ICPMS then compared with the corresponding theoretical content of these elements in Laponite (**Figure 6.3A**). In comparison to silicon, lithium showed a high degree of correlation (R^2 = 0.98) with discrete difference between measured and theoretical values (**Figure 6.3B**). Therefore, Lithium was selected as the marker element for Laponite quantification.

Clay Conc. (µg/mL)	Calculated Conc. (µg/mL)		Measured Conc. (µg/mL)	
	Li	Si	Li	Si
0	0	0	0	0
5	0.0135	1.5	0.007714	0.551
10	0.027	3	0.018824	1.448
25	0.0675	7.5	0.052762	3.9215
50	0.135	15	0.1083	7.942
100	0.27	30	0.17712	8.528

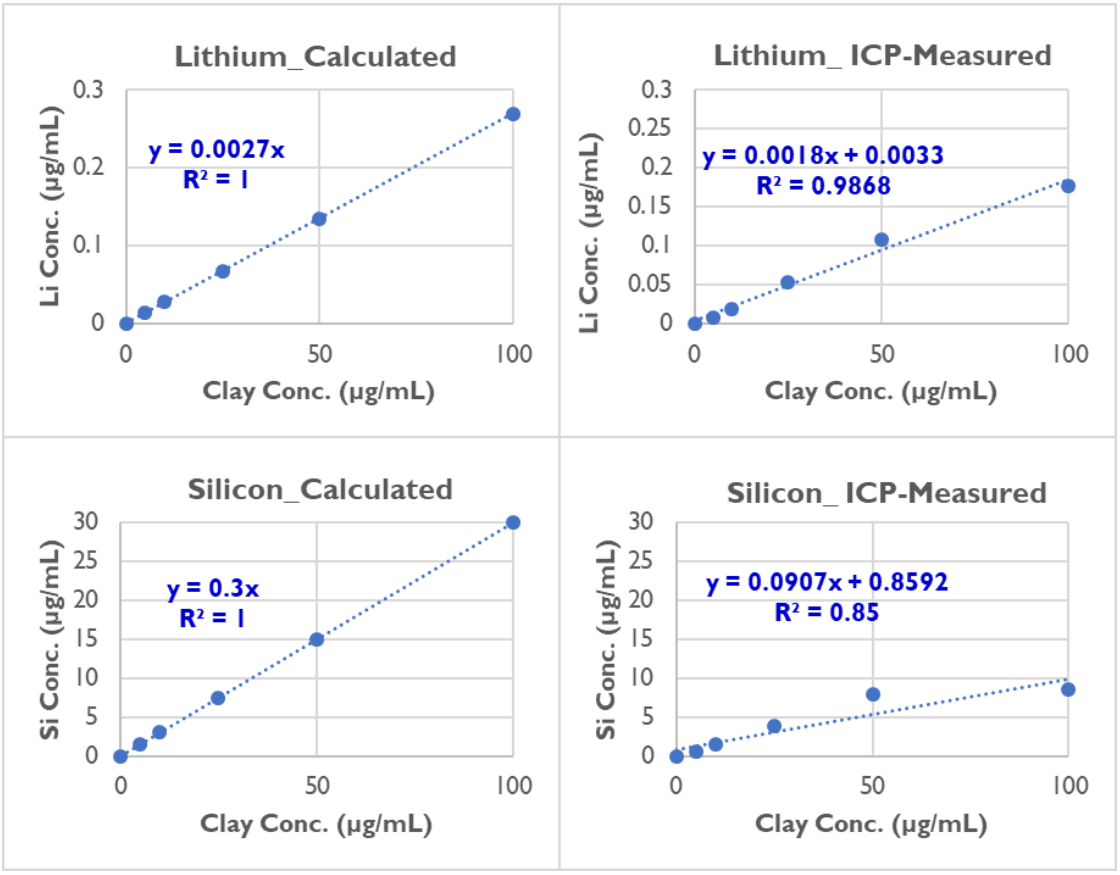

Figure 6. 3 Silicon vs lithium as a marker element for Laponite quantification by ICPMS.
(A) Theoretical vs measured Si & Li concentrations corresponding to Laponite doses 0-100 µg/mL. (B) Lithium showed a higher degree of correlation and ICP-measured values comparable to the expected/theoretical values

In agreement with the confocal microscopy data, Laponite cellular uptake exhibited a time-dependent significant increase ($P < 0.001$). At day 1 of clay-cell contact time, around 15 pg Laponite were internalized per cell. Levels of internalization reached ~30 pg/cell at day 3 and doubled to ~60 pg/cell at day 7 (**Figure 6.4A**). We then investigated distribution of Laponite particles in the cell culture system. The amount of Laponite particles internalized by the cell, adhered on cell membrane and free in the extracellular environment was measured by ICPMS are shown in **Figure 6.4B**. Around 98-99.3% of the initially applied clay particles remained extracellularly (not directly interacting with cells) while the conc. of internalized clay particles did not exceed 1.5%. However, despite that the amount of internalized Laponite particles did not exceed 1.5% it was a large amount relative to the cells which correspond to ~5 x 10^4 particles/cell at day 7 and is confirmed by the wide distribution of Laponite particles in the cell as shown by the confocal imaging discussed above. Around 0.5% of total Laponite applied was found attached/adhered to cell membrane as measured on the DPBS washes during ICPMS sample preparation.

Overall, these results demonstrate the strong affinity of Laponite for cellular uptake by hBMSCs in the form of aggregates distributed across the cell. The majority of Laponite particles applied to cells were observed to be retained extracellularly with a discrete proportion internalized. Level of nanoclay internalized were observed to increase with incubation time.

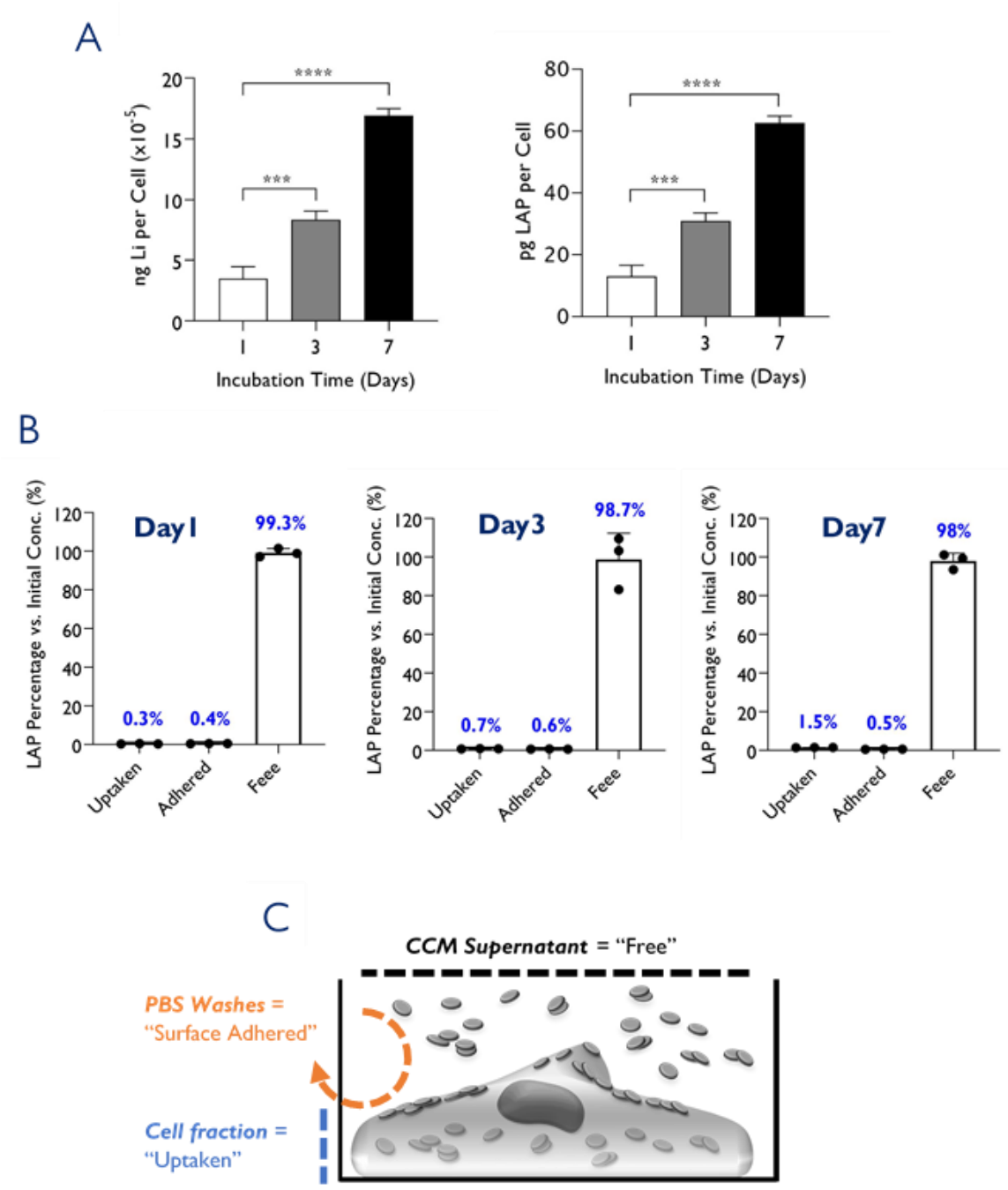

Figure 6. 4 Cellular uptake kinetics and distribution of Laponite across the cell culture system.

(A) The profile of Laponite nanoparticles taken up by cells increases in a time-dependent manner from 15 pg LAP/cell at day 1 to 60 pg LAP/cell at day 7. (B) The vast majority of the Laponite nanoparticles (98-99%) applied to cells remained in the extracellular space and only below 1.5% were internalized by cells. (C) Schematic representation demonstrating Laponite nanoparticles distribution in, on and outside the cells. Statistical analysis was performed using one-way ANOVA followed by Tukey's multiple comparisons test. Data represent mean ± SD, N = 3. ***P < 0.001; ****P < 0.0001.

6.4.3 Tracking Laponite distribution, intracellular transport pathway and fate using TEM-EDX

6.4.3.1 Laponite distribution and colocalization

Laponite nanoparticles were found distributed both extracellularly and intracellularly in the form of clusters/aggregates (**Figure 6.5**). This was confirmed by EDX analysis which showed Si and Mg peaks in the clay-treated groups but not in the negative control. In agreement with the confocal microscopy and ICPMS data, the internalized clay aggregates increased in size and number moving from day 3 to day 7 and were found distributed throughout the cytoplasm from the perinuclear region to near the plasma membrane. No Laponite particles were observed inside the nucleus.

Extracellularly, clusters of Laponite particles were distributed in the intercellular spaces and were also found in close proximity to the cell membrane. High magnification images showed extracellular Laponite particles as electron-dense rod/needle shaped particles with diameter range of ~ 30-50 nm (**Figure 6.6**). Intracellular Laponite particles were embedded within membrane-bound vesicles (endosomes/lysosomes) in the form of aggregates with various sizes (~0.5-1 µm), shapes and particle density (**Figure 6.7**). Laponite-containing lysosomes exhibited different stages of electron density/maturation and were found near mitochondria and the nuclear membrane. Some lysosomes with Laponite appeared fused with the endoplasmic reticulum and Golgi apparatus as shown by fusion of their membrane with ER in various location inside the cell. No clay particles were observed free in the cytoplasm – an observation confirmed through the absence of Si or Mg peaks upon EDX analysis of cytoplasmic regions. Golgi apparatus, endoplasmic reticulum and mitochondria all appeared free from clay particles across the timeframe. Secretory vesicles containing Laponite, as evidenced by EDX analysis, were observed fusing with plasma membrane potentially for Laponite exocytosis. Energy dispersive X-ray analysis confirmed the presence of Laponite particles inside endosomal/lysosomal bodies as evidenced by Si & Mg Kα peaks of the highlighted areas (**Figure 6.7**).

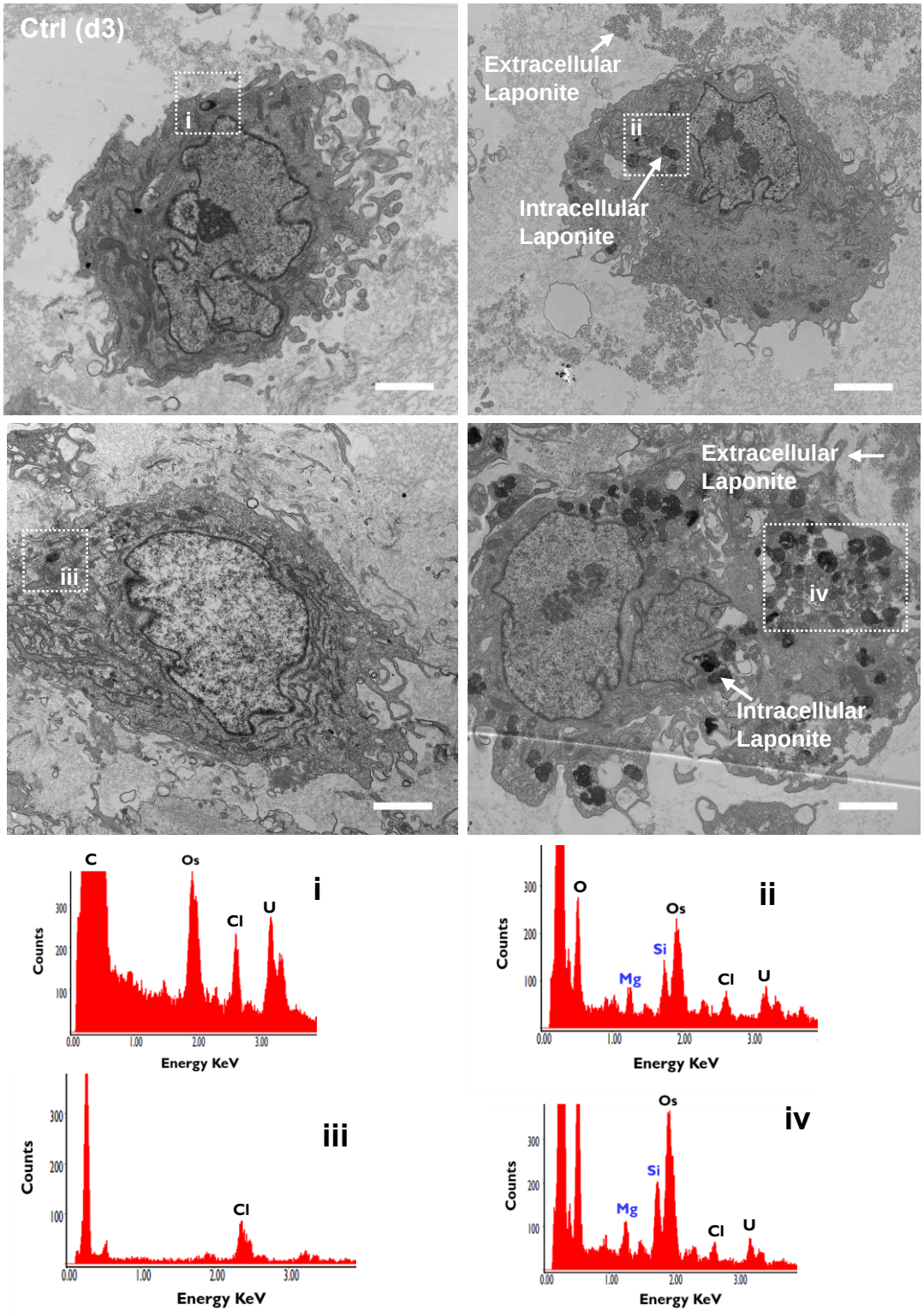

Figure 6. 5 Cellular uptake kinetics and extracellular vs intracellular distribution of Laponite.

Cells were cultured, alongside controls, with 100 µg/mL Laponite dispersion for 3 and 7 days. Laponite particles were found both extra- and intracellularly in the form of aggregates/clusters which increased in number with incubation time. Intracellular Laponite aggregates distributed throughout the cytoplasm. Images were taken at low magnifications of 6000x, using FEI Tecnai T12 Transmission Electron Microscope at 80 kV voltage. Scale bar = 2 µM. Boxes represent Laponite-free (i & iii) vs. Laponite-containing (ii & iv) lysosomes.

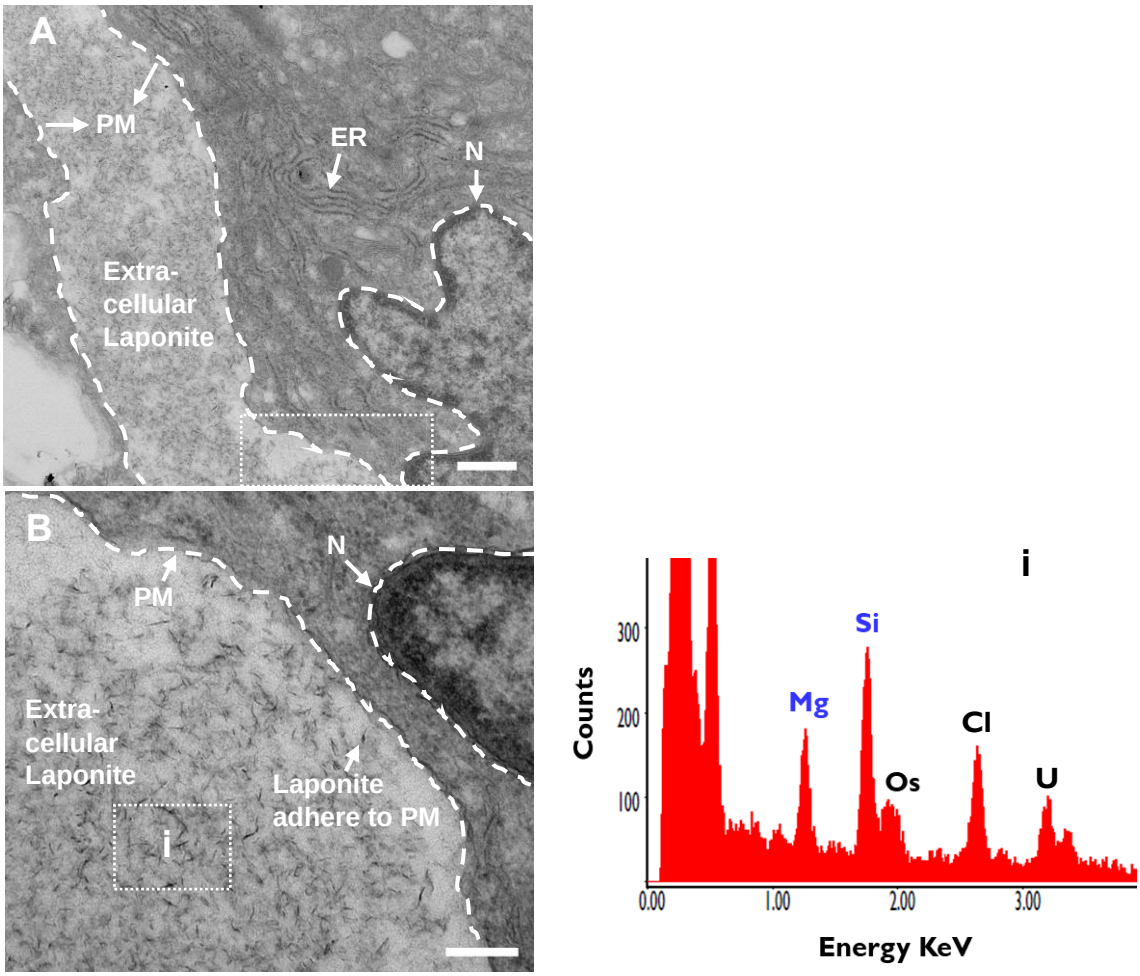

Figure 6. 6 Extracellular colocalisation of Laponite.
Laponite particles were found extracellularly in intercellular spaces and adhering to the plasma membrane as clusters of ~30-50 nm nanoparticles. Cells were treated with 100 µg/mL Laponite dispersion for 7 days then fixed and imaged using FEI Tecnai T12 Transmission Electron Microscope at 80 kV voltage. Image **A** was taken at magnification of 20500x (scale bar = 500 nm), while **B** is a higher magnification 60000x of selected area in image A (Scale bar = 200 nm). EDX analysis confirm presence of Laponite elemental peaks (Si & Mg) in highlighted areas of image **B** (box i which represent extracellular clay nanoparticles). PM = plasma membrane; ER = endoplasmic reticulum; N = nucleus.

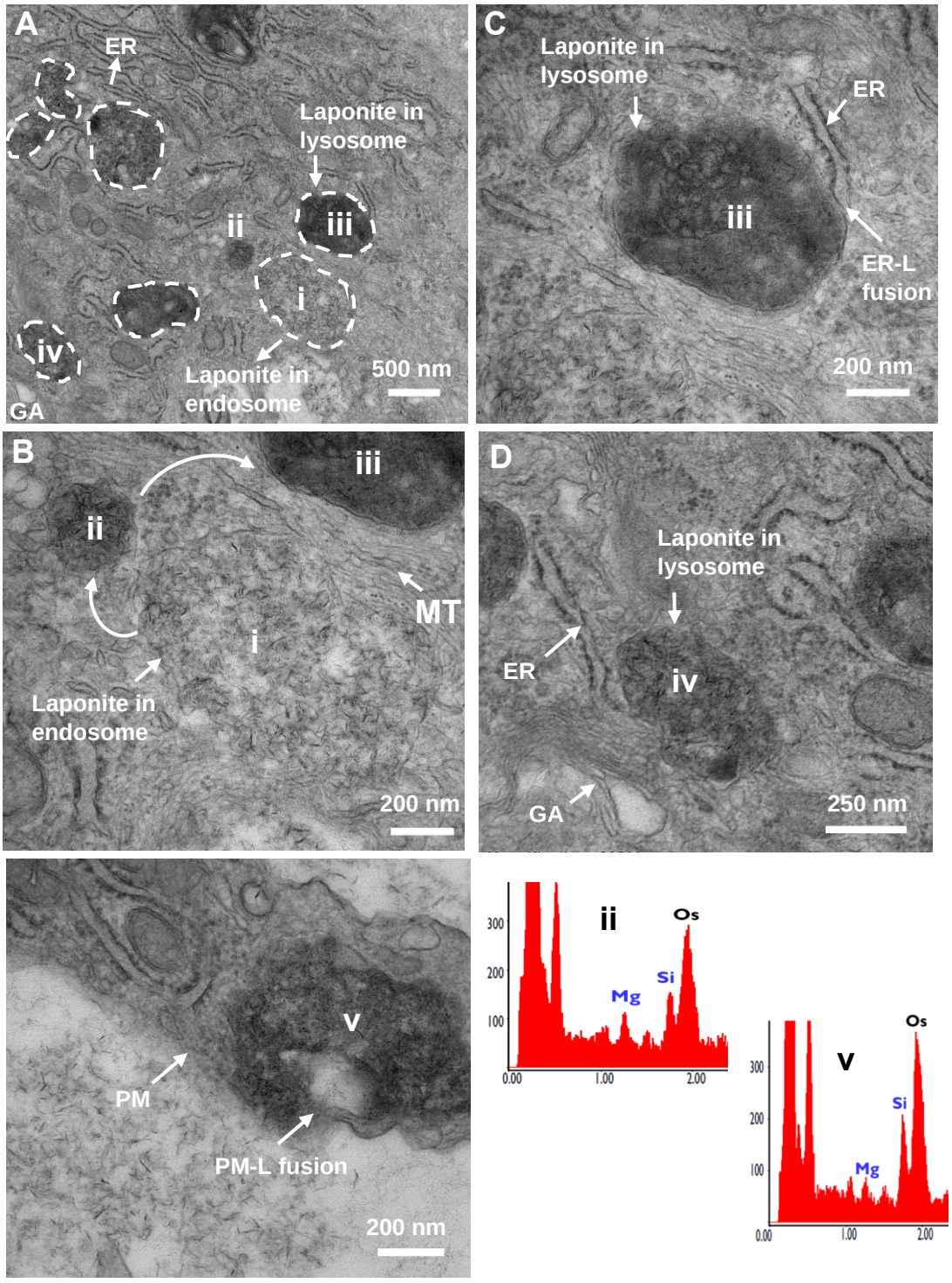

Figure 6. 7 Intracellular trafficking of Laponite in hBMSCs.
Laponite particles were found exclusively entrapped in endosomes (i) and lysosomes which, in some areas, fuse with ER (ii & iii), GA (iv) and plasma membrane (v) and exhibit various degrees of maturity (from i to v). Cells were treated with 100 µg/mL Laponite dispersion for 7 days then fixed and imaged using FEI Tecnai T12 Transmission Electron Microscope at 80 kV voltage. Image **A** was taken at magnification of 20500x (scale bar = 500 nm), while **B, C & D** are higher magnification of selected area (i, iii & iv) of image **A** (Scale bar = 200 nm). EDX analysis confirm presence of Laponite elemental peaks (Si & Mg) in selected area ii and v which represent lysosome and vesicle-membrane fusion respectively. ER = endoplasmic reticulum; GA = Golgi apparatus; L = lysosome; PM = plasma membrane; MT = microtubule.

6.4.3.2 Intracellular fate of Laponite nanoparticles

Laponite start its intracellular journey by interacting with the plasma membrane in the form of clusters for endocytosis as observed by the formation of membrane protrusions engulfing clay aggregates (**Figure 6.8**). Laponite particles at this stage are around 30-50 nm in size. When observed within endosomal compartments of lower maturation state (as indicated by their lower electron density) the particles display a similar size and morphology to extracellular Laponite. Interestingly within mature lysosomal bodies however, there is a marked decrease in particles size (< 10 nm) which is also attended by an increased Si/Mg EDX peak ratio compared to extracellular and endosomal clay. This observation is highly suggestive of intracellular degradation of Laponite nanoparticles in lysosomes with endo-/lysosomal maturation.

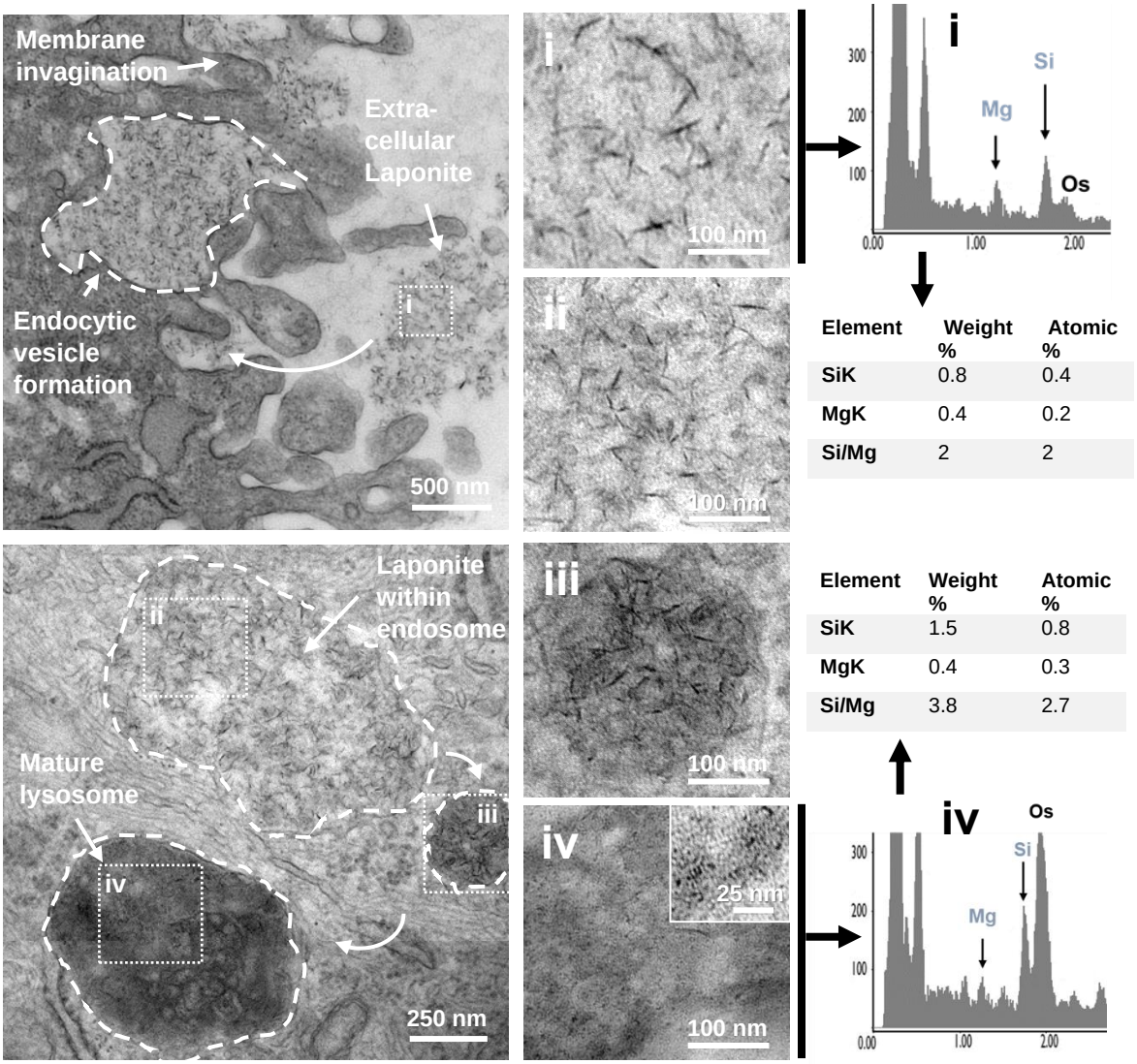

Figure 6. 8 Intracellular fate of endocytosed Laponite nanoparticles.
Laponite nanoparticles are endocytosed for subsequent entrapment within endosomal/lysosomal compartments and eventual degradation reflected in decrease in particle size and increase in Si/Mg ratio. Cells were treated with 100 µg/mL Laponite dispersion for 7 days. Images were taken using FEI Tecnai T12 Transmission Electron Microscope at 80 kV voltage. L = lysosome; PM = plasma membrane. i refers to extracellular (intact) Laponite nanoparticles (~30-50 nm), ii represent Laponite nanoparticles in endosomes, iii shows Laponite nanoparticles in lysosomes with higher degree of vesicle maturity and iv represents Laponite nanoparticles undergoing degradation within lysosomal bodies reducing Laponite particle size to < 10 nm. EDX analysis of areas i and iv suggests Laponite degradation as shown by increased Si/Mg peak ratios in response to Laponite uptake and processing within lysosomal bodies.

6.4.3.3 Cell response to Laponite internalization

A prominent feature of Laponite treated cells was the presence of double membrane-bound vesicles which were not observed in the control. A double membrane is a defining feature of autophagosomes and autolysosomes. The majority of such autophagosomes contained lamellar/residual bodies and fused with clay-lysosomes for autolysosome formation and clay and organelle degradation (**Figures 6.9**). They also colocalized with endoplasmic reticulum. Overall, our TEM images suggest a stimulatory role of Laponite on hBMSCs autophagy and Laponite colocalization with autophagosomes/autolysosomes for subsequent acidification, processing and degradation of clay particles and intracellular organelles.

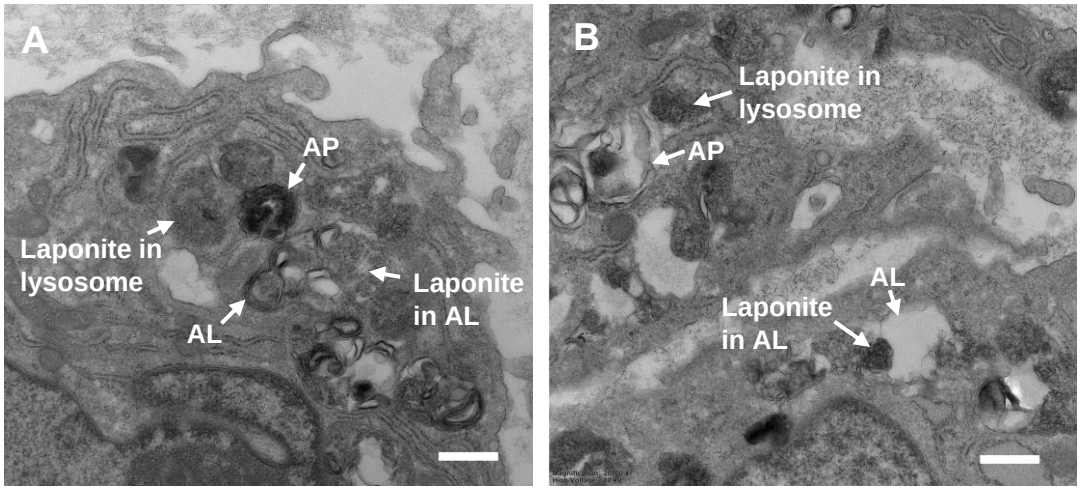

Figure 6. 9 Effect of internalized Laponite nanoparticles on hBMSCs autophagy. Cells were treated with 100 µg/mL Laponite dispersion for 3 (**A**) or 7 days (**B**). Laponite particles stimulate cell autophagy and colocalize with lamellar/residual bodies in autophagosomes for degradation. AP = autophagosome; AL = autolysosome. Images were taken magnifications of 20500x using FEI Tecnai T12 Transmission Electron Microscope. Scale bar = 500 nm

6.5 Discussion and analysis

In this study the interaction between Laponite nanoparticles and hBMSCs were tracked in terms of Laponite uptake kinetics, *in vitro* distribution, intracellular trafficking and fate and Laponite influence on cell organelles. Laponite was readily internalized by hBMSCs. Laponite uptake kinetics followed a linear increase with incubation time but did not reach saturation level even at 7 days of nanoclay exposure. Laponite nanoparticles were found both extracellularly, intracellularly as well as adhered on plasma membrane as clusters/aggregates with the extracellular portion represents the vast majority of initial applied Laponite particles. From the TEM at day 3 and 7 we can infer that Laponite starts its intracellular journey through interaction with plasma membrane as clusters which are subsequently endocytosed and entrapped within endosomal/lysosomal vesicles. These nanoclay/lysosomal compartments were distributed throughout the cytoplasm from the perinuclear to the peripheral regions and in some cases fused with the membrane of endoplasmic reticulum and Golgi apparatus. No Laponite particles were observed free in the cytoplasm or in any other cell organelle such as nucleus, mitochondria, endoplasmic reticulum and Golgi apparatus. TEM-EDX analysis suggested intracellular dissolution and exocytosis of internalized Laponite particles through endosomal-lysosomal maturation stages. On the other hand, the cell physiological behavior was significantly affected by Laponite endocytosis as evidenced by induced/enhanced autophagy which might represent an underlying mechanism for Laponite bioactivity.

When in contact with hBMSCs, Laponite was readily internalized and appeared well distributed across the cytoplasmic region. This is expected given the physicochemical properties of Laponite which give Laponite strong affinity for cellular uptake[265]. For example, the optimal particle size for cellular endocytosis is in the order of 25-30 nm[229] corresponding exactly with the surface plane of Laponite (25-30 nm sheets)[134,262]. In addition to particle size, the cationic edge charge of Laponite (Si-OH_2^+) allow direct/electrostatic interaction with the anionic glycoproteins and phospholipids of the cell membrane thus may also facilitate Laponite cellular interaction and uptake[131,179,231,348]. This is in agreement with various recent studies which reported strong affinity of Laponite for interaction with various cell types including stem and cancer cell models. For example, Laponite was readily internalized by hMSCs within 5 min[250] and enhanced the antitumor efficacy of

doxorubicin (DOX) drug primarily due to the observed much stronger cellular uptake of LAP/DOX than that of free DOX[349].

Next, we sought to track the kinetics of Laponite cellular uptake which is scarcely explored in the literature. It was observed that while the amount of internalized Laponite particles increases linearly with time, it does not appear to reach saturation level even at day 7 of nanoclay addition. Interestingly these data contrast with flow cytometry analysis presented by Carrow et al. - the only study reporting Laponite uptake kinetics which implied a more rapid association of Laponite nanoparticles with cells reaching saturation just at 5 min post-Laponite addition[250]. This might be attributed to various experimental factors such as the method of Laponite-culture media preparation, cell type and seeding density[339]. For example, therefore, it is possible that in this study Laponite nanoparticles exhibited more monodispersed state which allowed for more sustained delivery of suspended/dispersed particles to the cell monolayer over a wider time window through a slow diffusion-driven transport rather than a quick sedimentation-mediated process[350]. In support of this explanation, the dispersed form observed for extracellular Laponite particles using TEM in this study which also showed a particle size of 30-50 nm which is less than half that reported by Carrow et al (100 nm).

When investigating the *in vitro* distribution of Laponite nanoparticles across the hBMSCs culture system, it was observed that the amount of surface bound Laponite is nearly equivalent to the internalized portion until day 3. Although the approach adopted for the fractionation of the surface bound component in this study was rather crude, we can note that the fraction quantified is both consistent with other studies[131,193,351,352] and non-negligible when compared with the intracellular fraction. The influence of surface binding on observed phenotypic changes cannot therefore be discounted and may underlie previously reported ERK-MAPK mediated mechanical/cytoskeletal influences on cell phenotype[250].

Based on data provided in this study, in particular TEM-EDX, the intracellular journey of Laponite can be described as follows. Laponite interacts with the cell membrane as clusters of nanoscale particles (~30-50 nm) to undergo endocytosis. We have previously discussed how Laponite physicochemical properties (size & surface charge) give it strong affinity for interaction with cell membrane, but why it interacts

with the cell membrane as aggregates is still unclear. In fact, some studies indicate that nanoparticle clusters may have a higher chance and rate of internalization than single/individual nanoparticles as for example the case of silica nanoparticles[339,353,354]. In agreement with various experimental reports, Jin et al developed an interesting model which showed that nanoparticles diffuse to/on the cell membrane to form cluster with a size sufficient to generate a driving force that can overcome the elastic energy and entropic barriers associated with endocytosis[355] - something that does not occur with single particles[343].

Following endocytosis, Laponite particles/aggregates were observed entrapped within membrane bound endosomal/lysosomal vesicles – a similar intracellular trafficking pathway observed for various nanoparticles including gold[356,59], silica[309], silver[300] and anionic nanoclays[357]. Some of these vesicles were found in close proximity in the juxtanuclear region with different levels of electron density suggesting late endosome-lysosome fusion[358]. We did not detect any clay particles in the nucleus, free in the cytoplasm or embedded in other cytoplasmic organelles (endoplasmic reticulum, Golgi apparatus & mitochondria). However, the possibility that few particles may enter the nucleus cannot be excluded. In particular, the dispersed state of nanoparticles (~30-50 nm) in endosomes suggest that Laponite nanoparticles might escape the endosome and enter the nucleus and it is possible that particle passed inside the nucleus might be out of sectioning/plane. In support with this interpretation, Motskin et al.[235] showed nucleus entry of few hydroxyapatite nanoparticles with similar particle size (~50 nm) although not clearly observed in this study which might be due to particles out of sectioning/plane or the need for higher magnification imaging of the nucleus. This needs confirmation in the future studies.

We observed fusion of clay-entrapping vesicles with exocytic organelles (endoplasmic reticulum and Golgi apparatus) as well as with cell membrane suggesting an orchestrated interaction between endosomes, lysosomes, rough endoplasmic reticulum and Golgi apparatus for nanoclay processing and exocytosis[359]. Interestingly, similar intracellular trafficking pathway (endosome-lysosome-ER-Golgi-exocytosis) was reported for anionic nanoclay (layered double hydroxide) in human cells as confirmed by confocal imaging showing LDH co-localisation with early endosomes, lysosomes and Golgi apparatus[357]. In addition, the direct fusion of lysosomes with the plasma membrane infer another exocytic pathway

reported in literature (lysosomal exocytosis)[359,360]. Both scenarios have been observed in TEM of this study and are likely.

The absence of particles in the cytoplasm together with the active lysosomal processes observed is consistent with either, or both, of the following scenarios[342]: i) clay particles undergo degradation in lysosomes, which is the terminal degradative compartment of the endocytic pathway, and released in the cytoplasm as clay dissolution products Mg, Si, Na & Li; ii) clay particles are exocytosed, through the above discussed routes, either as intact or degraded particles. In fact, we observed various signs of Laponite nanoparticle degradation in lysosomes. For example, TEM imaging showed significant reduction in Laponite particle size in lysosomes (< 10 nm) compared particles in the extracellular environment or in early endosomes (~30-50 nm). It's worth noting that standard Laponite particle size in aqueous solution is 25-30 nm and in culture media around 100 nm according to literature[134,262]. Similar results were observed with mesoporous silica in lysosomes and cytoplasm of HUVECs in which particles underwent significant time-dependent reduction in their size (< 200 nm) compared to original particles (300-430 nm) initially applied to the cells[361]. The authors inferred particle degradation both in cytoplasm and lysosomes which was confirmed by confocal microscopy and inductively coupled plasma atomic emission spectroscopy (ICP-OES) analysis of cell lysate supernatant[361]. In addition to particle size change, the increase in Si/Mg weight or atomic ratio of lysosomal Laponite (3.8) compared to early endosomal or extracellular Laponite (2) is also suggestive of Laponite degradation. At pH below 9, as for example the lysosomal pH 4.5, H^+ first attack the edge of Laponite crystal (Mg-OH)[258] and the octahedral layer undergo predominant and faster dissolution over the tetrahedral network[257]. This will thus lead to quicker Mg^{2+} release than Si^{4+} and in turn higher Si/Mg peak ratio detected by EDX.

In agreement with the results presented in this study, the degradation of Laponite nanoparticles at pH < 9 is well documented in literature[134,294,243]. For example, recent work by Tang[246] and Yao[362] et al. provided evidence for Laponite nanorod and nanoplatelet degradation in cell culture media (pH = 7-7.4) as shown by significant time-dependent increase in the concentration of Si, Mg and Li ions in cell culture media extracts obtained from immersing Laponite-containing nanocomposites for 7 days. Moreover, anticancer drugs loaded on/in Laponite followed higher release rate

in acidic lysosomal-mimicking pH conditions than in physiological conditions[349,363] which might again be attributed to acid-enhanced nanoparticle degradation under these low pH conditions. The equation for this pH dependent dissolution is shown by Thompson and Butterworth equation below [134,243,364].

$Na_{0.8}Si_8Mg_{5.4}Li_{0.4}O_{20}(OH)_4 + 12H^+ + 8H_2O \rightarrow 0.8Na^+ + 8Si(OH)_4 + 5.4Mg^{2+} + 0.4Li^+$.

An interesting finding of this study is the indication that cellular uptake of Laponite may induce cell autophagy. This is suggested by the appearance, in Laponite treated cells, of double membrane vesicles - a typical feature of autophagosomes/autolysosomes[365]. Furthermore, Laponite nanoparticles were observed in autolysosomes resulting from fusion of autophagosomes with Laponite-entrapping lysosomes. Such nanoparticle-induced autophagy was also observed with other nanoparticles such as gold[343], silica[309], and silver[366]. Autophagy, which is a lysosome-based degradative pathway, has been reported to play an important role in promoting osteoblast differentiation *in vitro* and bone formation *in vivo*[367,368]. Interestingly, various nanoparticles stimulated cell osteogenic differentiation through autophagy induction which suggests autophagy as a potential mechanism behind clay nanoparticle osteogenic bioactivity. For example, addition of autophagy inhibitors 3-methyladenine (MA) and chloroquine (CQ) significantly reversed the gold[343] and silver[366] nanoparticles-enhanced ALP activity and mineralization of hMSCs bringing back to control levels compared to nanoparticles alone and silica nanoparticles were found in autolysosomes of differentiating osteoblasts[309]. Together these results infer that autophagy might be an underlying mechanism for Laponite osteogenic bioactivity and necessitate the need for further studies exploring this pathway. This could be achieved for example through confirming clay-induction of autophagy using biochemical markers such as LC3 and P62 proteins and investigating whether autophagy inhibition would influence the previous early observed clay-stimulation of hBMSCs osteogenesis.

Conclusion

This study answers key questions regarding the fate of Laponite following interaction with human bone marrow stromal cells which is critical for the successful control and manipulation of these nanomaterials not only for the regenerative medicine field but also for biomedical applications in general. Laponite was readily internalized by hBMSCs in a time dependent manner and the amount of Laponite distributed across the cell culture system was in the order extracellular > intracellular > surface bound. Laponite started its intracellular journey through endocytosis followed by entrapment exclusively in endosomal and lysosomal vesicles. This chapter also provides new evidence that Laponite undergoes degradation in lysosomes and exocytosis through direct lysosomal fusion with cell membrane and/or through lysosome-ER-Golgi orchestrated communication. Cell physiological function appears to be significantly affected due to Laponite internalization reflected in Laponite-induced autophagy which might be an underlying mechanism for Laponite bioactivity. Future experiments are warranted for exploring this pathway.

Chapter 7: Discussion

7.1 Achievements of the study

The main objective of this thesis was to explore the effect of Laponite clay nanoparticles on osteogenic differentiation of human bone marrow stromal cells, shed light on the role of Laponite endocytosis and release of degradation products in Laponite osteogenic bioactivity and track Laponite cellular uptake, intracellular trafficking and fate in hBMSCs which sets the basis for the successful harnessing of the potential afforded by nanoclay for the biomedical field. This project is a part of a long-term strategy to develop novel injectable osteogenic clay/stem cell microenvironments which can enhance bone regeneration at lower cost and minimal side effects. For this purpose, the project tested the hypothesis that Laponite clay nanoparticles induce/promote osteogenic differentiation of hBMSCs and that Laponite uptake and subsequent release of osteogenic degradation products play a significant role in Laponite osteogenic bioactivity.

This thesis achieved its aims by:

- The demonstration that Laponite clay nanoparticles are able to induce and promote osteogenic differentiation of bone marrow stromal cell population and that such Laponite osteogenic bioactivity strongly depend on nanoclay dose and exposure time
- Demonstrating that Laponite exert its osteogenic character through a direct nanoparticle-cell interaction and although Laponite endocytosis is essential for the ability of Laponite to promote hBMSCs osteogenesis, Laponite degradation products failed to play any significant role in Laponite osteogenic character, therefore, excluding a fundamental frequently cited mechanism for Laponite osteogenic bioactivity. This necessitates the need for turning attention to other physicochemical properties such as particles size and shape and cation exchange capacity which until now remain scarcely explored.
- Providing evidence for the intracellular transport route and fate of Laponite nanoparticles by hBMSCs - Laponite is readily internalized by cells, entrapped within endosomal/lysosomal compartments and activate cell autophagy and eventually degraded by the cells.

7.2 Summary of main findings

Before exploring the interaction mechanisms between Laponite nanoparticles and bone marrow stromal cells in chapters 4-6, chapter 3 was focused on confirming the biocompatibility and osteogenic properties of Laponite nanoparticles. This represented an opportunity to optimize methods and protocols in terms of clay dose and temporal stimulation for subsequent experiments to understand Laponite-hBMSCs interaction mechanisms most notably for osteogenesis. Laponite exhibited good biocompatibility on hBMSCs at doses ≤ 100 μg/mL with no significant influence on cell proliferation, adhesion and morphology as shown by stretched F-actin fibers and fibroblast-like morphology characteristic of mesenchymal cells. This dose range was further selected for assessing Laponite osteogenic bioactivity. Laponite significantly promoted osteogenic differentiation of hBMSCs in a dose- and time-dependent manner as demonstrated by enhanced ALP activity, osteogenic gene expression and extracellular matrix mineralisation. Interestingly, Laponite nanoparticle dispersions showed a unique ability to induce the formation of calcified bone-like nodules at two weeks of clay induction starting from primary cell culture (hBMSCs) although failed to be reproducible among different patients which might be attributed to sex, age, nutrition and the complex nature of patient variation. However, this opens the door for a new exciting research line of clay/regenerative medicine for terminal *in vitro* bone nodule formation starting from human primary stromal cells which is not widely reported – particularly at such an early time point.

Based on results from chapter 3, in chapter 4 we were interested in understanding how Laponite nanoparticles trigger such early enhancement of hBMSCs osteogenesis understood in this context in terms of ALP activity. We surveyed two different pathways including cell-independent, through direct Laponite-ALP interaction, and cell-dependent through Laponite endocytosis and release of degradation products Si^{4+}, Mg^{2+} and Li^{+}. Given the strong capacity of clay minerals, in general, to immobilise ALP enzyme and subsequently modulate its catalytic activity combined with the observed consistent ability of Laponite to strongly enhance ALP activity at an early stage (day 3), we started with exploring whether Laponite promotion of ALP activity is simply due to a direct interaction with the enzyme itself. Laponite showed a strong affinity for binding and immobilizing ALP enzyme and remarkably reduced (inhibited) its activity as shown by Michaelis–Menten parameter (increased K_m and

reduced V_{max}). This indicate that a direct binding of ALP by Laponite does not account for the previously observed ALP enhancement by nanoclay and turned our attention to the cell-dependent model. Based on surveying the literature, the fundamental frequently cited mechanism for nanoclay osteogenic bioactivity lie in nanoclay endocytosis and subsequent release of degradation products each of which is of relevance to osteogenic cell function. Therefore, almost, if not all, publications exploring the osteogenic bioactivity of clay rely on this mechanistic route in their interpretation but with no clear data to support this hypothesis. We started with exploring the role of Laponite endocytosis using a clathrin mediated endocytosis inhibitor at doses which proved biocompatible and able to efficiently block Laponite nanoparticle uptake. Interestingly, inhibition of Laponite endocytosis by hBMSCs strongly attenuated the as-observed clay enhancement of ALP activity suggesting Laponite endocytosis is crucial for its osteogenic action. Then, we moved to explore whether release of degradation products from Laponite, which might take place after fusion with lysosomes intracellularly, is responsible for Laponite osteogenic character. In contrast to intact Laponite particles, silicon, magnesium and lithium ions applied as salt solutions at conc. equivalent to that present in Laponite failed to trigger any significant influence on ALP activity of hBMSCs. This indicates that Laponite exert its osteogenic effect almost independent of its degradation products. However, it was essential to confirm excluding this route through the use of modified Laponite structures in terms of these elements (Si, Mg and Li) which provide a more consistent and reliable approach than simply the use of salts dispersed in culture media and to expand the osteogenic differentiation markers list (ALP activity, osteogenic gene expression and calcium mineralisation). Among these dissolution products, lithium ion was selected given its well known pharmacological action to promote bone formation both *in vitro* and *in vivo* and the frequent citation of its potential role in Laponite osteogenic bioactivity.

In chapter 5, we explored the role of lithium content of Laponite, as Wnt signaling activator, in Laponite osteogenic action on hBMSCs. This was achieved through the use of novel lithium modified clay formulations, in terms of both structural and adsorbed lithium, with BYK-ALTANA. Lithium content of Laponite was not sufficient to activate the Wnt signaling pathway demonstrated herein by Wnt reporter luciferase activity. Interestingly, results convincingly demonstrated that Laponite

exert its osteogenic action on hBMSCs almost independent of its lithium content, either incorporated in Laponite crystal structure or adsorbed on Laponite surface. This confirms against the hypothesized role of Laponite degradation products in imparting Laponite osteogenic bioactivity and turns attention towards intracellular biophysical model(s), mediated by intact particles, through for example acting as a nanocarrier of bioactive minerals/molecules or interacting with intracellular organelles to induce cell stress response such as ER stress and autophagy. However, an essential requirement before screening these various intracellular biophysical models is to explore the intracellular trafficking route and fate of Laponite nanoparticles by hBMSCs.

In chapter 6, we tracked how Laponite nanoparticles interact with hBMSCs in terms of Laponite uptake kinetics and *in vitro* distribution, Laponite intracellular transport route and fate as well as Laponite influence on physiological cell function. Laponite nanoparticles strongly interacted with and readily internalized by hBMSCs in a time-dependent manner in the form of aggregates of various sizes. These clay aggregates were localized in endosomal/lysosomal bodies and distributed from the perinuclear region to near the plasma membrane. However, such internalized amount of Laponite represent only ≤ 1.5% of the initial Laponite dispersion applied to the cells while the remaining percentage is represented by 0.5% adhered on cell membrane and 98-99.3% distributed in cell culture media extracellularly. These clay nanoparticles were found to enter the cell as aggregates/agglomerates via clathrin-mediated endocytosis and were not found free in any intracellular organelle other than endosomal and lysosomal vesicles some of which were fused with endoplasmic reticulum and Golgi apparatus. Moreover, TEM imaging showed that Laponite addition stimulated hBMSCs autophagy and Laponite co-localisation with autophagosomes/autolysosomes for its subsequent processing and degradation. Therefore, an interesting hypothesis we have drawn from this study is the role of autophagy as potential mechanism of Laponite osteogenic bioactivity which is currently under investigation.

7.3 Discussion of the main findings and their context to literature observations

The work presented in this thesis contributes to the field of biomaterials and regenerative medicine in a number of ways. Most importantly, it furthers the knowledge of the osteogenic effects of clay nanoparticles on human bone marrow stromal cells, clarifies the interaction mechanisms between clay nanoparticles and

hBMSCs and sets the basis for the successful control and manipulation of clay nanoparticles for reaching a clay/stem cell formula which easily be transferred to the clinic.

The finding that Laponite clay nanoparticles have intrinsic ability to induce osteogenic differentiation of human bone marrow stromal cells, combined with their well-established utility to impart attractive mechanical properties to biomaterial scaffolds and their classic use as drug delivery vehicles introduce an exciting new class of scaffolds/additives for enhanced bone regeneration. This represents an opportunity to enhance the osteoinductive properties of various scaffolds to induce bone formation even in absence of external osteogenic supplements which are known for their high expense and off-target effects[132].

Another important implication of this study is clarifying the mechanisms of interaction between Laponite clay nanoparticles and skeletal stem cells in terms of particle uptake, intracellular journey and fate. This understanding is essential to inform their use clinically and also future modifications of this technology. It is well known that the influence nanoparticles exert on cell function and fate strongly depend on the route and extent of their uptake[339,180]. Moreover, various studies have hypothesized the role of clay degradation products behind Laponite bioactivity but to date scarce information is available regarding their biodegradation, clearance profile and intracellular fate[265].Work in this thesis provides a clear understanding of such a pathway by demonstrating for the first time clay entrapment within lysosomal bodies and subsequent degradation. This is of importance for the biomedical field which requires biomaterial biodegradation into nontoxic products after achieving their target, for example as a template scaffold for regenerative medicine or after drug delivery to the targeted intracellular organelle[113]. This also supports a normal cellular route for Laponite nanoparticles by hBMSCs and supports the biocompatibility data provided above and increases the interest in harnessing the potential of such materials[339,342]. Moreover, the finding that clay nanoparticles are biocompatible and degrade intracellularly into nontoxic products combined with the well-known drug loading capacity of nanoclay make them an ideal candidate for drug delivery in cancer therapy for example[273,265,142]. However, the genotoxicity and *in vivo* distribution of these nanomaterials remain important unanswered questions.

Another interesting finding of this thesis is the Laponite induction of hBMSCs autophagy and colocalization with autophagosomes/autolysosomes which open a new promising direction to successfully understand how clay nanoparticles induce/promote hBMSCs osteogenic differentiation. Autophagy induction has been reported to promote osteoblast differentiation *in vitro* and *in vivo*[367,368] and various nanoparticles such as [343], silica[309], and silver[366] have been shown to induce osteogenic differentiation of responsive stem cell population through this pathway. However, until now no data are available in literature to discuss the role of autophagy in nanoclay osteogenic bioactivity.

7.4 Limitations of the current set of studies

Biosafety of nanoparticles, in general, is a prerequisite for their successful biomedical application and ultimate translation to the clinic. Although this thesis started with investigating the biocompatibility of Laponite nanoparticles, it did not explore the biodistribution, clearance profile and geno-/toxicity *in vivo*. We continued on excellent work reported by Gaharwar and colleagues which showed the evidence for *in vivo* Laponite biocompatibility[273] and biodegradability but with locally restricted inflammatory reactions especially with high clay doses[133,135] and with a paucity of information regarding their clearance profile and genotoxicity. This is important issue to address in future studies.

Another limitation of this study is that I relied on ALP activity as a key osteogenic marker for investigating the role of Laponite degradation products in Laponite osteogenic bioactivity, however, these data would have been more decisive and conclusive if supported by including other osteogenic markers such as extracellular matrix mineralization and osteogenic gene and protein expression over a wider culture timeframe. However, when referring back to data provided by the lithium modified Laponite nanoparticles, which are based on ALP activity, ECM mineralisation and bone-related gene expression, we found similar results confirming the negligible role of Laponite degradation products. In addition, when consulting data from the wide literature we find that they stand against a role of Laponite degradation products for two main reasons (discussed in chapter 4, section 4.5) : i) even assuming complete degradation of Laponite nanoparticles, the conc. of released ions is far below the limit to induce any significant influence on the cell osteogenic differentiation; ii) similar

clay-induced osteoblast differentiation was seen with other clay minerals which are free from Mg and Li ions in their composition.

Despite such interesting data observed in chapter 6 which indicate intracellular Laponite particle degradation within endosomal/lysosomal compartments, the data would be much stronger when supported with experiments exploring, through chemical analysis, how Laponite nanoparticles are processed in physiological conditions (cell culture medium) vs lysosome-mimicking ones (e.g. artificial lysosomal fluid) through the use of dialysis tubing and measuring the conc. of released degradation products via ICPMS. This is a fundamental experiment which needs exploration to support both the degradation data presented in chapter 4 and the Laponite fate results presented in chapter 6.

The observations of Laponite induction of cell autophagy and colocalisation with autolysosomes still need confirmation with confocal microscopy of fluorescently labeled Laponite and autophagosomes/autolysosomes and investigating the influence of Laponite on autophagy markers (LC3 & P62) both at the gene and protein levels. Once this nanoclay-activation of autophagy in hBMSCs is confirmed, the role of such pathway in Laponite osteogenic action can be investigated for example through the use of autophagy inhibitors such as 3MA and CQ. In fact, these experiments are currently under investigation by the Bone and Joint Group at Southampton General Hospital.

7.5 Future research directions

Based on results presented in this thesis, a number of future research directions can be proposed. First, it was found in chapter 3 that Laponite clay nanoparticles hold the potential to induce terminal *in vitro* osteogenic differentiation of human bone marrow stromal cells in the form of 3D bone-like nodules which is challenging to achieve starting from human primary bone marrow cultures[270] especially at early stage (day 14). These results necessitate the need for replicating such data with optimized/wider experimental design using multiple patients and with more-in-depth characterization of such clay-enhanced nodule formation. This can be achieved through characterizing the as-formed nodules morphologically and chemically using: i) SEM-EDX[280,281] for determination of nodule structure and elemental peaks/ratios such as calcium, phosphorus, and carbon combined with ii) Raman spectroscopy which is a non-

destructive technique that can be applied on live cells to detect functional groups for cells ECM and tissues [280,282] and compare them to native bone[280]. Subsequently, the cellular component of the as-formed nodules can be characterized by histological sectioning and staining to explore the presence and organization the three cell types, osteoblasts, osteocytes and fibroblasts[270].

Given that Laponite degradation products do not participate individually in imparting the osteogenic properties of Laponite, the role of other physicochemical properties such as particle size, shape and surface charge warrant further investigation. In fact subtle changes in these Laponite structural parameters (size, shape and charge) will modulate not only Laponite osteogenic bioactivity but its biocompatibility and biodegradation profile[179]. We have seen in chapter 5 how lithium modification of Laponite attenuated the effect of standard Laponite on hBMSCs gene expression although was not driven by Laponite lithium content. Understanding the response of skeletal stem cell populations to Laponite nanoparticles with varying structural properties, here particle size, shape and density of charge, is necessary for optimizing and tailoring the features of nanoclay for enhanced stem cell responses. Although a large number of studies have reported significant effect on stem cell differentiation due to modifying physicochemical properties of various nanoparticles, such as gold, silica and hydroxyapatite[343,369,308], no equivalent data are available regarding nanoclay.

The observation that Laponite clay nanoparticles accumulate on the cell membrane, are readily endocytosed by hBMSCs and subsequently entrapped within the endosomal/lysosomal bodies for ultimate particle degradation combined with its well utilized excellent drug loading capacity suggest these nanoparticles as promising biocompatible new class of nanomaterials for delivery of bioactive cues for regenerative medicine. Our group have utilized such drug delivery utility of Laponite gel for inducing bone formation at super low doses of BMP2[142] (around 3000 lower than currently employed in clinical practice) while preserving the bioactivity of loaded biomolecules. However, such utility of nanoclay for delivery of bioactive molecules is scarcely explored with individual nanoparticles. Therefore, harnessing this utility of clay nanoparticles can provide a safe and efficient approach for enhanced receptor-growth factor interaction and improved transport and intracellular release of bioactive agents such as calcium phosphate minerals/ions. Therefore,

harnessing the intrinsic osteogenic bioactivity of nanoclay combined with bioactive drug delivery capacity opens the door for these nanoparticles as a promising bioactive additives that can foster stem cell responses while minimizing the negative side effects associated with the use of supraphysiological doses of protein therapeutics for orthopedic applications.

Finally, based on reaching the exact mechanism underlying Laponite osteogenic bioactivity and understanding the role of key clay physicochemical properties, it will be important to generate a family of novel Laponite formulations that can induce bone formation as implantable 3D scaffold (e.g. nanoclay gel) both *in vitro* and *in vivo*. This will be the basis for reaching the clay/stem cell formula which successfully be translated to the clinic.

7.6 Concluding remarks

No previous studies have convincingly addressed how clay nanoparticles affect osteogenic differentiation of human bone marrow stromal cells and the mechanisms underlying nanoclay-hBMSCs interactions. This study provides evidence for the osteogenic bioactivity of nanoclay and screens for the various modes of influence nanoclay exert on skeletal stem cell functions. It convincingly demonstrated the ability of Laponite clay nanoparticles to induce osteogenic differentiation of hBMSCs. It shed the light on the role Laponite endocytosis as a crucial element for Laponite osteogenic character and corrects for a number of pathways misinterpreted in literature behind Laponite osteogenic bioactivity particularly the role of degradation products. Finally, it unravels the interaction mechanisms between Laponite nanoparticles and hBMSCs showing that clay nanoparticles are readily internalized by hBMSCs, subsequently transported within the degradative lysosomal pathway and ultimately degraded within endosomal/lysosomal compartments. It suggests new avenue for reaching the exact mechanism behind Laponite osteogenic bioactivity – i.e. Laponite-induced cell autophagy. Therefore, we believe that the work presented in this thesis sets a solid basis for the successful manipulation and control of such new class of biomaterials for ultimate clinical translation.

References

1. Marks, S. C. & Odgren, P. R. Structure and Development of the Skeleton. in *Principles of Bone Biology* 3–15 (2002).

2. Morgan, E. F., Barnes, G. L. & Einhorn, T. A. The Bone Organ System. Form and Function. in *Osteoporosis: Fourth Edition* 3–20 (2013).

3. Morrison, S. J. & Scadden, D. T. The bone marrow niche for haematopoietic stem cells. *Nature* **505**, 327–334 (2014).

4. Little, N., Rogers, B. & Flannery, M. Bone formation, remodelling and healing. *Surgery* **29**, 141–145 (2011).

5. Crockett, J. C., Rogers, M. J., Coxon, F. P., Hocking, L. J. & Helfrich, M. H. Bone remodelling at a glance. *Journal of Cell Science* **124**, 991–998 (2011).

6. Feng, X. Chemical and biochemical basis of cell-bone matrix interaction in health and disease. *Current Chemical Biology* **3**, 189–196 (2009).

7. Lacroix, D. Biomechanical aspects of bone repair. in *Bone Repair Biomaterials* 106–118 (2009).

8. Young, M. F. Bone matrix proteins: their function, regulation, and relationship to osteoporosis. *Osteoporosis international* **14 Suppl 3**, 35–42 (2003).

9. Teti, A. Regulation of cellular functions by extracellular matrix. *Journal of the American Society of Nephrology* **2**, S83 (1992).

10. Freemont, A. J. Basic bone cell biology. *International journal of experimental pathology* **74**, 411–6 (1993).

11. Rutkovskiy, A., Stensløkken, K.-O. & Vaage, I. J. Osteoblast Differentiation at a Glance. *Medical Science Monitor Basic Research* **22**, 95–106 (2016).

12. Florencio-Silva, R., Sasso, G. R. D. S., Sasso-Cerri, E., Simões, M. J. & Cerri, P. S. Biology of Bone Tissue: Structure, Function, and Factors That Influence Bone Cells. *BioMed Research International* **2015**, (2015).

13. Karsenty, G., Kronenberg, H. M. & Settembre, C. Genetic control of bone formation. *Annual Review of Cell and Developmental Biology* **25**, 629–648

(2009).

14. Fattore, A. Del, Teti, A. & Rucci, N. Bone cells and the mechanisms of bone remodelling. *Frontiers in Bioscience - Elite* **4 E**, 2302–2321 (2012).

15. Bonewald, L. F. The amazing osteocyte. *Journal of Bone and Mineral Research* **26**, 229–238 (2011).

16. Loiselle, A. E., Jiang, J. X. & Donahue, H. J. Gap junction and hemichannel functions in osteocytes. *Bone* **54**, 205–212 (2013).

17. Boyle, W. J., Simonet, W. S. & Lacey, D. L. Osteoclast differentiation and activation. *Nature* **423**, 337–342 (2003).

18. Yavropoulou, M. P. & Yovos, J. G. Osteoclastogenesis - Current knowledge and future perspectives. *Journal of Musculoskeletal Neuronal Interactions* **8**, 204–216 (2008).

19. Teitelbaum, S. L. Osteoclasts: What do they do and how do they do it? *American Journal of Pathology* **170**, 427–435 (2007).

20. Clarke, B. Normal bone anatomy and physiology. *Clinical journal of the American Society of Nephrology : CJASN* **3 Suppl 3**, S131–S139 (2008).

21. Dorozhkin, S. V. Calcium orthophosphates as bioceramics: State of the art. *Journal of Functional Biomaterials* **1**, 22–1074 (2010).

22. Lin, X., Patil, S., Gao, Y. G. & Qian, A. The Bone Extracellular Matrix in Bone Formation and Regeneration. *Frontiers in Pharmacology* **11**, (2020).

23. Elango, J. *et al.* Collagen Peptide Upregulates Osteoblastogenesis from Bone Marrow Mesenchymal Stem Cells through MAPK- Runx2. *Cells* **8**, 446 (2019).

24. Tsai, K. S. *et al.* Type I collagen promotes proliferation and osteogenesis of human mesenchymal stem cells via activation of ERK and Akt pathways. *Journal of Biomedical Materials Research - Part A* **94**, 673–682 (2010).

25. Nudelman, F. *et al.* The role of collagen in bone apatite formation in the presence of hydroxyapatite nucleation inhibitors. *Nature Materials* **9**, 1004–1009 (2010).

26. Roach, H. I. Why does bone matrix contain non-collagenous proteins? The

possible roles of osteocalcin, osteonectin, osteopontin and bone sialoprotein in bone mineralisation and resorption. *Cell Biology International* **18**, 617–628 (1994).

27. Gordon, J. A. R. *et al.* Bone sialoprotein expression enhances osteoblast differentiation and matrix mineralization in vitro. *Bone* **41**, 462–473 (2007).

28. Gericke, A. *et al.* Importance of phosphorylation for osteopontin regulation of biomineralization. *Calcified Tissue International* **77**, 45–54 (2005).

29. Huang, W. *et al.* Osteopontin is a negative regulator of proliferation and differentiation in MC3T3-E1 pre-osteoblastic cells. *Bone* **34**, 799–808 (2004).

30. Zoch, M. L., Clemens, T. L. & Riddle, R. C. New insights into the biology of osteocalcin. *Bone* **82**, 42–49 (2016).

31. Carvalho, M. S., Cabral, J. M. S., da Silva, C. L. & Vashishth, D. Synergistic effect of extracellularly supplemented osteopontin and osteocalcin on stem cell proliferation, osteogenic differentiation, and angiogenic properties. *Journal of Cellular Biochemistry* **120**, 6555–6569 (2019).

32. Termine, J. D. *et al.* Osteonectin, a bone-specific protein linking mineral to collagen. *Cell* **26**, 99–105 (1981).

33. Zhu, Y. Sen, Gu, Y., Jiang, C. & Chen, L. Osteonectin regulates the extracellular matrix mineralization of osteoblasts through P38 signaling pathway. *Journal of Cellular Physiology* **235**, 2220–2231 (2020).

34. David Shier, Ricki Lewis, J. B. *Hole's Human Anatomy and Physiology*. (McGraw-Hill Higher Education, 2015).

35. Tandon, B. *Essentials of Human Anatomy*. *Essentials of Human Anatomy* (Pearson, 2009).

36. Bianco, P. *et al.* The meaning, the sense and the significance: Translating the science of mesenchymal stem cells into medicine. *Nature Medicine* **19**, 35–42 (2013).

37. Bianco, P. & Robey, P. G. Skeletal stem cells. *Development (Cambridge)* **142**, 1023–1027 (2015).

38. Chan, C. K. F. *et al.* Identification of the Human Skeletal Stem Cell. *Cell* **175**, 43-56.e21 (2018).

39. Nombela-Arrieta, C., Ritz, J. & Silberstein, L. E. The elusive nature and function of mesenchymal stem cells. *Nature Reviews Molecular Cell Biology* **12**, 126–131 (2011).

40. Pittenger, M. F. *et al.* Multilineage potential of adult human mesenchymal stem cells. *Science* **284**, 143–147 (1999).

41. Prockop, D. J. Marrow stromal cells as stem cells for nonhematopoietic tissues. *Science* **276**, 71–74 (1997).

42. Méndez-Ferrer, S. *et al.* Mesenchymal and haematopoietic stem cells form a unique bone marrow niche. *Nature* **466**, 829–834 (2010).

43. Uccelli, A., Moretta, L. & Pistoia, V. Mesenchymal stem cells in health and disease. *Nature Reviews Immunology* **8**, 726–736 (2008).

44. Le Blanc, K. & Mougiakakos, D. Multipotent mesenchymal stromal cells and the innate immune system. *Nature Reviews Immunology* **12**, 383–396 (2012).

45. Caplan, A. I. & Correa, D. The MSC: An injury drugstore. *Cell Stem Cell* **9**, 11–15 (2011).

46. Beresford, J. N. Osteogenic stem cells and the stromal system of bone and marrow. *Clinical Orthopaedics and Related Research* 270–280 (1989).

47. Caplan, A. I. Mesenchymal stem cells. *Journal of Orthopaedic Research* **9**, 641–650 (1991).

48. Bianco, P., Kuznetsov, S. A., Riminucci, M. & Gehron Robey, P. Postnatal Skeletal Stem Cells. in *Methods in Enzymology* vol. 419 117–148 (2006).

49. Simmons, P. & Torok-Storb, B. Identification of stromal cell precursors in human bone marrow by a novel monoclonal antibody, STRO-1. *Blood* **78**, 55–62 (1991).

50. Gronthos, S., Graves, S. E., Ohta, S. & Simmons, P. J. The STRO-1+ fraction of adult human bone marrow contains the osteogenic precursors. *Blood* **84**, 4164–4173 (1994).

51. Tare, R. S., Mitchell, P. D., Kanczler, J. & Oreffo, R. O. C. Isolation, differentiation, and characterisation of skeletal stem cells from human bone marrow in vitro and in vivo. *Methods in Molecular Biology* **816**, 83–99 (2012).

52. Sacchetti, B. *et al.* Self-Renewing Osteoprogenitors in Bone Marrow Sinusoids Can Organize a Hematopoietic Microenvironment. *Cell* **131**, 324–336 (2007).

53. Quirici, N. *et al.* Isolation of bone marrow mesenchymal stem cells by anti-nerve growth factor receptor antibodies. *Experimental Hematology* **30**, 783–791 (2002).

54. Gang, E. J., Bosnakovski, D., Figueiredo, C. A., Visser, J. W. & Perlingeiro, R. C. R. SSEA-4 identifies mesenchymal stem cells from bone marrow. *Blood* **109**, 1743–1751 (2007).

55. Ambrosi, T. H., Longaker, M. T. & Chan, C. K. F. A Revised Perspective of Skeletal Stem Cell Biology. *Frontiers in Cell and Developmental Biology* **7**, (2019).

56. Böhm, A. M. *et al.* Activation of Skeletal Stem and Progenitor Cells for Bone Regeneration Is Driven by PDGFRβ Signaling. *Developmental Cell* **51**, 236-254.e12 (2019).

57. Quarto, R. *et al.* Repair of large bone defects with the use of autologous bone marrow stromal cells. *New England Journal of Medicine* **344**, 385–386 (2001).

58. Aubin, J. E. & Triffitt, J. T. Mesenchymal Stem Cells and Osteoblast Differentiation. in *Principles of Bone Biology* 59–81 (2002). doi:10.1016/b978-012098652-1.50106-2.

59. Yi, C., Liu, D., Fong, C. C., Zhang, J. & Yang, M. Gold nanoparticles promote osteogenic differentiation of mesenchymal stem cells through p38 MAPK pathway. *ACS Nano* **4**, 6439–6448 (2010).

60. Komori, T. *et al.* Targeted disruption of Cbfa1 results in a complete lack of bone formation owing to maturational arrest of osteoblasts. *Cell* **89**, 755–764 (1997).

61. Otto, F. *et al.* Cbfa1, a candidate gene for cleidocranial dysplasia syndrome, is essential for osteoblast differentiation and bone development. *Cell* **89**, 765–771

(1997).

62. Ducy, P., Zhang, R., Geoffroy, V., Ridall, A. L. & Karsenty, G. Osf2/Cbfa1: A transcriptional activator of osteoblast differentiation. *Cell* **89**, 747–754 (1997).

63. Nakashima, K. *et al.* The novel zinc finger-containing transcription factor Osterix is required for osteoblast differentiation and bone formation. *Cell* **108**, 17–29 (2002).

64. Zhou, X. *et al.* Multiple functions of Osterix are required for bone growth and homeostasis in postnatal mice. *Proceedings of the National Academy of Sciences of the United States of America* **107**, 12919–12924 (2010).

65. Karperien, M. *et al.* Tissue Formation during Embryogenesis. in *Tissue Engineering: Second Edition* 67–109 (2015).

66. Stein, G. S. & Lian, J. B. Molecular mechanisms mediating proliferation/differentiation interrelationships during progressive development of the osteoblast phenotype. *Endocrine Reviews* **14**, 424–442 (1993).

67. Franceschi, R. T. The developmental control of osteoblast-specific gene expression: Role of specific transcription factors and the extracellular matrix environment. *Critical Reviews in Oral Biology and Medicine* **10**, 40–57 (1999).

68. Aghajanian, P. & Mohan, S. The art of building bone: Emerging role of chondrocyte-to-osteoblast transdifferentiation in endochondral ossification. *Bone Research* (2018) doi:10.1038/s41413-018-0021-z.

69. Long, F. Building strong bones: Molecular regulation of the osteoblast lineage. *Nature Reviews Molecular Cell Biology* **13**, 27–38 (2012).

70. Majidinia, M., Sadeghpour, A. & Yousefi, B. The roles of signaling pathways in bone repair and regeneration. *Journal of Cellular Physiology* **233**, 2937–2948 (2018).

71. Gao, C., Peng, S., Feng, P. & Shuai, C. Bone biomaterials and interactions with stem cells. *Bone Research* **5**, 1–33 (2017).

72. Deng, Z. L. *et al.* Regulation of osteogenic differentiation during skeletal development. *Frontiers in Bioscience* **13**, 2001–2021 (2008).

73. Liu, X. *et al.* Wnt signaling in bone formation and its therapeutic potential for bone diseases. *Therapeutic Advances in Musculoskeletal Disease* **5**, 13–31 (2013).

74. Gong, Y. *et al.* LDL receptor-related protein 5 (LRP5) affects bone accrual and eye development. *Cell* **107**, 513–523 (2001).

75. Clevers, H. Wnt/β-Catenin Signaling in Development and Disease. *Cell* **127**, 469–480 (2006).

76. Kahn, M. Can we safely target the WNT pathway? *Nature Reviews Drug Discovery* **13**, 513–532 (2014).

77. Ling, L., Nurcombe, V. & Cool, S. M. Wnt signaling controls the fate of mesenchymal stem cells. *Gene* **433**, 1–7 (2009).

78. Liu, W. *et al.* Canonical Wnt signaling differently modulates osteogenic differentiation of mesenchymal stem cells derived from bone marrow and from periodontal ligament under inflammatory conditions. *Biochimica et Biophysica Acta - General Subjects* **1840**, 1125–1134 (2014).

79. Liu, G. *et al.* Canonical Wnts function as potent regulators of osteogenesis by human mesenchymal stem cells. *Journal of Cell Biology* **185**, 67–75 (2009).

80. De Boer, J. *et al.* Wnt signaling inhibits osteogenic differentiation of human mesenchymal stem cells. *Bone* **34**, 818–826 (2004).

81. Boland, G. M., Perkins, G., Hall, D. J. & Tuan, R. S. Wnt 3a promotes proliferation and suppresses osteogenic differentiation of adult human mesenchymal stem cells. *Journal of Cellular Biochemistry* **93**, 1210–1230 (2004).

82. Gaur, T. *et al.* Canonical WNT signaling promotes osteogenesis by directly stimulating Runx2 gene expression. *Journal of Biological Chemistry* **280**, 33132–33140 (2005).

83. Staal, F. J. T., Luis, T. C. & Tiemessen, M. M. Erratum: WNT signalling in the immune system: WNT is spreading its wings (Nature Reviews Immunology (2008) 8 (581-593)). *Nature Reviews Immunology* **15**, 329 (2015).

84. Liu, D., Yi, C., Zhang, D., Zhang, J. & Yang, M. Inhibition of proliferation and differentiation of mesenchymal stem cells by carboxylated carbon nanotubes. *ACS Nano* **4**, 2185–2195 (2010).

85. Chen, D. *et al.* Differential roles for bone morphogenetic protein (BMP) receptor type IB and IA in differentiation and specification of mesenchymal precursor cells to osteoblast and adipocyte lineages. *Journal of Cell Biology* **142**, 295–305 (1998).

86. Ryoo, H. M., Lee, M. H. & Kim, Y. J. Critical molecular switches involved in BMP-2-induced osteogenic differentiation of mesenchymal cells. *Gene* **366**, 51–57 (2006).

87. Wan, M. & Cao, X. BMP signaling in skeletal development. *Biochemical and Biophysical Research Communications* **328**, 651–657 (2005).

88. Chen, Q. *et al.* Fate decision of mesenchymal stem cells: Adipocytes or osteoblasts? *Cell Death and Differentiation* **23**, 1128–1139 (2016).

89. Jimi, E., Hirata, S., Shin, M., Yamazaki, M. & Fukushima, H. Molecular mechanisms of BMP-induced bone formation: Cross-talk between BMP and NF-κB signaling pathways in osteoblastogenesis. *Japanese Dental Science Review* **46**, 33–42 (2010).

90. Ge, C., Xiao, G., Jiang, D. & Franceschi, R. T. Critical role of the extracellular signal-regulated kinase-MAPK pathway in osteoblast differentiation and skeletal development. *Journal of Cell Biology* **176**, 709–718 (2007).

91. Xiao, G., Jiang, D., Gopalakrishnan, R. & Franceschi, R. T. Fibroblast growth factor 2 induction of the osteocalcin gene requires MAPK activity and phosphorylation of the osteoblast transcription factor, Cbfa1/Runx2. *Journal of Biological Chemistry* **277**, 36181–36187 (2002).

92. Hwang, J. H. *et al.* Extracellular matrix stiffness regulates osteogenic differentiation through MAPK activation. *PLoS ONE* **10**, e0135519 (2015).

93. Salasznyk, R. M., Klees, R. F., Hughlock, M. K. & Plopper, G. E. ERK signaling pathways regulate the osteogenic differentiation of human mesenchymal stem cells on collagen I and vitronectin. *Cell Communication*

and Adhesion **11**, 137–153 (2004).

94. You, J. *et al.* Osteopontin Gene Regulation by Oscillatory Fluid Flow via Intracellular Calcium Mobilization and Activation of Mitogen-activated Protein Kinase in MC3T3-E1 Osteoblasts. *Journal of Biological Chemistry* **276**, 13365–13371 (2001).

95. Kim, J. M. *et al.* The ERK MAPK pathway is essential for skeletal development and homeostasis. *International Journal of Molecular Sciences* **20**, 1803 (2019).

96. Patel, A. L. & Shvartsman, S. Y. Outstanding questions in developmental ERK signaling. *Development (Cambridge)* **145**, dev143818 (2018).

97. Kim, H. J. & Bar-Sagi, D. Modulation of signalling by sprouty: A developing story. *Nature Reviews Molecular Cell Biology* **5**, 441–450 (2004).

98. Nakamura, T. *et al.* Induction of osteogenic differentiation by hedgehog proteins. *Biochemical and Biophysical Research Communications* **237**, 465–469 (1997).

99. Van Der Horst, G., Farih-Sips, H., Löwik, C. W. G. M. & Karperien, M. Hedgehog stimulates only osteoblastic differentiation of undifferentiated KS483 cells. *Bone* **33**, 899–910 (2003).

100. Ornitz, D. M. & Marie, P. J. FGF signaling pathways in endochondral and intramembranous bone development and human genetic disease. *Genes and Development* **16**, 1446–1465 (2002).

101. Du, X., Xie, Y., Xian, C. J. & Chen, L. Role of FGFs/FGFRs in skeletal development and bone regeneration. *Journal of Cellular Physiology* **227**, 3731–3743 (2012).

102. Marie, P. J., Debiais, F. & Haÿ, E. Regulation of human cranial osteoblast phenotype by FGF-2, FGFR-2 and BMP-2 signaling. *Histology and Histopathology* **17**, 877–885 (2002).

103. Boilly, B., Vercoutter-Edouart, A. S., Hondermarck, H., Nurcombe, V. & Le Bourhis, X. FGF signals for cell proliferation and migration through different pathways. *Cytokine and Growth Factor Reviews* **11**, 295–302 (2000).

104. Huang, W., Yang, S., Shao, J. & Li, Y. P. Signaling and transcriptional regulation in osteoblast commitment and differentiation. *Frontiers in Bioscience* **12**, 3068–3092 (2007).

105. Green, E., Lubahn, J. D. & Evans, J. Risk factors, treatment, and outcomes associated with nonunion of the midshaft humerus fracture. *Journal of surgical orthopaedic advances* **14**, 64–72 (2005).

106. Van Staa, T. P., Dennison, E. M., Leufkens, H. G. M. & Cooper, C. Epidemiology of fractures in England and Wales. *Bone* **29**, 517–522 (2001).

107. Panteli, M., Pountos, I., Jones, E. & Giannoudis, P. V. Biological and molecular profile of fracture non-union tissue: Current insights. *Journal of Cellular and Molecular Medicine* **19**, 685–713 (2015).

108. Mills, L. A. & Simpson, A. H. R. W. The relative incidence of fracture non-union in the Scottish population (5.17 million): A 5-year epidemiological study. *BMJ Open* **3**, (2013).

109. Wang, W. & Yeung, K. W. K. Bone grafts and biomaterials substitutes for bone defect repair: A review. *Bioactive Materials* **2**, 224–247 (2017).

110. Dimitriou, R., Jones, E., McGonagle, D. & Giannoudis, P. V. Bone regeneration: Current concepts and future directions. *BMC Medicine* **9**, 1–10 (2011).

111. Campana, V. *et al.* Bone substitutes in orthopaedic surgery: from basic science to clinical practice. *Journal of Materials Science: Materials in Medicine* **25**, 2445–2461 (2014).

112. Blokhuis, T. J., Calori, G. M. & Schmidmaier, G. Autograft versus BMPs for the treatment of non-unions: What is the evidence? *Injury* **44**, S40–S42 (2013).

113. O'Brien, F. J. Biomaterials & scaffolds for tissue engineering. *Materials Today* **14**, 88–95 (2011).

114. Khan, S. N. *et al.* The biology of bone grafting. *The Journal of the American Academy of Orthopaedic Surgeons* **13**, 77–86 (2005).

115. Roberts, T. T. & Rosenbaum, A. J. Bone grafts, bone substitutes and

orthobiologics the bridge between basic science and clinical advancements in fracture healing. *Organogenesis* **8**, 114–124 (2012).

116. Betz, R. R. Limitations of autograft and allograft: New synthetic solutions. *Orthopedics* **25**, 561–70 (2002).

117. Bhatt, R. A. & Rozental, T. D. Bone Graft Substitutes. *Hand Clinics* **28**, 457–468 (2012).

118. Kurien, T., Pearson, R. G. & Scammell, B. E. Bone graft substitutes currently available in orthopaedic practice: The evidence for their use. *Bone and Joint Journal* **95 B**, 583–597 (2013).

119. Langer, R. & Vacanti, J. P. Tissue engineering. *Science* **260**, 920–926 (1993).

120. Luo, Z. *et al.* Peptide-incorporated 3D porous alginate scaffolds with enhanced osteogenesis for bone tissue engineering. *Colloids and Surfaces B: Biointerfaces* **143**, 243–251 (2016).

121. Zhang, K. *et al.* Advanced smart biomaterials and constructs for hard tissue engineering and regeneration. *Bone Research* **6**, 1–15 (2018).

122. Qu, H., Fu, H., Han, Z. & Sun, Y. Biomaterials for bone tissue engineering scaffolds: A review. *RSC Advances* **9**, 26252–26262 (2019).

123. Andrée, L., Barata, D., Sutthavas, P., Habibovic, P. & van Rijt, S. Guiding mesenchymal stem cell differentiation using mesoporous silica nanoparticle-based films. *Acta Biomaterialia* **96**, 557–567 (2019).

124. Fathi-Achachelouei, M. *et al.* Use of nanoparticles in tissue engineering and regenerative medicine. *Frontiers in Bioengineering and Biotechnology* **7**, 113 (2019).

125. Shi, J., Votruba, A. R., Farokhzad, O. C. & Langer, R. Nanotechnology in drug delivery and tissue engineering: From discovery to applications. *Nano Letters* **10**, 3223–3230 (2010).

126. J Hill, M. *et al.* Nanomaterials for bone tissue regeneration: Updates and future perspectives. *Nanomedicine* **14**, 2987–3006 (2019).

127. Dawson, J. I. & Oreffo, R. O. C. Clay: New opportunities for tissue

regeneration and biomaterial design. *Advanced Materials* **25**, 4069–4086 (2013).

128. Chimene, D., Alge, D. L. & Gaharwar, A. K. Two-Dimensional Nanomaterials for Biomedical Applications: Emerging Trends and Future Prospects. *Advanced Materials* **27**, 7261–7284 (2015).

129. Kerativitayanan, P., Carrow, J. K. & Gaharwar, A. K. Nanomaterials for Engineering Stem Cell Responses. *Advanced Healthcare Materials* **4**, 1600–1627 (2015).

130. Gaharwar, A. K. *et al.* Bioactive silicate nanoplatelets for osteogenic differentiation of human mesenchymal stem cells. *Advanced Materials* **25**, 3329–3336 (2013).

131. Mihaila, S. M. *et al.* The osteogenic differentiation of SSEA-4 sub-population of human adipose derived stem cells using silicate nanoplatelets. *Biomaterials* **35**, 9087–9099 (2014).

132. Xavier, J. R. *et al.* Bioactive nanoengineered hydrogels for bone tissue engineering: A growth-factor-free approach. *ACS Nano* **9**, 3109–3118 (2015).

133. Gaharwar, A. K. *et al.* Shear-thinning nanocomposite hydrogels for the treatment of hemorrhage. *ACS Nano* **8**, 9833–9842 (2014).

134. Thompson, D. W. & Butterworth, J. T. The nature of laponite and its aqueous dispersions. *Journal of Colloid And Interface Science* **151**, 236–243 (1992).

135. Paul, A. *et al.* Nanoengineered biomimetic hydrogels for guiding human stem cell osteogenesis in three dimensional microenvironments. *Journal of Materials Chemistry B* **4**, 3544–3554 (2016).

136. Kerativitayanan, P. *et al.* Nanoengineered Osteoinductive and Elastomeric Scaffolds for Bone Tissue Engineering. *ACS Biomaterials Science and Engineering* **3**, 590–600 (2017).

137. Su, D., Jiang, L., Chen, X., Dong, J. & Shao, Z. Enhancing the Gelation and Bioactivity of Injectable Silk Fibroin Hydrogel with Laponite Nanoplatelets. *ACS Applied Materials and Interfaces* **8**, 9619–9628 (2016).

138. Ambre, A. H., Katti, D. R. & Katti, K. S. Nanoclays mediate stem cell differentiation and mineralized ECM formation on biopolymer scaffolds. *Journal of Biomedical Materials Research - Part A* **101 A**, 2644–2660 (2013).

139. Hong, S. *et al.* 3D Printing: 3D Printing of Highly Stretchable and Tough Hydrogels into Complex, Cellularized Structures. *Advanced materials (Deerfield Beach, Fla.)* **27**, 4034 (2015).

140. Mehrali, M. *et al.* Nanoreinforced Hydrogels for Tissue Engineering: Biomaterials that are Compatible with Load-Bearing and Electroactive Tissues. *Advanced Materials* **29**, 1603612 (2017).

141. Dawson, J. I., Kanczler, J. M., Yang, X. B., Attard, G. S. & Oreffo, R. O. C. Clay gels for the delivery of regenerative microenvironments. *Advanced Materials* **23**, 3304–3308 (2011).

142. Gibbs, D. M. R. *et al.* Bone induction at physiological doses of BMP through localization by clay nanoparticle gels. *Biomaterials* **99**, 16–23 (2016).

143. Brigatti, M. F., Galán, E. & Theng, B. K. G. Structure and Mineralogy of Clay Minerals. in *Developments in Clay Science* vol. 5 21–81 (2013).

144. Güven, N. Crystal Structures of Clay Minerals and Their X-ray Identification. *Clays and Clay Minerals* **30**, 80–80 (1982).

145. Yuan, P., Tan, D. & Annabi-Bergaya, F. Properties and applications of halloysite nanotubes: Recent research advances and future prospects. *Applied Clay Science* **112**–**113**, 75–93 (2015).

146. Lvov, Y. M., DeVilliers, M. M. & Fakhrullin, R. F. The application of halloysite tubule nanoclay in drug delivery. *Expert Opinion on Drug Delivery* **13**, 977–986 (2016).

147. Van Olphen, H. *An introduction to clay colloid chemistry. By H van Olphen. Interscience Publishers, Div. of John Wiley & Sons, 605 Third Ave., New York 16, N. Y, 1963. xvi + 301 pp. 15.5 × 23 cm. Price $10*. *Journal of Pharmaceutical Sciences* vol. 53 (1964).

148. Neumann, B. S. & Sansom, K. G. The rheological properties of dispersions of Laponite, a synthetic hectorite-like clay, in electrolyte solutions. *Clay Minerals*

9, 231–243 (1971).

149. Martin, R. T. Data Handbook for Clay Materials and Other Non-Metallic Minerals. *Clays and Clay Minerals* **28**, 160 (1980).

150. Drever, J. I. *The geochemistry of natural waters. The geochemistry of natural waters.* (Prentice-Hall, Inc., Englewood Cliffs, N.J, 1982).

151. Swartzen-Allen, S. Lee, and E. M. Surface and Colloid Chemistry of Clays. *Chemical Reviews* **74**, 385–400 (1974).

152. Ruzicka, B. & Zaccarelli, E. A fresh look at the Laponite phase diagram. *Soft Matter* **7**, 1268–1286 (2011).

153. Galan, E. Properties and applications of palygorskite-sepiolite clays. *Clay Minerals* **31**, 443–453 (1996).

154. Jones, B. F. & Galan, E. H. Sepiolite and palygorskite. *Reviews in Mineralogy* **19**, 631–674 (1988).

155. Theng, B. K. G. Polymer-clay nanocomposites. in *Developments in Clay Science* vol. 4 201–241 (2012).

156. Thakur, A. *et al.* Injectable shear-thinning nanoengineered hydrogels for stem cell delivery. *Nanoscale* **8**, 12362–12372 (2016).

157. Waters, R. *et al.* Stem cell secretome-rich nanoclay hydrogel: A dual action therapy for cardiovascular regeneration. *Nanoscale* **8**, 7371–7376 (2016).

158. Nojoomi, A., Tamjid, E., Simchi, A., Bonakdar, S. & Stroeve, P. Injectable polyethylene glycol-laponite composite hydrogels as articular cartilage scaffolds with superior mechanical and rheological properties. *International Journal of Polymeric Materials and Polymeric Biomaterials* **66**, 105–114 (2017).

159. Haraguchi, K., Takehisa, T. & Fan, S. Effects of clay content on the properties of nanocomposite hydrogels composed of poly(N-isopropylacrylamide) and clay. *Macromolecules* **35**, 10162–10171 (2002).

160. Lee, J. H. *et al.* Thermal and mechanical characteristics of poly(L-lactic acid) nanocomposite scaffold. *Biomaterials* **24**, 2773–2778 (2003).

161. Lee, Y. H. *et al.* Electrospun dual-porosity structure and biodegradation morphology of Montmorillonite reinforced PLLA nanocomposite scaffolds. *Biomaterials* **26**, 3165–3172 (2005).

162. Bitinis, N., Hernandez, M., Verdejo, R., Kenny, J. M. & Lopez-Manchado, M. A. Recent advances in clay/polymer nanocomposites. *Advanced Materials* **23**, 5229–5236 (2011).

163. Theng. Clay-polymer interactions: summary and perspectives. *Clay and Clay Minerals* **30**, 1–10 (1982).

164. Ray, S. S. Recent trends and future outlooks in the field of clay-containing polymer nanocomposites. *Macromolecular Chemistry and Physics* **215**, 1162–1179 (2014).

165. Ahlfeld, T. *et al.* Development of a clay based bioink for 3D cell printing for skeletal application. *Biofabrication* **9**, 034103 (2017).

166. Jin, Y., Liu, C., Chai, W., Compaan, A. & Huang, Y. Self-Supporting Nanoclay as Internal Scaffold Material for Direct Printing of Soft Hydrogel Composite Structures in Air. *ACS Applied Materials and Interfaces* **9**, 17456–17465 (2017).

167. Aguzzi, C., Cerezo, P., Viseras, C. & Caramella, C. Use of clays as drug delivery systems: Possibilities and limitations. *Applied Clay Science* **36**, 22–36 (2007).

168. Yu, W. H. *et al.* Adsorption of proteins and nucleic acids on clay minerals and their interactions: A review. *Applied Clay Science* **80**–**81**, 443–452 (2013).

169. Zheng, J. P., Luan, L., Wang, H. Y., Xi, L. F. & Yao, K. D. Study on ibuprofen/montmorillonite intercalation composites as drug release system. *Applied Clay Science* **36**, 297–301 (2007).

170. Park, J. K. *et al.* Controlled release of donepezil intercalated in smectite clays. *International Journal of Pharmaceutics* **359**, 198–204 (2008).

171. Pongjanyakul, T., Khunawattanakul, W. & Puttipipatkhachorn, S. Physicochemical characterizations and release studies of nicotine-magnesium aluminum silicate complexes. *Applied Clay Science* **44**, 242–250 (2009).

172. Joshi, G. V., Kevadiya, B. D., Patel, H. A., Bajaj, H. C. & Jasra, R. V. Montmorillonite as a drug delivery system: Intercalation and in vitro release of timolol maleate. *International Journal of Pharmaceutics* **374**, 53–57 (2009).

173. Viseras, C., Cerezo, P., Sanchez, R., Salcedo, I. & Aguzzi, C. Current challenges in clay minerals for drug delivery. *Applied Clay Science* **48**, 291–295 (2010).

174. Jafarbeglou, M., Abdouss, M., Shoushtari, A. M. & Jafarbeglou, M. Clay nanocomposites as engineered drug delivery systems. *RSC Advances* **6**, 50002–50016 (2016).

175. Xue, J. *et al.* Electrospun microfiber membranes embedded with drug-loaded clay nanotubes for sustained antimicrobial protection. *ACS Nano* **9**, 1600–1612 (2015).

176. Takahashi, T., Yamada, Y., Kataoka, K. & Nagasaki, Y. Preparation of a novel PEG-clay hybrid as a DDS material: Dispersion stability and sustained release profiles. *Journal of Controlled Release* **107**, 408–416 (2005).

177. Ding, X., Gao, J., Wang, Z., Awada, H. & Wang, Y. A shear-thinning hydrogel that extends in vivo bioactivity of FGF2. *Biomaterials* **111**, 80–89 (2016).

178. Lvov, Y. M., Shchukin, D. G., Möhwald, H. & Price, R. R. Halloysite clay nanotubes for controlled release of protective agents. *ACS Nano* **2**, 814–820 (2008).

179. Albanese, A., Tang, P. S. & Chan, W. C. W. The effect of nanoparticle size, shape, and surface chemistry on biological systems. *Annual Review of Biomedical Engineering* **14**, 1–16 (2012).

180. Panariti, A., Miserocchi, G. & Rivolta, I. The effect of nanoparticle uptake on cellular behavior: Disrupting or enabling functions? *Nanotechnology, Science and Applications* **5**, 87–100 (2012).

181. Vergaro, V. *et al.* Cytocompatibility and uptake of halloysite clay nanotubes. *Biomacromolecules* **11**, 820–826 (2010).

182. Naumenko, E. A., Guryanov, I. D., Yendluri, R., Lvov, Y. M. & Fakhrullin, R. F. Clay nanotube-biopolymer composite scaffolds for tissue engineering.

Nanoscale **8**, 7257–7271 (2016).

183. Lai, X. *et al.* Proteomic profiling of halloysite clay nanotube exposure in intestinal cell co-culture. *Journal of Applied Toxicology* **33**, 1316–1329 (2013).

184. Chiriaco, F. *et al.* Cytotoxicity measurements of Halloysite Nanotubes for nanomedicine applications. *IEEE MeMeA 2014 - IEEE International Symposium on Medical Measurements and Applications, Proceedings* 1–4 (2014).

185. Paola, M. Di *et al.* Surface coating highly improves cytocompatibility of halloysite nanotubes: A metabolic and ultrastructural study. *IEEE Transactions on Nanotechnology* **15**, 770–774 (2016).

186. Kommireddy, D. S., Ichinose, I., Lvov, Y. M. & Mills, D. K. Nanoparticle Multilayers: Surface Modification for Cell Attachment and Growth. *Journal of Biomedical Nanotechnology* **1**, 286–290 (2006).

187. Zhou, W. Y. *et al.* Poly(vinyl alcohol)/Halloysite nanotubes bionanocomposite films: Properties and in vitro osteoblasts and fibroblasts response. *Journal of Biomedical Materials Research - Part A* **93**, 1574–1587 (2010).

188. Huang, B., Liu, M., Long, Z., Shen, Y. & Zhou, C. Effects of halloysite nanotubes on physical properties and cytocompatibility of alginate composite hydrogels. *Materials Science and Engineering C* **70**, 303–310 (2017).

189. Nitya, G., Nair, G. T., Mony, U., Chennazhi, K. P. & Nair, S. V. In vitro evaluation of electrospun PCL/nanoclay composite scaffold for bone tissue engineering. *Journal of Materials Science: Materials in Medicine* **23**, 1749–1761 (2012).

190. Jing, X., Mi, H. Y. & Turng, L. S. Comparison between PCL/hydroxyapatite (HA) and PCL/halloysite nanotube (HNT) composite scaffolds prepared by co-extrusion and gas foaming. *Materials Science and Engineering C* **72**, 53–61 (2017).

191. Robinson, D., Karnik, S. & Mills, D. K. Stem cell proliferation and differentiation through capped clay nanotubes. *Proceedings - 32nd Southern Biomedical Engineering Conference, SBEC 2016* 25–26 (2016).

192. Mieszawska, A. J. *et al.* Clay enriched silk biomaterials for bone formation. *Acta Biomaterialia* **7**, 3036–3041 (2011).

193. Li, P. R. *et al.* Evaluation on cytotoxicity and genotoxicity of the exfoliated silicate nanoclay. *ACS Applied Materials and Interfaces* **2**, 1608–1613 (2010).

194. Baek, M., Lee, J. A. & Choi, S. J. Toxicological effects of a cationic clay, montmorillonite in vitro and in vivo. *Molecular and Cellular Toxicology* **8**, 95–101 (2012).

195. Costa, R. *et al.* Osteoblast, fibroblast and in vivo biological response to poly(vinylidene fluoride) based composite materials. *Journal of Materials Science: Materials in Medicine* **24**, 395–403 (2013).

196. Sandri, G. *et al.* Montmorillonite-chitosan-silver sulfadiazine nanocomposites for topical treatment of chronic skin lesions: In vitro biocompatibility, antibacterial efficacy and gap closure cell motility properties. *Carbohydrate Polymers* **102**, 970–977 (2014).

197. Lordan, S., Kennedy, J. E. & Higginbotham, C. L. Cytotoxic effects induced by unmodified and organically modified nanoclays in the human hepatic HepG2 cell line. *Journal of Applied Toxicology* **31**, 27–35 (2011).

198. Salcedo, I. *et al.* In vitro biocompatibility and mucoadhesion of montmorillonite chitosan nanocomposite: A new drug delivery. *Applied Clay Science* **55**, 131–137 (2012).

199. Lin, F. H., Chen, C. H., Cheng, W. T. K. & Kuo, T. F. Modified montmorillonite as vector for gene delivery. *Biomaterials* **27**, 3333–3338 (2006).

200. Zhuang, H., Zheng, J. P., Gao, H. & De Yao, K. In vitro biodegradation and biocompatibility of gelatin/montmorillonite- chitosan intercalated nanocomposite. *Journal of Materials Science: Materials in Medicine* **18**, 951–957 (2007).

201. Rawat, K., Agarwal, S., Tyagi, A., Verma, A. K. & Bohidar, H. B. Aspect Ratio Dependent Cytotoxicity and Antimicrobial Properties of Nanoclay. *Applied Biochemistry and Biotechnology* **174**, 936–944 (2014).

202. Haroun, A. A., Gamal-Eldeen, A. & Harding, D. R. K. Preparation, characterization and in vitro biological study of biomimetic three-dimensional gelatin-montmorillonite/cellulose scaffold for tissue engineering. *Journal of Materials Science: Materials in Medicine* **20**, 2527–2540 (2009).

203. Da Silva, G. R. *et al.* Montmorillonite clay based polyurethane nanocomposite as substrate for retinal pigment epithelial cell growth. *Journal of Materials Science: Materials in Medicine* **24**, 1309–1317 (2013).

204. Popryadukhin, P. V. *et al.* Composite materials based on chitosan and montmorillonite: Prospects for use as a matrix for cultivation of stem and regenerative cells. *Cell and Tissue Biology* **6**, 82–88 (2012).

205. Katti, K. S., Katti, D. R. & Dash, R. Synthesis and characterization of a novel chitosan/montmorillonite/ hydroxyapatite nanocomposite for bone tissue engineering. *Biomedical Materials* **3**, 034122 (2008).

206. Bongartz, R. *et al.* Folic acid-modified clay: Targeted surface design for cell culture applications. *Journal of Materials Chemistry B* **1**, 522–528 (2013).

207. Barlas, F. B. *et al.* Folic acid modified clay/polymer nanocomposites for selective cell adhesion. *Journal of Materials Chemistry B* **2**, 6412–6421 (2014).

208. Ambre, A., Katti, K. S. & Katti, D. R. In situ mineralized hydroxyapatite on amino acid modified nanoclays as novel bone biomaterials. *Materials Science and Engineering C* **31**, 1017–1029 (2011).

209. Ambre, A. H., Katti, D. R. & Katti, K. S. Biomineralized hydroxyapatite nanoclay composite scaffolds with polycaprolactone for stem cell-based bone tissue engineering. *Journal of Biomedical Materials Research - Part A* **103**, 2077–2101 (2015).

210. Katti, K. S., Ambre, A. H., Payne, S. & Katti, D. R. Vesicular delivery of crystalline calcium minerals to ECM in biomineralized nanoclay composites. *Materials Research Express* **2**, 045401 (2015).

211. Gaharwar, A. K., Schexnailder, P. J., Kline, B. P. & Schmidt, G. Assessment of using Laponite® cross-linked poly(ethylene oxide) for controlled cell adhesion and mineralization. *Acta Biomaterialia* **7**, 568–577 (2011).

212. Zhai, X. *et al.* 3D-Printed High Strength Bioactive Supramolecular Polymer/Clay Nanocomposite Hydrogel Scaffold for Bone Regeneration. *ACS Biomaterials Science and Engineering* **3**, 1109–1118 (2017).

213. Schexnailder, P. J., Gaharwar, A. K., Bartlett, R. L., Seal, B. L. & Schmidt, G. Tuning Cell Adhesion by Incorporation of Charged Silicate Nanoparticles as Cross-Linkers to Polyethylene Oxide. *Macromolecular Bioscience* **10**, 1416–1423 (2010).

214. Gaharwar, A. K. *et al.* Highly extensible bio-nanocomposite films with Direction-dependent properties. *Advanced Functional Materials* **20**, 429–436 (2010).

215. Peak, C. W., Carrow, J. K., Thakur, A., Singh, A. & Gaharwar, A. K. Elastomeric Cell-Laden Nanocomposite Microfibers for Engineering Complex Tissues. *Cellular and Molecular Bioengineering* **8**, 404–415 (2015).

216. Gaharwar, A. K. *et al.* Physically Crosslinked Nanocomposites from Silicate-Crosslinked PEO: Mechanical Properties and Osteogenic Differentiation of Human Mesenchymal Stem Cells. *Macromolecular Bioscience* **12**, 779–793 (2012).

217. Haraguchi, K., Takehisa, T. & Ebato, M. Control of cell cultivation and cell sheet detachment on the surface of polymer/clay nanocomposite hydrogels. *Biomacromolecules* **7**, 3267–3275 (2006).

218. Jain, M. & Matsumura, K. Polyampholyte- and nanosilicate-based soft bionanocomposites with tailorable mechanical and cell adhesion properties. *Journal of Biomedical Materials Research - Part A* **104**, 1379–1386 (2016).

219. Chang, C. W., Van Spreeuwel, A., Zhang, C. & Varghese, S. PEG/clay nanocomposite hydrogel: A mechanically robust tissue engineering scaffold. *Soft Matter* **6**, 5157–5164 (2010).

220. Jain, M. & Matsumura, K. Thixotropic injectable hydrogel using a polyampholyte and nanosilicate prepared directly after cryopreservation. *Materials Science and Engineering C* **69**, 1273–1281 (2016).

221. Han, L. *et al.* Mussel-Inspired Adhesive and Tough Hydrogel Based on

Nanoclay Confined Dopamine Polymerization. *ACS Nano* **11**, 2561–2574 (2017).

222. Gaharwar, A. K. *et al.* Nanoclay-enriched poly(€-caprolactone) electrospun scaffolds for osteogenic differentiation of human mesenchymal stem cells. *Tissue Engineering - Part A* **20**, 2088–2101 (2014).

223. Wang, C. *et al.* Preparation of laponite bioceramics for potential bone tissue engineering applications. *PLoS ONE* **9**, e99585 (2014).

224. Kerativitayanan, P. & Gaharwar, A. K. Elastomeric and mechanically stiff nanocomposites from poly(glycerol sebacate) and bioactive nanosilicates. *Acta Biomaterialia* **26**, 34–44 (2015).

225. Gaharwar, A. K., Rivera, C. P., Wu, C. J. & Schmidt, G. Transparent, elastomeric and tough hydrogels from poly(ethylene glycol) and silicate nanoparticles. *Acta Biomaterialia* **7**, 4139–4148 (2011).

226. Wang, S. *et al.* Electrospun laponite-doped poly(lactic-co-glycolic acid) nanofibers for osteogenic differentiation of human mesenchymal stem cells. *Journal of Materials Chemistry* **22**, 23357–23367 (2012).

227. Castro-Smirnov, F. A. *et al.* Cellular uptake pathways of sepiolite nanofibers and DNA transfection improvement. *Scientific Reports* **7**, 1–10 (2017).

228. Zhang, S., Gao, H. & Bao, G. Physical Principles of Nanoparticle Cellular Endocytosis. *ACS Nano* **9**, 8655–8671 (2015).

229. Zhang, S., Li, J., Lykotrafitis, G., Bao, G. & Suresh, S. Size-dependent endocytosis of nanoparticles. *Advanced Materials* **21**, 419–424 (2009).

230. Gratton, S. E. A. *et al.* The effect of particle design on cellular internalization pathways. *Proceedings of the National Academy of Sciences of the United States of America* **105**, 11613–11618 (2008).

231. Arvizo, R. R. *et al.* Effect of nanoparticle surface charge at the plasma membrane and beyond. *Nano Letters* **10**, 2543–2548 (2010).

232. Pomeransky, A. A. & Khriplovich, I. B. Equations of motion of spinning relativistic particle in external fields. *Journal of Experimental and Theoretical*

Physics volume **86**, 839–849 (1998).

233. Choi, S. J. & Choy, J. H. Layered double hydroxide nanoparticles as target-specific delivery carriers: Uptake mechanism and toxicity. *Nanomedicine* **6**, 803–814 (2011).

234. Oh, J. M., Choi, S. J., Kim, S. T. & Choy, J. H. Cellular uptake mechanism of an inorganic nanovehicle and its drug conjugates: Enhanced efficacy due to clathrin-mediated endocytosis. *Bioconjugate Chemistry* **17**, 1411–1417 (2006).

235. Motskin, M. *et al.* Hydroxyapatite nano and microparticles: Correlation of particle properties with cytotoxicity and biostability. *Biomaterials* **30**, 3307–3317 (2009).

236. Napierska, D. *et al.* Size-dependent cytotoxicity of monodisperse silica nanoparticles in human endothelial cells. *Small* **5**, 846–853 (2009).

237. Park, M. V. D. Z. *et al.* In vitro developmental toxicity test detects inhibition of stem cell differentiation by silica nanoparticles. *Toxicology and Applied Pharmacology* **240**, 108–116 (2009).

238. Drury, J. L. & Mooney, D. J. Hydrogels for tissue engineering: Scaffold design variables and applications. *Biomaterials* **24**, 4337–4351 (2003).

239. Gaharwar, A. K., Schexnailder, P. J., Jin, Q., Wu, C. J. & Schmidt, G. Addition of chitosan to silicate cross-linked PEO for tuning osteoblast cell adhesion and mineralization. *ACS Applied Materials and Interfaces* **2**, 3119–3127 (2010).

240. van Wachem, P. B. *et al.* Interaction of cultured human endothelial cells with polymeric surfaces of different wettabilities. *Biomaterials* **6**, 403–408 (1985).

241. Samani, F., Kokabi, M., Soleimani, M. & Valojerdi, M. R. Fabrication and characterization of electrospun fibrous nanocomposite scaffolds based on poly(lactide-co-glycolide)/poly(vinyl alcohol) blends. *Polymer International* **59**, 901–909 (2010).

242. Hynes, R. O. Integrins: Bidirectional, allosteric signaling machines. *Cell* **110**, 673–687 (2002).

243. Jatav, S. & Joshi, Y. M. Chemical stability of Laponite in aqueous media.

Applied Clay Science **97**–**98**, 72–77 (2014).

244. Ishikawa, K., Akasaka, T., Yawaka, Y. & Watari, F. High functional expression of osteoblasts on imogolite, aluminosilicate nanotubes. *Journal of Biomedical Nanotechnology* **6**, 59–65 (2010).

245. Shi, P. *et al.* Self-Assembling Nanoclay Diffusion Gels for Bioactive Osteogenic Microenvironments. *Advanced Healthcare Materials* **7**, 1800331 (2018).

246. Tang, L. *et al.* LAPONITE® nanorods regulating degradability, acidic-alkaline microenvironment, apatite mineralization and MC3T3-E1 cells responses to poly(butylene succinate) based bio-nanocomposite scaffolds. *RSC Advances* **8**, 10794–10805 (2018).

247. Sadjadi, M. S., Ebrahimi, H. R., Meskinfam, M. & Zare, K. Silica enhanced formation of hydroxyapatite nanocrystals in simulated body fluid (SBF) at 37 °c. *Materials Chemistry and Physics* **130**, 67–71 (2011).

248. Miyaji, F., Kim, H. M., Handa, S., Kokubo, T. & Nakamura, T. Bonelike apatite coating on organic polymers: Novel nucleation process using sodium silicate solution. *Biomaterials* **20**, 913–919 (1999).

249. Henry Teng, H. How ions and molecules organize to form crystals. *Elements* **9**, 189–194 (2013).

250. Carrow, J. K. *et al.* Widespread changes in transcriptome profile of human mesenchymal stem cells induced by two-dimensional nanosilicates. *Proceedings of the National Academy of Sciences of the United States of America* **115**, E3905–E3913 (2018).

251. Yoshizawa, S., Brown, A., Barchowsky, A. & Sfeir, C. Magnesium ion stimulation of bone marrow stromal cells enhances osteogenic activity, simulating the effect of magnesium alloy degradation. *Acta Biomaterialia* **10**, 2834–2842 (2014).

252. Cheng, P. *et al.* High-purity magnesium interference screws promote fibrocartilaginous entheses regeneration in the anterior cruciate ligament reconstruction rabbit model via accumulation of BMP-2 and VEGF.

Biomaterials **81**, 14–26 (2016).

253. Zreiqat, H. *et al.* Mechanisms of magnesium-stimulated adhesion of osteoblastic cells to commonly used orthopaedic implants. *Journal of Biomedical Materials Research* **62**, 175–184 (2002).

254. Reffitt, D. M. *et al.* Orthosilicic acid stimulates collagen type 1 synthesis and osteoblastic differentiation in human osteoblast-like cells in vitro. *Bone* **32**, 127–135 (2003).

255. Hedgepeth, C. M. *et al.* Activation of the Wnt signaling pathway: A molecular mechanism for lithium action. *Developmental Biology* **185**, 82–91 (1997).

256. Wang, Z. *et al.* Attapulgite-doped electrospun poly(lactic-co-glycolic acid) nanofibers enable enhanced osteogenic differentiation of human mesenchymal stem cells. *RSC Advances* **5**, 2383–2391 (2015).

257. Sokolova, T. A. Decomposition of clay minerals in model experiments and in soils: Possible mechanisms, rates, and diagnostics (analysis of literature). *Eurasian Soil Science* **46**, 182–197 (2013).

258. Mohanty, R. P. & Joshi, Y. M. Chemical stability phase diagram of aqueous Laponite dispersions. *Applied Clay Science* **119**, 243–248 (2016).

259. Shih, Y. R. V. *et al.* Calcium phosphate-bearing matrices induce osteogenic differentiation of stem cells through adenosine signaling. *Proceedings of the National Academy of Sciences of the United States of America* **111**, 990–995 (2014).

260. Boonrungsiman, S. *et al.* The role of intracellular calcium phosphate in osteoblast-mediated bone apatite formation. *Proceedings of the National Academy of Sciences of the United States of America* **109**, 14170–14175 (2012).

261. Sathy, B. N. *et al.* RALA complexed α-TCP nanoparticle delivery to mesenchymal stem cells induces bone formation in tissue engineered constructs in vitro and in vivo. *Journal of Materials Chemistry B* **5**, 1753–1764 (2017).

262. Cross, L. M., Carrow, J. K., Ding, X., Singh, K. A. & Gaharwar, A. K. Sustained and Prolonged Delivery of Protein Therapeutics from Two-

Dimensional Nanosilicates. *ACS Applied Materials and Interfaces* **11**, 6741–6750 (2019).

263. Ladewig, K., Zhi, P. X. & Gao, Q. L. Layered double hydroxide nanoparticles in gene and drug delivery. *Expert Opinion on Drug Delivery* **6**, 907–922 (2009).

264. Yang, D. *et al.* Enhanced transcription and translation in clay hydrogel and implications for early life evolution. *Scientific Reports* **3**, (2013).

265. Mousa, M., Evans, N. D., Oreffo, R. O. C. & Dawson, J. I. Clay nanoparticles for regenerative medicine and biomaterial design: A review of clay bioactivity. *Biomaterials* **159**, 204–214 (2018).

266. Moore, T. L. *et al.* Nanoparticle administration method in cell culture alters particle-cell interaction. *Scientific Reports* **9**, 1–9 (2019).

267. Moore, T. L. *et al.* Nanoparticle colloidal stability in cell culture media and impact on cellular interactions. *Chemical Society Reviews* **44**, 6287–6305 (2015).

268. Li, T. *et al.* Impact of bone marrow mesenchymal stem cell immunomodulation on the osteogenic effects of laponite. *Stem Cell Research and Therapy* **9**, 100 (2018).

269. Wei, M., Li, S. & Le, W. Nanomaterials modulate stem cell differentiation: biological interaction and underlying mechanisms. *Journal of nanobiotechnology* **15**, 75 (2017).

270. Schecroun, N. & Delloye, C. Bone-like nodules formed by human bone marrow stromal cells: Comparative study and characterization. *Bone* **32**, 252–260 (2003).

271. Bigham, J. M. Clay Mineralogy: Spectroscopic and Chemical Determinative Methods. *Journal of Environmental Quality* **24**, 795–795 (1995).

272. Li, Y. *et al.* PH sensitive Laponite/alginate hybrid hydrogels: Swelling behaviour and release mechanism. *Soft Matter* **7**, 6231–6238 (2011).

273. Li, K. *et al.* Enhanced in vivo antitumor efficacy of doxorubicin encapsulated

within laponite nanodisks. *ACS Applied Materials and Interfaces* **6**, 12328–12334 (2014).

274. Unfried, K. *et al.* Cellular responses to nanoparticles: Target structures and mechanisms. *Nanotoxicology* **1**, 52–71 (2007).

275. Golub, E. E. & Boesze-Battaglia, K. The role of alkaline phosphatase in mineralization. *Current Opinion in Orthopaedics* **18**, 444–448 (2007).

276. Orimo, H. The mechanism of mineralization and the role of alkaline phosphatase in health and disease. *Journal of Nippon Medical School* **77**, 4–12 (2010).

277. Matsubara, T. *et al.* BMP2 regulates osterix through Msx2 and Runx2 during osteoblast differentiation. *Journal of Biological Chemistry* **283**, 29119–29125 (2008).

278. Komori, T. Regulation of bone development and extracellular matrix protein genes by RUNX2. *Cell and Tissue Research* **339**, 189–195 (2010).

279. Kim, Y. J., Lee, M. H., Wozney, J. M., Cho, J. Y. & Ryoo, H. M. Bone morphogenetic protein-2-induced alkaline phosphatase expression is stimulated by Dlx5 and repressed by Msx2. *Journal of Biological Chemistry* **279**, 50773–50780 (2004).

280. Gentleman, E. *et al.* Comparative materials differences revealed in engineered bone as a function of cell-specific differentiation. *Nature Materials* **8**, 763–770 (2009).

281. Gough, J. E., Jones, J. R. & Hench, L. L. Nodule formation and mineralisation of human primary osteoblasts cultured on a porous bioactive glass scaffold. *Biomaterials* **25**, 2039–2046 (2004).

282. Ghita, A., Pascut, F. C., Sottile, V. & Notingher, I. Monitoring the mineralisation of bone nodules in vitro by space- and time-resolved Raman micro-spectroscopy. *Analyst* **139**, 55–58 (2014).

283. Robey, P. G. Noncollagenous Bone Matrix Proteins. in *Principles of Bone Biology* 335–349 (2008).

284. Boskey, A. L. & Robey, P. G. The Regulatory Role of Matrix Proteins in Mineralization of Bone. in *Osteoporosis: Fourth Edition* 235–255 (2013).

285. Butler, W. T. The nature and significance of osteopontin. *Connective Tissue Research* **23**, 123–136 (1989).

286. Xie, H., Wang, P. & Wu, J. Effect of exposure of osteoblast-like cells to low-dose silver nanoparticles: uptake, retention and osteogenic activity. *Artificial Cells, Nanomedicine and Biotechnology* **47**, 260–267 (2019).

287. Liu, W. *et al.* Alpl prevents bone ageing sensitivity by specifically regulating senescence and differentiation in mesenchymal stem cells. *Bone Research* **6**, 1–15 (2018).

288. WHYTE, M. P. Hypophosphatasia and the Role of Alkaline Phosphatase in Skeletal Mineralization*. *Endocrine Reviews* **15**, 439–461 (1994).

289. Prins, H. J. *et al.* In vitro induction of alkaline phosphatase levels predicts in vivo bone forming capacity of human bone marrow stromal cells. *Stem Cell Research* **12**, 428–440 (2014).

290. Siddappa, R., Licht, R., van Blitterswijk, C. & de Boer, J. Donor variation and loss of multipotency during in vitro expansion of human mesenchymal stem cells for bone tissue engineering. *Journal of Orthopaedic Research* (2007).

291. Makboul, H. E. & Ottow, J. C. G. Alkaline phosphatase activity and michaelis constant in the presence of different clay minerals. *Soil Science* **128**, 129–135 (1979).

292. Shindo, H. *et al.* Adsorption, activity, and kinetics of acid phosphatase as influenced by selected oxides and clay minerals. *Soil Science and Plant Nutrition* **48**, 763–767 (2002).

293. Zhu, Y., Wu, F., Feng, W., Liu, S. & Giesy, J. P. Interaction of alkaline phosphatase with minerals and sediments: Activities, kinetics and hydrolysis of organic phosphorus. *Colloids and Surfaces A: Physicochemical and Engineering Aspects* **495**, 46–53 (2016).

294. Gaharwar, A. K. *et al.* 2D Nanoclay for Biomedical Applications: Regenerative Medicine, Therapeutic Delivery, and Additive Manufacturing. *Advanced*

Materials **31**, 1900332 (2019).

295. Carlisle, E. M. Silicon: A possible factor in bone calcification. *Science* **167**, 279–280 (1970).

296. Han, P., Wu, C. & Xiao, Y. The effect of silicate ions on proliferation, osteogenic differentiation and cell signalling pathways (WNT and SHH) of bone marrow stromal cells. *Biomaterials Science* **1**, 379–392 (2013).

297. Yousef, N. S., Farouq, R. & Hazzaa, R. Adsorption kinetics and isotherms for the removal of nickel ions from aqueous solutions by an ion-exchange resin: application of two and three parameter isotherm models. *Desalination and Water Treatment* **57**, 21925–21938 (2016).

298. MORELAND, B. H. Lippincott's Illustrated Reviews: Biochemistry. *Biochemical Society Transactions* **16**, 907–908 (1988).

299. Francia, V., Reker-Smit, C., Boel, G. & Salvati, A. Limits and challenges in using transport inhibitors to characterize how nano-sized drug carriers enter cells. *Nanomedicine* **14**, 1533–1549 (2019).

300. Greulich, C. *et al.* Uptake and intracellular distribution of silver nanoparticles in human mesenchymal stem cells. *Acta Biomaterialia* **7**, 347–354 (2011).

301. Heining, E., Bhushan, R., Paarmann, P., Henis, Y. I. & Knaus, P. Spatial segregation of BMP/smad signaling affects osteoblast differentiation in C2C12 cells. *PLoS ONE* **6**, (2011).

302. Ghiaci, M., Aghaei, H., Soleimanian, S. & Sedaghat, M. E. Enzyme immobilization: Part 2. Immobilization of alkaline phosphatase on Na-bentonite and modified bentonite. *Applied Clay Science* **43**, 308–316 (2009).

303. Sedaghat, M. E., Ghiaci, M., Aghaei, H. & Soleimanian-Zad, S. Enzyme immobilization. Part 4. Immobilization of alkaline phosphatase on Na-sepiolite and modified sepiolite. *Applied Clay Science* **46**, 131–135 (2009).

304. Carrasco, M. S., Rad, J. C. & González-Carcedo, S. Immobilization of alkaline phosphatase by sorption on Na-sepiolite. *Bioresource Technology* **51**, 175–181 (1995).

305. Tietjen, T. & Wetzel, R. G. Extracellular enzyme-clay mineral complexes: Enzyme adsorption, alteration of enzyme activity, and protection from photodegradation. *Aquatic Ecology* **37**, 331–339 (2003).

306. Servagent-Noinville, S., Revault, M., Quiquampoix, H. & Baron, M. H. Conformational changes of bovine serum albumin induced by adsorption on different clay surfaces: FTIR analysis. *Journal of Colloid and Interface Science* **221**, 273–283 (2000).

307. Schmidt, M. P. & Martínez, C. E. Kinetic and Conformational Insights of Protein Adsorption onto Montmorillonite Revealed Using in Situ ATR-FTIR/2D-COS. *Langmuir* **32**, 7719–7729 (2016).

308. Yang, X. *et al.* The stimulatory effect of silica nanoparticles on osteogenic differentiation of human mesenchymal stem cells. *Biomedical Materials* **12**, 015001 (2016).

309. Ha, S. W., Neale Weitzmann, M. & Beck, G. R. Bioactive silica nanoparticles promote osteoblast differentiation through stimulation of autophagy and direct association with LC3 and p62. *ACS Nano* **8**, 5898–5910 (2014).

310. Zhang, L., Yang, C., Li, J., Zhu, Y. & Zhang, X. High extracellular magnesium inhibits mineralized matrix deposition and modulates intracellular calcium signaling in human bone marrow-derived mesenchymal stem cells. *Biochemical and Biophysical Research Communications* **450**, 1390–1395 (2014).

311. Zhang, X. *et al.* Ion channel functional protein kinase TRPM7 regulates Mg ions to promote the osteoinduction of human osteoblast via PI3K pathway: In vitro simulation of the bone-repairing effect of Mg-based alloy implant. *Acta Biomaterialia* **63**, 369–382 (2017).

312. Wang, J. *et al.* Magnesium Ions Promote the Biological Behaviour of Rat Calvarial Osteoblasts by Activating the PI3K/Akt Signalling Pathway. *Biological Trace Element Research* **179**, 284–293 (2017).

313. Zhu, Z. *et al.* Lithium stimulates human bone marrow derived mesenchymal stem cell proliferation through GSK-3β-dependent β-catenin/Wnt pathway

activation. *FEBS Journal* **281**, 5371–5389 (2014).

314. De Boer, J., Wang, H. J. & Van Blitterswijk, C. Effects of Wnt Signaling on Proliferation and Differentiation of Human Mesenchymal Stem Cells. *Tissue Engineering* **10**, 393–401 (2004).

315. Wu, Y. *et al.* A Bi-lineage conducive scaffold for osteochondral defect regeneration. *Advanced Functional Materials* **24**, 4473–4483 (2014).

316. Xing, M., Wang, X., Wang, E., Gao, L. & Chang, J. Bone tissue engineering strategy based on the synergistic effects of silicon and strontium ions. *Acta Biomaterialia* **72**, 381–395 (2018).

317. Valerio, P., Pereira, M. M., Goes, A. M. & Leite, M. F. The effect of ionic products from bioactive glass dissolution on osteoblast proliferation and collagen production. *Biomaterials* **25**, 2941–2948 (2004).

318. Tsigkou, O., Jones, J. R., Polak, J. M. & Stevens, M. M. Differentiation of fetal osteoblasts and formation of mineralized bone nodules by 45S5 Bioglass® conditioned medium in the absence of osteogenic supplements. *Biomaterials* **30**, 3542–3550 (2009).

319. Naruphontjirakul, P., Tsigkou, O., Li, S., Porter, A. E. & Jones, J. R. Human mesenchymal stem cells differentiate into an osteogenic lineage in presence of strontium containing bioactive glass nanoparticles. *Acta Biomaterialia* (2019) doi:10.1016/j.actbio.2019.03.038.

320. Von Moos, N., Bowen, P. & Slaveykova, V. I. Bioavailability of inorganic nanoparticles to planktonic bacteria and aquatic microalgae in freshwater. *Environmental Science: Nano* **1**, 214–232 (2014).

321. Habibovic, P. & Barralet, J. E. Bioinorganics and biomaterials: Bone repair. *Acta Biomaterialia* **7**, 3013–3026 (2011).

322. Zamani, A., Omrani, G. R. & Nasab, M. M. Lithium's effect on bone mineral density. *Bone* **44**, 331–334 (2009).

323. Wilting, I. *et al.* Lithium use and the risk of fractures. *Bone* **40**, 1252–1258 (2007).

324. Jin, Y. *et al.* Lithium chloride enhances bone regeneration and implant osseointegration in osteoporotic conditions. *Journal of Bone and Mineral Metabolism* **35**, 497–503 (2017).

325. Tang, L., Chen, Y., Pei, F. & Zhang, H. Lithium chloride modulates adipogenesis and osteogenesis of human bone marrow-derived mesenchymal stem cells. *Cellular Physiology and Biochemistry* **37**, 143–152 (2015).

326. Li, L. *et al.* Acceleration of bone regeneration by activating Wnt/β-catenin signalling pathway via lithium released from lithium chloride/calcium phosphate cement in osteoporosis. *Scientific Reports* **7**, 45204 (2017).

327. Han, P. *et al.* Lithium release from β-tricalcium phosphate inducing cementogenic and osteogenic differentiation of both hPDLCs and hBMSCs. *Biomaterials Science* **2**, 1230–1243 (2014).

328. Hoeppner, L. H., Secreto, F. J. & Westendorf, J. J. Wnt signaling as a therapeutic target for bone diseases. *Expert Opinion on Therapeutic Targets* **13**, 485–496 (2009).

329. R. Wagner, E. *et al.* The Therapeutic Potential of the Wnt Signaling Pathway in Bone Disorders. *Current Molecular Pharmacology* **4**, 14–25 (2011).

330. Klein, P. S. & Melton, D. A. A molecular mechanism for the effect of lithium on development. *Proceedings of the National Academy of Sciences of the United States of America* **93**, 8455–8459 (1996).

331. Stambolic, V., Ruel, L. & Woodgett, J. R. Lithium inhibits glycogen synthase kinase-3 activity and mimics wingless signalling in intact cells. *Current Biology* **6**, 1664–1669 (1996).

332. Satija, N. K., Sharma, D., Afrin, F., Tripathi, R. P. & Gangenahalli, G. High Throughput Transcriptome Profiling of Lithium Stimulated Human Mesenchymal Stem Cells Reveals Priming towards Osteoblastic Lineage. *PLoS ONE* **8**, e55769 (2013).

333. Kim, G. J. *et al.* Effect of nano-montmorillonite on osteoblast differentiation, mineral density, and osteoclast differentiation in bone formation. *Nanomaterials* **10**, 230 (2020).

334. Kang, H. R. *et al.* Mg–Al and Zn–Al Layered Double Hydroxides Promote Dynamic Expression of Marker Genes in Osteogenic Differentiation by Modulating Mitogen-Activated Protein Kinases. *Advanced Healthcare Materials* **7**, 1700693 (2018).

335. Huang, K. *et al.* Halloysite Nanotube Based Scaffold for Enhanced Bone Regeneration. *ACS Biomaterials Science and Engineering* **5**, 4037–4047 (2019).

336. Wang, Z. *et al.* Attapulgite-doped electrospun poly(lactic-co-glycolic acid) nanofibers enable enhanced osteogenic differentiation of human mesenchymal stem cells. *RSC Advances* (2015) doi:10.1039/c4ra09839k.

337. Jaber, M., Komarneni, S. & Zhou, C. H. Synthesis of clay minerals. in *Developments in Clay Science* vol. 5 223–241 (2013).

338. Fleischer, C. C. & Payne, C. K. Nanoparticle-cell interactions: Molecular structure of the protein corona and cellular outcomes. *Accounts of Chemical Research* **47**, 2651–2659 (2014).

339. Behzadi, S. *et al.* Cellular uptake of nanoparticles: Journey inside the cell. *Chemical Society Reviews* **46**, 4218–4244 (2017).

340. Pan, T. *et al.* MiR-29b-Loaded Gold Nanoparticles Targeting to the Endoplasmic Reticulum for Synergistic Promotion of Osteogenic Differentiation. *ACS Applied Materials and Interfaces* **8**, 19217–19227 (2016).

341. Iversen, T. G., Skotland, T. & Sandvig, K. Endocytosis and intracellular transport of nanoparticles: Present knowledge and need for future studies. *Nano Today* **6**, 176–185 (2011).

342. Donahue, N. D., Acar, H. & Wilhelm, S. Concepts of nanoparticle cellular uptake, intracellular trafficking, and kinetics in nanomedicine. *Advanced Drug Delivery Reviews* **143**, 68–96 (2019).

343. Zhang, Y., Kong, N., Zhang, Y., Yang, W. & Yan, F. Size-dependent effects of gold nanoparticles on osteogenic differentiation of human periodontal ligament progenitor cells. *Theranostics* **7**, 1214–1224 (2017).

344. Saito, A. *et al.* Endoplasmic reticulum stress response mediated by the PERK-

eIF2α-ATF4 pathway is involved in osteoblast differentiation induced by BMP2. *Journal of Biological Chemistry* **286**, 4809–4818 (2011).

345. Furmanik, M. & Shanahan, C. M. ER stress regulates alkaline phosphatase gene expression in vascular smooth muscle cells via an ATF4-dependent mechanism. *BMC Research Notes* **11**, 483 (2018).

346. Murakami, T. *et al.* Signalling mediated by the endoplasmic reticulum stress transducer OASIS is involved in bone formation. *Nature Cell Biology* **11**, 1205–1211 (2009).

347. Schrand, A. M., Schlager, J. J., Dai, L. & Hussain, S. M. Preparation of cells for assessing ultrastructural localization of nanoparticles with transmission electron microscopy. *Nature Protocols* **5**, 744–757 (2010).

348. Zhu, M. *et al.* Physicochemical properties determine nanomaterial cellular uptake, transport, and fate. *Accounts of Chemical Research* **46**, 622–631 (2013).

349. Wang, S. *et al.* Laponite nanodisks as an efficient platform for doxorubicin delivery to cancer cells. *Langmuir* **29**, 5030–5036 (2013).

350. Rischitor, G. *et al.* Quantification of the cellular dose and characterization of nanoparticle transport during in vitro testing. *Particle and Fibre Toxicology* **13**, 47 (2016).

351. Veernala, I. *et al.* Effect of Fluoride Doping in Laponite Nanoplatelets on Osteogenic Differentiation of Human Dental Follicle Stem Cells (hDFSCs). *Scientific Reports* **9**, 1–15 (2019).

352. Liao, J. *et al.* Nano-Bio interactions of clay nanotubes with colon cancer cells. *Colloids and Surfaces A: Physicochemical and Engineering Aspects* **586**, 124242 (2020).

353. Chaudhuri, A., Battaglia, G. & Golestanian, R. The effect of interactions on the cellular uptake of nanoparticles. *Physical Biology* **8**, 046002 (2011).

354. Halamoda-Kenzaoui, B. *et al.* The agglomeration state of nanoparticles can influence the mechanism of their cellular internalisation. *Journal of Nanobiotechnology* **15**, 1–15 (2017).

355. Jin, H., Heller, D. A., Sharma, R. & Strano, M. S. Size-dependent cellular uptake and expulsion of single-walled carbon nanotubes: Single particle tracking and a generic uptake model for nanoparticles. *ACS Nano* **3**, 149–158 (2009).

356. Chithrani, B. D., Ghazani, A. A. & Chan, W. C. W. Determining the size and shape dependence of gold nanoparticle uptake into mammalian cells. *Nano Letters* **6**, 662–668 (2006).

357. Chung, H. E., Park, D. H., Choy, J. H. & Choi, S. J. Intracellular trafficking pathway of layered double hydroxide nanoparticles in human cells: Size-dependent cellular delivery. *Applied Clay Science* **65**–**66**, 24–30 (2012).

358. Luzio, J. P., Pryor, P. R. & Bright, N. A. Lysosomes: Fusion and function. *Nature Reviews Molecular Cell Biology* vol. 8 622–632 (2007).

359. Sakhtianchi, R. *et al.* Exocytosis of nanoparticles from cells: Role in cellular retention and toxicity. *Advances in Colloid and Interface Science* **201**–**202**, 18–29 (2013).

360. Sikora, B. *et al.* Mammalian cell defence mechanisms against the cytotoxicity of NaYF4:(Er,Yb,Gd) nanoparticles. *Nanoscale* **9**, 14259–14271 (2017).

361. Zhai, W. *et al.* Degradation of hollow mesoporous silica nanoparticles in human umbilical vein endothelial cells. *Journal of Biomedical Materials Research - Part B Applied Biomaterials* **100 B**, 1397–1403 (2012).

362. Yao, Q., Fuglsby, K. E., Zheng, X. & Sun, H. Nanoclay-functionalized 3D nanofibrous scaffolds promote bone regeneration. *Journal of Materials Chemistry B* **8**, 3842–3851 (2020).

363. Gonçalves, M. *et al.* PH-sensitive Laponite®/doxorubicin/alginate nanohybrids with improved anticancer efficacy. *Acta Biomaterialia* **10**, 300–307 (2014).

364. Bibi, I., Singh, B. & Silvester, E. Dissolution kinetics of soil clays in sulfuric acid solutions: Ionic strength and temperature effects. *Applied Geochemistry* **51**, 170–183 (2014).

365. Eskelinen, E. L. To be or not to be? Examples of incorrect identification of autophagic compartments in conventional transmission electron microscopy of

mammalian cells. *Autophagy* **4**, 257–260 (2008).

366. He, W. *et al.* Silver nanoparticles stimulate osteogenesis of human mesenchymal stem cells through activation of autophagy. *Nanomedicine* **15**, 337–353 (2020).

367. Liu, F. *et al.* Suppression of autophagy by FIP200 deletion leads to osteopenia in mice through the inhibition of osteoblast terminal differentiation. *Journal of Bone and Mineral Research* **28**, 2414–2430 (2013).

368. Mizushima, N. & Levine, B. Autophagy in mammalian development and differentiation. *Nature Cell Biology* **12**, 823–830 (2010).

369. Li, J. *et al.* Gold nanoparticle size and shape influence on osteogenesis of mesenchymal stem cells. *Nanoscale* **8**, 7992–8002 (2016).